Elaboration of advanced photocatalytic materials by Atomic layer Deposition (ALD)

Syreina Alsayegh

THÈSE POUR OBTENIR LE GRADE DE DOCTEUR DE L'UNIVERSITÉ DE MONTPELLIER

En Chimie et Physico-chimie des matériaux

École doctorale Science Chimique Balard (ED459)

Unité de recherche : Institut Européen des Membranes (IEM)

Elaboration of Advanced Photocatalytic Materials by Atomic layer Deposition (ALD)

Présentée par Syreina ALSAYEGH
Le 17 décembre 2021

Sous la direction de Mikhael BECHELANY
Et l'encadrement de Antonio-Carlo RAZZOUK, François ZAVISKA, Geoffroy LESAGE and Juliette ESTEPHAN

Devant le jury composé de

M. Mikhael BECHELANY, directeur de recherche CNRS, Université de Montpellier	Directeur de thèse
M. Antonio-Carlo RAZZOUK, professeur, Université Libanaise	Co-directeur de thèse
M. François ZAVISKA, maître de conférence, Université de Montpellier	Co-encadrant
M. Geoffroy LESAGE, maître de conférence, Université de Montpellier	Co-encadrant
M. Lionel SANTINACCI, chargé de recherche CNRS, Université Aix Marseille	Rapporteur
M. Alain ESTEVE, directeur de recherche CNRS, Université de Toulouse	Rapporteur (Président)
Mme. Valérie KELLER, directeur de recherche CNRS, Université de Strasbourg	Examinatrice
Mme. Nathanaëlle SCHNEIDER, chargé de recherche CNRS, Chimie Paris Tech	Examinatrice

UNIVERSITÉ DE MONTPELLIER

"Nothing that is worthwhile is ever easy.

Remember that!"

Nicholas Sparks

To my parents, my colleagues, my friends and Fadi,

With all my gratitude

My deep gratitude goes first to my director Dr. Mikhael Bechelany, who guided me during these 3 years of research. His scientific advices and optimism make it much easier even in the hard moments. Thank you for believing in my capacities and encouraging me always to go further. Thank you for your patience, your enthusiasm, your motivation, I know you believed in me even when I had doubts about it.

My appreciation also goes to my co-director Pr. Antonio-Carlo Razzouk for believing in me and encouraging me to do a PhD. Thanks to Juliette Estephan for accepting to supervise this work with the collaboration between the Lebanese University and University of Montpellier.

I would like to express the deepest appreciation for my supervisors Francois Zaviska and Geoffroy Lesage for their guidance and constant supervision whenever I asked for it.

A special recognition for the directories of the institute Pr. Philippe Mielle and Pr. David Cornu.

I would like to express my gratitude for the member of juries that accepted to supervise this thesis: M. Lionel Santinacci, M. Alain Esteve, Mme Valerie Keller and Mme Nathanaëlle Schneider.

The biggest thanks goes to my colleagues and IEM workers. Throw-out these years, I have met so many people in this lab with whom we shared good moment. The list is maybe long but I want to make sure to thank each and every one of them. A special thanks to Danae, Sakhti, Matthieu, Octavio, Carlos, Jeanne, Fanny, Amr, Orlane, Hana. A big thanks for my Lebanese friends: Fida, Elissa, Ghenwa, Joelle, Sara, Maya, Ghady, Cynthia, George, Petros, Marleine. Fida, Elissa and Mahmoud, thank you for your support and for staying my friends after the last few months of thesis. Fida, thank you for the late night staying supports and for all the cooking. No words can describe my gratitude for the best colleagues in our team that are now like family. A special thanks to Carole, my French friend, we shared many tears together but so many laughs and talks and shopping. Finally thanks for Habib for his support and guidance during these 3 years; I asked so many questions but he was always there to answer them. Thank You all for making these 3 years so special with lots of memories that I will never forget.

I would not forget all the IEM stuff, for helping me in all the technical and analysis issues: Eddy Le Petit, Jim Cartier and Christophe Charmette. During this thesis, I spent plenty of time in the workshop of IEM and learned so much from all of you Bruno Navara, Patrice Montelz and Daniel Valenza. Thank you for helping me to find solution and repair the instruments.

Thanks to Catherine Scognamiglio, Christelle Floutier, Florence Leroy and Fabienne Biondi.

Finally, thanks to my parents and brothers for believing in me and encouraging me every day. You encouraged me to follow my dreams even if it meant to be far away from you. The goodbyes were not easy every time I went to visit you but deep inside you continued to encourage me without showing your tears. I love you and so thankful for you, without you I was not who I am today. Thanks to Fadi for supporting during the good and bad moments. His encouragement everyday by telling me I am doing a great job was so helpful.

Without all these peoples and their support especially during COVID and after the economic crisis in Lebanon, I was not here today submitting my work.

Table of contents

Abstract

Due to the increasing contamination of our natural water resources by a wide range of organic micropollutant (OMPs), there is a need for developing new energy-efficient advanced oxidation processes for the treatment of water contaminated by such refractory pollutants.

Photocatalysis has attracted much attention, due to its ability to degrade toxic organic compounds in wastewater into CO_2 and water. Among the various photocatalytic materials, titanium dioxide (TiO_2) has been widely used due to its high photocatalytic efficiency, high stability and low toxicity. However, fast charge recombination and the narrow absorption range in the UV spectrum; limit its photocatalytic efficiency under visible-light irradiation.

In this work, the elaboration of different TiO_2 structure by combining two techniques have been performed. One of the main objectives is to elaborate highly catalytic material with great stability. In the first part of this thesis, TiO_2 nanofibers were synthesized by electrospinning method. In order to improve the photocatalytic activity under visible light, a developed process based on atomic layer deposition (ALD) was used to grow boron nitride (BN) and palladium (Pd) on these fibers. The second part of this work was to elaborate TiO_2 nanotubes (NTs) by ALD and compare their photoactivity with TiO_2 NFs. The tubular structure allows orthogonal separation of charge carriers which promotes degradation. The morphological, structural and optical properties of all synthesized materials were investigated by several characterization techniques such as Fourier-transform infrared spectroscopy (FTIR), scanning electron microscopy (SEM), Raman spectroscopy, X-ray diffraction (XRD), transmission electron microscopy (TEM) and X-ray photoelectron spectroscopy (XPS). Moreover, the optical and electrochemical properties of the catalyst have been also assessed. The influence of chemical and physical properties on the photocatalytic degradation of acetaminophen has been investigated. Promising results in enhancement of the degradation of ACT were seen with nanocomposite material TiO_2-BN-Pd compared to pristine TiO_2 NFs. Moreover, TiO_2 nanotubes (NTs) has shown better photoactivity under visible light than TiO_2 NFs. In parallel, a better understanding of the photocatalytic oxidation pathways (based on by-product analysis) coupled with toxicity tests (*Vibrio Fisheri*, Microtox) was investigated.

Promising results were obtained, where the synthesized TiO_2 shows higher catalytic activity and good stability under visible light irradiation. Therefore, a major concern limits the use of these suspended photocatalysts in water treatment. Hence, the combination of two processes using an immobilized catalyst by coupling advanced separation and oxidation (membrane/photocatalysis) appears to be an interesting solution in order to improve the micropollutant/catalyst contact. The first step of this third part of the study consists in developing photocalytic membranes by ALD deposition of photocatalyst on conventional ceramic membranes. Once these membranes have been developed, a photocatalytic reactor was specifically designed to be able to test these membranes and evaluate their performance for micropollutant degradation. Much work is still needed to improve the hydrodynamics as well as the irradiation efficiency of the photocatalyst.

Résumé

En raison de la contamination croissante de nos ressources en eau naturelles par une large gamme de micropolluants organiques (MP), il est nécessaire de développer de nouveaux procédés d'oxydation avancés économes en énergie pour le traitement des eaux contaminées par de tels polluants réfractaires.

La photocatalyse a attiré beaucoup d'attention, en raison de sa capacité à dégrader les composés organiques toxiques dans les eaux usées en composés non toxiques tels que le CO_2 et l'eau. Parmi les divers matériaux photocatalytiques, le dioxyde de titane (TiO_2) a été largement utilisé en raison de son efficacité photocatalytique élevée, de sa stabilité élevée et de sa faible toxicité. Cependant, la recombinaison de charge rapide et la plage d'absorption étroite dans le spectre UV; limite son efficacité photocatalytique sous irradiation en lumière visible.

Dans ce travail, l'élaboration de différentes structures de TiO_2 en combinant deux techniques a été réalisé avec succès. L'un des principaux objectifs est d'élaborer un matériau stable à haute performance catalytique. Dans la première partie de cette thèse, des nanofibres de TiO_2 ont été synthétisées par électrofilage. Afin d'améliorer l'activité photocatalytique sous lumière visible, un procédé développé basé sur le dépôt de couche atomique (ALD) a été utilisé pour déposer du nitrure de bore (BN) et du palladium (Pd) sur ces fibres. Dans la deuxième partie de ce travail, des nanotubes de TiO_2 ont été élaboré par ALD et leur photoactivité a été comparé avec les nanofibres de TiO_2. La structure tubulaire permet une séparation orthogonale des porteurs de charge ce qui favorise la dégradation. Les propriétés morphologiques, structurelles et optiques de tous les matériaux synthétisés ont été étudiées par plusieurs techniques de caractérisation telles que la spectroscopie infrarouge à transformée de Fourier (FTIR), la microscopie électronique à balayage (MEB), la spectroscopie Raman, la diffraction des rayons X (XRD), la microscopie électronique à transmission (MET) et la spectroscopie photoélectronique aux rayons X (XPS). De même les propriétés optiques et électrochimiques des matériaux ont été évaluées. L'influence des propriétés chimiques et physiques sur la dégradation photocatalytique de l'acétaminophène a été étudiée. Des résultats prometteurs en termes d'amélioration de la dégradation de l'ACT ont été observé avec le matériau nanocomposite TiO_2-BN-Pd par rapport aux fibre de TiO_2 vierges. De plus, les

nanotubes de TiO_2 ont montré une meilleure photoactivité sous lumière visible que les nanofibres. En parallèle, une meilleure compréhension des voies d'oxydation photocatalytique (basée sur l'analyse des sous-produits) couplée à des tests de toxicité (*Vibrio Fisheri*, Microtox) ont été étudiée.

En vue des résultats prometteurs obtenue dans les 2 première partie, la récupération de ces catalyseurs en suspension limitent leur utilisation pour le traitement des eaux. Le couplage des procédés de séparation/oxydation avancée (membrane/photocatalyse) apparait comme une solution intéressante afin d'améliorer le contact micropolluant-catalyseur. La première étape de cette troisième partie d'étude à consister à élaborer des membranes photocalytiques par déposition ALD de photocatalyseur sur des membranes céramiques conventionnelles. Une fois ces membranes développées, un réacteur photocatalytique a été spécifiquement conçu pour pouvoir tester ces membranes et évaluer leur performance pour la dégradation de micropolluant. De nombreux travaux sont encore nécessaires afin d'améliorer l'hydrodynamique ainsi que le rendement d'irradiation du photocatalyseur.

List of Figures

List of Tables

Abbreviations

0D: zero dimensional

1D: one dimensional

2D: two-dimensional

3D: three-dimensional

ACT: acetaminophen

ALD: Atomic Layer Deposition

BN: boron nitride

MO: methyl orange

NFs: nanofibers

NTs: nanotubes

Pd: palladium

TiO_2: titanium dioxide

UV: Ultra Violet

VOCs: Volatile Organic Compounds

WWTPs: Waste Water Treatment Plants

Vis: Visible

e^-/h^+: electron-holes

AOPs: Advanced oxidation processes

PMR: photocatalytic membrane reactor

General Introduction

The purity of our water resources is affected by variety of human activities, with more people on the planet and more products and chemicals in use. Emerging pollutants have been introduced from agriculture, industry and our homes into our water. The use of everyday products such as detergent, personal care products and medicines resulting from our daily habits. When we use these products residues are flashed out the drain in the wastewater. Factories and industries release many chemicals substances into atmosphere and water when producing goods of everyday use. Cars fuels are also in important source of chemicals in air and water. The use of fertilizers and pesticides in production of our food is another significant source of emerging pollutants. The pollutants with all these activities end in our water: seawater, ground water, surface water and wastewater. As wastewater facilities treat our sewage, most pollutants are removed from the water before their release in the environment. In addition, our drinking water is purified before consuming. However, with the continuous increase of environmental pollution from air to soil and water, many new pollutants are detected. Some of these pollutants cannot be removed by the conventional wastewater treatments, traces of these pollutants has been detected in drinking water and environment. Current water sources contain traces of emerging pollutants.

Emerging micropollutants need to be effectively removed from water, accordingly new processes have been developed such as nanofiltration, reverse osmosis, granular activated carbon adsorption and advanced oxidation processes (AOP). Many researches have been focusing on advanced oxidation process and ceramic membrane filtration in several European countries and in the world. These innovative studies have been mixed with conventional wastewater treatment. They may filter the emerging pollutants by ceramic membranes, or the use of ozone or UV light to destroy the pollutants. The combination of several technologies could be effective to reach maximum removal of persistent pollutants but the shift to these new technologies have high implementation. Photocatalysis is an advanced oxidation process that has been developed in order to remove micropollutants from water based on light sources. This technique is cost-effective and highly efficient for the removal of pharmaceuticals. This technique is based on the activation of semiconductor with a light source that will allow the excitation of the electron from the valence band to the conduction band and the formation of photogenerated carriers that will participate in the oxydo-

reduction reactions. The most used semiconductor is TiO_2 due to his wide advantages. Nevertheless, TiO_2 possess a wide band gap and the recombination of the electron-holes is fast. Several techniques were used for the modification of TiO_2 by doping with metals and non-metals, coupling to other semiconductors.

Atomic layer deposition is a promising technique for the preparation or modification of TiO_2 catalysts. It is based on sequential pulses of gas precursors and allows the formation of thin layer with high thickness control on the angstrom level and pinhole free deposition. The aim of this thesis is the elaboration or modification of photocatalytic materials by ALD used in the water purification process. During this work, elaboration of TiO_2 with different aspects was studied for the degradation of pharmaceutical pollutants: acetaminophen and carbamazepine. First, elaboration of TiO_2 nanofibers was performed by electrospinning, and these NFs were modified by ALD by deposition of BN and Pd in order to shift the degradation under visible light and to reduce the e^-/h^+ recombination. Then, TiO_2 NTs were elaborated by ALD and compared to TiO_2 NFs. These NTs were also modified and their degradation efficiency was studied under Visible light. Finally, the conception of a new system for photocatalytic filtration using ceramic membrane have been developed. Alumina Ceramic membranes have been modified by ALD to enhance their photocatalytic activity and tune their properties. The morphological, structural and optical properties of the synthesized nanostructures were investigated using different characterization techniques such as scanning electron microscopy, transmission electron microscopy, energy-dispersive X-ray spectroscopy, BET measurements, X-ray diffraction, Raman spectroscopy, Fourier-transform infrared spectrometer, UV–VIS spectrophotometer and photoluminescence.

To achieve the above objectives, the following topics were investigated:

- Chapter 1: A literature review about environmental pollution and recent progress in water treatment by photocatalysis and elaboration of catalyst by ALD
- Chapter 2: Tunable TiO_2-BN-Pd nanofibers by combining electrospinning and Atomic Layer Deposition to enhance photodegradation of acetaminophen
- Chapter 3: N-doped TiO_2 Nanotubes synthesized by Atomic Layer Deposition for the degradation of acetaminophen
- Chapter 4: Elaboration of photocatalytic membranes with TiO_2 coating by ALD and evaluation of photocatalytic membrane reactor performance for degradation of ACT

Chapter 1: Literature Review

Table of contents

1. Environmental pollution

Environmental pollution is known as the presence of harmful substances on human's health and other organisms in the environment. Some scientists think that human activities plays a major role in the increase of pollutants concentration[1]. The increase of pollution is also caused by the population growth, the global warming, agriculture and industrialization. In addition, transboundary movement of pollutants in-between countries could be an important factor too. Pollutants are substances released in the environment that can cause several diseases and affect humans health and other living organisms even at low concentration[2–4]. These pollutants can affect air, water and soil quality and can be highly persistent[5]. Pollutants are divided in many categories: micropollutants known also as emerging pollutants[6], persistent organic pollutants (POPs)[7,8] and heavy metals[9].

1.1. Air pollution

Air pollution could be caused by a wide variety of pollutants reported in **Figure 1. 1**, that can cause severe health problems such as respiratory, cardiovascular, mental, and perinatal disorders[1]. These pollutants could be generated by both natural and anthropogenic sources[10]. Exposure to air pollutants can be divided into two groups, short term and long term exposure. The effect of the short term exposure are cough, shortness of breath, wheezing, asthma, respiratory disease, and high rates of hospitalization. The long term exposure can cause chronic asthma, pulmonary insufficiency, cardiovascular diseases, and cardiovascular mortality. Herein, air pollution does not affect only human health but also could have a high influence on degradation of groundwater and soil quality[11].

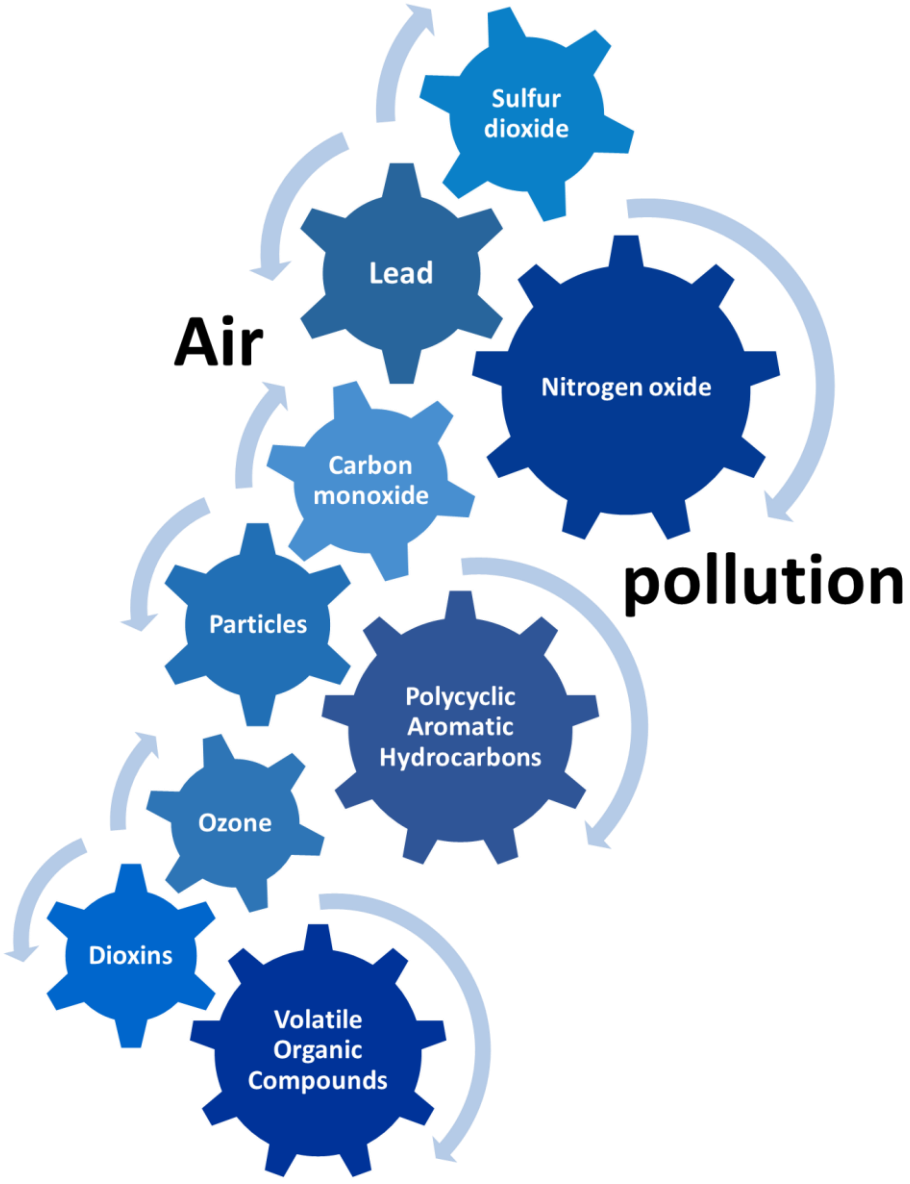

Figure 1. 1. Chemical compounds that causes decrease in the air quality.

1.2. Soil contamination

Several sources may be responsible of soil contamination, some of them are represented in **Figure 1. 2**. The accumulation of contaminants in soils may be caused by human activities or natural resources over hundred of years. Deposition of contaminants in soil by air is very common; the contaminants could be carry out by rain or dry deposition. Higher risk of soil contamination is directly associated to higher air pollution[12]. Thus, the soil contamination could be also caused by irrigation with polluted water and the abuse of use of pesticides and herbicides. This can be elucidate by local contamination of soils with higher pollutant's

concentration. One more source of contamination could be internal, by the replication and reaction of toxic elements[13,14]. These contaminants may be then transferred from soil to crops and grazing animals than to human food chain. These persistent contaminants may also emerge in watercourses which may accumulate in freshwater sources[15,16].

Figure 1. 2. Different sources of soil contamination and their impact on human and living organisms

1.3. Water pollution

Every year more than 3.5 million people die because of polluted water. When many people take water for guaranteed, more than 7 million people on earth, do not have access to safe drinking water. Our source of water either it comes from surface water like rivers, lacs and reservoir or from groundwater is affected by what happens in the environment[13]. Human daily activities plays a major role in polluting the water resources: air pollution, industrial discharges, agriculture abuse use of fertilizers and pesticides, fuels[17]. As a result, these sources of water are polluted and considered as raw water unsafe to drink.

Different aspects of pollutants could be found such as heavy metals, micropollutants and biological pollutants. In this work, we focused on micropollutants also known as emerging contaminants. Over the last decades, these contaminants has drawn much attention since

they can resist to wastewater treatment plants and could be found in tap water[18]. These pollutants, as of natural or anthropogenic origin, include pharmaceuticals, personal care products, steroid hormones and agrochemicals[19]. Anthropogenic sources consist of contamination due to domestic wastes, insecticides and herbicides, food processing waste, pollutants from livestock operations, VOCs, heavy metals from electronic wastes, chemical waste, and medical wastes[20].

1.3.1. Pharmaceuticals

There are over 3000 pharmaceutical products on the French market and some of these are available without prescriptions such as acetaminophen, ibuprofen, aspirin. The most common pharmaceuticals are antibiotics, analgesics, anti-inflammatories, painkillers, and hormones. These pharmaceuticals ends up in water sources at trace levels[21]. When humans take medicines, part of them are not fully adsorbed by the body and are excreted in their native form or in their metabolites form. These pollutants ends up in the sewage and are than discharged into aquatic systems such as rivers and lakes. Moreover other sources of contamination could be triggered by the industries, hospitals or even wastewater treatment plants effluents (**Figure 1.** 3)[22]. Hence, the removal of many of them by conventional wastewater treatment plants remains impossible[23]. Some of these micropollutants are discharged from WWTPs in the sediments while others could make it to our drinking water[24].

The presence of micropollutants in surface water has recently been widely reported. The fate of many of these compounds remain unpredictable. These micropolluttants can be converted to more toxic by-products by chemical or biological degradation. European regulations have fixed some new regulations regarding some pollutants, but many other remains unregulated[25,26]. Many new technologies have focused on detection of micropollutants in surface water, wastewater effluents and drinking water. These techniques allowed the detection and occurrence of many products in different water sources and during different seasons [27–31].

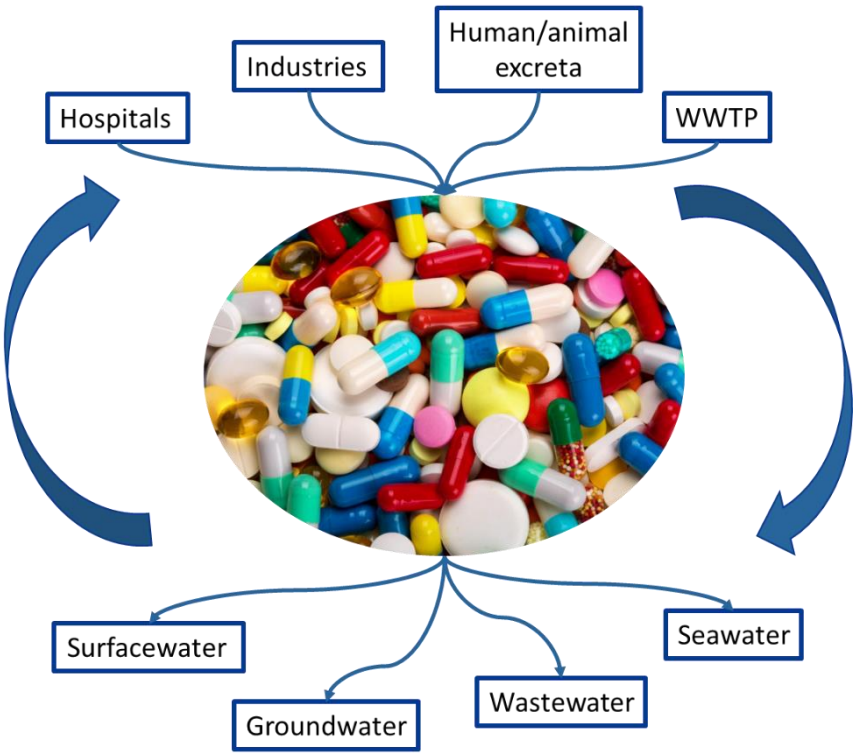

Figure 1. 3. Sources and pathways of pharmaceuticals in water cycle

1.3.2. Pharmaceuticals occurrence in water

Pharmaceuticals are considered as hazardous emerging pollutants due to their persistence in the environment, bioaccumulation, and toxicological profile. They can be found in trace levels in surface waters, wastewaters, ground water and drinking water[32–34]. Even though they are found in very low concentration in environment, these levels(ng/l and µg/l) have shown important adverse effects on humans health and wildlife[35,36]. Herein, we will present some pharmaceutical products and their occurrence in water resources.

Pharmaceuticals could be divided according to their therapeutic classes into analgesic, anti-inflammaory drugs, antibiotics, antiepileptics, antidepressants, antineoplastics and antitumor agents and steroidal hormones. Recent studies reported concentration of more than 100 pharmaceutical products found in sewage water and wastewater effluents in several countries. **Figure 1.** 4 resume some of these drugs found in treated sewage and surface water (data were collected from several articles)[32].

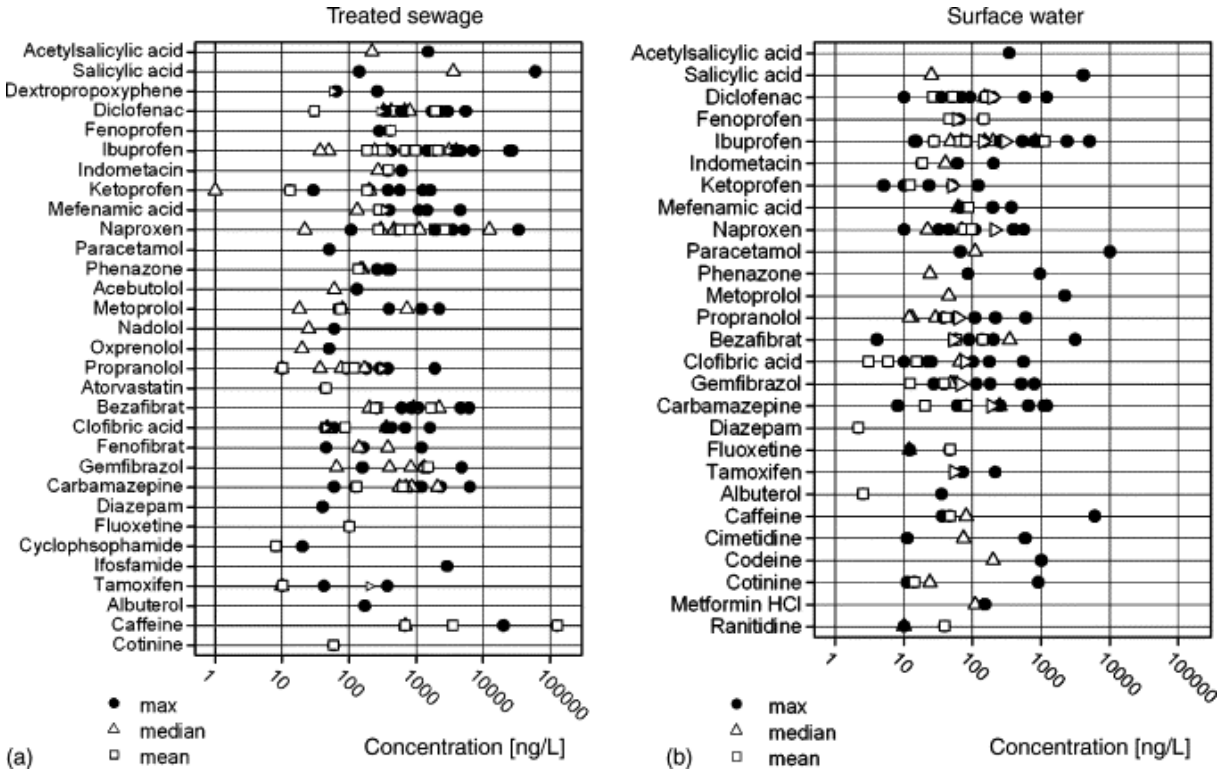

Figure 1. 4. Concentration of pharmaceuticals in (a) treated wastewater (b) and surface[32].

Herein, some reports on detection of different pharmaceutical products in surface water (river, lacs), ground water and wastewater plants. Since 1998, more than 32 pharmaceuticals were detected in German municipal effluents and rivers[37]. In 2002, kolpin *et al.* reported the study of 95 micropollutants found in streams downstream of urban areas and livestock production across the U.S.A[38]. Moreover, average levels of micropoluttants in 44 rivers in USA were estimated to 60ng/L[39]. Same pharmaceuticals with concentration raging between 4 and 2370 ng/L were detected in the Tyne estuary in the U.K.[33]. Calamari *et al.* reported the presence of many pollutants in the rivers Po and Lambro in Italy such as antibiotics and B-blockers drugs[40].

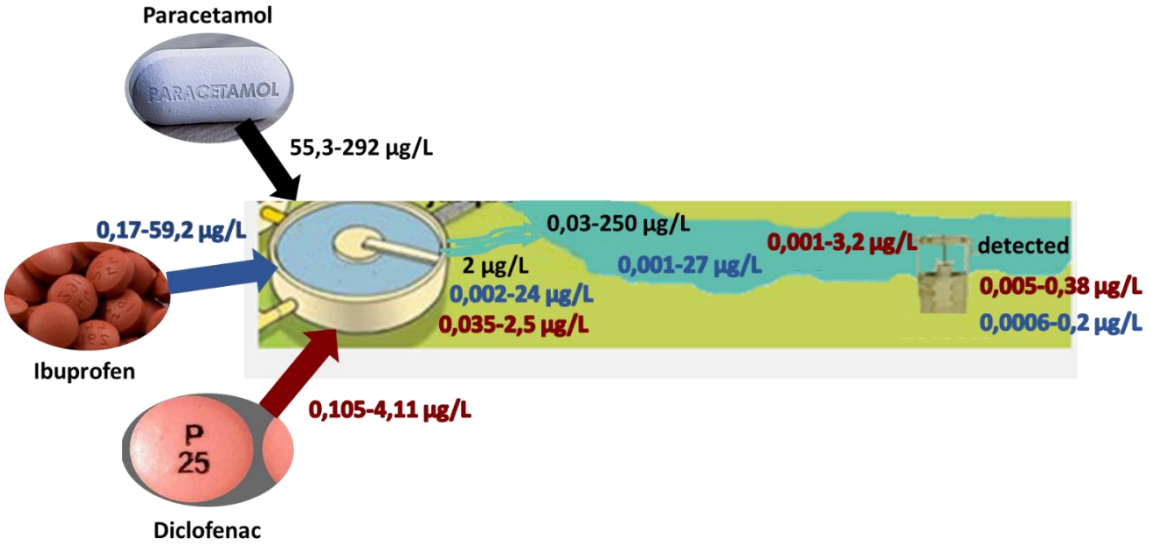

Figure 1. 5. Occurrence of some pharmaceutical drugs before they enter to WWTPs and after their discharges in surface water[32].

In Europe, recent studies have shown the persistence of pharmaceuticals products to the WWTPs and their concentrations before and after the treatment (**Figure 1.** 5). The removal efficiencies of these three drugs are variable. These values are assigned not only to the different chemical properties of the compounds but also to the treatment steps and the seasonal temperature. Since paracetamol, known as acetaminophen, possesses a high concentration in influent and effluent in many countries, we selected it as model pollutant in our study. Acetaminophen is in analgesic drug available without medical prescription. As we can see in **Table 1.** 1, concentration of this molecule is highly variable between countries and even between different sources in the same country. These variations could be explained by the degradation and dilution factors of the molecules in wastewater treatment plants. Moreover, surface sources are not exposed to the same sewage effluents and hospital discharges. Higher environmental pollution could be detected in highly industrialized areas[41,42]. In addition, acetaminophen (ACT) is not stable to some degradation techniques and could decompose into sub-products[43].

Table 1. 1. Occurrence of acetaminophen in different water sources of several countries

	Concentration (ng/L)	Water resources	Country	References
Acetaminophen	78170	Surface water	Serbia	44
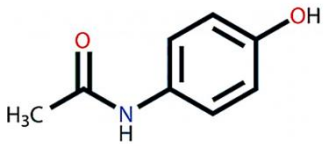	5-127 5-9 13406-56944	Surface water WWTP effluent WTTP influent	Korea Korea Korea	45
	4.1-7.3 1.9-19	Surface water WTTP effluent	Korea Korea	46
	24600-29000 32-4300	WTTP influent WTTP effluent	Spain Spain	47
	380	Ground water	USA	48
	62250	Hospital effluent	Taiwan	49
	N.D-200	Surface water	France	50
	10.6-72.3 108.1-11308.9 N.D-210.1	Surface water WTTP effluent Drinking water	France (Herault)	51

To further understand the variation efficiency of removal of pollutants in the treatment facilities, we will describe the steps that water go through in wastewater treatment plants before it is qualified as drinking water.

2. Water Treatment

There is two types of water treatment plants: Potable water and Wastewater treatment. The first one uses surface water such as rivers, lacs and reservoirs for drinking water. Whereas, the second one use household sewage and industrial discharges.

2.1. Drinking water treatment plants

The process for cleaning water could take from 24 to 73 hours. The steps followed are presented in **Figure 1.** 6 using surface water and not sewage water. In this case, dirty water of rivers or lacs or reservoirs are used and turn into drinking water as follow:

2.1.1. Primary treatment step

- **Coagulation and flocculation**

In these water sources, amounts of sediments, leafs, wood, bacteria and many other organic matters are recognized. To remove these particles, chemicals known as coagulants are added to the water right at the inlet of the water plant. These chemicals will allow the particles to stick together. Than the water is transferred to mixing basins where the flocculation will happen. In these basins, slow mixing of the solution of water with coagulants will allow the formation of floc particles. The mixing time depend on the water quality in flocculation basins. Than the water is moved to sedimentation basins. The goal of this process, will allow the deposition of the flocs into the sediment. The flocs particles will settle out to the bottom of the basins as sludge. The sludge is taken away to handling facilities. The top water, being the cleanest, flows to the next stage of process. In other plants, dissolved air flotation tanks are used in place of sedimentation basins. In these cases, air is pumped in the bottom of the tanks creating bubbles. As these bubbles flow to the bottom, they take with them the flocs to the surface. Film of floc is formed on the surface of the basins, and these flocs are pushed away with a sweeper arm and then collected to be removed as sludge; the cleaner water is this time in the bottom and will be used in the next step. There is no regulations on the techniques used during the cleaning steps of the water, all what matters is the quality of water pumped to the city[52].

2.1.2. Secondary treatment step

Once the majority of solids have been removed by flocculation, coagulation and sedimentation, filtration is being proceeded. The water at this point is clear, but suspended solids and bacteria remain in the water. Sand filters are used in this step to ensure clean water. Membranes filtration is also another technology that is being applied in some cases in these steps. Particles get caught when the water pass through them and

they are considered as highly efficient. Turbidity at this time is measured to quantify the quantity of particles remaining in the water. If the water contain low quantity of particles, an unnecessary step could be added, active carbon basins that help the remove of microparticles. This step is not mandatory, but it help to improve taste and odor of the water[53].

2.1.3. Final treatment step

Disinfection step is the last step in water treatment plants. There are three main ways of disinfection that could be used combined all together or just used individually to kill microorganisms.

- **Chlorine treatment**

In this step, chlorine dioxide or monochloramine are added to the water. However, these chemicals could react with other organic material in the water and create disinfection by-products that are harmful for human health. Even though, chlorine is the most used technique in the treatment plants. Some of the chlorine residuals will be released with tap water and allow the disinfection of the water after they leave the plants and kills the pathogens that can infect the water treated after they leave the facility.

- **Ozone treatment**

Ozonation (O_3) kills the bacteria in the water as wee as improves the taste of the water. In this case, chemicals should be used after the disinfection process to remove the O_3 remaining in the water no to cause harmful effects to the city population.

- **Ultra Violet (UV) radiation treatment**

UV light is shined through the water, that will allow to freeze the reproduction of bacteria. Nevertheless, no residuals stays in this water, which means if this water was infected after the treatment, the bacteria's could not be removed. In some other cases, membrane are used in this last step for the disinfection of the water.

Once the water is treated, it is ready to be pumped into the city pipe's network . The water flowing out of the plants is tested for various levels of chemicals, particles etc. This permeate is settled by the regulation accountability fixed by each country.

2.2. Wastewater treatment plants

This treatment plants relies on the use of rainwater and sewage water to clean them before they are released again in surface waters (**Figure 1.** 6)[54].

Only 3% of the water on the earth is fresh water. More than ¾ of this water is frozen in glaciers and less than 1% is found underground and in rivers and lacs[55]. In 2020, one-in-four people lives in lack of safe drinking water. Thereby, the need of alternative resources other than the surface water is a necessity. Normally after the treatment of sewage water, the cleaned water considered as grey water is used for irrigation of the crops in agriculture, in industries and for domestic needs (flushing, gardening) in some countries.

Hence, the increase in water demand and water scarcity has led to the use of wastewater as drinking water. In most cases, this effluent is released in rivers or other water source. In rare case, for example in Africa, this water is directly discharged in other water treatment plant for consumption. This is considered as full cycle water reuse[56]. However, the conventional wastewater treatment plants have shown inefficiency in removal of micropollutants as discussed in section 1.3. Consequently, new technologies are being developed from several years to replace or to be combined with the existent steps of cleaning water[57–60]. Nam *et al.* reported that the removal efficiencies of micropollutants detected in a WTP ranged from 6% to 100%[61]. Contamination of environmental waters, surface waters and groundwaters as well as of waters intended for human consumption by trace levels of organic substances is a subject of increasing concern globally.

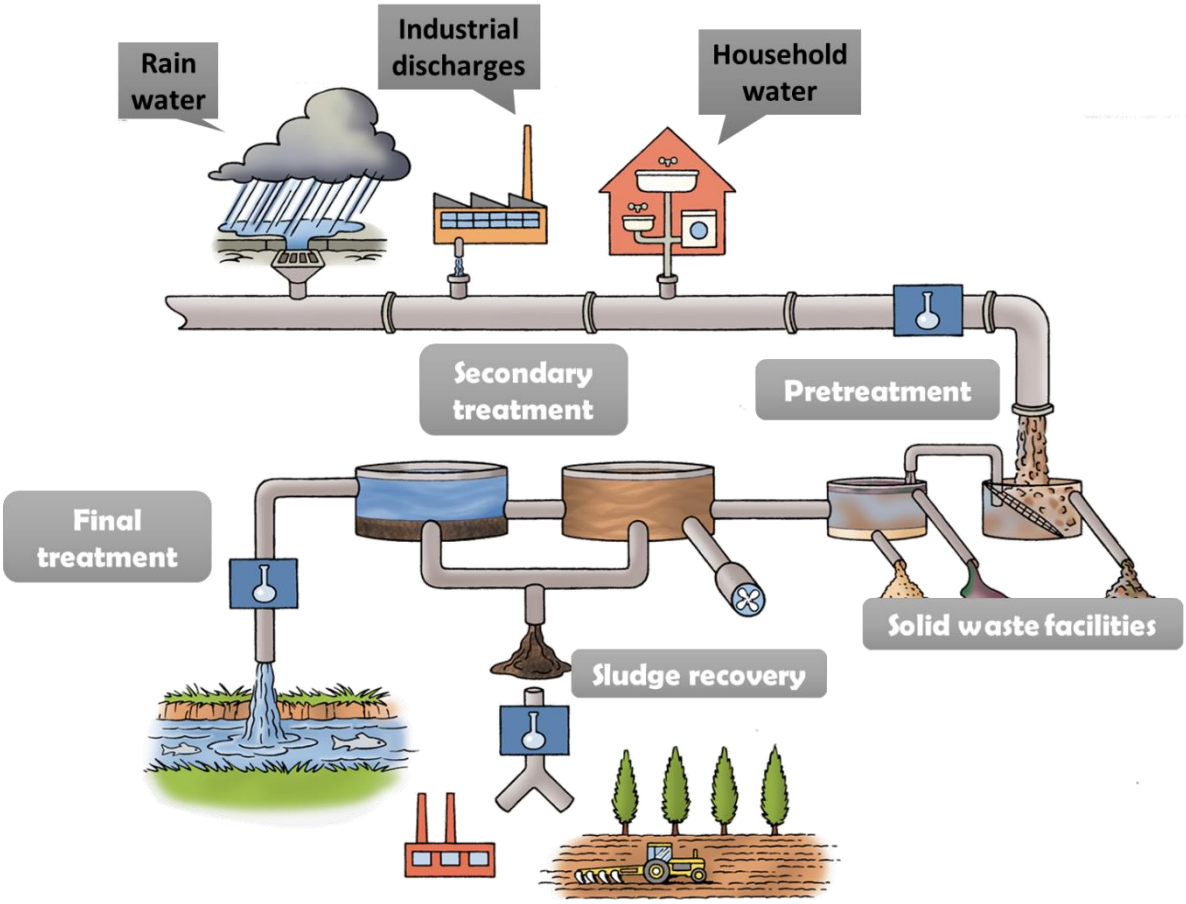

Figure 1. 6. Steps of cleaning sewage water in wastewater treatment plants (https://www.idea.be/fr/cycle-eau/assainissement-des-eaux-usees/comment-fonctionne-une-station-d-epuration.html).

2.3. Conventional waste water treatment

In water treatment plants, diverse techniques are operational. For instance, a combination of physical, chemical and biological technologies have been used such as flocculation, coagulation, precipitation, evaporation, carbon adsorption, membrane filtration, electrochemistry, biodegradation and phytoremediation[62–68]. Researchers over the years focused on developing these techniques to find the best route. None of these techniques was confirmed to be the best and most adequate since many factors should be taken into consideration. Each treatment presents advantages and drawbacks in terms of efficiency, cost, feasibility and environmental impact. Hence, with the increase of environmental pollution and the introduction of new pollutants, these techniques are inefficient. It was evidenced in the literature, the detection of persistent pollutant in tap water[69,70]. Even though, these chemicals

are found in trace levels, their adverse impact on human health and wildlife have been already reported[54].

2.4. Advanced oxidation process

With the increase of pollution and the increase of water demand, technological innovation is important for the drinking and wastewater sector to ensure the long-term sustainability and quality of water resources. Since the currently employed methods are not effective, a great deal of attention has been given for Advanced Oxidation Processes (AOPs) over the two last decades[71,72]. These techniques are promising for removal of wide range of persistent pollutants from water. These physicochemical processes are based on generation of reactive species in the presence or not of a catalyst that will convert organic pollutants into carbon dioxide (CO_2) and water[73]. For instance, AOPs are not envisioned to replace conventional systems but to complement existing systems for better quality effluent. They should be introduced in pre-treatment steps or/and in post treatment steps[74].

Two types of AOPs have been already revealed: homogeneous and heterogeneous methods. These methods will generate radicals by activating different factors such as UV, ozone, catalyst, electrochemical. Amongst the chemically active species produced are ozone (O_3), hydrogen peroxide (H_2O_2), singlet oxygen (O), hydroxyl radical (OH·), and others. In contrary to conventional treatments, this technique does not generate toxic products. While the conventional treatments like chlorination, reverse osmosis, flocculation …. produce toxic by-products that could be mutagenic and carcinogenic to human health[75,76].

The number of publications in this field is interesting and reveal the potential of these innovative techniques in the removal and decomposition of pollutants from water, soil and air. Herein, we will shortly describe the different existing AOPs techniques before getting into details in photocatalysis and elaboration of effective catalyst for higher removal efficiency of pollutants. It is worth noting that all AOPs techniques involve two steps:

- ✓ In-situ formation of reactive oxidative species
- ✓ Reaction of oxidants with target molecules

2.4.1. Electrochemical AOPs

EAOPs are based on the electrochemical generation of strong oxidants such as hydroxyl radicals (OH°) (**Figure 1. 7**). Some of the most reported EAOPS are: anodic oxidation (AO), anodic oxidation with electrogenerated H_2O_2 (AO-H_2O_2), electro-Fenton (EF) and photoelectro-Fenton (PEF)[77].

Anodic oxidation is the most popular EAOP technique, based on the oxidation of organics on the anode surface by direct electron transfer or/ and indirect oxidation of OH radicals or agents present in the solution O_3, H_2O_2, persulfate….[78,79].

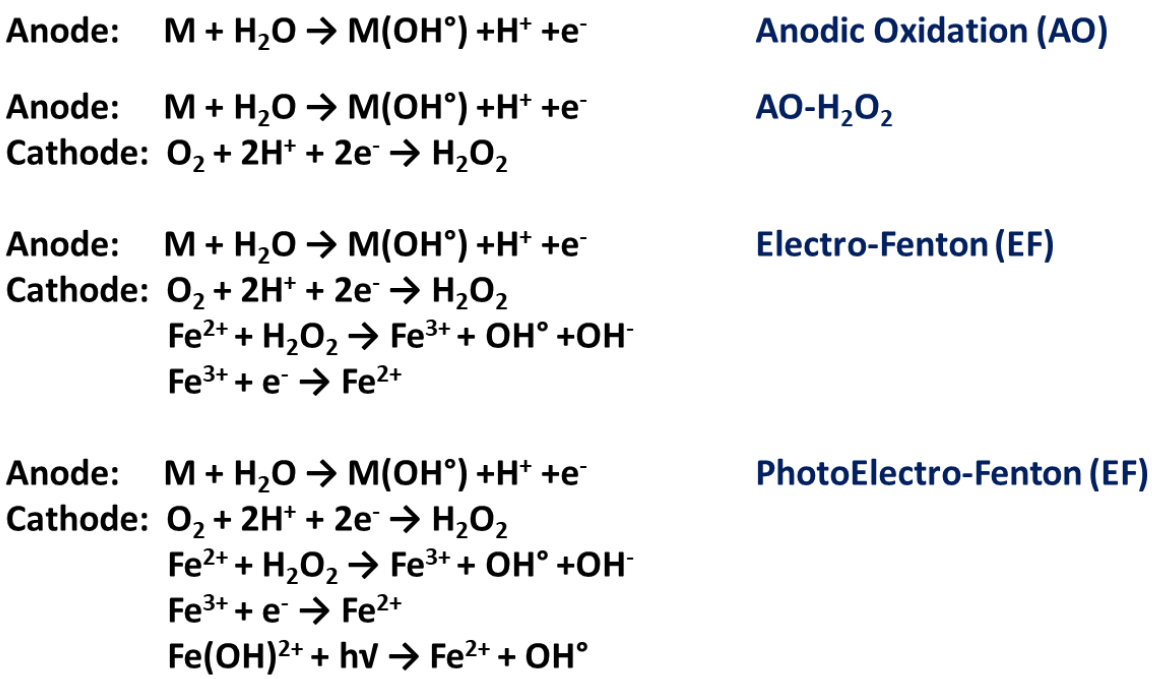

Figure 1. 7. Main reaction of three EAOPs mechanisms

EAPOs has been widely investigated for water treatment with different electrode types and materials have such as SnO_2, doped TiO_2, PbO_2, Boron-doped diamond (BDD)….However, BDD-electrodes are the most applied EAOP method due to their relatively low production costs compared to other electrodes and high stability of the diamond layer under anodic polarization[80]. Degradation of different organic pollutants such as dyes, pharmaceuticals, pesticides were exploited with these techniques. Brillas *et al.* reported the degradation of paracetamol using anodic oxidation with comparing BDD and Pt efficiency used as anode. The

author proved the efficiency of this method for the complete mineralization of the pharmaceutical pollutant within a pH from 2 to 12. The degradation using BDD as anode was achieved within 240 min whereas it took 360 min for a complete degradation with Pt[81].

2.4.2. Physical AOPs

Initiation of physical processes could be done by Electrohydraulic discharge (Plasma), ultrasound (sonochemical), microwave assisted or electron beam. Therefore, these techniques are still considered inefficient for full-scale application in water treatment regarding their many disadvantages. As an example, the application of ultrasound is highly energy intensive and results in a very low electrical efficiency of this AOP in comparison to other technologies. Consequently these techniques have been combined with other AOPs techniques for better results[82–84].

2.4.3. UV based AOPs

Since 1996, the use of UV has been extended from disinfection purposes to AOPs processes (**Figure 1.** 8) The process is known as photolysis that induce degradation of contaminants by light exposure and absorption of photons. This absorption of photons causes the outer electrons in a compound to become unstable, and thus they become reactive or split. The most used source of light is UV but it could be replaced by sunlight that reduces the limitation of the system. Since UV lamps has limited operator hours, and fouling of UV lamp could generate high maintenance cost. Furthermore, UV lamps could require higher energy than other processes, not to mention that some compounds could reduce the UV light absorbance such as iron and nitrate[76].

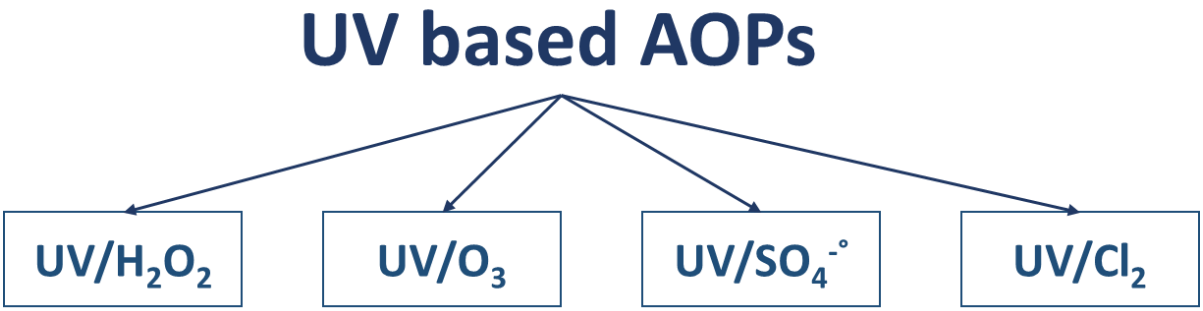

Figure 1. 8. Different types of UV based advanced oxidation process depending on the radical promoter added to the solution

It should be cleared that these processes depends on many factors that were well debated in the literature, which make it harder to confirm the best route[85,86]. Some of these factors are listed below:

- Pollutant type
- Target compound
- Pollutant concentration
- Water quality (pH, temperature, Interferent, source of water…)
- Light source
- Radicals generation
- Concentration of radicals promoters

2.4.4. Ozone based AOPs

Ozone has been already used as an oxidant and disinfectant in water treatment. As an oxidant, ozone is very selective and attacks primarily electron-rich functional groups like double bonds, amines, and activated aromatic rings (e.g. phenol) .Hence ozone based AOPs are rarely used alone, they are either combined to UV techniques or applied in the presence of catalyst for more efficient results. The reaction for the formation of OH°, between ozone and hydroxide ions, is quite slow. Hence, methods to actively initiate formation of radicals include the ozonation at elevated pH and the combinations O_3/H_2O_2, O_3/UV, and O_3/catalysts. Furthermore, H_2O_2/O_3 has an advantage over UV processes because of the lack of related equipment and maintenance, which can reduce energy requirements. Residual H_2O_2 might have to be destroyed before discharging the treated water to the receiving aqueous environment[87].

Wardenier *et al.* showed that plasma-ozonation is more efficient than the conventional UV, O_3 and H_2O_2 AOPs, in terms of removal and energy efficiency. The study was performed on four different micropollutants. The authors found that ozonation based processes are more reliable than UV based ones. In addition, plasma-ozonation method allows a complete elimination (>99.8% removal) of the target compounds within 20 min of treatment. Although the energy efficiency of plasma-ozonation falls between the energy cost of O_3 and UV-based

AOPs, the removal kinetics generally proceed faster compared to other AOPs. Moreover, new setups could be promising in decreasing energy cost of the combined techniques[88].

2.4.5. Catalytic AOPs

Catalytic AOPs denote catalytic ozonation, photocatalytic ozonation and heterogeneous photocatalysis processes. Among these, the most two studied catalytic AOPs are Photo-Fenton process and heterogeneous photocatalysis.

- **Homogeneous Photo-Fenton process**

Fenton reaction starts when a combination of ferrous iron (Fe(II)) and H_2O_2 at acidic conditions reacts together and form hydroxyl radicals (OH°) (equation (**i-ii**)). Iron acts as a catalyst with maximum catalytic activity at pH=3, particularly due to the precipitation of ferric oxyhydroxide at higher pH value. This process is activated by light source in order to increase the degradation efficiency and is called Photo-Fenton (**iii-iv**). One important limitation of this technique is the high cost, applying heterogeneous catalyst or solar energy and integrating biological treatment technologies in the treatment process could lower the costs[89].

$$Fe^{2+} + H_2O_2 \rightarrow Fe^{3+} + OH^\circ + OH^- \quad \textbf{(i)}$$

$$Fe^{3+} + H_2O_2 \rightarrow Fe^{2+} + HO_2^\circ + H^+ \quad \textbf{(ii)}$$

$$Fe(OH)^{2+} + h\nu \rightarrow Fe^{2+} + OH^\circ \quad \textbf{(iii)}$$

$$H_2O_2 + h\nu \rightarrow 2 \times OH^\circ \quad \textbf{(iv)}$$

- **Heterogeneous photocatalysis process**

This process is established by the activation of photo-active catalyst for the generation of charge carriers that will participate in the oxydo-reduction reaction of the pollutant. Photocatalytic process has drawn much attention due to its high degradation efficiency and ability of removal of different micropollutants from water. More details of the process and the reaction that could take place will be discussed broadly in section 3.

There are thousands of publications in AOPs techniques for removal of harmful pollutants from water. Here is some recent works using single or combined AOPs processes for removal of pharmaceutical compounds from water (**Table 1.** 2).

Table 1. 2. AOPs processes reported recently for degradation of pharmaceutical products

Pharmaceutical product	AOP process	Single/ combined process	Removal efficiency (%)	Water source	References
Norfloxacin	gamma-ray irradiation	single	~82 75	Pure/Surface waste	[90]
Amoxicillin	O_3/H_2O_2	combined	79	effluent	[91]
Paracetamol	H_2O_2/UV O_3	combined	30 40	Pure	[92]
Carbamazepine	UV/$S_2O_8^{2-}$	combined	~99	Pure	[93]
carbamazepine	UV/H_2O_2	combined	100	Pure	[94]
Paracetamol Sulfamethoxazole	membrane bioreactor-nanofiltration-ozonation	combined	~80 ~90	waste	[95]

2.4.6. AOPs limitations

Although advanced oxidation technologies are relevant for the removal of a wide range of organic pollutants due to the high oxidative potential and efficiency, one of the shortcomings is that single advanced oxidation technology is not capable of removing the pollutants yet. In some cases, generation of recalcitrants, inhibitory and intermediate by-products is commonly witnessed. With the intention of achieving complete degradation of water pollutants, process combination has showed encouraging results[96,97].

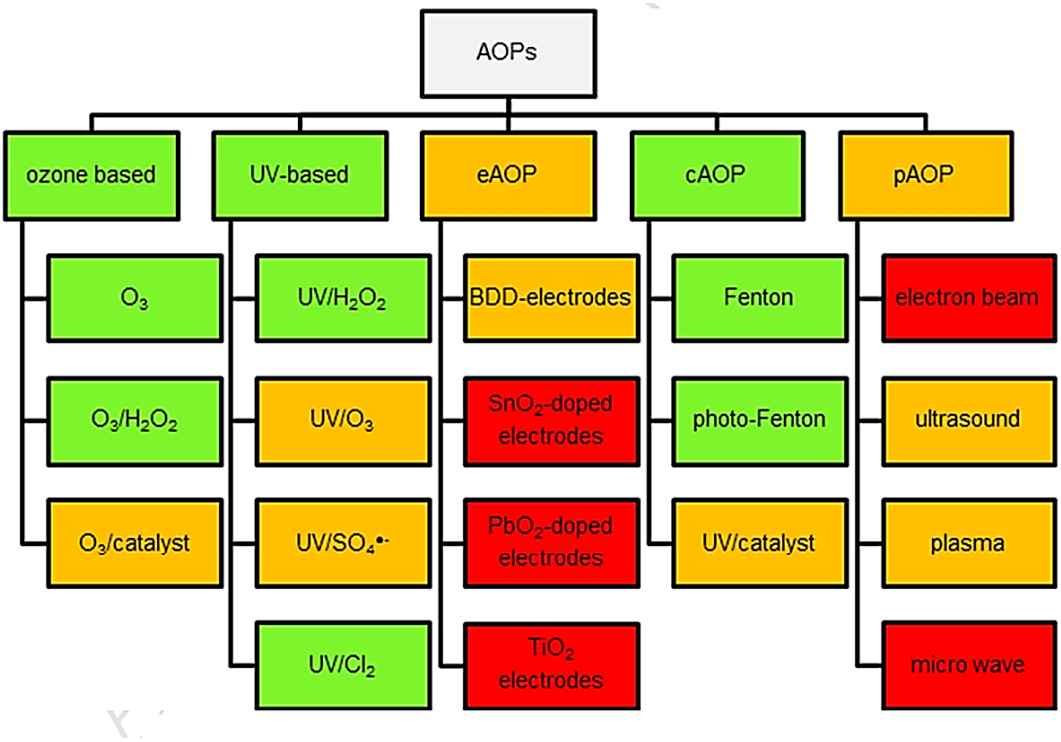

Figure 1. 9. Classification of different AOPs, with in red the methods tested at lab scale, in orange systems experienced at pilot and lab- scale and in green techniques established at full scale[80] (figure reported from article as it is).

Some of these techniques have already been used in full-scale systems while other systems still not efficient (**Figure 1.** 9) For instance, Fenton process have been used in wastewater treatment plants before coagulation step. Iron chloride and hydrogen peroxide are added with the polluted water, where the oxidation process will proceed before transferring the water to neutralization basins and then to flocculation step. Hence, Fenton process could generate metal residue that should be eliminated which will increase the cost of treatment[98]. Moreover, all UV, OZONE and Plasma induced AOPs are high cost and energy consumption. This is why further studies and investigations are still needed in this field. Among these different AOPs methods, photocatalysis is promising since it does not relay on high-energy cost and could be induced by solar light for the generation of radicals. Next, we will discuss the mechanism of photocatalysis and the advantages in wastewater treatment techniques.

3. Photocatalysis

Among all the techniques cited above, photocatalysis is the most favorable technique for water treatment regarding its benefits: cost efficiency, non-toxic nature and absence of further pollution[99]. Photocatalysis is considered as “green technology” process, based on the activation of semiconductor under light irradiation. It does not require any addition of chemicals or gases that could generate secondary contaminants[100]. Moreover, it is not energy consuming since it can be activated even under solar light irradiation. Since 1965, photocatalysis have been widely explored and many modifications were brought to increase the removal of different pollutants from water, air and environment such as dyes, pesticides, heavy metals, pharmaceuticals…[101–104].

3.1. Principle

Heterogeneous photocatalysis based on semiconductor has demonstrated its efficiency in degradation of water’s pollutants. The degradation mechanism is presented in **Figure 1.** 10 where a source of light with an energy equal to or greater than the semiconductor band-gap E_G ($h\nu \geq E_G$) will activate the semiconductor. The photo-excited semiconductor generate electron (e^-) and holes (h^+) between the valence and the conduction band. The holes generated at the valance band absorbs water molecule and create hydroxyl radical (OH°), whereas electron in the conduction band reacts with the oxygen to form anionic superoxide radicals (O^{-}_{2}°)[105,106]. Than the degradation and mineralization of pollutant could take place by indirect or direct mechanism.

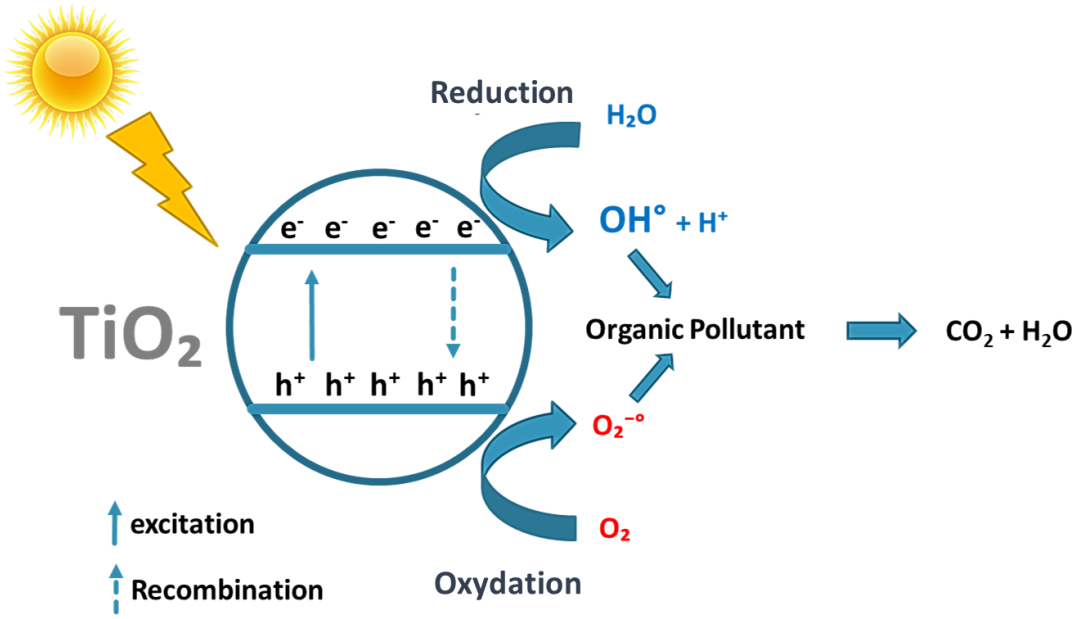

Figure 1. 10. Mechanism of photocatalysis based on activation of semiconductor.

3.1.1. Indirect photocatalytic mechanism

The radicals formed (OH° and O^{-}_{2}°) will oxidize the organic molecules and the intermediates formed during the process. The oxydo-reduction reaction take place both on the surface of the catalyst[107]. A detailed mechanism of degradation is given by the following equations (**v-x**):

$$\text{Catalyst} + h\nu \rightarrow e^- + h^+ \quad \textbf{(v)}$$

$$h^+ + H_2O \rightarrow OH + H^+ \quad \textbf{(vi)}$$

$$2e^- + O_2 \rightarrow O_2^{-\circ} \quad \textbf{(vii)}$$

$$O_2^{-\circ} + e^- + 2H^+ \rightarrow H_2O_2 \quad \textbf{(viii)}$$

$$H_2O_2 + e^- \rightarrow OH^\circ + OH^- \quad \textbf{(ix)}$$

$$\text{Pollutant} + OH^\circ \rightarrow \text{intermediates} \rightarrow CO_2 + H_2O \quad \textbf{(x)}$$

3.1.2. Direct photocatalytic mechanism

In this mechanism, two approaches are addressed: the Langmuir–Hinshelwood and the Eley–Rideal process. The first approach is based on the generation of electrons and holes by

the irradiation of the photocatalyst. The holes are then trapped by the adsorbed pollutant molecule on the catalyst surface to form reactive radicals, that will react with an electron. Subsequently, the catalyst is regenerated for further use[108]. The process is expressed as given below:

$$\frac{1}{r} = \frac{1}{k_r} + \frac{1}{k_r k_a C} \quad \textbf{(xi)}$$

where *r* is the reaction rate for the oxidation of reactant (mg/L min), k_r is the specific reaction rate constant for the oxidation of the reactant (mg/L min), k_a is the equilibrium constant of the reactant (L/mg) and *C* is the pollutant concentration.

When the concentration of the pollutant is two small, the equation is simplified:

$$\ln \frac{C_0}{C} = kKt = k_{app} t \quad \textbf{(xii)}$$

The plot of $\ln \frac{C_0}{C} = \textbf{f(t)}$ represents a straight line, where the linear regression is equal to the apparent first-order rate constant (k_{app}). Generally first-order kinetics is suitable for the concentration of substrate range up to few ppm, numerous studies were available where this kinetic model well fitted[109].

Whereas the Eley–Rideal process is based on trapping of the holes by the surface defects (S)[110]. These active surfaces will than react with the pollutant following the equations (**xiii-xvi**):

Catalyst + hν → e^- + h^+ **(xiii)**

S + h^+ → S^+ **(xiv)**

S^+ + e^- → S **(xv)**

(S-pollutant)$^+$ → S + products **(xvi)**

Several semiconductors have been used and reported for the degradation of organic pollutants: ZnO, TiO_2, gC_3N_4, vanadium oxides V_2O_5, SnO_2…[111–114]. Thi *et al.* reported 99% removal of paracetamol from aqueous solution after 3h visible irradiation using lanthanum doped ZnO photocatalyst[115]. Yang *et al.* studied the effect of active species (h^+, OH°, O_2^{-}°, HO_2°, and H_2O_2) on the degradation of ACT under UV light using TiO_2-P25. The authors found that

hydroxyl radicals are the major active reactant during the photocatalysis process[116]. Rostami *et al.* synthesized zinc ferrite–graphene nano-hybrids with variation of graphene percentage. They found that zinc ferrite ($ZnFe_2O_4$) nano powders were inactive under visible irradiation and no degradation of paracetamol occurred. Hence, the combination of $ZnFe_2O_4$ with 4% graphene leads to a complete degradation of paracetamol after 3h visisble irradiation[117]. The photocatalytic activity of these semiconductors depends essentially on the band gap, surface area, and generation of electron–hole pair for degradation of pharmaceutical products present in water. Hence, many other factors could affect their efficiency, more details will be presented in section 3.3.

3.2. Titanium dioxide semiconductor

Regarding all the semiconductors used for photoctatalytic degradation, TiO_2 is still one of the most promising catalyst that have been widely reported in literature[118–122]. This photocatalyst holds a strong oxidizing power with a high thermal stability, low cost and toxicity and most importantly, it is easy to synthesize. Hence, TiO_2 has a wide band gap and fast recombination of the photogenerated charges which limits his efficiency under UV irradiation[123]. Since UV range is only 4% of the solar irradiation, upscaling of this technique for water treatment is still limited. Thus, proper exploitation involve operational photocatalyst under visible light. The researchers have widely reported modification of TiO_2 by different methods to improve the reaction under visible or solar light irradiation to meet industrial requirements[124–126]. Different techniques have shown good influence in modification of TiO_2 and shift of the band gap for higher degradation efficiency under visible light. Some of the most viable modification are metal doping, non-metal doping, coupling with other semiconductor to form heterojunction, composite and morphology control.

3.2.1. Metal doping

Materials used as metals for TiO_2 in order to improve its catalytic ability are Palladium (Pd), platinum (Pt), silver (Ag) and gold (Au)… . Noble metals are often adopted due to their high stability and effectivity[127,128]. Doping TiO_2 with these metals favors the generation of hydroxyl radicals that contribute in the degradation of molecules[129–135]. Dlugokecka *et al.* successfully prepared TiO_2-Pd by microemulsion for phenol degradation. The higher photocatlytic activity was obtained with the addition of 0.1 mol% of Pd with an average diameter of the catalyst 2.4

nm. These values were 3 times higher than pristine TiO_2[133]. Lopes *et al.* reported the elaboration of Ag/ TiO_2 composite on immobilized substrate. A complete degradation of anthracene (polycyclic aromatic hydrocarbons) was obtained within 2h at 40 °C using the composites. The authors reported the effect of silver on the absorbance of the sample by diffuse reflectance. They found that the absorbance of Ag/TiO_2 sample is enhanced within the whole range of visible light (466-789 nm). This is due to the electronic transition interactions between Ag ions and TiO_2 which confirm the better photoactivity of Ag/TiO_2 and contributes to the expansion of the photocatalyst using sunlight[136]. The wavelength of the radiation responsible for activation of resonance is controlled by the size of the metallic nanoparticle.

3.2.2. Non-metal doping

Non metal dopants used to modify TiO_2 catalytic efficiency has also shown worthy results in the literature some of them are carbon (C), Phosphorus (P), Boron (B), nitrogen (N)[124,137]…. A one-step hydrothermal method was used for elaboration of Phosphorous-doped titanium oxide. The samples obtained had much higher crystallinity than usual TiO_2 samples prepared by other techniques. Moreover, an increase in hydroxyl groups was observed when doping with phosphorous which reduced the O vacancies in the sample. This resulted in higher degradation of methylene blue (dye) compared to commercial TiO_2[138]. Boron- doping of TiO_2 has been widely reported, this photocatalyst exhibit stronger absorption in visible region with a higher surface area and a good photocatalytic activity for dye degradation[139]. Another form of modification has also attracted much attention by doping simultaneously two types of non-metal atoms into TiO_2. Tunable synergic effect of the electronic structure increase the visible-light photocatalytic activity to some extent. N, S co-doped TiO_2 have been reported for degradation of pharmaceutical products. Two structure morphologies were compared as well as all the photocatalysis parameters: catalyst loading, pharmaceutical concentration, reaction time, and radical scavengers. BET results showed that N, S-TiO_2 nanoparticle has a large BET surface area (132 $m^2.g^{-1}$) that N, S-TiO_2 nanosheets (64 $m^2.g^{-1}$). The high photocatalytic activity under solar irradiation using N,S-TiO_2 may be due to synergistic effects of nitrogen and sulfur co-doping into TiO_2, resultant in better separation of e^--h^+ and higher-visible light adsorption[104].

3.2.3. Composite

Composite structure has been considered as an effective method for extending the spectral response of TiO_2 to visible light[140–142]. Different composites structures could be elaborated by coupling TiO_2 with another semiconductor which will create an heterojunction between the two oxides, such as SiO_2, ZrO_2, WO_3, Cu_2O, Al_2O_3 and BN…[143–146]. Another way to develop composite materials is by co-metal dopants or metal-non metal dopants[147] .

- **Composite semiconductor**

The composites of different semiconductors based on the nanoscale coupling effect for photocatalytic application has been a very important research topic, but very challenging. This composite design could highly affect the optical properties of TiO_2 by reducing the recombination of the photogenerated carriers and shifting the band gap to visible range. Moreover, this structure could be extended to the design of other composite photocatalyst (tertiary, quaternary…) with the purpose of enhancing activity by coupling suitable wide and narrow band-gap semiconductors, which is inspiring for the practical environmental purification[148,149]. **Figure 1.** 11 shows composite formation according to their energy levels.

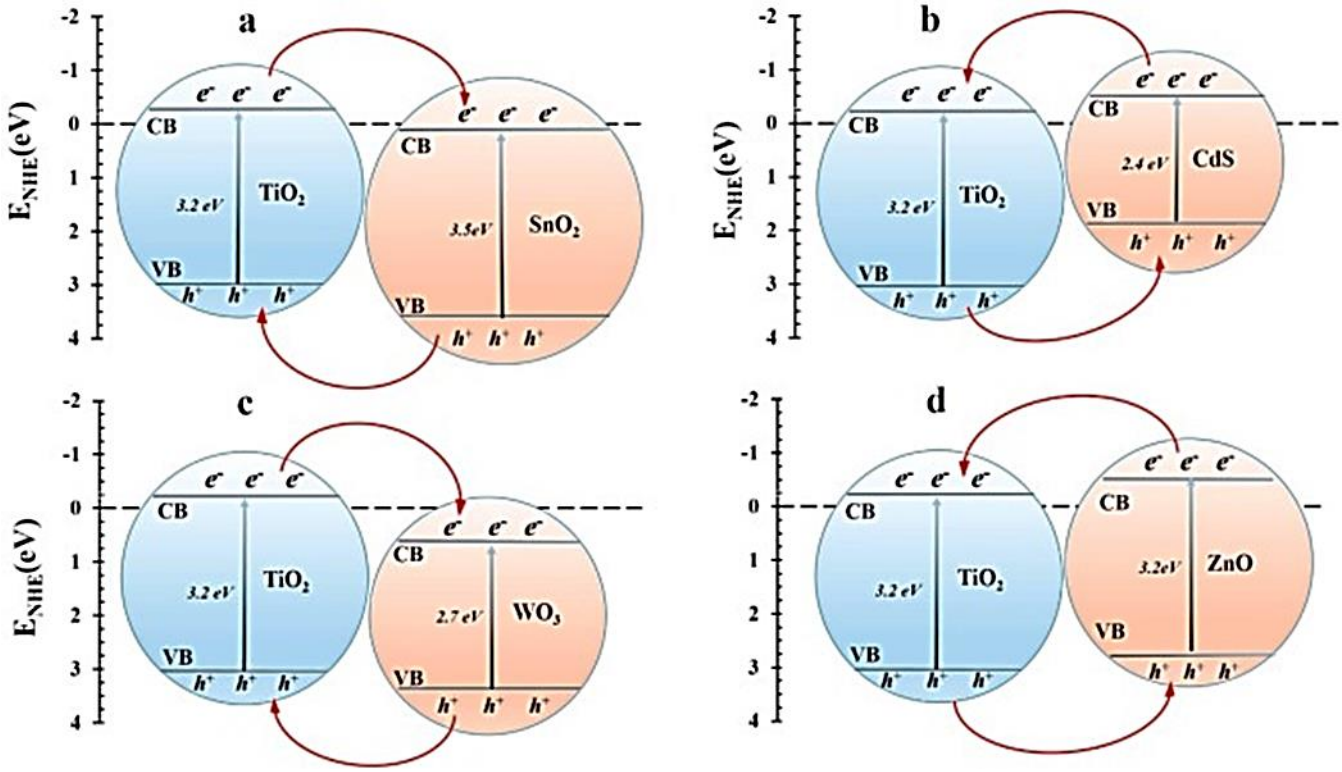

Figure 1. 11. Schematic energy levels of composite materials a) TiO_2/SnO_2, b) TiO_2/CdS, c) TiO_2/WO_3, d) TiO_2/ZnO (data extracted from [121])

- **Co-metal dopants**

Co-metal doping has not been widely investigated; some examples have shown a better dispersion of the metal which promotes the visible effect of the catalyst with a lower recombination of the generated carriers by improving the internal electron transfer. In other words, incorporating metal dopants produced oxygen vacancies in the TiO_2 lattice, reducing Ti^{4+} into Ti^{3+}[150–152].

- **Metal/non-metal co-dopants**

Dopant components in the TiO_2 lattice, including metal and non-metal, produce doping energy levels in the TiO_2 band gap that improve visible light absorption and result in higher photocatalytic performance **Figure 1.** 12[153].

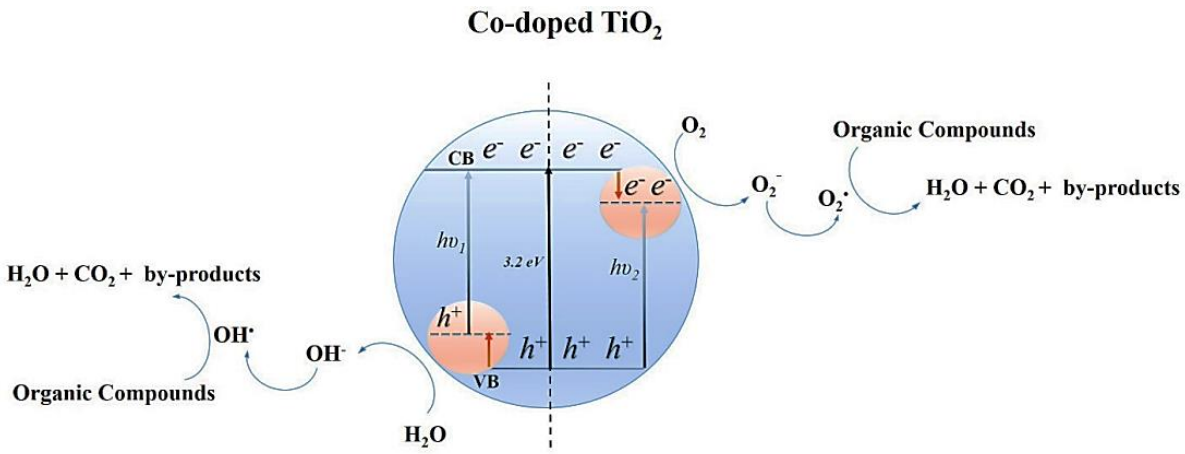

Figure 1. 12. Example of schematic energy level of co-doped **TiO_2**/metal/non-metal (extracted from [121])

3.3. Factors affecting the mechanism of photocatalysis

Titanium dioxide has been already tested with a wide range of organic compounds like pesticides, pharmaceuticals, dyes… whereas degradation efficiency have varied from an experiment to another. There is different factors that could interact during the degradation process and affect the degradation efficiency. Optimal conditions relay on many factors affecting the process: catalyst concentration, catalyst morphology, pollutant concentration and morphology, matrix (pH, temperature…), source of light and reactor's design.

3.3.1. pH

The pH of water (wastewater, ground water, ….) has a complex effect on photocatalytic oxidation rates. The electrostatic interaction between catalyst surfaces, substrates, and radicals are determined regarding the pH of the matrix[74]. The surface charge properties of the photocatalyst is directly affected by the pH of the solution. Recent study have shown the effect of pH on the degradation of paracetamol by TiO_2 nanotubes (NTs)[154]. In **Figure 1.13**, when pH values are between 2.5 and 4.5, the reaction rate constants are low because the OH° in the reagent medium interacts weakly with the paracetamol molecules. At a pH value of 6.5, the higher photodegradation efficiency is observed, due to the excess of hydroxyl radicals on the substrate surface. When pH values are between 8.5 and 10.5, the photodegradation rate decreases. This is because paracetamol at pH> pKa exists as anion form. Thus, the increase in

the pH gradually increases the electrostatic repulsion between the surface of the nanocatalyst and paracetamol, this considerably reduces the adsorption of paracetamol.

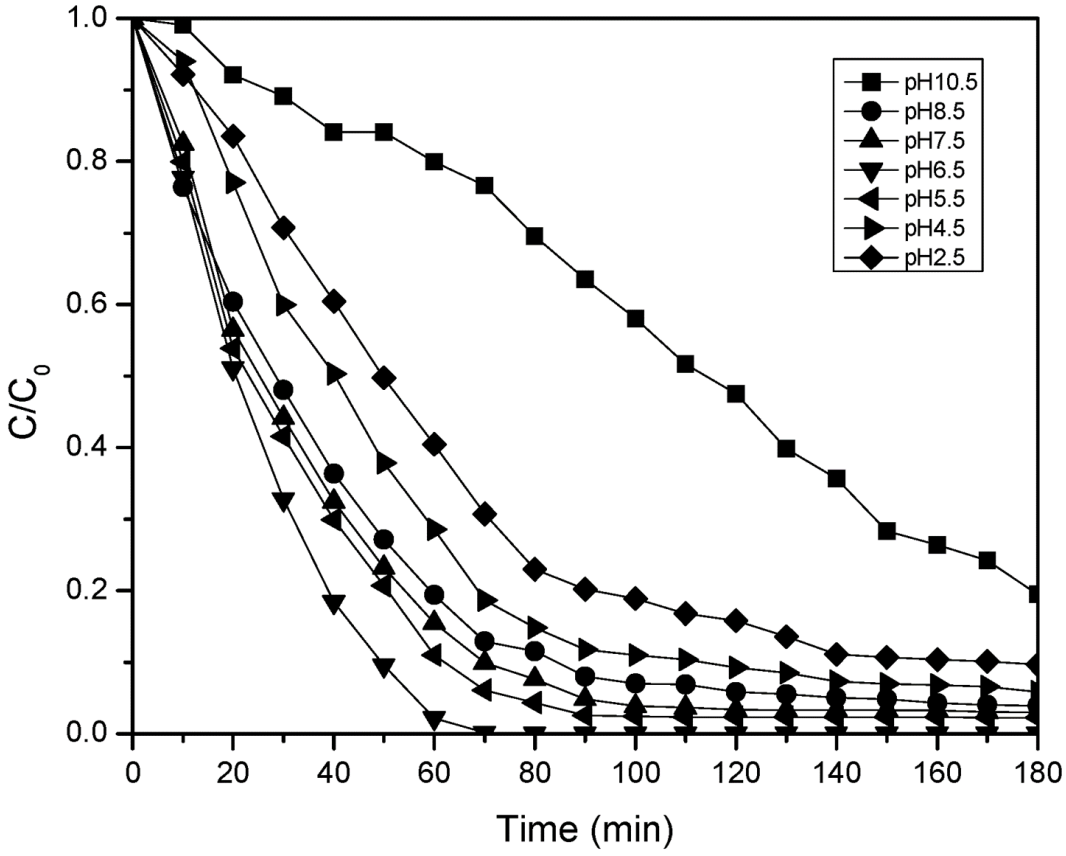

Figure 1.13. Effect of pH on degradation efficiency of paracetamol using TiO_2 NTs as catalyst (extracted from refrence [154])

3.3.2. Catalyst/pollutant ratio

The catalyst/ pollutant ratio is one of the most important factor that have been extensively reported. To find the best ratio of catalyst, many factors should be taken into concentration such as solution pH and pollutant pKa[155]. The use of excessive amounts of catalyst may decrease the degradation efficiency by decreasing the amount of energy transferred into the solution because of catalyst opacity[156]. Reactor's design may also affect the degradation efficiency of the pollutant; uniform irradiation of the catalyst surface should be reached.

3.3.3. Light intensity

The light intensity affect directly the degradation efficiency of pollutants. An increase in light intensity can improve the photocatalytic performance only up to a certain limit. Beside

that, energy loss due to light reflection, transmission and energy loss as heat is inevitable in the process[157]. This limitation largely invited more research in the modification of TiO_2 to reduce these energy loss and improve the degradation performance[158].

3.3.4. TiO_2 morphology

The easily synthesizable and modifiable nature of TiO_2 is a major benefit that allows the elaboration of numerous forms of TiO_2 by different methods. This advantage tolerate the manipulation of appropriate photocatalyst exhibiting desired physical properties, activity and stability for particular application. During the years, the correlation between the surface properties, the synthesis route and the rational development have favored the application of photocatalytic degradation on a wide range of micropollutants[159]. The different synthesis route allow the control of catalyst morphology, from crystallinity to structure to number of active sites and band gap. TiO_2 can exist in a range of morphologies (**Figure 1. 14**): zero-dimensional such as TiO_2 spheres, one-dimensional with TiO_2 fibers, rods and tubes, two-dimensional with TiO_2 nanosheets and three-dimensional with interconnected architectures[160–163].

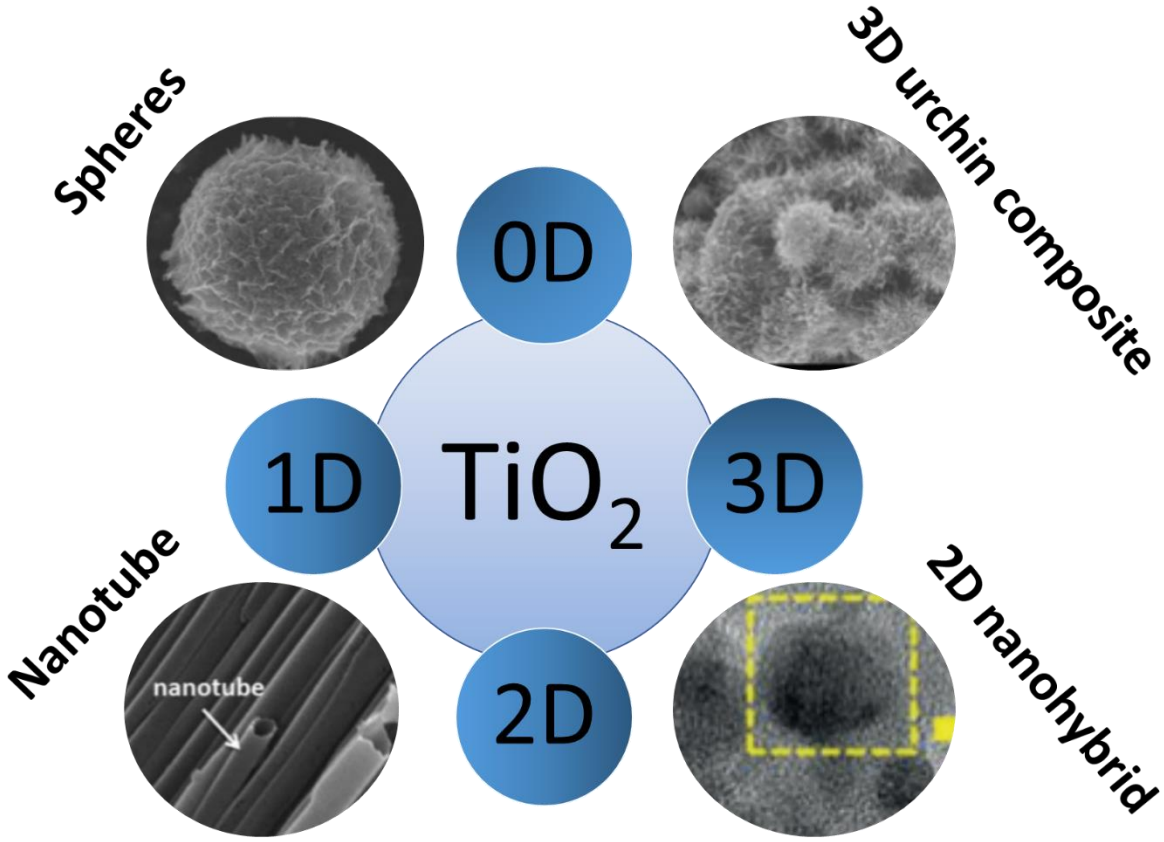

Figure 1. 14. Different TiO_2 photocatalyst structures reported in the litterature[164–167].

Numerous forms of TiO_2 have been synthesized with different methods to elaborate an optimal photocatalyst used in suspension for water treatment. Therefore, the design and implementation of novel TiO_2-based photocatalysts deposited onto suitable substrates to obtain exploitable materials for specifically addressing environmental applications remains challenging.

3.4. Photocatalytic membranes

Photocatalysis application in wastewater treatment plant have been successfully established. Hence, the necessity of designing immobilized catalyst is still misplaced. Membrane filtration and separation have shown powerful efficiency in wastewater treatment for the removal of persistent micropollutants[168,169]. This promising result have lead the scientists to enhance the performance of photocatalytic membranes and to intensify their studies in this field. Various membranes including inorganic, polymeric, and mixed matrix

membranes have been studied so far. However limitations remains in the material properties and reactor design[170,171]. To date, different reactor designs were routed: photocatalytic membrane reactor (PMR) with different light, feed, membrane position…, biomembrane photocatalytic reactor, annular photocatalytic reactor, tubular photocatalytic reactor and bed-fixed membrane photocatalytic reactor. In this thesis, we are interested in photocatalytic membrane reactor whereas we elaborate ceramic membrane by atomic layer deposition. The detailed process will be defined in the last chapter of this manuscript. **Figure 1. 15** describes the main difference between several PMR systems that have been already developed.

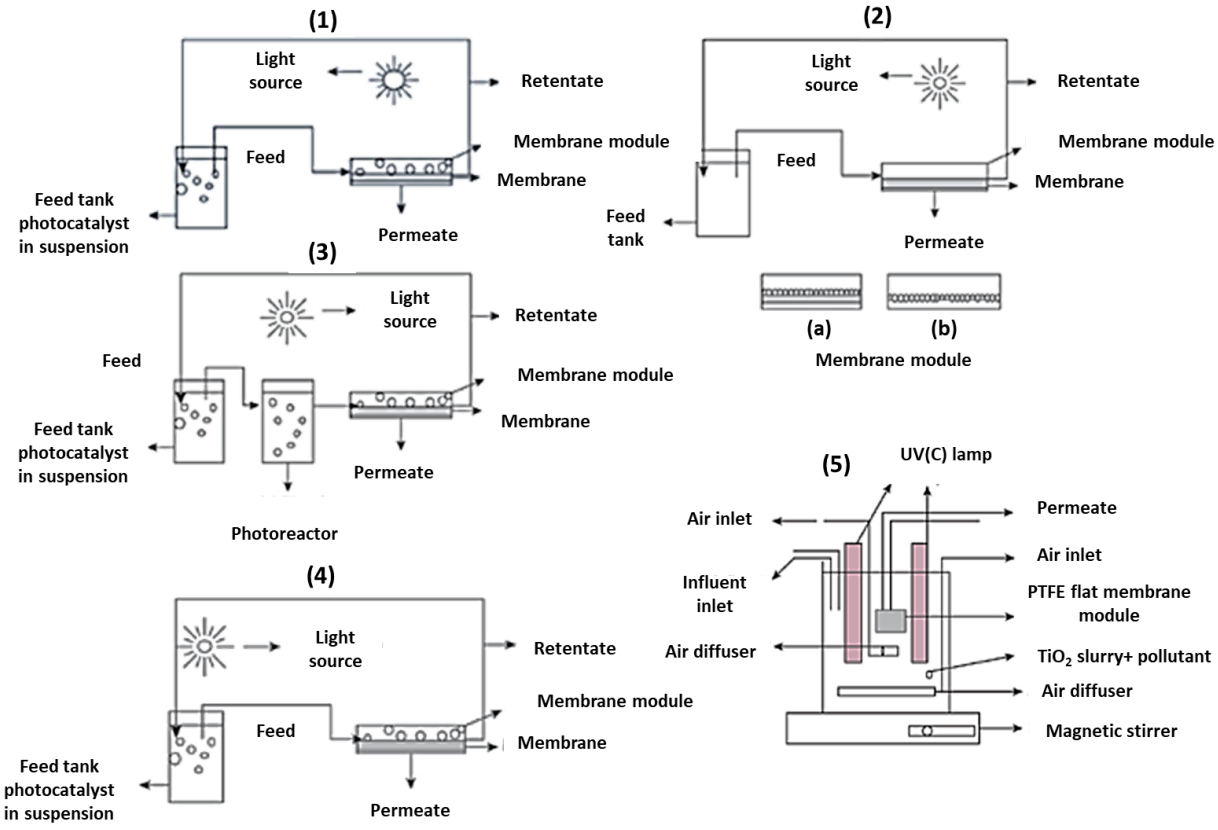

Figure 1. 15. Different photocatalytic membrane reactor systems.

Functionalization of polymeric membranes with TiO_2 catalyst have already shown to be promising for photodegradation of dissolved organic matter, humic acids and bacteria. Ceramic membranes, even though less exploited so far, have many advantages over polymeric membranes for filtration applications, since they have typically superior thermal properties, and a better resistance against corrosion and chemicals. These membranes can also be used

for highly acidic effluents. Moreover, ceramic membranes are much less susceptible to deterioration by the attack of OH radicals, which might be a problem for long life use of polymer membranes. Ceramic membranes have been fabricated with catalytic nanoparticles (titania, alumina, silica, silver) for synergistic effects on the membrane performance. The effect of catalytic nanoparticles have shown improvement of the membrane efficiency in the field of water and wastewater treatment including fouling mitigation, improvement of permeate. Hence, potential risks of nanoparticles release into the environment should be taken into consideration.[172] A study using heterogeneous photocatalysis assisted by supported TiO_2 as a tertiary treatment process in a conventional wastewater treatment plant shows encouraging results[173]. Additionally, functionalization with TiO_2 prevents fouling of the membranes, which is a major concern in membrane use for water treatment. [174] In most studies, however, PMs may encounter various technical problems such as membrane structure deterioration, low photocatalytic activity and loss of deposited TiO_2 layer over time[175]. To prevent the problems associated with the TiO_2 membrane coating, atomic layer deposition technique is promising since a controllable thickness deposition and pore diameter is possible[176].

4. Synthesis and modification of TiO_2

With all the challenges of photocatalysis for water treatment, several requirements are established for the design of highly active catalyst. Since TiO_2 semiconductor is not efficient for degradation under visible light, new structures and modifications are pointed. The goal is to design a photocatalysts with increased lifetime or charge separation of the photogenerated electron–hole species. In addition, higher photoefficiency is a must, as the ability of the catalyst to absorb light and convert it is essential for generation of radicals. Moreover, the reactant matrix should be taken into consideration during the fabrication of the material. Briefly, the photocatalytic activity of catalysts is governed by many properties, including its specific surface area, pore volume and distribution, crystal structure, phase composition, particle size and morphology[154].

To respond to these requirements, various methods were applied in the synthesis of titanium dioxide photocatalyst. As described in section 3.3, doping TiO_2 with metal, non-metal

or coupling with other semiconductors and creation of composite materials were all already assessed. The methods for elaboration of such materials are divided into two main groups, wet chemistry methods and dry method. In some cases, multiple methods are combined together in order to obtain the desired material aspect. These preparation methods include sol-gel, hydrothermal process, chemical vapor deposition, hydrothermal methods, electrospinning and atomic layer deposition[177–179].

4.1. Sol-gel method

The sol–gel technique is a wet chemical technique that has been extensively used for preparation of photocatalysts[180–182]. It is also a cheap and low-temperature solution route technique. Different shapes of material could be obtained in form of powder, ceramic coating, fibers, thin layers, and porous materials. Hence, in order to enhance the photocatalytic activity of the material, combination with another technique may be required[183–185].

Gombak *et al.* prepared B-N-TiO_2 specimens by co-sol gel technique. The successfully obtained a nanostructured powder with high surface area and higher crystallinity when increasing the B dopant. The efficiency of the catalyst was tested out on the degradation of methyl orange (MO). The best photocatalytic performance was obtained upon using TiO_2-B9-N5. Such a phenomenon was related to the simultaneous generation of intra-gap empty electronic states and filled Ti 3d levels. The adopted technique was valuable for preparation of such photocatalyst[186].

4.2. Hydrothermal

Hydrothermal/solvothermal methods are powerful techniques for synthesizing metal oxide, chalcogenide nanomaterials and various 3D photocatalyst. The process impose a high pressure and temperature treatment, which in some cases could be an advantageous but in others it would have a major drawback. Hence, tuning different conditions allow the fabrication of nanomaterials with various morphologies and structures (**Figure 1.** 16). Hydrothermal process could be used as an one-step route or could be combined with sol-gel or microwave assisted processes[187].

Santhi *et al.* prepared TiO_2 nanorods by hydrothermal technique under different pHs. The characterization techniques confirmed the successful elaboration of TiO_2. XRD analysis confirms the formation of anatase phase of TiO_2, moreover, FESEM micrograph confirms the formation of nanorods. The calculated band gap values of TiO_2 nanorods was found to decrease with increasing pH from the optical absorption spectra. Photocatalytic activity of TiO_2 nanorods against methyl orange (MO) was examined and their results have shown highest degradation (51%) of MO within 150 min[188].

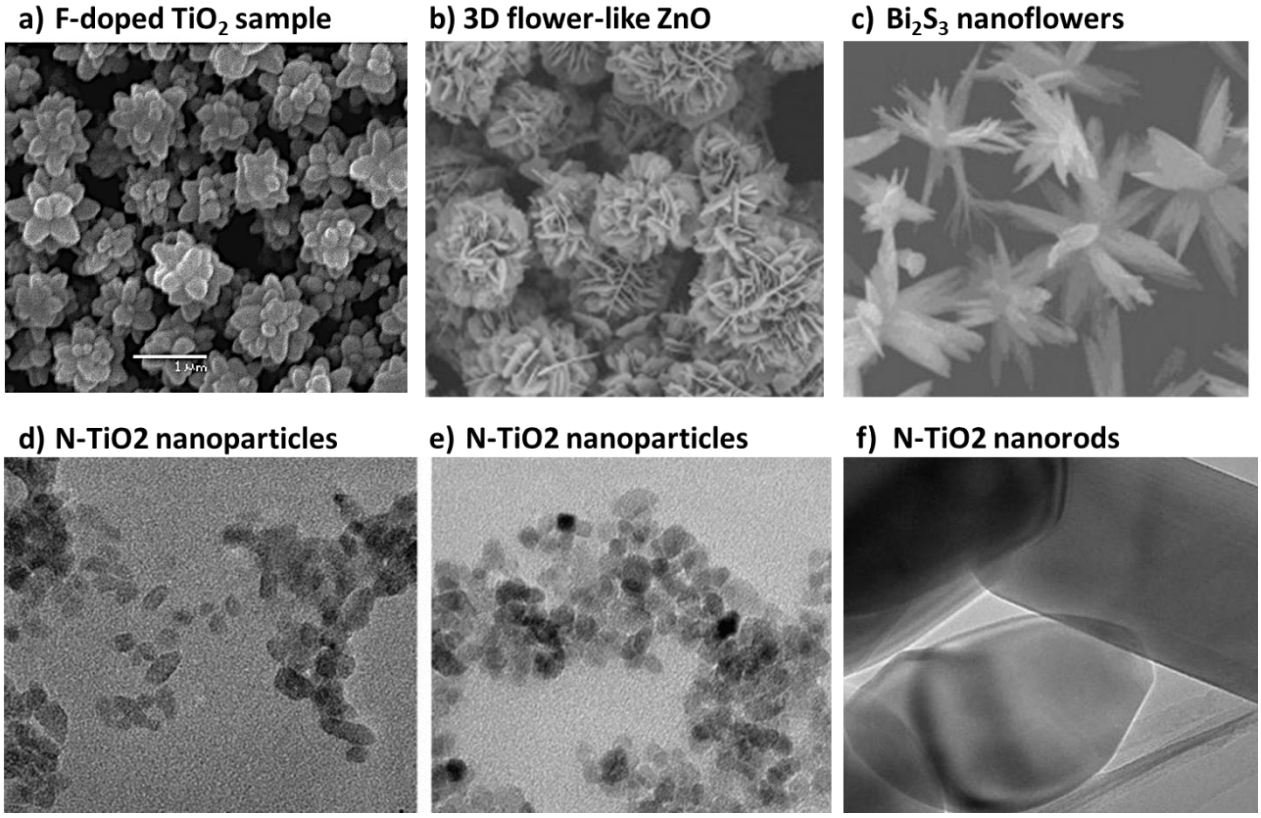

Figure 1. 16. SEM images of different materials elaborated by hydrothermal process: a) F-doped TiO_2[189], b) 3D flower like ZnO[190] c) Bi_2S_3 nanoflowers[191], d-e) N-TiO_2 nanoparticles[192] and f) N-TiO_2 nanorods[188].

4.3. Electrospinning

Electrospinning is an efficient way to fabricate nanofibres and various shaped fibers such as hollow tubes, ribbons and filled tubes[193]. This method is a simple fabrication route and leads to a wide range of suitable materials, with high production efficiency. Up to now, more than hundred types of natural and synthetic polymer have been electrospun into NFs,

including poly(vinyl pyrrolidone) (PVP), polyvinyl alcohol (PVA), polyacrylonitrile (PAN) and others[194,195]. More recently, the fabrication of electrospun ceramic or other inorganic NFs has been reported[196]. **Figure 1. 17** describes the electrospinning process. It is a simple technique where a polymeric solution is pumped out of the syringe with a controllable flow. High voltage is added between the nozzle and the collector and the pendent drop of the solution at the nozzle of the spinneret will become highly electrified. When increasing the value of voltage, the electrostatic forces will overcome the surface tension of the electrospinnable solution and the ejection of a liquid jet from the nozzle is possible. Subjected to a stretching and whipping process, this electrified jet forms a long and thin thread. Evaporation of the solvent will take place and formation of fibers on the rotating drum will be initiated. Once the process is complete, the fibers are collected from the collector and a thermal treatment is applied in the case of TiO_2 NFs to remove the polymeric fraction.

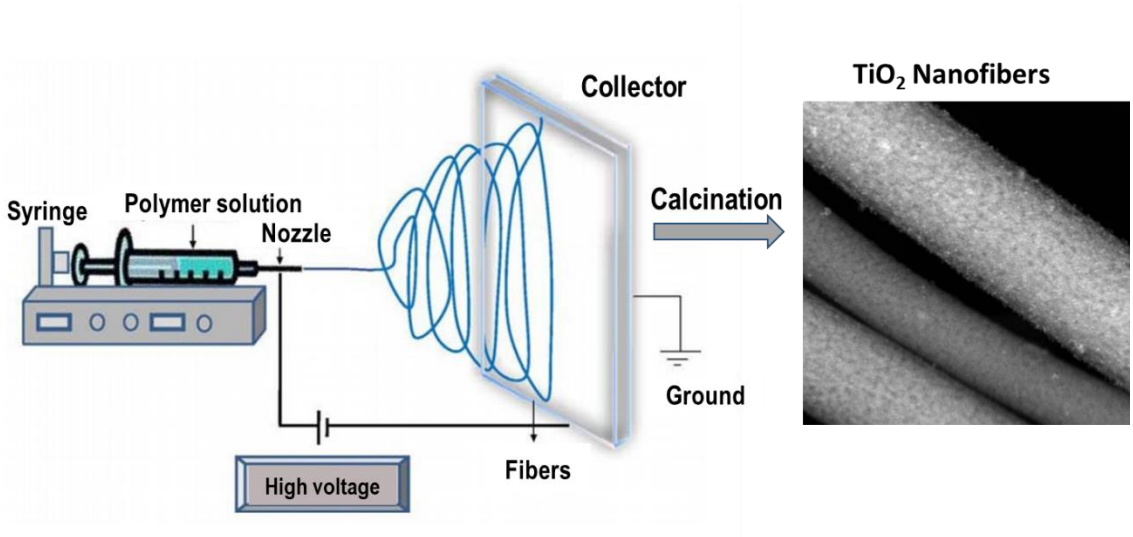

Figure 1. 17. Schematic illustration of electrospinning setup.

Nasr *et al.* synthesized graphene oxide (rGO)/TiO_2 nanofibers by electrospinning with different rGO ratio (2, 5 and 7%). The synthesized material were used as photocatalysts for degradation of MO. The authors found that 2% rGO was the optimum, which was confirmed by UV-Vis absorbance spectroscopy. The absorption edges of rGO/TiO_2 composite nanofibers are red-shifted and rGO (2 wt %)/ TiO_2 has the lowest band gap. This nanocomposite exhibits higher degradation efficiency of MO above all the synthesized samples. Electrospinning is a promising technique in elaboration of TiO_2 based photocatalyst with well dispersed nanofibers

and easily integration of other materials to create composites[197]. The same authors, fabricated Ag/TiO_2 and BN–Ag/TiO_2 composite nanofibers also by electrospinning. They studied the effect of coupling TiO_2 semiconductor with co-dopants. Nanofibers diameter increased with the incorporation of BN and Ag, same as the surface area. The importance of this study is to show that electrospinning allow the modification of TiO_2 catalyst with an improvement in surface area, active sites, band gap and photocatalysis effectiveness. The elaborated nanocomposite also shows a good antibacterial properties and maybe used ad in antibacterial material for biomedical use and water disinfection.[198]

4.4. Atomic Layer Deposition (ALD)

Among vapor deposition techniques, Atomic layer deposition (ALD) has drawn recently much attention in elaboration of catalysts. The principle of this technique and the researches that have been done till now will be reviewed in section **5**. The importance of this technique for water purification is noteworthy, since the need of nanomaterials with controllable size and morphology is promising for upscaling[199,200].

4.5. Limitations of conventional methods

The catalyst preparation method is one key parameter that should be considered for photocatalytic uses. Many limitations have been pointed out and limit the use of photocatalysis in real wastewater treatment plants. First of all, the conventional preparation techniques of TiO_2 with doping metals or non-metals cannot control the concentration of the dopants. Hence when metal loading concentration is beyond optimum value, electron transfer from TiO_2 to metal dopants could deform the potential field in TiO_2 particles and charge metal centers negatively which could lead to an increase in the recombination rate. Moreover, the doping procedure of non-metal requires thermal treatment at high temperatures (400-850 ºC) or a long preparation time requiring high energy. For this reason, the need of new deposition techniques for the elaboration of nanocomposites is of utmost importance. Another drawback is that the direct application of NPs for photocatalytic degradation suffers from aggregation of NPs. As a result, it affects the stability and recyclability of NPs. To overcome this limitation, supported catalyst system is of utmost importance. Moreover, suitable techniques with well-defined procedures and equipment are required[179].

Table 1.3. Comparison between the different methods for elaboration of composite catalyst

Synthesis Technique	Advantages	Limitations
Hydrothermal method	Cost effective Low energy consumption	Need expensive autoclave Reusability is not easy
Sol-gel method	Easy preparation High surface area	High precursor cost Product bandage is weak
Coating method	Efficient Fast	Inhomogeneous layer thickness
Atomic Layer Deposition	Conformal layer Thickness control Control of heterostructure interface	Cost

Atomic Layer Deposition is a promising candidate to respond to these difficulties. It is an efficient technique to coat NPs on suitable substrate. It allows the incorporation of nanoparticles into a polymer, metal, or ceramic matrix to upgrade their novel properties—mechanical stability, good optical features, low water/gas permeability, and high thermal conductivity. Moreover, high control of thickness and particle diameters is also possible.

5. Atomic Layer Deposition (ALD) for catalysis

With the increase of water pollution and the higher demand for clean drinking water, new technologies are in need. Photocatalysis is a promising technique for water treatment plants to remove the persistent pollutant. Hence, the design of material that respond to this demand is still missing. New design of nanomaterials with controllable thickness and morphology is utmost importance. Moreover, upscaling of photocatalysis procedure needs to improve supported materials design for photocatalytic membranes reactor. Among many techniques, ALD is a great candidate for tuning catalyst characteristic by enhancing the separation of the photogenerated charges, shifting the band gap to visible range and creating heterojunction materials. Herein, we will present the principle of Atomic Layer Deposition and we will review

the development of this technique in the catalysis field. This section will display the importance of ALD in elaboration of controllable materials for enhancement of degradation of pollutants under UV and visible light. Moreover, functionalization of already exiting catalyst has been widely reported by doping with metals; non-metals, creating heterojunction and composite materials. Elaboration of TiO_2 semiconductor and composite based TiO_2 catalysts will be mainly discussed. The catalytic efficiency of these materials will be reported on the removal of pollutants and generation of hydrogen.

5.1. ALD principle

ALD is a vapor phase thin film deposition technique that has gained considerable attractiveness in recent years. Atomic Layer Deposition (ALD) was created in 1960 and was known as ALE "atomic Layer epitaxy" or molecular layering. It was first developed and used for elaboration of semiconductors in microelectronic field[201,202]. Before gaining fast attention into many other applications such as bio-medical, catalysis and energy conversion[203,204]. Tremendous efforts and research have led to the industrialization of this technique in fabrication of semiconductor for microelectronics[205].

ALD is based on the sequential pulses of gas phase precursors separated in time. It is a self limiting reaction that allows the deposition of thin films and overlayer in the nanometer range. A typical ALD cycle is represented by pulse of the first precursor into the ALD chamber. The precursor will react with active sites of the substrate during the exposure time. The self-limiting character of this technique is the key to the desirable film properties such as conformal coating of high aspect ratio features, pinhole free films, and digital growth control, followed by a purge with an inert gas than the pulse of the co-reactant followed by exposure and purge. Than a carrier gas is introduced into the room to remove surplus precursor and reaction products from the reactor. If the ALD co-reactant is introduced to the reactor before all of the first precursor is removed, gas phase CVD reactions will take place. After ensuring in off time of purge, the second half cycle start with the pulse of the co-reactant to react with the chemisorbed precursor. A purge phase is initiated to remove the excess products and the cycle is repeated until the desired film thickness obtained. **Figure 1.** 18 denote the typical mechanism of Al_2O_3 deposition by ALD. The precursors used in this case are the trimethylaluminum (TMA) and H_20 as co-reactant[206].

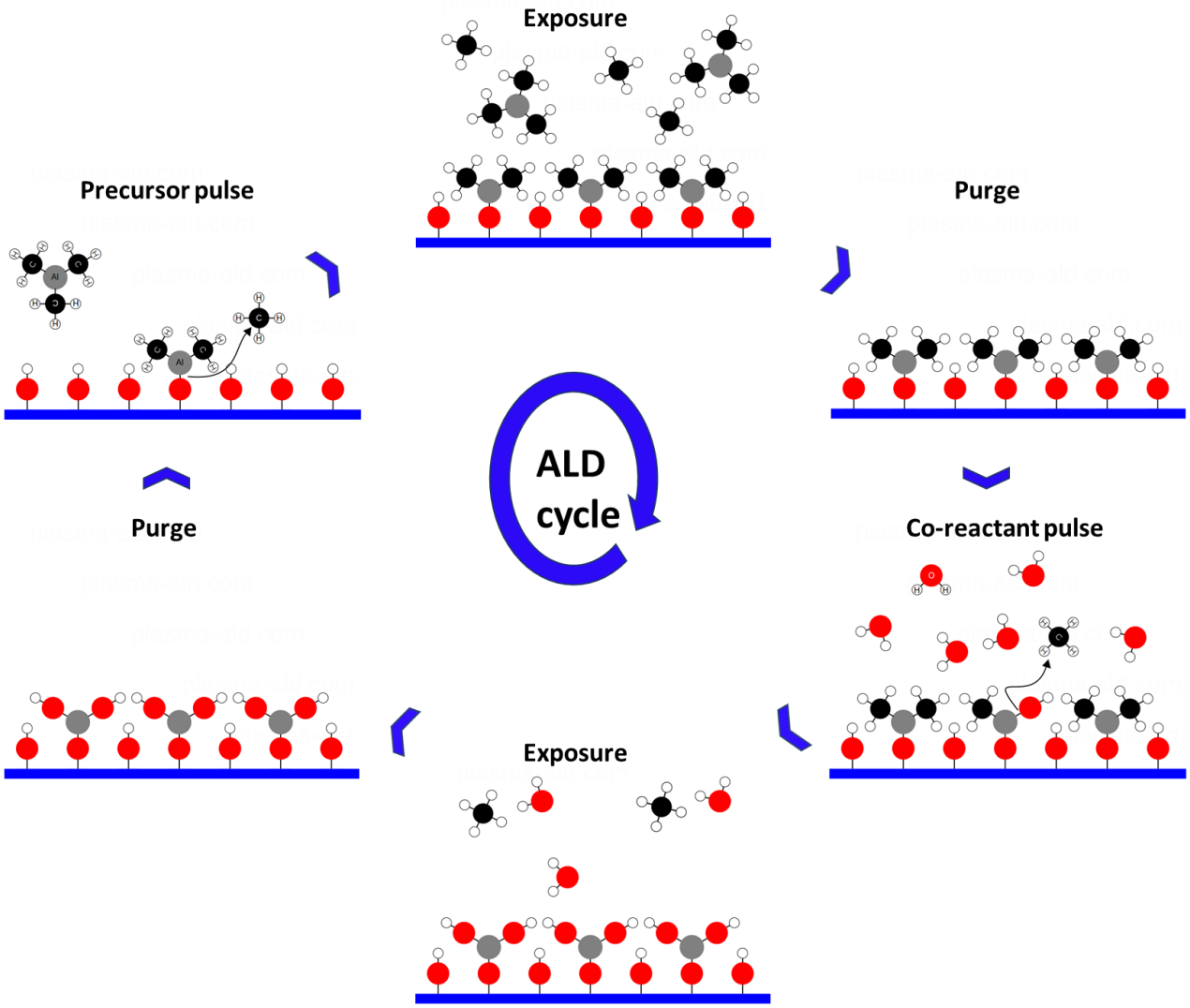

Figure 1. 18. Schematic representation of one cycle of Atomic Layer Deposition of aluminum oxide Al_2O_3 via trimethylaluminum (TMA) and water.

5.1. ALD precursors and deposited materials

Wide range of materials have been already synthesized by ALD including oxides, nitrides, sulfides, fluorides, metals, ternaries, quaternaries, chalcogenides[207,208]. It stems from the fact that various precursors could be used during the ALD process and the deposition could happen in a broad range of temperature. Any precursors could be used in ALD as long as they encounter three main criteria's, they should be highly reactive, volatile and thermally stable. The precursors should react rapidly with the substrate and with each other's without

generating toxic sub-products. Some of the materials generated by ALD are listed below[209–212]:

Oxides: ZnO, $Al2O_3$, ZrO_2, TiO_2, SiO_2, HfO_2, MgO, V_2O_5, SnO_2….

Nitrides: AIN, BN, TiN, ZrN, SiN, HfN, …

Sulfides: ZnS, SrS, PbS, …

Fluorides: CaF_2, ZnF_2, MgF_2, …

Metals: Pd, Pt, Cu, Ru, Fe, Ni, …

Carbides: TiC, NbC, TaC, …

5.2. Specialized ALD systems

With the increase demand for ALD technique in many fields, different type of ALD where developed to enhance the feasibility of this process and respond to high demand in different fields. The principle still the same but minor modifications are implemented to overcome the limitations of this technique.

5.2.1. Thermal ALD

Substrates to be coated with an ALD film are placed in a heated reactor under vacuum. The restricted temperature window for self-limited regime of ALD deposition and high investment costs of the tools/precursors represent main drawback of nowadays ALDs, but these are overcome step by step by continuous improvements in the ALD technology listed below.

5.2.2. Molecular Layer Deposition (MLD)

This derivative technique from ALD allow the deposition of polymeric thin films with growth control at the molecular level. In this process, molecules are loaded on the substrates one by one in order of preference with a growth per cycle higher than ALD rate. This vapor-phase method does not require solvents or catalysts and is promising for the fabrication of functional ultrathin polymeric layers. One of the most material deposited by MLD is alucone based on sequential pulsed of TMA and ethylene glycol (EG)[213].

5.2.3. Plasma enhanced ALD (PEALD)

Thermal ALD processes present some drawbacks with the deposition at lower temperatures. Potential precursors exist but are not highly reactive with the typical thermal ALD. PEALD was first reported in 2001 for deposition of thin film at lower temperature with plasma processing. Plasmas gases such as O_2 enable high reactivity without adding lots of heat. Radicals are many times more reactive than molecular co-reactants and can improve the ALD process in several ways. Compared to thermal ALD, PEALD showed several advantages such as increased film growth rate, low process temperature and no explicit purge step. Moreover, this technique allowed the deposition of a wide range of materials such as $SrTiO_{3n}$ TiN, $BaTiO_3$…[214,215] Hence, the surface chemistry for the plasma process is not nearly as clean as that for the thermal ALD process[216].

5.2.4. Solution ALD (sALD)

Wu *et al.* successfully elaborated MgO by solution ALD (sALD) based on hydrolysis reaction between titanium isopropoxide and diethyl ether solution[217]. The same principal of ALD is used but with the incorporation of dissolved precursors. This could be a good opportunity to overcome the need of volatile and high thermal stability precursor.

5.2.5. Atomic Layer Deposition on Particles

Another advance was brought by replacing the conventional reactor by a rotary or fluidized bed reactor for a better particle coating. This technique allow the deposition of a uniform layer on nanoparticles and was used for the modification of powder catalysts[218].

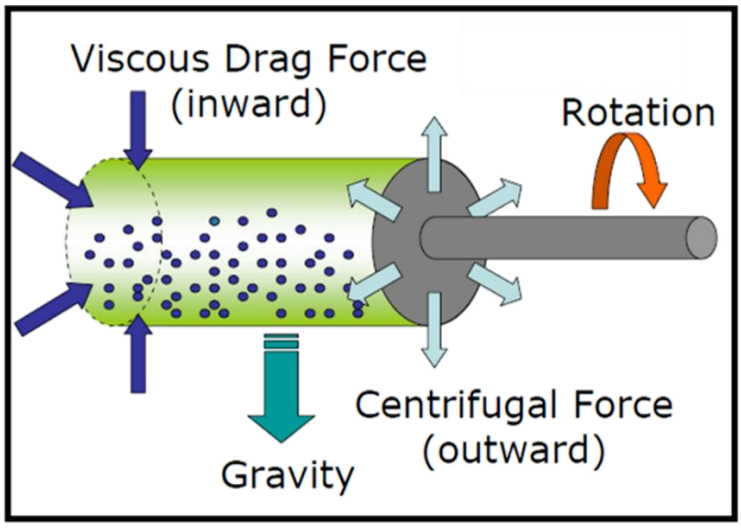

Figure 1. 19. Conception of new rotary reactor for deposition of uniform coating on particles[219].

5.2.6. Spatial ALD

One major drawback of ALD is the low deposition rate, which make ALD less attractive for high throughput processing. Spatial atomic layer deposition could adverse this limitation where the half-reactions are separated spatially instead of through the use of purge steps. This increase the growth per cycle without compromising the typical ALD assets[220]. Spatial ALD is certainly a route towards further industrialization of atomic layer deposition.

5.3. ALD Advantages

The broad popularity of this technique is explained by its many advantages over conventional techniques. This technique allows the deposition of conformal layer with a high thickness control and pinhole free even on 3D materials. Excellent step coverage is obtained on high aspect ratio substrates with no particle generation. The potential deposition at low temperatures allow the use of wide substrates. Lastly, multilayers could be easily obtained by doping different materials or create nanolaminates[206,208,221].

5.4. Applications

Early interest in ALD was widely driven by semiconductor applications, particularly high-k materials for DRAM capacitors and transistor gate dielectrics. Hence, application of ALD in many other active areas in microelectronics research has vastly increased to deposition of electrode metals, diffusion barriers, and seed layers. Recent years have seen the spread of ALD films into a broad spectrum of applications outside of the "traditional" semiconductor space as solar catalysis batteries, fuel cells encapsulation, energy storage, optical devices, sensors, bio-medical field, membranes and catalysis[222–226].

5.5. ALD for elaboration and functionalization of catalysts

Heteregenoeus catalysis is the most used technique, whereas synthesis of nanoparticles or films depends on the desired application. Nanoparticles such as oxides, sulfides, metals and alloys are usually deposit to activate the catalyst support. Different catalyst supports have been used such as nanopowders[186], porous substrates[211,227], nanotubes[66], nanowires[228],

aerogel[229] and metal organic framework (MOF)[230]. For thin film deposition, ALD allow a conformal deposition to tune the surface properties of the catalyst.

Several reviews have been written about ALD for catalysis application[231–235], herein we will discuss the newest researches made in this field and we will focus on the deposition and functionalization of TiO_2 catalyst by ALD.

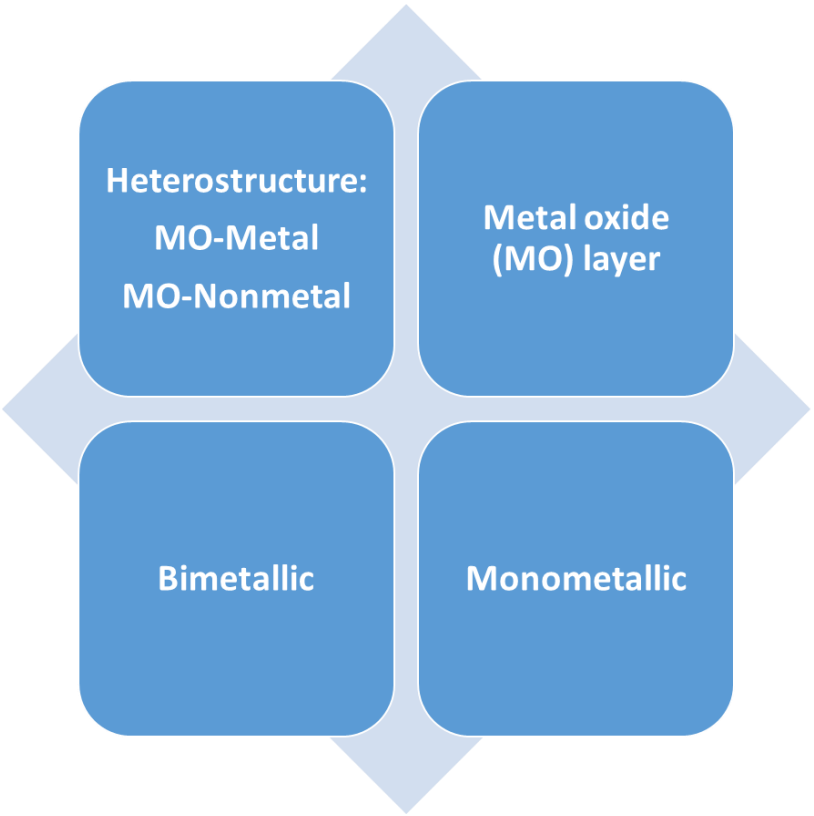

5.5.1. Conformal Metal oxides coating-tuning the substrate morphology

Specific property of ALD method in photocatalysis, is the ability to deposit conformal thin films on different type of substrates with nanometer-scale thickness control. Catalyst were prepared to be used in suspension in the solution, whereas new technologies have been working on elaboration of immobilized catalyst. Herein, we will report deposition of conformal oxide layers on different substrate types: nanofibers, nanopowders, ceramic membranes, nanotubes, etc..

- **Deposition on highly porous substrates**

Even though ALD has shown a high impact in catalysis, different parameters should be taken into consideration specially when coating porous substrates[236]. Moreover, deposition temperature could highly affect the synthesized material. The tuning of the structure of the catalyst have a major effect on its catalytic properties. If the structure is coated with a thick oxide layer, a decrease in the photocatalytic activity of the substrate could be generated. Justh *et al.* confirmed that when coating porous carbon nanostructures by TiO_2 layer, no improvement in the degradation of MO was approved. This might be due to the change in the functional properties of the substrate during the ALD process. Hence, it is important to pay attention on the change of density and specific area of the catalyst as well as crystallinity in order to improve the catalytic degradation[229]. Levchuk *et al.* reported the successful deposition of TiO_2 on aluminum foam by ALD. They evaluated the prepared material for the degradation of formic acid and phenol degradation[237].

- **Carbon based material**

Atomic Layer deposition allows the elaboration of different structure materials that could be highly active. Recently, researchers have found that deposition of amorphous TiO_2 layer on fullerene C60 substrate presented a high photocatalytic activity regarding the degradation of MO. The precursors used were $[Ti(OC_3H_7)_4]$ and H_2O at 80 and 160°C and the layer deposited has a thickness of 1-1.5 nm[238]. This phenomenon is related to the fact that the crystallinity of the materials, deposited by ALD, depends on several factors, such as: deposition temperature, type of reactants, presence of impurities, substrates, film thickness, etc… Marchetti *et al.* used $TiCl_4$ and water for deposition of TiO_2 on graphene substrate. The crystallinity of TiO_2 film was affected by the number of cycles, when less than 200 cycles is applied, the film was amorphous. With increasing the number of cycles, a crystalline structure was obtained. The photocatalytic degradation of methyl red increased with number of ALD cycles. The authors also confirmed that when depositing TiO_2 directly on Silicon substrate no degradation was generated. Thus enhancement of photodegradation of methyl red is due to the hybrid structure of TiO_2/Graphene where higher efficiency in electron-hole separation is obtained[239]. Another study has also reported the effect of ALD parameters on the structure of synthesized TiO_2 films. TiO_2 thin films were deposited on Si substrate in a Picosun SUNALE R-150 ALD

reactor operated under nitrogen atmosphere at approximately 10 mbar. The films were grown using $TiCl_4$ and deionized water at deposition temperatures between 150 and 400 ◦C using a number of growth cycles ranging from 250 to 3000, corresponding to the film thickness up to 160 nm[240]. The authors tried to establish a relationship between thickness, crystalline structure and photocatalytic activity. When the deposition temperature increases, the crystalline structure is more developed. As well, the increase of thickness at a deposition temperature of 350°C, lead to the formation of TiO_2 crystalline structure with both phases anatase and rutile. The degradation efficiency of TiO_2 is directly correlated with its structure. The photocatalytic activity of deposited films towards hydroxyl radical generation has been tested in the reaction of hydroxyterephthalate (TAOH) formation from terephthalate (TA). Higher radical generation is stated when the thickness increase until an optimum before decreasing (**Figure 1.** 20)[240]. Guo *et al.* stated that the photocatalytic activity of TiO_2 is also dependent on the nature and density of defect sites. The adsorption states and reaction of adsorbates on TiO_2 surface are highly affected by the dominant defects on the surface and in the bulk[241].

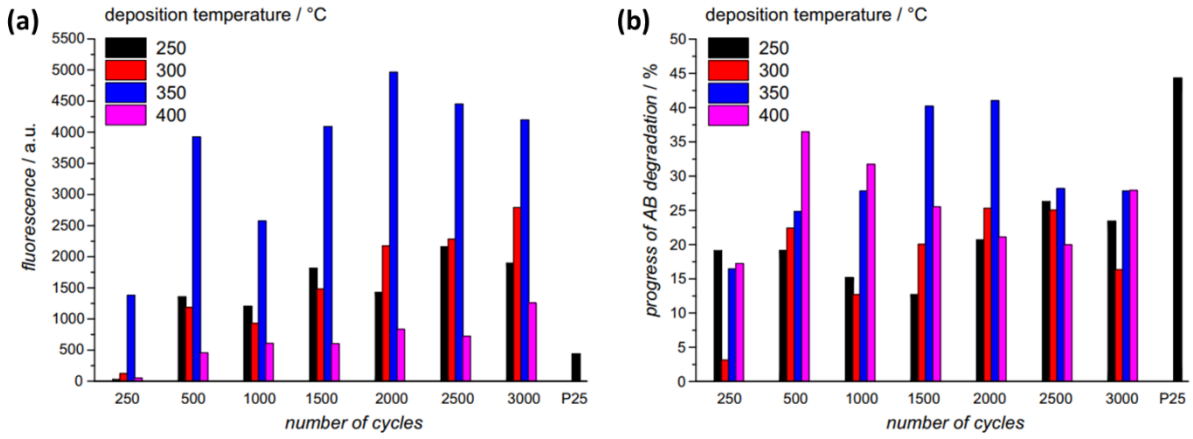

Figure 1. 20. Photocatalytic activity of TiO_2 layers: (A) oxidation of TA to TAOH, (B) degradation of AB. The reaction progress after 90 min of irradiation[240].

Kumari *et al.* have also studied the effect of thickness on the catalytic efficiency of TiO_2 deposit on stainless steel substrate by ALD. They found that the impact of the number of ALD deposition cycles on the metal oxide thin films could affect not only the crystallinity and roughness but also the microstructure of the deposited layers. The photocatalytic efficiency

was highly dependent on the thickness of the material and this is in relation with the light diffusion and penetration within the material. The TiO_2 deposition was performed at 250 °C via Plasma Enhanced – ALD (PE-ALD) with Tetrakis(dimethylamido) titanium (TDMAT) and O_2 plasma as precursors. The light absorbed and transmitted within the semiconductor is attenuated due to the intrinsic properties of the materials including the refractive index (η), extinction coefficient (κ) and dielectric constant constants (εr). This study demonstrated the dependency of photo-catalytic performance on the thickness of the material by correlating the fundamentals of light-matter interactions with the obtained experimental results[242].

Another interesting metal oxide that was widely used in preparation of catalyst is zinc oxide (ZnO). A possible way of immobilization of these nanostructure on complex substrates is offered by ALD. Moreover, ALD does not only ensure a stable bond between the catalyst and the support but can also affect the photocatalytic activity of ZnO. This is possible by finding the optimal operating conditions (e.g. the deposition temperature and ALD cycles and the number of cycles). In this study, ZnO films were deposited on glass substrate with DEZ and H_2O as precursor and co-reactant, respectively. At high temperature deposition (250°C), various nanograin shapes were obtained while at lower temperature nanograins were not properly formed. The structure of these catalysts is directly correlated with the degradation efficiency. Another important parameter that could influence the catalytic activity is the film thickness. An optimal film thickness of 50 nm was enough to ensure a good degradation efficiency, above this value the film thickness could adversely affect the efficiency[243].

Due to their unique combination of properties, the functionalization of the CNTs by ALD with a metal oxide semiconductor such as ZnO is a quite challenging and actual research topic. This configuration is an excellent photocatalyst nanocomposite material candidate, since these photocatalysts are not dispersed in solution but they are supported on solid substrate thus avoiding large quantities of catalyst and time consuming separation procedure[244]. ZnO/CNTs nanocomposite with different ALD cycles 25, 50, 100 and 200 cycles were synthesized using diethylzinc and ozone as oxygen precursor. The morphology of the deposited ZnO film highly affect the photocatalytic behavior. The best degradation of RhB was produced with 100 cycles of ALD, and this was related to the granular morphology increase of ZnO while increasing ALD number of cycles (**Figure 1. 21**). Another study have also confirmed

the influence of ZnO nanostructure on photocatalytic degradation. The well nanostructured ZnO can produce various reactive oxygen species (ROS), such as the hydroxyl radical, superoxide anion, and singlet oxygen, by UV-A light irradiation in water. The competing effects of film thickness, the catalytic quantum yield, and optical properties could affect the photocatalytic activity of ZnO.

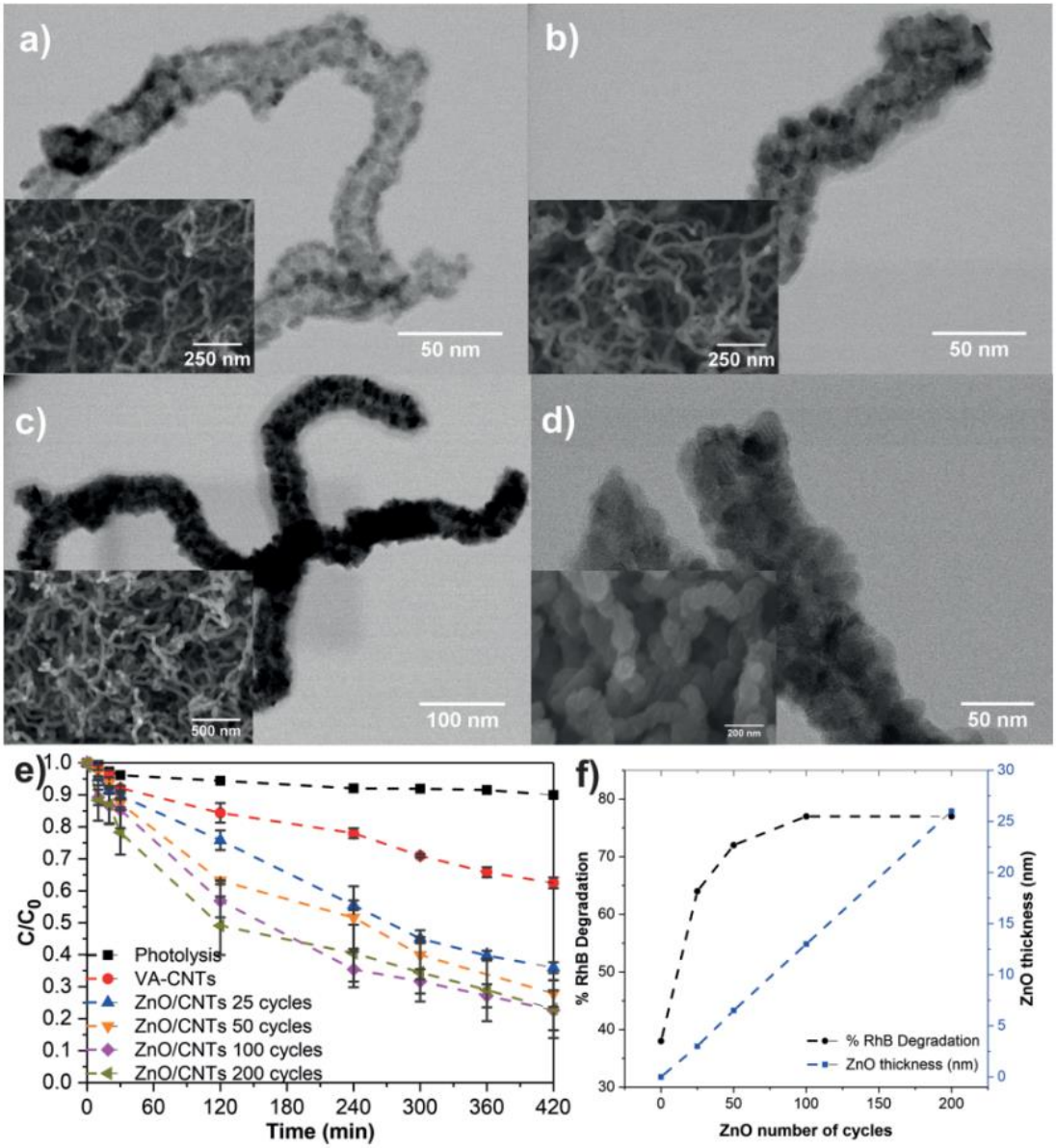

Figure 1. 21. BF-TE-STEM images of carbon nanotubes decorated with ZnO after: (a) 25, (b) 50, (c) 100, and (d) 200 ALD cycles. Inset images: SEM images of the CNTs coated with ZnO after: (a) 25, (b) 50, (c) 100, and (d) 200 ALD cycles. (e) Evolution of the normalized concentration (C/C0) of RhB under UV (365 nm LED) irradiation of the ZnO/VA-CNTs nanostructures, as-prepared CNTs and photolysis (absence of catalyst). (f) %RhB degradation vs. the ZnO number of cycles and film thickness. The film thickness increased linearly with

increasing number of deposition cycles, and ALD of ZnO process is precisely controlled by the number of ALD cycles applied. The lines represent trendlines[244].

- **Powders**

Atomic Layer deposition was not only used to elaborate new catalyst but also modify existing catalysts. This technique is very promising for tuning the properties of existing material. It could be used as a coating for photo-active material or a surface protection layer to increase the life-time of the catalyst by enhancing its stability. Commercial TiO_2 nanopowders were successfully coated by an ultrathin layer of Fe_2O_3. The deposition was done in a fluidized bed reactor to uniformly coat the powders. The authors studied the effect of ALD number of cycle on the degradation of MO under visible light. They found that ALD allows the deposition of a uniform layer on the surface of the powder (**Figure 1.22 a-b**) and the degradation efficiency could be highly dependent on the layer thickness. The optimal rate was found with 200 cycles of Fe_2O_3 confirmed by the optical characterizations. Enhancement of the band gap of the heterostructure was verified and the mechanism of charge transfer was proposed. ALD allowed the formation of an heterostructure between the interface of TiO_2 and Fe_2O_3. Photogenerated electrons were formed by the excitation of Fe_2O_3 and thus transferred to TiO_2 conduction band by the built-in electric field and the concentration gradient of electrons, while holes remain in VB of Fe_2O_3 (**Figure 1.22. e**) Therefore, the separation efficiency of photoinduced electron–hole pairs can be improved and higher degradation efficiency is obtained[245].

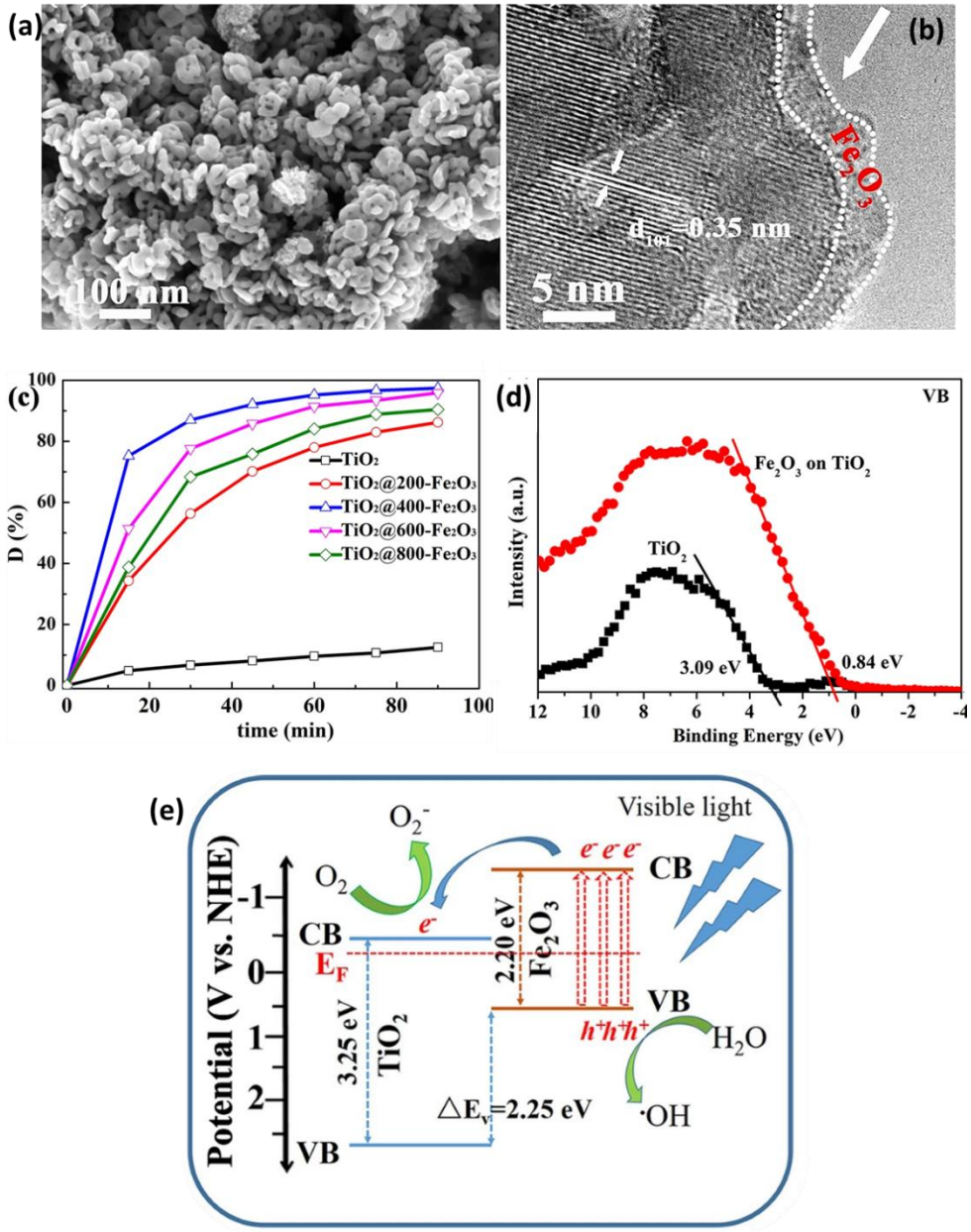

Figure 1.22. a-b) SEM images of TiO_2@Fe_2O_3, c) degradation efficiency of MO with different photocatalyst, d) UV-vis absorbance spectrum and e) schematic presentation of fermi level[245].

- **Ceramic membranes as catalyst support**

Ceramic membranes are becoming more attractive for challenging water purification processes than inorganic supports. Functionalization of the membrane surface with conventional methods is not efficient due to aggregation of the photocatalytic particles, detachment, membrane damage, and pore blocking. Hence, ALD could face these challenges and tune the ceramic membrane surface with the highest precision coating layer or with

deposition of long term stability nanoparticles[246]. ALD will reach not only the surface of the membrane but can also tune the membrane pores because of its ability to deposit on high aspect ratio structures. Enhancement of the mechanical, thermal and chemical stability of the membrane increase their photocatalytic efficiency by improving their permeability and reducing membrane fouling. Berger *et al.* used TiO_2 coated ceramic membrane by ALD in a single-pass flow-through process (**Figure 1. 23**). The authors reported the effect of TiO_2 layer on the degradation of dye molecules. The authors compared different ceramic substrates; they found that the layer deposit on the surface of the membrane was homogeneous. However, the TiO_2 layer thickness within the bulk of the membrane is inhomogeneous. This non-uniform coating could be caused by a non-optimized conditions regarding the time of diffusion of the precursor into the membrane pores. The modified membrane showed a promising results for removal of pollutants from water under light irradiation[247]. Atomic layer deposition allows the increase of number of reactive species on the surface of the membrane as well as the permeability of the membrane with a high control of pore size.

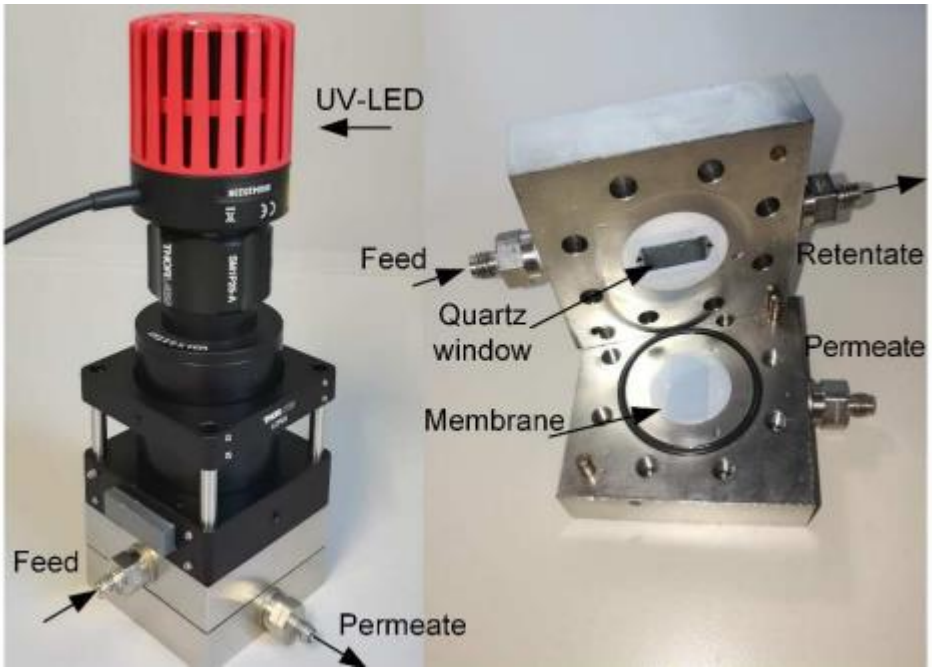

Figure 1. 23. Photographs of the (left) closed photocatalytic membrane cell with attached UV LED and (right) open photocatalytic membrane cell[247].

Table 1 : Thin film layer deposition by ALD

Catalyst	Substrate	ALD	Nbr of cycles	Pollutant	Degradation efficiency	Time (min)	Reference
TiO_2-Fe_2O_3	TiO_2 powder	Fe_2O_3	400	MO	97.4%	90	[245]
MgO-Ag/TiO_2	Ag/TiO_2	MgO	5	Phenol	95%	120	[248]
C60-TiO_2	C60 fullerene	TiO_2	80	MO	30%	330	[238]
ZnO/Al_2O_3 NTs 20%	PAN	ZnO, Al_2O_3	100 20	MO	98%	45	[249]
VA-CNT	CNT	ZnO	100	RhB	77%	420	[244]
ZnS/g-C_3N_4	g-C_3N_4	ZnS	5	MB	90%	100	[250]

5.5.2. Supported monometallic catalyst

Besides metal oxide semiconductor itself, novel metals, such as Pd, Pt, Au, , have been added to further increase the photocatalytic performance. This is because when these metals are presented on the metal oxide semiconductor surface, metal/semiconductor heterojunctions are formed, which could effectively prevent the combination of electrons and holes[251–253]. In the presence of irradiation, electrons are excited on the metal oxide semiconductor and can migrate from semiconductor surface (with higher Fermi energy) to metal surface (with lower Fermi energy). The metal NPs prevent the combination of electrons and holes, and increase lifetime of charged carriers thus photocatalytic performance is increased by the Mott-Schottky effect[253,254].

TiO_2 based materials have been widely doped with metals for the increase of their photocatalytic activity. Pt is the most efficient co-catalyst for the H_2 generation reaction. These NPs can enable efficient electron transfer at the TiO_2 surface by favoring a solid-state junction to TiO_2, and additionally catalyze the hydrogen[228]. Atomic Layer deposition is an effected technique for metal doping since it allow the control of the particle size and their density on the substrate. Another advantage is the possibility of decoration of high aspect ratio materials such as NTs and NFs. Yoo *et al.* reported the deposition of Pt nanoparticles by ALD varying the number of cycle that affects the nanoparticle diameter size. The quantum yield of H_2

generation was depending on both the source of irradiation and the size diameter of Pt NPs. The TiO_2-NPs composite acted as a good catalyst for generation of H_2. The optimum Pt size for solar light was obtained at 26 cycles (~7 nm) while for 325 nm light the maximum occurred at 40 cycles (~11 nm). These values could be attributed to the effect of the light penetration depth, where a competition occurs between the positive effect of the Pt nanoparticle loading and the negative effect caused by shading of the TiO_2 surface[255]. Same results were reported by ozkan *et al.* after elaboration of Pt-decorated spaced (SP) TiO_2 NTs by ALD. The authors compared the effect of substrate on the photocatalytic H_2 evolution. The inner and the outer walls of NTs were uniformly decorated by Pd NPs owing to the originality of ALD in coating 3D substrates. The photocatalytic activity for H_2 evolution strongly depends on the size and density of Pt nanoparticles, driven by the number of ALD cycles. SEM images shows the effect of ALD cycle number on the density of the NPs. When the number of cycle is too high, coalescence can occur on the surface of the semiconductor and film deposition occur on the inside and outside of the NTs. Ultimately, the photocatalytic H_2 generation rate enhances initially with increasing Pt content, reaches a maximum, and then declines once the Pt content is beyond an optimized amount. The photocatalytic activity decreased due to two possible phenomena: 1) oxide shading effect by Pt, caused by the large amount of Pt shades on the photosensitive TiO_2 surface or hinders the light absorption, 2) larger Pt particles or higher metal loadings may provide more recombination sites for photogenerated electrons and holes.[256]

Palladium is also a good candidate owing to its higher chemical stability than Ag and Pt and better thermal resistance than Au[129,257]. Deposition of Palladium was extended from metal oxide substrate to Carbon nanotubes substrates, MOF and BN as an innovative support material[230,258,259]. Merenda *et al.* fabricated Pd-TiO_2 heterojunction on TiO_2 NTs by ALD. The Pd catalytic interface and resulting active site density was tailored by varying the nanoparticle growth and coalescence via ALD, leading to Pd-TiO_2 junctions with distinctive morphological aspects and interface properties (**Figure 1. 24**). These catalysts were used for the degradation of methylene blue under visible light irradiation. The higher degradation efficiency of Pd-TiO_2 was attributed to the Surface Plasmon Resonance effect and correlated to the variation of the catalyst morphology tuned by ALD[260]. Assaud *et al.* tested the efficiency of TiO_2 NTs-Pd for

ethanol electrooxidation. XPS analysis showed that as-prepared Pd nanoparticles are present in the metallic state, whereas after ethanol electrooxidation 40% of surface Pd is transformed to PdOx. Among the prepared electrocatalysts (N = 400–900 ALD cycles), the 500 ALD Pd/TNTs system showed the best catalytic activity and satisfactory stability in alkaline media. The electrochemical characterizations have demonstrated that these Pd/TNTs systems exhibit high current densities and low onset potential if compared to the literature and commercial catalysts[251].

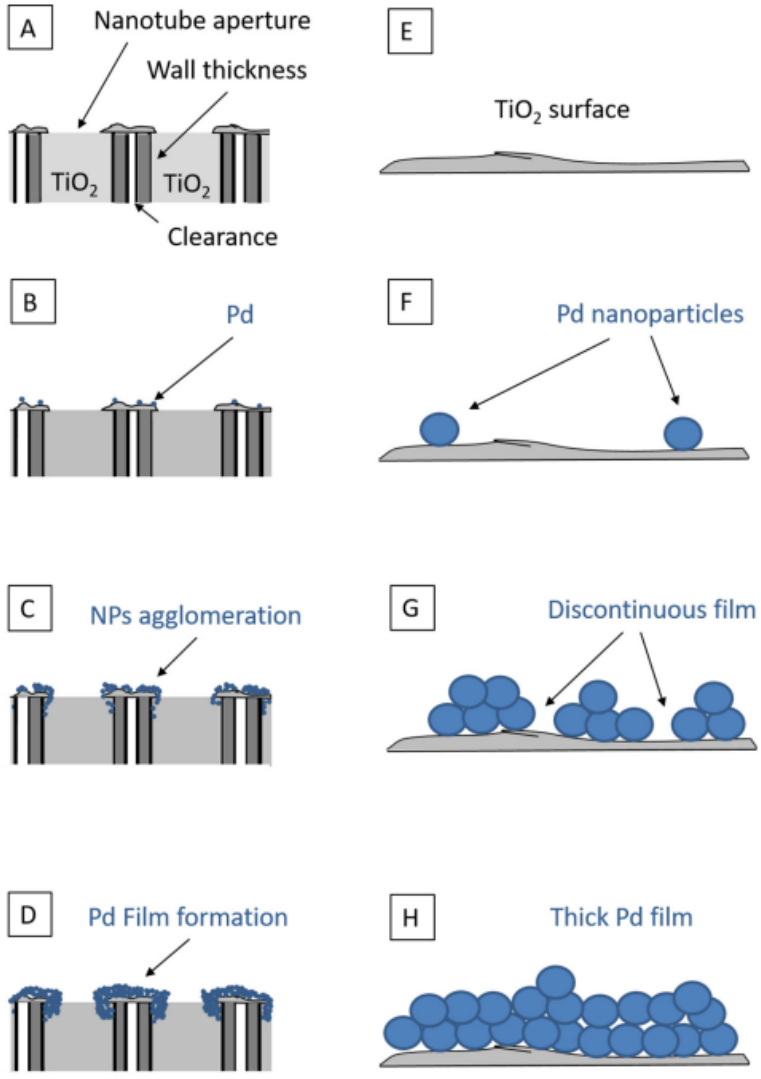

Figure 1. 24. Pd deposition mechanism for as-annealed (A) TiO_2 and upon 50, 100 and 250 ALD cycles, (B), (C), (D) respectively. Pd-TiO_2 catalytic junction, formation, growth and coalescence of catalytic interfaces upon 50, 100 and 250 catalytic cycles, (F), (G) and (H) respectively[260].

Ag-TiO_2 NTs was successfully prepared by ALD, for TiO_2 preparation anodisc aluminum was used as a template and removed after TiO_2 deposition by calcination[261]. The authors reported the uniform dispersion of Ag NPs on the inner and outer walls of TiO_2 (**Figure 1.** 25). The authors studied the degradation efficiency of the prepared catalyst under UV light. Hence, the effect of this catalyst should be tested under visible or solar light to confirm their efficiency[261].

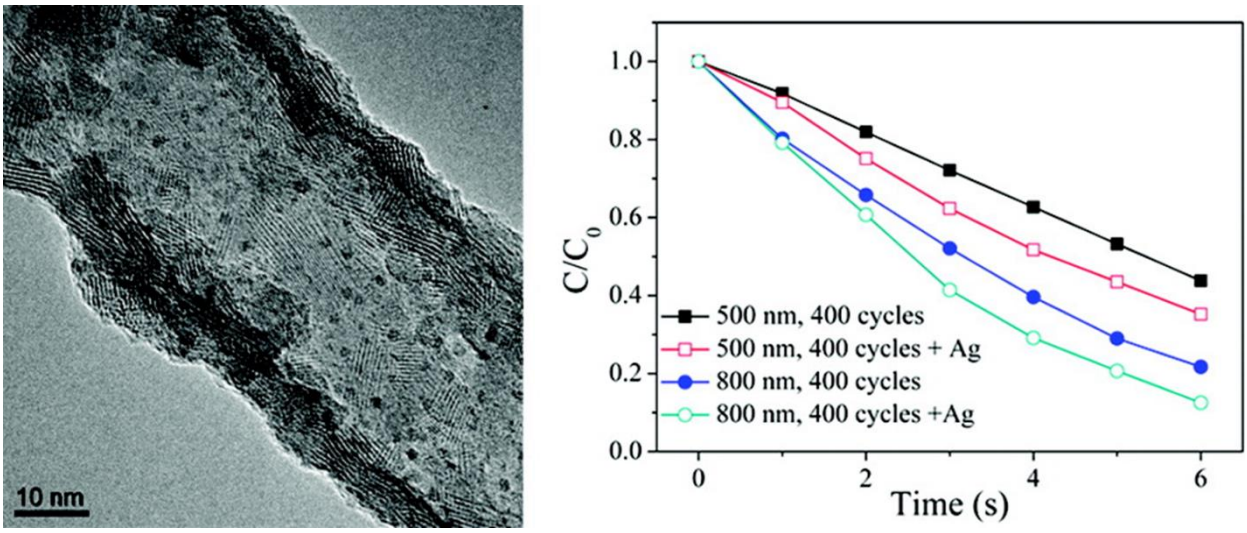

Figure 1. 25. TEM image of well dispersed Ag on **TiO_2** NTs prepared by ALD (left) and the degradation efficiency of MO under UV light irradiation (right)[261].

Copper NPs were also successfully deposited on TiO_2 surface to create heterojunction material and enhance the photocatalytic activity of TiO_2[255]. For Atomic Layer deposition process, $Cu(hfac)_2$ and deionized water were used as Cu precursor and reducing agent, respectively. Prior to deposition, TiO_2 NTs were modified into H-TiO_2 for generation of more active sites. Since no evident difference in the crystal structure and absorption ability was seen after the deposition, chemical state of Cu was devoted. The authors examined the chemical states of Cu to understand weather the enhancement in degradation is directly correlated with the chemical state of the metal (Cu_0, Cu^+, and Cu^{2+}). ALD technique has shown potential in depositing Cu with different chemical states and the role Cu plays in photocatalytic CO_2 reduction has been proved important. It was found that $Cu_0/^+$ plays a major role in the achieving high photocatalytic activity, even higher than Ti^{3+} [262].

5.5.3. Supported bimetallic catalyst

Bimetallic nanoparticles are an important class of materials with properties higher than their monometallic form due to synergistic effects. Traditional techniques experienced difficulties in obtaining a precise size diameter and composition of the bimetallic structure. Without these conditions, the catalyst does not have potential degradation efficiency. To improve the morphology of the bimetallic catalyst, the materials should be compatible with each other's and the deposition conditions should be the same. Moreover, the second metal should selectively grow on the first one and not on the substrate. With modification of ALD parameter this structure is possible[263].

Assaud *et al.* reported the elaboration of well-defined Pd/Ni nanocatalysts grown by ALD for the electrooxidation of formic acid. The authors concluded that the oxidized Ni is a suitable substrate for three-dimensional growth of Pd islands. The Pd/Ni bimetallic systems demonstrates a high activity toward the electrooxidation reaction of formic acid and reaches the higher level for Pd(40 ALD cycles)/ Ni(1000 ALD cycles). Lower Pd content was supports a higher interaction between Pd and Ni because of the electronic effects between the alloyed Pd/Ni metals or because of the mass transport effect in 3D nanostructures. This explains the trend of higher peak current densities for the electrooxidation of formic acid at a lower Pd content in the Pd/Ni nanocatalysts[264]. Weber *et al.* successfully prepared a core-shell bimetallic structure with Pd and Pt (**Figure 1.** 26) [265].

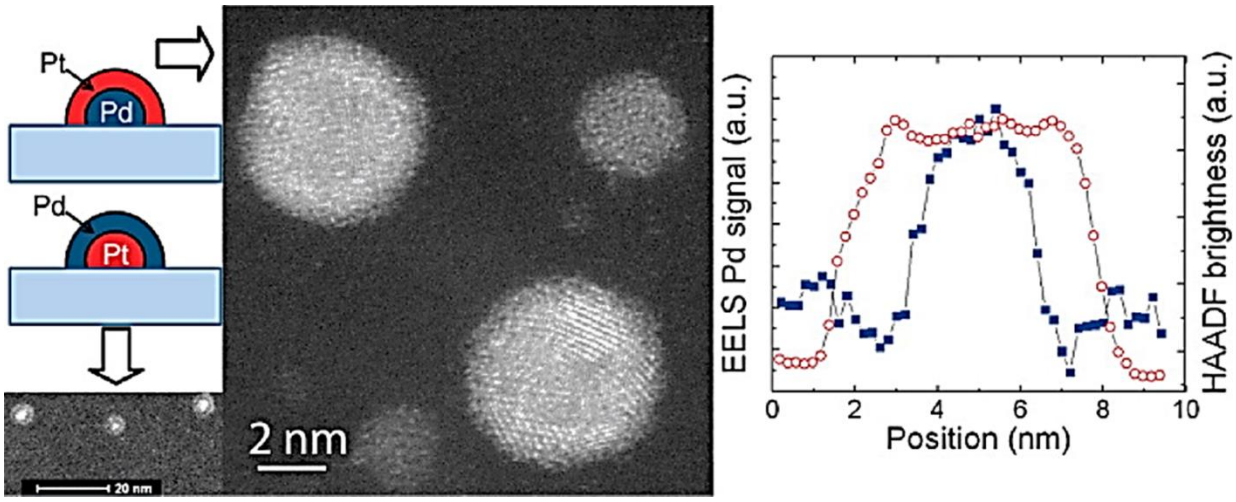

Figure 1. 26. Image representing the schematic formation of highly dispersed Pd/Pt and Pt/Pd nanoparticles)[265].

5.5.4. Selective area deposition

The use of selective area deposition in creating composite has shown a potential way to create 3D nanostructured catalyst. This technique allow the fabrication of different material structure such as core-shell structure, embedded deposition structures and discontinuous coating structures. The elaboration of these structures are possible by monitoring the parameter of ALD such as pressure, temperature, precursor or cycle number allow the [266–268]. For more details the reader is referred to another review on selective are deposition for elaboration of catalysts[232]. Due to its advantages, ALD can be applied to reveal the catalytic mechanism by deliberately designing catalysts with a clear structure, even in confined and synergetic environments.

- **Site selective decoration by ALD**

This technique allow the selective deposition of oxide films on sites of the catalyst. The addition of ALD oxide coating is used to introduce promoters on the catalyst surface. This will engender an increase in the heterojunction facet without completely coating the initial catalyst surface. TiO_2 was site selectively deposited on g-C_3N_4 nanosheets and the composite was used for dye degradation and hydrogen generation[269]. The authors found that increasing the number of ALD cycles generated a continuous film of TiO_2 that attenuated the reactivity of the catalyst. Hence, the optimal ALD condition was 35 cycles of TiO_2, where higher degradation efficiency and H_2 generation were found under visible light. This is due to the heterojunction created between TiO_2 and g-C_3N_4 that facilitates the separation of photo-generated charges and rapid transfer of the electrons to the surface of composite catalyst. Moreover, the activity of the synthesized material was compared between UV-Vis and Visible light (**Figure 1.27**). It was found that the catalyst react differently, since under UV light the TiO_2 will be excited and participate in the degradation step. This confirm that ALD plays a major role in tuning the structure of the material by a high control of the active sites to have suitable band positions and the maximum atom efficiency in the photocatalytic reactions.

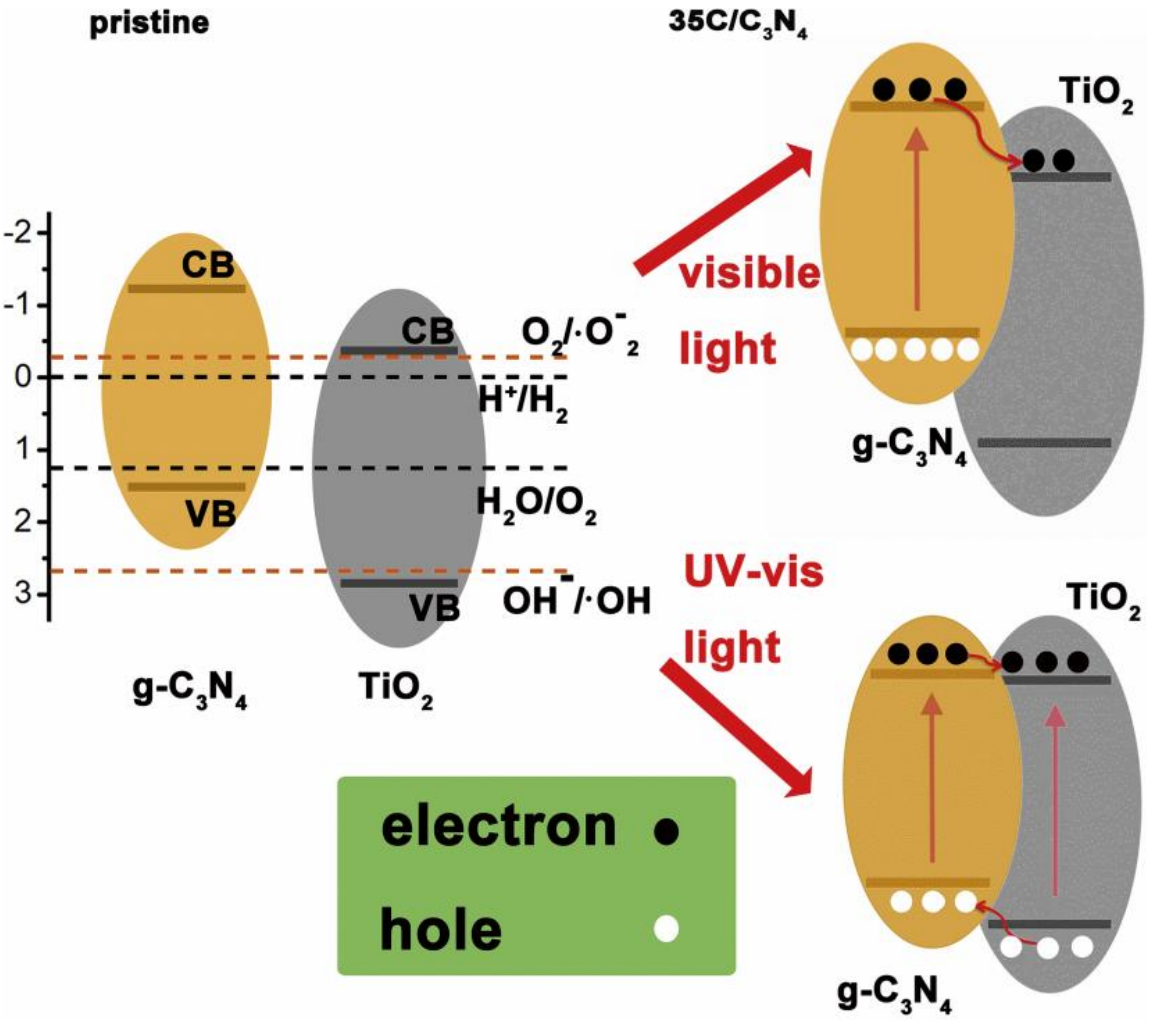

Figure 1.27. Schematic diagrams of the 35C/C3N4 involved in photocatalytic reactions using both visible light and UV–vis light[269].

- **Bimetallic alloy NPs**

By choosing the right precursor and co-reactant in the ALD process, Yang *et al.* reported the selective deposition of Pd on Au NPs in $BaZrO_3$/Au composites. SEM and TEM images confirm that the Pd nanoparticles are selectively deposited on Au nanoparticles, formatting Au-Pd, instead of depositing on $BaZrO_3$ surface. This mechanism is possible by tuning the ALD parameters with the choice of precursor and co-reactant used. The precursors used will be selectively adsorbed on the metal NPs. The increase of ALD cycle number increased the diameter of Pd NPs as well.

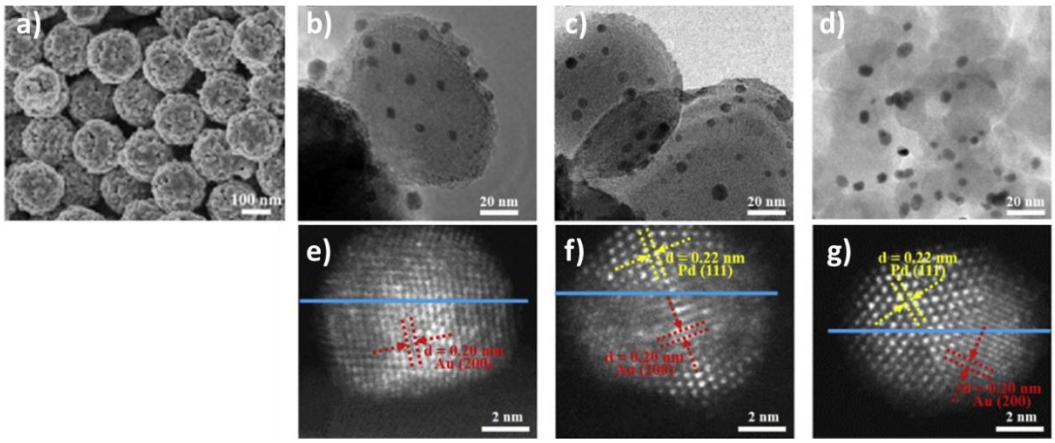

Figure 1.28. a)SEM image of $BaZO_3$ particles and HRTEM images of b-e)$BaZO_3$/Au, c-f) $BaZO_3$/Au/ Pd10c and d-g) $BaZO_3$/Au/Pd20c[270].

The photocatalytic performance of the synthesized catalyst was investigated by the degradation of RhB under UV irradiation. $BaZrO_3$/Au/Pd10c shows the higher degradation efficiency of RhB, with the complete removal of RhB after 90 min irradiation. The increase of the degradation efficiency of this photocatalyst was confirmed by the improvement of optical and electrochemical properties. The lower PL intensity, higher photocurrent and the increase in the separation of the photogenerated charges were assessed. It should be noted that when higher Pd NPs amount was deposited, the photodegradation was decreased. This finding confirms the ability of ALD to control the nanoparticles diameter in nm scale and moreover allows the tuning of the substrate properties by selective deposition of NPs leading to an increase of electron/hole separation under irradiation[270].

6. Conclusion and challenges

While the word is facing real water pollution crisis, the request for clean drinking water keep increasing. Organic pollutants have been detected in nearly all water resources (surface water, ground water, seawater) of many countries. These pollutants were also detected in drinking water, and their impact on human health have been investigated. Researches confirmed that conventional wastewater treatment plants are not able to remove these pollutants from water. In order to produce water of superior quality, new water treatment technologies have been addressed. Among these technologies, advanced oxidation processes

were widely investigated due to their low energy consumption and their high degradation efficiency.

Photocatalysis, known as an environmentally friendly technology, is based on photonic activation mode of catalyst instead of the thermal activation mechanism. The activation of a semiconductor in the presence of light, will generated electrons and holes that are directly involved in the degradation process. Titanium dioxide is one of the most promising photocatalysts for degradation of organic pollutants in water due to its high oxidizing ability, photostability and non-toxicity. Hence, this semiconductor possess low activity under visible light irradiation due to its large band gap and fast recombination of the photogenerated species. The band gap and photocatalytic activity of TiO_2 are highly influenced by the design and the morphology structure of the material. Doping TiO_2 with metals, non-metals and coupling with other semi-conductors exhibited a valid process for narrowing the band gap and demonstrated a more appropriate solution for extending the photocatalytic activity of TiO_2 into the visible region. Today different strategies for preparation and modification of TiO_2 were reported. Some of these techniques have limitations in the control of the internal and external surface of the catalyst. Moreover, the elaborated catalysts are not stable and could lose their photocatalytic activity after the first cycle.

The need for highly structured materials with high morphology control and stability, exhibit the development of new strategies for the preparation of semiconductor's catalysts. Moreover, the choice of the material support for immobilized catalysts is definitely important for improving the long-term stability of the catalyst. Membrane processes trend to be the technology of choice for many wastewater treatment applications. The combination of this process with photocatalysis seems to be very promoter. The main challenges in any membrane process is to avoid the membrane fouling. Activation of the membrane surface with a TiO_2 layer have proved to be an efficient way to reduce fouling and enhance the photocatalytic activity. Hence, the complex structure of membranes exhibit appropriate techniques for functionalization and modification not only the surface of the membrane but also the pores. To prevent membrane fouling caused by TiO_2 deposition, atomic layer deposition was recently nominated.

ALD has shown to be an effective technique to provide functionalized photocatalyst over the conventional methods. The well-structured monocatalyst or doped cocatalyst have shown higher degradation efficiency due to the precise control in the angstrom levels. ALD allow the synthetization of advanced catalyst with high separation of photogenerated carriers, higher stability and selectivity. Moreover, it allows the modification of an existing catalyst by doping with metal NPs, or coupling with other semi-conductor or deposition of a conformal active layer on the surface. It is also a very promising technique for immobilized catalyst on different substrates, especially membranes. Hence, the main challenge remains in upscaling ALD for preparation of catalysts, due to its higher costs regrading other techniques.

Finally, the use of these new-designed catalysts in real wastewater treatment is still missing. Without this application, the mechanism of degradation by photocatalysis and the fate of these pollutants will not be well recognized. The photocatalysis mechanism is affected by many parameters, not only the catalyst but also the concentration of the catalyst, the pollutant, the light intensity, the matrix etc. Hence, the comparison between different catalyst efficiencies is not possible yet and better degradation mechanism should be settled for the possibility of scaling-up these prepared catalysts.

7. Thesis objectives

The aim of this thesis is to synthesize highly active photocatalyst under visible light for degradation of organic pollutants. Model materials were elaborated by combining two major techniques electrospinning and Atomic layer Deposition. These model materials were used in order to understand the effect of modification of TiO_2 by doping with metals, non-metals and coupling with other semiconductors. First, we tried to understand two phenomena: the influence of the formation of heterostructure and/or doping on the separation of electron-holes by combining TiO_2 NFs with BN. Than the effect of combination of TiO_2 with metallic NPs on the band gap shifts was investigated after deposition of Pd NPs by ALD. In addition, the influence of TiO_2 morphologies on photocatalysis phenomena was also considered. We tried to understand the effect of the morphology of TiO_2 on the separation of the photogenerated carriers. Nanofibers elaborated by electrospinning were compared to nanotubes elaborated by ALD. The impact of these designs on the band gap shift and the separation of electron holes

was depicted by optical and electrochemical characterization techniques. Once, we understood the effect of TiO_2 morphology, we further modified the nanotubes with non-metal dopant (nitrogen). Several characterization techniques such as EIS, PL, UV-Vis diffuse reflectance, XPS, BET were used to determine the properties of these elaborated materials.

After the materials were optimized, photocatalysis experiments were performed on the degradation of pharmaceutical pollutant, acetaminophen, under light irradiation. The stability of the elaborated photocatalysts was also achieved. In addition, we tried to understand the degradation mechanism of ACT, as well as define the active species responsible of this degradation by performing scavengers tests. Finally, toxicity monitoring during the degradation was followed up to define the toxicity of the by-products formed after the decomposition of the parental molecule.

After optimizing the effect of the material design on the degradation using powder materials in suspension, we moved forward in our research and we tried to elaborate immobilized catalysts on ceramic membranes as support. Integrating the photocatalysts with membrane technology is significant, as the photocatalysts are used in continuous process which save the operation time and cost due to the elimination of additional separation step. In this work, we functionalized commercial ceramic membrane with coating TiO2 layers by ALD. The influence of TiO2 layer thickness on membrane permeability was investigated.

References

1. Manisalidis I, Stavropoulou E, Stavropoulos A, Bezirtzoglou E. Environmental and Health Impacts of Air Pollution: A Review. *Front Public Health*. 2020;8:14. doi:10.3389/fpubh.2020.00014

2. Briggs D. Environmental pollution and the global burden of disease. *Br Med Bull*. 2003;68(1):1-24. doi:10.1093/bmb/ldg019

3. Marshall AP, Willsey T, Reeves M, Amidon F, Miller S. Wetlands of the Mariana Islands. In: Goldstein MI, DellaSala DA, eds. *Encyclopedia of the World's Biomes*. Elsevier; 2020:295-315. doi:10.1016/B978-0-12-409548-9.12443-1

4. Barboza LGA, Cózar A, Gimenez BCG, Barros TL, Kershaw PJ, Guilhermino L. Chapter 17 - Macroplastics Pollution in the Marine Environment. In: Sheppard C, ed. *World Seas: An Environmental Evaluation (Second Edition)*. Academic Press; 2019:305-328. doi:10.1016/B978-0-12-805052-1.00019-X

5. Ma J, Hung H, Tian C, Kallenborn R. Revolatilization of persistent organic pollutants in the Arctic induced by climate change. *Nat Clim Change*. 2011;1(5):255-260. doi:10.1038/nclimate1167

6. Feng N-X, Yu J, Zhao H-M, et al. Efficient phytoremediation of organic contaminants in soils using plant–endophyte partnerships. *Sci Total Environ*. 2017;583:352-368. doi:10.1016/j.scitotenv.2017.01.075

7. Cindoruk SS, Sakin AE, Tasdemir Y. Levels of persistent organic pollutants in pine tree components and ambient air. *Environ Pollut*. 2020;256:113418. doi:10.1016/j.envpol.2019.113418

8. Pasquale Avino and Mario Vincenzo Russo*. A Comprehensive Review of Analytical Methods for Determining Persistent Organic Pollutants in Air, Soil, Water and Waste. *Curr Org Chem*. 2018;22(10):939-953. doi:10.2174/1385272822666180404144834

9. Awa SH, Hadibarata T. Removal of Heavy Metals in Contaminated Soil by Phytoremediation Mechanism: a Review. *Water Air Soil Pollut*. 2020;231(2):47. doi:10.1007/s11270-020-4426-0

10. Lee BXY, Hadibarata T, Yuniarto A. Phytoremediation Mechanisms in Air Pollution Control: a Review. *Water Air Soil Pollut*. 2020;231(8):437. doi:10.1007/s11270-020-04813-6

11. Wilson WE, Suh HH. Fine Particles and Coarse Particles: Concentration Relationships Relevant to Epidemiologic Studies. *J Air Waste Manag Assoc*. 1997;47(12):1238-1249. doi:10.1080/10473289.1997.10464074

12. Gupta N, Yadav KK, Kumar V, Kumar S, Chadd RP, Kumar A. Trace elements in soil-vegetables interface: Translocation, bioaccumulation, toxicity and amelioration - A review. *Sci Total Environ*. 2019;651:2927-2942. doi:10.1016/j.scitotenv.2018.10.047

13. McKone TE. Pollution, Soil. In: Wexler P, ed. *Encyclopedia of Toxicology (Second Edition)*. Elsevier; 2005:489-496. doi:10.1016/B0-12-369400-0/00781-X

14. Wang X, Sheng J, Gong P, Xue Y, Yao T, Jones KC. Persistent organic pollutants in the Tibetan surface soil: Spatial distribution, air–soil exchange and implications for global cycling. *Environ Pollut*. 2012;170:145-151. doi:10.1016/j.envpol.2012.06.012

15. Fu J, Mai B, Sheng G, et al. Persistent organic pollutants in environment of the Pearl River Delta, China: an overview. *Environ Public Health Manag*. 2003;52(9):1411-1422. doi:10.1016/S0045-6535(03)00477-6

16. Devi NL. Persistent Organic Pollutants (POPs): Environmental Risks, Toxicological Effects, and Bioremediation for Environmental Safety and Challenges for Future Research. In: Saxena G, Bharagava RN, eds. *Bioremediation of Industrial Waste for Environmental Safety: Volume I: Industrial Waste and Its Management*. Springer Singapore; 2020:53-76. doi:10.1007/978-981-13-1891-7_4

17. Nghiem LD, Fujioka T. Removal of emerging contaminants for water reuse by membrane technology. In: *Emerging Membrane Technology for Sustainable Water Treatment*. Elsevier Science Oxford; 2016:217-247.

18. Kim M-K, Zoh K-D. Occurrence and removals of micropollutants in water environment. *Environ Eng Res*. 2016;21(4):319-332.

19. Quesada HB, Baptista ATA, Cusioli LF, Seibert D, de Oliveira Bezerra C, Bergamasco R. Surface water pollution by pharmaceuticals and an alternative of removal by low-cost adsorbents: A review. *Chemosphere*. 2019;222:766-780. doi:10.1016/j.chemosphere.2019.02.009

20. Ukaogo PO, Ewuzie U, Onwuka CV. 21 - Environmental pollution: causes, effects, and the remedies. In: Chowdhary P, Raj A, Verma D, Akhter Y, eds. *Microorganisms for Sustainable Environment and Health*. Elsevier; 2020:419-429. doi:10.1016/B978-0-12-819001-2.00021-8

21. Stackelberg PE, Gibs J, Furlong ET, Meyer MT, Zaugg SD, Lippincott RL. Efficiency of conventional drinking-water-treatment processes in removal of pharmaceuticals and other organic compounds. *Sci Total Environ*. 2007;377(2):255-272. doi:10.1016/j.scitotenv.2007.01.095

22. Snyder SA, Westerhoff P, Yoon Y, Sedlak DL. Pharmaceuticals, personal care products, and endocrine disruptors in water: implications for the water industry. *Environ Eng Sci*. 2003;20(5):449-469.

23. Capdeville MJ, Budzinski H. Trace-level analysis of organic contaminants in drinking waters and groundwaters. *TrAC Trends Anal Chem*. 2011;30(4):586-606. doi:10.1016/j.trac.2010.12.006

24. Gibs J, Stackelberg PE, Furlong ET, Meyer M, Zaugg SD, Lippincott RL. Persistence of pharmaceuticals and other organic compounds in chlorinated drinking water as a

function of time. *Sci Total Environ*. 2007;373(1):240-249. doi:10.1016/j.scitotenv.2006.11.003

25. Faust SD, Aly OM. *Adsorption Processes for Water Treatment*. Elsevier; 2013.

26. Huschek G, Hansen PD, Maurer HH, Krengel D, Kayser A. Environmental risk assessment of medicinal products for human use according to European Commission recommendations. *Environ Toxicol Int J*. 2004;19(3):226-240.

27. Cahill JD, Furlong ET, Burkhardt MR, Kolpin D, Anderson LG. Determination of pharmaceutical compounds in surface- and ground-water samples by solid-phase extraction and high-performance liquid chromatography–electrospray ionization mass spectrometry. *J Chromatogr A*. 2004;1041(1):171-180. doi:10.1016/j.chroma.2004.04.005

28. Márta Z, Bobály B, Fekete J, Magda B, Imre T, Szabó PT. Simultaneous determination of ten nonsteroidal anti-inflammatory drugs from drinking water, surface water and wastewater using micro UHPLC-MS/MS with on-line SPE system. *J Pharm Biomed Anal*. 2018;160:99-108. doi:10.1016/j.jpba.2018.07.016

29. Tanwar S, Di Carro M, Magi E. Innovative sampling and extraction methods for the determination of nonsteroidal anti-inflammatory drugs in water. *SI Anal Approaches*. 2015;106:100-106. doi:10.1016/j.jpba.2014.10.027

30. Paíga P, Lolić A, Hellebuyck F, Santos LHMLM, Correia M, Delerue-Matos C. Development of a SPE–UHPLC–MS/MS methodology for the determination of non-steroidal anti-inflammatory and analgesic pharmaceuticals in seawater. *SI Anal Approaches*. 2015;106:61-70. doi:10.1016/j.jpba.2014.06.017

31. Paíga P, Santos LHMLM, Delerue-Matos C. Development of a multi-residue method for the determination of human and veterinary pharmaceuticals and some of their metabolites in aqueous environmental matrices by SPE-UHPLC–MS/MS. *J Pharm Biomed Anal*. 2017;135:75-86. doi:10.1016/j.jpba.2016.12.013

32. Fent K, Weston AA, Caminada D. Ecotoxicology of human pharmaceuticals. *Aquat Toxicol*. 2006;76(2):122-159. doi:10.1016/j.aquatox.2005.09.009

33. Roberts PH, Thomas KV. The occurrence of selected pharmaceuticals in wastewater effluent and surface waters of the lower Tyne catchment. *Sci Total Environ*. 2006;356(1):143-153. doi:10.1016/j.scitotenv.2005.04.031

34. Quintana JB, Weiss S, Reemtsma T. Pathways and metabolites of microbial degradation of selected acidic pharmaceutical and their occurrence in municipal wastewater treated by a membrane bioreactor. *Water Res*. 2005;39(12):2654-2664.

35. Klatte S, Schaefer H-C, Hempel M. Pharmaceuticals in the environment – A short review on options to minimize the exposure of humans, animals and ecosystems. *Sustain Chem Pharm*. 2017;5:61-66. doi:10.1016/j.scp.2016.07.001

36. Tanoue R, Nomiyama K, Nakamura H, et al. Uptake and Tissue Distribution of Pharmaceuticals and Personal Care Products in Wild Fish from Treated-Wastewater-Impacted Streams. *Environ Sci Technol*. 2015;49(19):11649-11658. doi:10.1021/acs.est.5b02478

37. Ternes TA. Occurrence of drugs in German sewage treatment plants and rivers. *Water Res*. 1998;32(11):3245-3260.

38. Kolpin DW, Furlong ET, Meyer MT, et al. Pharmaceuticals, hormones, and other organic wastewater contaminants in US streams, 1999− 2000: A national reconnaissance. *Environ Sci Technol*. 2002;36(6):1202-1211.

39. Thacker PD. Pharmaceutical data elude researchers. *Environ Sci Technol*. 2005;39(9):193A-194A.

40. Calamari D, Zuccato E, Castiglioni S, Bagnati R, Fanelli R. Strategic survey of therapeutic drugs in the rivers Po and Lambro in northern Italy. *Environ Sci Technol*. 2003;37(7):1241-1248.

41. Vystavna Y, Le Coustumer P, Huneau F. Monitoring of trace metals and pharmaceuticals as anthropogenic and socio-economic indicators of urban and industrial impact on surface waters. *Environ Monit Assess*. 2013;185(4):3581-3601.

42. Vulliet E, Cren-Olivé C. Screening of pharmaceuticals and hormones at the regional scale, in surface and groundwaters intended to human consumption. *Environ Pollut*. 2011;159(10):2929-2934.

43. Yamamoto H, Nakamura Y, Moriguchi S, et al. Persistence and partitioning of eight selected pharmaceuticals in the aquatic environment: laboratory photolysis, biodegradation, and sorption experiments. *Water Res*. 2009;43(2):351-362.

44. Grujić S, Vasiljević T, Laušević M. Determination of multiple pharmaceutical classes in surface and ground waters by liquid chromatography–ion trap–tandem mass spectrometry. *J Chromatogr A*. 2009;1216(25):4989-5000.

45. Choi K, Kim Y, Park J, et al. Seasonal variations of several pharmaceutical residues in surface water and sewage treatment plants of Han River, Korea. *Sci Total Environ*. 2008;405(1-3):120-128.

46. Kim SD, Cho J, Kim IS, Vanderford BJ, Snyder SA. Occurrence and removal of pharmaceuticals and endocrine disruptors in South Korean surface, drinking, and waste waters. *Water Res*. 2007;41(5):1013-1021.

47. Gómez MJ, Bueno MM, Lacorte S, Fernández-Alba AR, Agüera A. Pilot survey monitoring pharmaceuticals and related compounds in a sewage treatment plant located on the Mediterranean coast. *Chemosphere*. 2007;66(6):993-1002.

48. Barnes KK, Kolpin DW, Furlong ET, Zaugg SD, Meyer MT, Barber LB. A national reconnaissance of pharmaceuticals and other organic wastewater contaminants in the United States—I) Groundwater. *Sci Total Environ*. 2008;402(2-3):192-200.

49. Lin AY-C, Tsai Y-T. Occurrence of pharmaceuticals in Taiwan's surface waters: Impact of waste streams from hospitals and pharmaceutical production facilities. *Sci Total Environ*. 2009;407(12):3793-3802.

50. Celle-Jeanton H, Schemberg D, Mohammed N, et al. Evaluation of pharmaceuticals in surface water: Reliability of PECs compared to MECs. *Environ Int*. 2014;73:10-21. doi:10.1016/j.envint.2014.06.015

51. Togola A, Budzinski H. Multi-residue analysis of pharmaceutical compounds in aqueous samples. *J Chromatogr A*. 2008;1177(1):150-158. doi:10.1016/j.chroma.2007.10.105

52. Bratby J. Coagulation and Flocculation in Water and Wastewater Treatment - Second Edition. *Water Intell Online*. 2006;5. doi:10.2166/9781780402321

53. grégorio C. Non-Conventional Low-Cost Adsorbents for Dye Removal: A Review. *Bioresour Technol*. 2006;97:1061-1085. doi:10.1016/j.biortech.2005.05.001

54. grégorio C, Lichtfouse E. Wastewater Treatment: An Overview. In: ; 2018:1-21. doi:10.1007/978-3-319-92111-2_1

55. Jackson RB, Carpenter SR, Dahm CN, et al. WATER IN A CHANGING WORLD. *Ecol Appl*. 2001;11(4):1027-1045. doi:https://doi.org/10.1890/1051-0761(2001)011[1027:WIACW]2.0.CO;2

56. Sonune A, Ghate R. Developments in Wastewater Treatment Methods. *Desalination*. 2004;167:55-63. doi:10.1016/j.desal.2004.06.113

57. Villaescusa I, Fiol N, Poch J, Bianchi A, Bazzicalupi C. Mechanism of paracetamol removal by vegetable wastes: The contribution of π–π interactions, hydrogen bonding and hydrophobic effect. *Desalination*. 2011;270(1):135-142. doi:10.1016/j.desal.2010.11.037

58. Baccar R, Sarrà M, Bouzid J, Feki M, Blánquez P. Removal of pharmaceutical compounds by activated carbon prepared from agricultural by-product. *Chem Eng J*. 2012;211-212:310-317. doi:10.1016/j.cej.2012.09.099

59. Domínguez JR, González T, Palo P, Cuerda-Correa EM. Removal of common pharmaceuticals present in surface waters by Amberlite XAD-7 acrylic-ester-resin: Influence of pH and presence of other drugs. *Desalination*. 2011;269(1-3):231-238.

60. Barakat M. New Trends in Removing Heavy Metals from Industrial Wastewater. *Arab J Chem*. 2011;4:361-377. doi:10.1016/j.arabjc.2010.07.019

61. Nam S-W, Jo B-I, Yoon Y, Zoh K-D. Occurrence and removal of selected micropollutants in a water treatment plant. *Chemosphere*. 2014;95:156-165. doi:10.1016/j.chemosphere.2013.08.055

62. Trinh TK, Kang LS. Response surface methodological approach to optimize the coagulation–flocculation process in drinking water treatment. *Chem Eng Res Des*. 2011;89(7):1126-1135. doi:10.1016/j.cherd.2010.12.004

63. Wu Y-F, Liu W, Gao N-Y, Tao T. A study of titanium sulfate flocculation for water treatment. *Water Res*. 2011;45(12):3704-3711. doi:10.1016/j.watres.2011.04.023

64. Nasrollahzadeh M, Sajjadi M, Iravani S, Varma RS. Carbon-based sustainable nanomaterials for water treatment: State-of-art and future perspectives. *Chemosphere*. 2021;263:128005. doi:10.1016/j.chemosphere.2020.128005

65. Chenab KK, Sohrabi B, Jafari A, Ramakrishna S. Water treatment: functional nanomaterials and applications from adsorption to photodegradation. *Mater Today Chem*. 2020;16:100262. doi:10.1016/j.mtchem.2020.100262

66. Ali S, Rehman SAU, Luan H-Y, Farid MU, Huang H. Challenges and opportunities in functional carbon nanotubes for membrane-based water treatment and desalination. *Sci Total Environ*. 2019;646:1126-1139. doi:10.1016/j.scitotenv.2018.07.348

67. Banerjee A, Ray A. 13 - A survey of adsorption process parameter optimization related to degradation of environmental pollutants. In: Bhattacharyya S, Mondal NK, Platos J, Snášel V, Krömer P, eds. *Intelligent Environmental Data Monitoring for Pollution Management*. Academic Press; 2021:289-309. doi:10.1016/B978-0-12-819671-7.00013-0

68. Garcia-Segura S, Nienhauser AB, Fajardo AS, et al. Disparities between experimental and environmental conditions: Research steps toward making electrochemical water treatment a reality. *Environ Electrochem ● Phys Nano Electrochem*. 2020;22:9-16. doi:10.1016/j.coelec.2020.03.001

69. Mompelat S, Le Bot B, Thomas O. Occurrence and fate of pharmaceutical products and by-products, from resource to drinking water. *Environ Int*. 2009;35(5):803-814.

70. Tran NH, Reinhard M, Gin KY-H. Occurrence and fate of emerging contaminants in municipal wastewater treatment plants from different geographical regions-a review. *Water Res*. 2018;133:182-207.

71. Luiz D, Silva G, Vaz E, José H, Moreira R. Evaluation of hybrid treatments to produce high quality reuse water. *Water Sci Technol*. 2011;63(9):2046-2051.

72. Oller I, Malato S, Sánchez-Pérez Ja. Combination of advanced oxidation processes and biological treatments for wastewater decontamination—a review. *Sci Total Environ*. 2011;409(20):4141-4166.

73. Stasinakis A. Use of selected advanced oxidation processes (AOPs) for wastewater treatment–a mini review. *Glob NEST J*. 2008;10(3):376-385.

74. Ikehata K, Jodeiri Naghashkar N, Gamal El-Din M. Degradation of Aqueous Pharmaceuticals by Ozonation and Advanced Oxidation Processes: A Review. *Ozone Sci Eng*. 2006;28(6):353-414. doi:10.1080/01919510600985937

75. Kasprzyk-Hordern B, Dinsdale RM, Guwy AJ. The removal of pharmaceuticals, personal care products, endocrine disruptors and illicit drugs during wastewater treatment and its impact on the quality of receiving waters. *Water Res*. 2009;43(2):363-380.

76. Fast SA, Gude VG, Truax DD, Martin J, Magbanua BS. A critical evaluation of advanced oxidation processes for emerging contaminants removal. *Environ Process*. 2017;4(1):283-302.

77. Moreira FC, Boaventura RAR, Brillas E, Vilar VJP. Electrochemical advanced oxidation processes: A review on their application to synthetic and real wastewaters. *Appl Catal B Environ*. 2017;202:217-261. doi:10.1016/j.apcatb.2016.08.037

78. Panizza M, Cerisola G. Direct and mediated anodic oxidation of organic pollutants. *Chem Rev*. 2009;109(12):6541-6569.

79. Martinez-Huitle CA, Ferro S. Electrochemical oxidation of organic pollutants for the wastewater treatment: direct and indirect processes. *Chem Soc Rev*. 2006;35(12):1324-1340.

80. Miklos DB, Remy C, Jekel M, Linden KG, Drewes JE, Hübner U. Evaluation of advanced oxidation processes for water and wastewater treatment – A critical review. *Water Res*. 2018;139:118-131. doi:10.1016/j.watres.2018.03.042

81. Brillas E, Sirés I, Arias C, et al. Mineralization of paracetamol in aqueous medium by anodic oxidation with a boron-doped diamond electrode. *Chemosphere*. 2005;58(4):399-406.

82. Torres R, Abdelmalek F, Combet E, Pétrier C, Pulgarin C. A comparative study of ultrasonic cavitation and Fenton's reagent for bisphenol A degradation in deionised and natural waters. *J Hazard Mater*. 2007;146(3):546-551.

83. Oturan MA, Aaron J-J. Advanced Oxidation Processes in Water/Wastewater Treatment: Principles and Applications. A Review. *Crit Rev Environ Sci Technol*. 2014;44(23):2577-2641. doi:10.1080/10643389.2013.829765

84. Bo L, Quan X, Chen S, Zhao H, Zhao Y. Degradation of p-nitrophenol in aqueous solution by microwave assisted oxidation process through a granular activated carbon fixed bed. *Water Res*. 2006;40(16):3061-3068.

85. Jabbari F, Eslami A, Mahmoudian J. Degradation of Diclofenac in Water Using the O_3/UV/S_2O_8 Advanced Oxidation Process. *Health Scope*. 2020;9(2):e99436. doi:10.5812/jhealthscope.99436

86. Chavoshan S, Khodadadi M, Nasseh N. Photocatalytic degradation of penicillin G from simulated wastewater using the UV/ZnO process: isotherm and kinetic study. *J Environ Health Sci Eng*. 2020;18(1):107.

87. Reisz E, Schmidt W, Schuchmann H-P, von Sonntag C. Photolysis of ozone in aqueous solutions in the presence of tertiary butanol. *Environ Sci Technol*. 2003;37(9):1941-1948.

88. Wardenier N, Liu Z, Nikiforov A, Van Hulle SWH, Leys C. Micropollutant elimination by O3, UV and plasma-based AOPs: An evaluation of treatment and energy costs. *Chemosphere*. 2019;234:715-724. doi:10.1016/j.chemosphere.2019.06.033

89. Rahim Pouran S, Abdul Aziz AR, Wan Daud WMA. Review on the main advances in photo-Fenton oxidation system for recalcitrant wastewaters. *J Ind Eng Chem*. 2015;21:53-69. doi:10.1016/j.jiec.2014.05.005

90. Sayed M, Khan JA, Shah LA, et al. Degradation of quinolone antibiotic, norfloxacin, in aqueous solution using gamma-ray irradiation. *Environ Sci Pollut Res*. 2016;23(13):13155-13168.

91. Alaton IA, Dogruel S, Baykal E, Gerone G. Combined chemical and biological oxidation of penicillin formulation effluent. *J Environ Manage*. 2004;73(2):155-163.

92. Andreozzi R, Caprio V, Marotta R, Vogna D. Paracetamol oxidation from aqueous solutions by means of ozonation and H2O2/UV system. *Water Res*. 2003;37(5):993-1004.

93. Deng J, Shao Y, Gao N, et al. Degradation of the antiepileptic drug carbamazepine upon different UV-based advanced oxidation processes in water. *Chem Eng J*. 2013;222:150-158.

94. Vogna D, Marotta R, Andreozzi R, Napolitano A, d'Ischia M. Kinetic and chemical assessment of the UV/H2O2 treatment of antiepileptic drug carbamazepine. *Chemosphere*. 2004;54(4):497-505. doi:10.1016/S0045-6535(03)00757-4

95. Yacouba ZA, Mendret J, Lesage G, Zaviska F, Brosillon S. Removal of organic micropollutants from domestic wastewater: The effect of ozone-based advanced oxidation process on nanofiltration. *J Water Process Eng*. 2021;39:101869. doi:10.1016/j.jwpe.2020.101869

96. Tijani JO, Fatoba OO, Madzivire G, Petrik LF. A Review of Combined Advanced Oxidation Technologies for the Removal of Organic Pollutants from Water. *Water Air Soil Pollut*. 2014;225(9):2102. doi:10.1007/s11270-014-2102-y

97. Urtiaga A, Rueda A, Anglada Á, Ortiz I. Integrated treatment of landfill leachates including electrooxidation at pilot plant scale. *J Hazard Mater*. 2009;166(2-3):1530-1534.

98. Zaviska F, Drogui P, Mercier G, Blais J-F. Procédés d'oxydation avancée dans le traitement des eaux et des effluents industriels: Application à la dégradation des polluants réfractaires. *Rev Sci EauJournal Water Sci*. 2009;22(4):535-564.

99. Li D, Shi W. Recent developments in visible-light photocatalytic degradation of antibiotics. *Chin J Catal*. 2016;37(6):792-799.

100. Long Z, Li Q, Wei T, Zhang G, Ren Z. Historical development and prospects of photocatalysts for pollutant removal in water. *J Hazard Mater*. 2020;395:122599. doi:10.1016/j.jhazmat.2020.122599

101. Natarajan S, Bajaj HC, Tayade RJ. Recent advances based on the synergetic effect of adsorption for removal of dyes from waste water using photocatalytic process. *J Environ Sci*. 2018;65:201-222. doi:10.1016/j.jes.2017.03.011

102. Poursani AS, Nilchi A, Hassani A, Shariat SM, Nouri J. The synthesis of nano TiO 2 and its use for removal of lead ions from aqueous solution. *J Water Resour Prot*. 2016;8(04):438.

103. Ani I, Akpan U, Olutoye M, Hameed B. Photocatalytic degradation of pollutants in petroleum refinery wastewater by TiO2-and ZnO-based photocatalysts: recent development. *J Clean Prod*. 2018;205:930-954.

104. Eslami A, Amini MM, Yazdanbakhsh AR, Mohseni-Bandpei A, Safari AA, Asadi A. N, S co-doped TiO2 nanoparticles and nanosheets in simulated solar light for photocatalytic degradation of non-steroidal anti-inflammatory drugs in water: a comparative study. *J Chem Technol Biotechnol*. 2016;91(10):2693-2704.

105. Herrmann J-M. Heterogeneous photocatalysis: fundamentals and applications to the removal of various types of aqueous pollutants. *Catal Today*. 1999;53(1):115-129. doi:10.1016/S0920-5861(99)00107-8

106. Wankhade Atul V, Gaikwad G, Dhonde M, Khaty N, Thakare S. Removal of organic pollutant from water by heterogenous photocatalysis: a review. *Res J Chem Env*. 2013;17:84-94.

107. Rauf MA, Ashraf SS. Fundamental principles and application of heterogeneous photocatalytic degradation of dyes in solution. *Chem Eng J*. 2009;151(1):10-18. doi:10.1016/j.cej.2009.02.026

108. Machado AEH, de Miranda JA, de Freitas RF, et al. Destruction of the organic matter present in effluent from a cellulose and paper industry using photocatalysis. *J Photochem Photobiol Chem*. 2003;155(1-3):231-241.

109. Nasr M, Viter R, Eid C, Habchi R, Miele P, Bechelany M. Enhanced photocatalytic performance of novel electrospun BN/TiO2 composite nanofibers. *New J Chem*. 2017;41(1):81-89. doi:10.1039/C6NJ03088B

110. Serpone N, Emeline AV. Suggested terms and definitions in photocatalysis and radiocatalysis. *Int J Photoenergy*. 1900;4:943970. doi:10.1155/S1110662X02000144

111. Wen J, Xie J, Chen X, Li X. A review on g-C3N4-based photocatalysts. *2nd Int Symp Energy Environ Photocatalytic Mater*. 2017;391:72-123. doi:10.1016/j.apsusc.2016.07.030

112. Kuzhalosai V, Subash B, Shanthi M. A novel sunshine active cerium loaded zinc oxide photocatalyst for the effective degradation of AR 27 dye. *Mater Sci Semicond Process*. 2014;27:924-933.

113. Qi K, Cheng B, Yu J, Ho W. Review on the improvement of the photocatalytic and antibacterial activities of ZnO. *J Alloys Compd*. 2017;727:792-820.

114. Ibrahim NS, Leaw WL, Mohamad D, Alias SH, Nur H. A critical review of metal-doped TiO2 and its structure–physical properties–photocatalytic activity relationship in hydrogen production. *Int J Hydrog Energy*. Published online 2020.

115. Thi VH-T, Lee B-K. Effective photocatalytic degradation of paracetamol using La-doped ZnO photocatalyst under visible light irradiation. *Proc Int Conf Adv Funct Mater AFM 2016*. 2017;96:171-182. doi:10.1016/j.materresbull.2017.04.028

116. Yang L, Yu LE, Ray MB. Photocatalytic Oxidation of Paracetamol: Dominant Reactants, Intermediates, and Reaction Mechanisms. *Environ Sci Technol*. 2009;43(2):460-465. doi:10.1021/es8020099

117. Rostami M, Zamani RM, Aghajanzadeh KM, Danafar H. Sol–gel synthesis and characterization of zinc ferrite–graphene nano-hybrids for photo-catalytic degradation of the paracetamol. *J Pharm Investig*. 2018;48(6):657-664. doi:10.1007/s40005-017-0362-4

118. Nasr M, Eid C, Habchi R, Miele P, Bechelany M. Recent Progress on Titanium Dioxide Nanomaterials for Photocatalytic Applications. *ChemSusChem*. 2018;11(18):3023-3047. doi:10.1002/cssc.201800874

119. Al-Mamun M, Kader S, Islam M, Khan M. Photocatalytic activity improvement and application of UV-TiO2 photocatalysis in textile wastewater treatment: A review. *J Environ Chem Eng*. 2019;7(5):103248.

120. Daghrir R, Drogui P, Robert D. Modified TiO2 for environmental photocatalytic applications: a review. *Ind Eng Chem Res*. 2013;52(10):3581-3599.

121. Shayegan Z, Lee C-S, Haghighat F. TiO2 photocatalyst for removal of volatile organic compounds in gas phase–A review. *Chem Eng J*. 2018;334:2408-2439.

122. Lee S-Y, Park S-J. TiO2 photocatalyst for water treatment applications. *J Ind Eng Chem*. 2013;19(6):1761-1769.

123. Namshah KS, Mohamed RM. WO3–TiO2 nanocomposites for paracetamol degradation under visible light. *Appl Nanosci*. 2018;8(8):2021-2030. doi:10.1007/s13204-018-0888-4

124. Bhanvase BA, Shende TP, Sonawane SH. A review on graphene–TiO2 and doped graphene–TiO2 nanocomposite photocatalyst for water and wastewater treatment. *Environ Technol Rev*. 2017;6(1):1-14. doi:10.1080/21622515.2016.1264489

125. Shen HL, Hu HH, Liang DY, et al. Effect of calcination temperature on the microstructure, crystallinity and photocatalytic activity of TiO2 hollow spheres. *J Alloys Compd*. 2012;542:32-36. doi:10.1016/j.jallcom.2012.07.080

126. Jin C, Park S, Kim H, Lee C. Ultrasensitive multiple networked Ga2O3-core/ZnO-shell nanorod gas sensors. *Sens Actuators B Chem*. 2012;161(1):223-228. doi:https://doi.org/10.1016/j.snb.2011.10.023

127. Gopinath KP, Madhav NV, Krishnan A, Malolan R, Rangarajan G. Present applications of titanium dioxide for the photocatalytic removal of pollutants from water: A review. *J Environ Manage*. 2020;270:110906. doi:10.1016/j.jenvman.2020.110906

128. Thomas J, Yoon M. Facile synthesis of pure TiO2 (B) nanofibers doped with gold nanoparticles and solar photocatalytic activities. *Appl Catal B Environ*. 2012;111\112:502-508. doi:10.1016/j.apcatb.2011.10.039

129. Nguyen CH, Fu C-C, Juang R-S. Degradation of methylene blue and methyl orange by palladium-doped TiO2 photocatalysis for water reuse: Efficiency and degradation pathways. *J Clean Prod*. 2018;202:413-427. doi:10.1016/j.jclepro.2018.08.110

130. Banerjee AN, Hamnabard N, Joo SW. A comparative study of the effect of Pd-doping on the structural, optical, and photocatalytic properties of sol–gel derived anatase TiO2 nanoparticles. *Ceram Int*. 2016;42(10):12010-12026. doi:10.1016/j.ceramint.2016.04.128

131. Mohapatra SK, Kondamudi N, Banerjee S, Misra M. Functionalization of Self-Organized TiO2 Nanotubes with Pd Nanoparticles for Photocatalytic Decomposition of Dyes under Solar Light Illumination. *Langmuir*. 2008;24(19):11276-11281. doi:10.1021/la801253f

132. Singh J, Tripathi N, Mohapatra S. Synthesis of Ag–TiO2 hybrid nanoparticles with enhanced photocatalytic activity by a facile wet chemical method. *Nano-Struct Nano-Objects*. 2019;18:100266. doi:10.1016/j.nanoso.2019.100266

133. Długokęcka M, Łuczak J, Polkowska Ż, Zaleska-Medynska A. The effect of microemulsion composition on the morphology of Pd nanoparticles deposited at the surface of TiO2 and photoactivity of Pd-TiO2. *Appl Surf Sci*. 2017;405:220-230. doi:10.1016/j.apsusc.2017.02.014

134. Yilmaz P, Lacerda AM, Larrosa I, Dunn S. Photoelectrocatalysis of Rhodamine B and Solar Hydrogen Production by TiO2 and Pd/TiO2 Catalyst Systems. *Electrochimica Acta*. 2017;231:641-649. doi:10.1016/j.electacta.2017.02.035

135. Santos LM, Machado WA, França MD, et al. Structural characterization of Ag-doped TiO 2 with enhanced photocatalytic activity. *RSC Adv*. 2015;5(125):103752-103759.

136. Lopes FCSMR, da Rocha M da GC, Bargiela P, Sousa Ferreira H, Pires CA de M. Ag/TiO2 photocatalyst immobilized onto modified natural fibers for photodegradation of anthracene. *Chem Eng Sci*. 2020;227:115939. doi:10.1016/j.ces.2020.115939

137. Xiang Q, Yu J, Wang W, Jaroniec M. Nitrogen self-doped nanosized TiO2 sheets with exposed 001 facets for enhanced visible-light photocatalytic activity. *Chem Commun*. 2011;47(24):6906-6908. doi:10.1039/C1CC11740H

138. Jin C, Zheng R, Guo Y, Xie J, Zhu Y, Xie Y. Hydrothermal synthesis and characterization of phosphorous-doped TiO2 with high photocatalytic activity for methylene blue degradation. *J Mol Catal Chem*. 2009;313(1-2):44-48.

139. Xu J, Ao Y, Chen M, Fu D. Low-temperature preparation of Boron-doped titania by hydrothermal method and its photocatalytic activity. *J Alloys Compd*. 2009;484(1-2):73-79.

140. Liu Q, Guo Y, Chen Z, Zhang Z, Fang X. Constructing a novel ternary Fe(III)/graphene/g-C3N4 composite photocatalyst with enhanced visible-light driven photocatalytic activity via interfacial charge transfer effect. *Appl Catal B Environ*. 2016;183:231-241. doi:10.1016/j.apcatb.2015.10.054

141. Liu W, Shen J, Yang X, Liu Q, Tang H. Dual Z-scheme g-C3N4/Ag3PO4/Ag2MoO4 ternary composite photocatalyst for solar oxygen evolution from water splitting. *Appl Surf Sci*. 2018;456:369-378. doi:10.1016/j.apsusc.2018.06.156

142. Zhang X, Wang C, Yu C, et al. Application of Ag/AgBr/GdVO4 composite photocatalyst in wastewater treatment. *J Environ Sci*. 2018;63:68-75. doi:10.1016/j.jes.2017.06.020

143. Zhang W, Li R, Yang B. Porous TiO2-Al2O3 composite photocatalyst prepared by sol-gel method: the role of calcination temperature. *Nanosci Nanotechnol-Asia*. 2012;2(1):59-65.

144. Jiao J, Xu Q, Li L. Porous TiO2/SiO2 composite prepared using PEG as template direction reagent with assistance of supercritical CO2. *J Colloid Interface Sci*. 2007;316(2):596-603.

145. Neppolian B, Wang Q, Yamashita H, Choi H. Synthesis and characterization of ZrO 2–TiO 2 binary oxide semiconductor nanoparticles: Application and interparticle electron transfer process. *Appl Catal -Gen - APPL CATAL -GEN*. 2007;333:264-271. doi:10.1016/j.apcata.2007.09.026

146. Singh B, kaur G, Singh P, et al. Nanostructured BN–TiO2 composite with ultra-high photocatalytic activity. *New J Chem*. 2017;41(20):11640-11646. doi:10.1039/C7NJ02509B

147. Luna AL, Dragoe D, Wang K, et al. Photocatalytic Hydrogen Evolution Using Ni–Pd/TiO2: Correlation of Light Absorption, Charge-Carrier Dynamics, and Quantum Efficiency. *J Phys Chem C*. 2017;121(26):14302-14311. doi:10.1021/acs.jpcc.7b01167

148. Teixeira S, Mora H, Blasse L-M, et al. Photocatalytic degradation of recalcitrant micropollutants by reusable Fe3O4/SiO2/TiO2 particles. *J Photochem Photobiol Chem*. 2017;345:27-35. doi:10.1016/j.jphotochem.2017.05.024

149. Abbasi-Asl H, Sabzehmeidani MM, Ghaedi M. Efficient degradation of metronidazole antibiotic by TiO2/Ag3PO4/g–C3N4 ternary composite photocatalyst in a continuous flow-loop photoreactor. *J Environ Chem Eng*. 2021;9(5):105963. doi:10.1016/j.jece.2021.105963

150. Pham T-D, Lee B-K. Selective removal of polar VOCs by novel photocatalytic activity of metals co-doped TiO2/PU under visible light. *Chem Eng J*. 2017;307:63-73. doi:10.1016/j.cej.2016.08.068

151. Gao W, Zhang X, Su X, et al. Construction of bimetallic Pd-Ag enhanced AgBr/TiO2 hierarchical nanostructured photocatalytic hybrid capillary tubes and devices for continuous photocatalytic degradation of VOCs. *Chem Eng J*. 2018;346:77-84. doi:10.1016/j.cej.2018.04.017

152. Zhang C, Liu F, Zhai Y, et al. Alkali-Metal-Promoted Pt/TiO2 Opens a More Efficient Pathway to Formaldehyde Oxidation at Ambient Temperatures. *Angew Chem Int Ed*. 2012;51(38):9628-9632. doi:10.1002/anie.201202034

153. Dong F, Wang H, Wu Z, Qiu J. Marked enhancement of photocatalytic activity and photochemical stability of N–doped TiO2 nanocrystals by Fe3+/Fe2+ surface modification. *J Colloid Interface Sci*. 2010;343(1):200-208. doi:10.1016/j.jcis.2009.11.012

154. Lozano-Morales SA, Morales G, López Zavala MÁ, Arce-Sarria A, Machuca-Martínez F. Photocatalytic Treatment of Paracetamol Using TiO2 Nanotubes: Effect of pH. *Processes*. 2019;7(6). doi:10.3390/pr7060319

155. Castilla-Caballero D, Machuca-Martínez F, Bustillo-Lecompte C, Colina-Márquez J. Photocatalytic Degradation of Commercial Acetaminophen: Evaluation, Modeling, and Scaling-Up of Photoreactors. *Catalysts*. 2018;8(5). doi:10.3390/catal8050179

156. Sakthivel S, Neppolian B, Shankar MV, Arabindoo B, Palanichamy M, Murugesan V. Solar photocatalytic degradation of azo dye: comparison of photocatalytic efficiency of ZnO and TiO2. *Sol Energy Mater Sol Cells*. 2003;77(1):65-82. doi:10.1016/S0927-0248(02)00255-6

157. Elaziouti A, Ahmed B. ZnO-assisted photocatalytic degradation of congo Red and benzopurpurine 4B in aqueous solution. *J Chem Eng Process Technol*. 2011;2:1-9.

158. Bagheri S, TermehYousefi A, Do T-O. Photocatalytic pathway toward degradation of environmental pharmaceutical pollutants: structure, kinetics and mechanism approach. *Catal Sci Technol*. 2017;7(20):4548-4569. doi:10.1039/C7CY00468K

159. Chun H, Yizhong W, Hongxiao T. Destruction of phenol aqueous solution by photocatalysis or direct photolysis. *Chemosphere*. 2000;41(8):1205-1209. doi:10.1016/S0045-6535(99)00539-1

160. Xu Z, Meng X. Size effects of nanocrystalline TiO2 on As(V) and As(III) adsorption and As(III) photooxidation. *J Hazard Mater*. 2009;168(2):747-752. doi:10.1016/j.jhazmat.2009.02.084

161. Nakata K, Fujishima A. TiO2 photocatalysis: Design and applications. *J Photochem Photobiol C Photochem Rev*. 2012;13(3):169-189. doi:10.1016/j.jphotochemrev.2012.06.001

162. Wu Y, Yu J, Liu H-M, Xu B-Q. One-Dimensional TiO2 Nanomaterials: Preparation and Catalytic Applications. *J Nanosci Nanotechnol*. 2010;10(10):6707-6719. doi:10.1166/jnn.2010.2531

163. Ge M, Li Q, Cao C, et al. One-dimensional TiO2 Nanotube Photocatalysts for Solar Water Splitting. *Adv Sci*. 2017;4(1):1600152. doi:10.1002/advs.201600152

164. Yu H, Yu J, Cheng B, Liu S. Novel preparation and photocatalytic activity of one-dimensional TiO2hollow structures. *Nanotechnology*. 2007;18(6):065604. doi:10.1088/0957-4484/18/6/065604

165. Zheng Z, Huang B, Qin X, Zhang X, Dai Y. Strategic Synthesis of Hierarchical TiO2 Microspheres with Enhanced Photocatalytic Activity. *Chem – Eur J*. 2010;16(37):11266-11270. doi:10.1002/chem.201001280

166. Lee JY, Jo W-K. Application of ultrasound-aided method for the synthesis of CdS-incorporated three-dimensional TiO2 photocatalysts with enhanced performance. *Ultrason Sonochem*. 2017;35:440-448. doi:10.1016/j.ultsonch.2016.10.023

167. Jo YK, Kim IY, Gunjakar JL, et al. Unique Properties of 2 D Layered Titanate Nanosheets as a Building Block for the Optimization of the Photocatalytic Activity and Photostability of TiO2-Based Nanohybrids. *Chem – Eur J*. 2014;20(32):10011-10019. doi:10.1002/chem.201402726

168. Hu C, Wang M-S, Chen C-H, Chen Y-R, Huang P-H, Tung K-L. Phosphorus-doped g-C3N4 integrated photocatalytic membrane reactor for wastewater treatment. *J Membr Sci*. 2019;580:1-11. doi:10.1016/j.memsci.2019.03.012

169. Szymański K, Morawski AW, Mozia S. Effectiveness of treatment of secondary effluent from a municipal wastewater treatment plant in a photocatalytic membrane reactor and hybrid UV/H2O2 – ultrafiltration system. *Chem Eng Process - Process Intensif*. 2018;125:318-324. doi:10.1016/j.cep.2017.11.015

170. Hatat-Fraile M, Liang R, Arlos MJ, et al. Concurrent photocatalytic and filtration processes using doped TiO2 coated quartz fiber membranes in a photocatalytic membrane reactor. *Chem Eng J*. 2017;330:531-540. doi:10.1016/j.cej.2017.07.141

171. Sathishkumar P, Pugazhenthiran N, Mangalaraja RV, Guesh K, Contreras D, Anandan S. Contemporary Achievements of Visible Light-Driven Nanocatalysts for the Environmental Applications. In: *Photocatalytic Functional Materials for Environmental Remediation*. John Wiley & Sons, Ltd; 2019:69-129. doi:https://doi.org/10.1002/9781119529941.ch3

172. Kim J, Van der Bruggen B. The use of nanoparticles in polymeric and ceramic membrane structures: Review of manufacturing procedures and performance improvement for

water treatment. *Environ Pollut*. 2010;158(7):2335-2349. doi:10.1016/j.envpol.2010.03.024

173. Murgolo S, Petronella F, Ciannarella R, et al. UV and solar-based photocatalytic degradation of organic pollutants by nano-sized TiO2 grown on carbon nanotubes. *Environ Appl Adv Oxid Process – EAAOP3*. 2015;240:114-124. doi:10.1016/j.cattod.2014.04.021

174. Geltmeyer J, Teixido H, Meire M, et al. TiO2 functionalized nanofibrous membranes for removal of organic (micro)pollutants from water. *Sep Purif Technol*. 2017;179:533-541. doi:10.1016/j.seppur.2017.02.037

175. Chong MN, Jin B, Chow CWK, Saint C. Recent developments in photocatalytic water treatment technology: A review. *Water Res*. 2010;44(10):2997-3027. doi:10.1016/j.watres.2010.02.039

176. Weber M, Julbe A, Ayral A, Miele P, Bechelany M. Atomic Layer Deposition for Membranes: Basics, Challenges, and Opportunities. *Chem Mater*. 2018;30(21):7368-7390. doi:10.1021/acs.chemmater.8b02687

177. Xu H, Ouyang S, Liu L, Reunchan P, Umezawa N, Ye J. Recent advances in TiO 2-based photocatalysis. *J Mater Chem A*. 2014;2(32):12642-12661.

178. Sinha I, De AK. Chapter 1 - An overview of synthesis techniques for preparing doped photocatalysts. In: Singh P, Borthakur A, Mishra PK, Tiwary D, eds. *Nano-Materials as Photocatalysts for Degradation of Environmental Pollutants*. Elsevier; 2020:1-13. doi:10.1016/B978-0-12-818598-8.00001-8

179. Arif Z, Sethy NK, Kumari L, Mishra PK, Upadhyay SN. Chapter 3 - Recent advances in functionalized polymer-based composite photocatalysts for wastewater treatment. In: Singh P, Borthakur A, Mishra PK, Tiwary D, eds. *Nano-Materials as Photocatalysts for Degradation of Environmental Pollutants*. Elsevier; 2020:39-64. doi:10.1016/B978-0-12-818598-8.00003-1

180. Bazli L, Siavashi M, Shiravi A. A review of carbon nanotube/TiO2 composite prepared via sol-gel method. *J Compos Compd*. 2019;1(1):1-9. doi:10.29252/jcc.1.1.1

181. Tseng TK, Lin YS, Chen YJ, Chu H. A Review of Photocatalysts Prepared by Sol-Gel Method for VOCs Removal. *Int J Mol Sci*. 2010;11(6):2336-2361. doi:10.3390/ijms11062336

182. Akpan UG, Hameed BH. The advancements in sol–gel method of doped-TiO2 photocatalysts. *Appl Catal Gen*. 2010;375(1):1-11. doi:10.1016/j.apcata.2009.12.023

183. Nickheslat A, Amin MM, Izanloo H, Fatehizadeh A, Mousavi SM. Phenol Photocatalytic Degradation by Advanced Oxidation Process under Ultraviolet Radiation Using Titanium Dioxide. Kelishadi R, ed. *J Environ Public Health*. 2013;2013:815310. doi:10.1155/2013/815310

184. Macwan DP, Dave PN, Chaturvedi S. A review on nano-TiO2 sol–gel type syntheses and its applications. *J Mater Sci*. 2011;46(11):3669-3686. doi:10.1007/s10853-011-5378-y

185. Sood S, Kumar S, Umar A, Kaur A, Mehta SK, Kansal SK. TiO2 quantum dots for the photocatalytic degradation of indigo carmine dye. *J Alloys Compd*. 2015;650:193-198. doi:10.1016/j.jallcom.2015.07.164

186. Gombac V, De Rogatis L, Gasparotto A, et al. TiO2 nanopowders doped with boron and nitrogen for photocatalytic applications. *Doping Funct Photoactive Semicond Met Oxides*. 2007;339(1):111-123. doi:10.1016/j.chemphys.2007.05.024

187. Wong CL, Tan YN, Mohamed AR. Photocatalytic Degradation of Phenol Using Immobilized Nanotube Photocatalysts. Kolmakov A, ed. *J Nanotechnol*. 2011;2011:904629. doi:10.1155/2011/904629

188. Santhi K, Navaneethan M, Harish S, Ponnusamy S, Muthamizhchelvan C. Synthesis and characterization of TiO2 nanorods by hydrothermal method with different pH conditions and their photocatalytic activity. *Appl Surf Sci*. 2020;500:144058. doi:10.1016/j.apsusc.2019.144058

189. Wu G, Wang J, Thomas DF, Chen A. Synthesis of F-Doped Flower-like TiO2 Nanostructures with High Photoelectrochemical Activity. *Langmuir*. 2008;24(7):3503-3509. doi:10.1021/la703098g

190. Zhao X, Lou F, Li M, Lou X, Li Z, Zhou J. Sol–gel-based hydrothermal method for the synthesis of 3D flower-like ZnO microstructures composed of nanosheets for photocatalytic applications. *Ceram Int*. 2014;40(4):5507-5514. doi:10.1016/j.ceramint.2013.10.140

191. Zhang M, Chen D-J, Wang R-Z, Feng J-J, Bai Z, Wang A-J. D-penicillamine assisted hydrothermal synthesis of Bi2S3 nanoflowers and their electrochemical application. *Mater Sci Eng C*. 2013;33(7):3980-3985. doi:10.1016/j.msec.2013.05.037

192. Wu D, Long M, Cai W, Chen C, Wu Y. Low temperature hydrothermal synthesis of N-doped TiO2 photocatalyst with high visible-light activity. *J Alloys Compd*. 2010;502(2):289-294. doi:10.1016/j.jallcom.2010.04.189

193. Chen J, Liao W, Jiang Y, et al. Facile Fabrication of ZnO/TiO2 Heterogeneous Nanofibres and Their Photocatalytic Behaviour and Mechanism towards Rhodamine B. *Nanomater Nanotechnol*. 2016;6:9. doi:10.5772/62291

194. Abi Younes P, Sayegh S, Nada AA, et al. Elaboration of porous alumina nanofibers by electrospinning and molecular layer deposition for organic pollutant removal. *Colloids Surf Physicochem Eng Asp*. 2021;628:127274. doi:10.1016/j.colsurfa.2021.127274

195. Zhu S, Nie L. Progress in fabrication of one-dimensional catalytic materials by electrospinning technology. *J Ind Eng Chem*. 2021;93:28-56. doi:10.1016/j.jiec.2020.09.016

196. Xia Y, Yang P, Sun Y, et al. One-Dimensional Nanostructures: Synthesis, Characterization, and Applications. *Adv Mater*. 2003;15(5):353-389. doi:10.1002/adma.200390087

197. Nasr M, Balme S, Eid C, Habchi R, Miele P, Bechelany M. Enhanced Visible-Light Photocatalytic Performance of Electrospun rGO/TiO2 Composite Nanofibers. *J Phys Chem C*. 2017;121(1):261-269. doi:10.1021/acs.jpcc.6b08840

198. Nasr M, Soussan L, Viter R, et al. High photodegradation and antibacterial activity of BN–Ag/TiO2 composite nanofibers under visible light. *New J Chem*. 2018;42(2):1250-1259. doi:10.1039/C7NJ03183A

199. Bethi B, Sonawane SH, Bhanvase BA, Gumfekar SP. Nanomaterials-based advanced oxidation processes for wastewater treatment: A review. *Chem Eng Process - Process Intensif*. 2016;109:178-189. doi:10.1016/j.cep.2016.08.016

200. Das S, Mukherjee A, Sengupta G, Singh VK. Chapter 18 - Overview of nanomaterials synthesis methods, characterization techniques and effect on seed germination. In: Singh P, Borthakur A, Mishra PK, Tiwary D, eds. *Nano-Materials as Photocatalysts for Degradation of Environmental Pollutants*. Elsevier; 2020:371-401. doi:10.1016/B978-0-12-818598-8.00018-3

201. Goodman CH, Pessa MV. Atomic layer epitaxy. *J Appl Phys*. 1986;60(3):R65-R82.

202. Puurunen RL. A Short History of Atomic Layer Deposition: Tuomo Suntola's Atomic Layer Epitaxy. *Chem Vap Depos*. 2014;20(10-11-12):332-344. doi:10.1002/cvde.201402012

203. Maina JW, Merenda A, Weber M, et al. Atomic layer deposition of transition metal films and nanostructures for electronic and catalytic applications. *Crit Rev Solid State Mater Sci*. Published online September 20, 2020:1-22. doi:10.1080/10408436.2020.1819200

204. Skoog SA, Elam JW, Narayan RJ. Atomic layer deposition: medical and biological applications. *Int Mater Rev*. 2013;58(2):113-129. doi:10.1179/1743280412Y.0000000009

205. Raaijmakers IJ. (Invited) Current and Future Applications of ALD in Micro-Electronics. *ECS Trans*. 2019;41(2):3-17. doi:10.1149/1.3633649

206. George SM. Atomic Layer Deposition: An Overview. *Chem Rev*. 2010;110(1):111-131. doi:10.1021/cr900056b

207. Mackus AJ, Schneider JR, MacIsaac C, Baker JG, Bent SF. Synthesis of doped, ternary, and quaternary materials by atomic layer deposition: a review. *Chem Mater*. 2018;31(4):1142-1183.

208. Johnson RW, Hultqvist A, Bent SF. A brief review of atomic layer deposition: from fundamentals to applications. *Mater Today*. 2014;17(5):236-246. doi:10.1016/j.mattod.2014.04.026

209. Delabie A, Puurunen RL, Brijs B, et al. Atomic layer deposition of hafnium oxide on germanium substrates. *J Appl Phys*. 2005;97(6):064104.

210. Arts K, Utriainen M, Puurunen RL, Kessels WM, Knoops HC. Film conformality and extracted recombination probabilities of O atoms during plasma-assisted atomic layer deposition of SiO2, TiO2, Al2O3, and HfO2. *J Phys Chem C*. 2019;123(44):27030-27035.

211. Puurunen R, Root A, Sarv P, et al. Growth of aluminium nitride on porous silica by atomic layer chemical vapour deposition. *Appl Surf Sci*. 2000;165(2-3):193-202.

212. Schneider N, Lincot D, Donsanti F. Atomic layer deposition of copper sulfide thin films. *Thin Solid Films*. 2016;600:103-108.

213. Dameron A, Seghete D, Burton B, et al. Molecular layer deposition of alucone polymer films using trimethylaluminum and ethylene glycol. *Chem Mater*. 2008;20(10):3315-3326.

214. Elers K-E, Winkler J, Weeks K, Marcus S. TiCl[sub 4] as a Precursor in the TiN Deposition by ALD and PEALD. *J Electrochem Soc*. 2005;152(8):G589. doi:10.1149/1.1938108

215. Schindler P, Kim Y, Thian D, An J, Prinz FB. Plasma-enhanced atomic layer deposition of BaTiO3. *Viewp Set No 57 Contemp Innov Thermoelectr Res Dev*. 2016;111:106-109. doi:10.1016/j.scriptamat.2015.08.026

216. Napari M, Lahtinen M, Veselov A, Julin J, Østreng E, Sajavaara T. Room-temperature plasma-enhanced atomic layer deposition of ZnO: Film growth dependence on the PEALD reactor configuration. *Surf Coat Technol*. 2017;326:281-290. doi:10.1016/j.surfcoat.2017.07.056

217. Wu Y, Döhler D, Barr M, et al. Atomic layer deposition from dissolved precursors. *Nano Lett*. 2015;15(10):6379-6385.

218. King DM, Liang X, Zhou Y, et al. Atomic layer deposition of TiO2 films on particles in a fluidized bed reactor. *Powder Technol*. 2008;183(3):356-363.

219. George S. Atomic Layer Deposition on Particles. In: IOP Publishing; 2006:831.

220. Poodt P, Cameron DC, Dickey E, et al. Spatial atomic layer deposition: A route towards further industrialization of atomic layer deposition. *J Vac Sci Technol Vac Surf Films*. 2012;30(1):010802.

221. Weimer AW. Particle atomic layer deposition. *J Nanoparticle Res*. 2019;21(1):9. doi:10.1007/s11051-018-4442-9

222. Puurunen RL, Saarilahti J, Kattelus H. Implementing ALD layers in MEMS processing. *ECS Trans*. 2007;11(7):3.

223. Sayegh S, Lee J-H, Yang D-H, et al. Humidity-resistant gas sensors based on SnO2 nanowires coated with a porous alumina nanomembrane by molecular layer deposition. *Sens Actuators B Chem*. 2021;344:130302. doi:10.1016/j.snb.2021.130302

224. Graniel O, Weber M, Balme S, Miele P, Bechelany M. Atomic layer deposition for biosensing applications. *Biosens Bioelectron*. 2018;122:147-159. doi:https://doi.org/10.1016/j.bios.2018.09.038

225. Jung YS, Cavanagh AS, Dillon AC, Groner MD, George SM, Lee S-H. Enhanced stability of LiCoO2 cathodes in lithium-ion batteries using surface modification by atomic layer deposition. *J Electrochem Soc*. 2009;157(1):A75.

226. Sun X, Xie M, Wang G, et al. Atomic layer deposition of TiO2 on graphene for supercapacitors. *J Electrochem Soc*. 2012;159(4):A364.

227. Chan C-C, Chang C-C, Hsu W-C, Wang S-K, Lin J. Photocatalytic activities of Pd-loaded mesoporous TiO2 thin films. *Chem Eng J*. 2009;152(2):492-497. doi:10.1016/j.cej.2009.05.012

228. Wang C-C, Hsueh Y-C, Su C-Y, Kei C-C, Perng T-P. Deposition of uniform Pt nanoparticles with controllable size on TiO2-based nanowires by atomic layer deposition and their photocatalytic properties. *Nanotechnology*. 2015;26(25):254002. doi:10.1088/0957-4484/26/25/254002

229. Justh N, Mikula GJ, Bakos LP, et al. Photocatalytic properties of TiO2@polymer and TiO2@carbon aerogel composites prepared by atomic layer deposition. *Carbon*. 2019;147:476-482. doi:10.1016/j.carbon.2019.02.076

230. Weber M, Bechelany M. Combining nanoparticles grown by ALD and MOFs for gas separation and catalysis applications. *Pure Appl Chem*. 2019;92. doi:10.1515/pac-2019-0109

231. Singh JA, Yang N, Bent SF. Nanoengineering Heterogeneous Catalysts by Atomic Layer Deposition. *Annu Rev Chem Biomol Eng*. 2017;8(1):41-62. doi:10.1146/annurev-chembioeng-060816-101547

232. Cao K, Cai J, Liu X, Chen R. Review Article: Catalysts design and synthesis via selective atomic layer deposition. *J Vac Sci Technol A*. 2017;36(1):010801. doi:10.1116/1.5000587

233. Wang H, Zhang L, Chen Z, et al. Semiconductor heterojunction photocatalysts: design, construction, and photocatalytic performances. *Chem Soc Rev*. 2014;43(15):5234-5244. doi:10.1039/C4CS00126E

234. Fonseca J, Lu J. Single-Atom Catalysts Designed and Prepared by the Atomic Layer Deposition Technique. *ACS Catal*. 2021;11(12):7018-7059. doi:10.1021/acscatal.1c01200

235. Cao K, Cai J, Liu X, Chen R. Review Article: Catalysts design and synthesis via selective atomic layer deposition. *J Vac Sci Technol A*. 2018;36(1):010801. doi:10.1116/1.5000587

236. Omerzu A, Peter R, Jardas D, et al. Large enhancement of photocatalytic activity in ZnO thin films grown by plasma-enhanced atomic layer deposition. *Surf Interfaces*. 2021;23:100984. doi:10.1016/j.surfin.2021.100984

237. Levchuk I, Guillard C, Dappozze F, Parola S, Leonard D, Sillanpää M. Photocatalytic activity of TiO2 films immobilized on aluminum foam by atomic layer deposition technique. *J Photochem Photobiol Chem*. 2016;328:16-23. doi:10.1016/j.jphotochem.2016.03.034

238. Justh N, Firkala T, László K, Lábár J, Szilágyi IM. Photocatalytic C60-amorphous TiO2 composites prepared by atomic layer deposition. *Appl Surf Sci*. 2017;419:497-502. doi:10.1016/j.apsusc.2017.04.243

239. Marchetti F, Laidani N, Scarpa M, Gottardi G, Moser E. Graphene films decorated with TiO2 grown by atomic layer deposition: Characterization and photocatalytic activity study under UV–visible light. *Appl Surf Sci*. 2019;470:484-495. doi:10.1016/j.apsusc.2018.11.136

240. Buchalska M, Surówka M, Hämäläinen J, Iivonen T, Leskelä M, Macyk W. Photocatalytic activity of TiO2 films on Si support prepared by atomic layer deposition. *8th Eur Meet Sol Chem Photocatal Environ Appl*. 2015;252:14-19. doi:10.1016/j.cattod.2014.09.032

241. Guo Q, Ma Z, Zhou C, Ren Z, Yang X. Single Molecule Photocatalysis on TiO2 Surfaces. *Chem Rev*. 2019;119(20):11020-11041. doi:10.1021/acs.chemrev.9b00226

242. Kumari P, Bahadur N, O'Dell LA, et al. Nanoscale 2D semi-conductors – Impact of structural properties on light propagation depth and photocatalytic performance. *Sep Purif Technol*. 2021;258:118011. doi:10.1016/j.seppur.2020.118011

243. Park K-H, Han GD, Kim BJ, et al. Effects of atomic layer deposition conditions on the formation of thin ZnO films and their photocatalytic characteristics. *Ceram Int*. 2019;45(15):18823-18830. doi:10.1016/j.ceramint.2019.06.115

244. Oliveira IE, Silva RM, Girão AV, Faria JL, Silva CG, Silva RF. Facile Preparation of ZnO/CNTs Nanocomposites via ALD for Photocatalysis Applications. *Eur J Inorg Chem*. 2020;2020(18):1743-1750. doi:10.1002/ejic.202000032

245. Cao Y-Q, Zi T-Q, Zhao X-R, et al. Enhanced visible light photocatalytic activity of Fe2O3 modified TiO2 prepared by atomic layer deposition. *Sci Rep*. 2020;10(1):13437. doi:10.1038/s41598-020-70352-z

246. Weber M, Julbe A, Kim SS, Bechelany M. Atomic layer deposition (ALD) on inorganic or polymeric membranes. *J Appl Phys*. 2019;126(4):041101. doi:10.1063/1.5103212

247. Berger TE, Regmi C, Schäfer AI, Richards BS. Photocatalytic degradation of organic dye via atomic layer deposited TiO2 on ceramic membranes in single-pass flow-through operation. *J Membr Sci*. 2020;604:118015. doi:10.1016/j.memsci.2020.118015

248. Scott T, Zhao H, Deng W, Feng X, Li Y. Photocatalytic degradation of phenol in water under simulated sunlight by an ultrathin MgO coated Ag/TiO2 nanocomposite. *Chemosphere*. 2019;216:1-8. doi:10.1016/j.chemosphere.2018.10.083

249. Nasr M, Viter R, Eid C, Habchi R, Miele P, Bechelany M. Optical and structural properties of Al2O3 doped ZnO nanotubes prepared by ALD and their photocatalytic application. *Sel Pap "E-MRS 2017 – Symp Q."* 2018;343:24-29. doi:10.1016/j.surfcoat.2017.11.060

250. Kim WJ, Jang E, Park TJ. Enhanced visible-light photocatalytic activity of ZnS/g-C3N4 type-II heterojunction nanocomposites synthesized with atomic layer deposition. *Appl Surf Sci*. 2017;419:159-164. doi:10.1016/j.apsusc.2017.05.012

251. Assaud L, Brazeau N, Barr MK, et al. Atomic layer deposition of Pd nanoparticles on TiO2 nanotubes for ethanol electrooxidation: synthesis and electrochemical properties. *ACS Appl Mater Interfaces*. 2015;7(44):24533-24542.

252. Zhou Y, King DM, Liang X, Li J, Weimer AW. Optimal preparation of Pt/TiO2 photocatalysts using atomic layer deposition. *Appl Catal B Environ*. 2010;101(1):54-60. doi:10.1016/j.apcatb.2010.09.005

253. Gao F, Jiang J, Du L, Liu X, Ding Y. Stable and highly efficient Cu/TiO2 nanocomposite photocatalyst prepared through atomic layer deposition. *Appl Catal Gen*. 2018;568:168-175. doi:10.1016/j.apcata.2018.10.006

254. Ribao P, Corredor J, Rivero MJ, Ortiz I. Role of reactive oxygen species on the activity of noble metal-doped TiO2 photocatalysts. *SI Photocatal Trend*. 2019;372:45-51. doi:10.1016/j.jhazmat.2018.05.026

255. Yoo J, Zazpe R, Cha G, et al. Uniform ALD deposition of Pt nanoparticles within 1D anodic TiO2 nanotubes for photocatalytic H2 generation. *Electrochem Commun*. 2018;86:6-11. doi:10.1016/j.elecom.2017.10.017

256. Ozkan S, Yoo J, Nguyen NT, et al. Spaced TiO2 nanotubes enable optimized Pt atomic layer deposition for efficient photocatalytic H2 generation. *ChemistryOpen*. 2018;7(10):797.

257. Lei Y, Lu J, Luo X, et al. Synthesis of Porous Carbon Supported Palladium Nanoparticle Catalysts by Atomic Layer Deposition: Application for Rechargeable Lithium–O2 Battery. *Nano Lett*. 2013;13(9):4182-4189. doi:10.1021/nl401833p

258. Weber M, Lamboux C, Navarra B, et al. Boron Nitride as a Novel Support for Highly Stable Palladium Nanocatalysts by Atomic Layer Deposition. *Nanomaterials*. 2018;8(10). doi:10.3390/nano8100849

259. Najem M, Nada AA, Weber M, et al. Palladium/Carbon Nanofibers by Combining Atomic Layer Deposition and Electrospinning for Organic Pollutant Degradation. *Materials*. 2020;13(8). doi:10.3390/ma13081947

260. Merenda A, Weber M, Bechelany M, et al. Fabrication of Pd-TiO2 nanotube photoactive junctions via Atomic Layer Deposition for persistent pesticide pollutants degradation. *Appl Surf Sci*. 2019;483:219-230. doi:10.1016/j.apsusc.2019.03.285

261. Liang Y-C, Wang C-C, Kei C-C, Hsueh Y-C, Cho W-H, Perng T-P. Photocatalysis of Ag-Loaded TiO2 Nanotube Arrays Formed by Atomic Layer Deposition. *J Phys Chem C*. 2011;115(19):9498-9502. doi:10.1021/jp202111p

262. Liu M, Zheng L, Bao X, et al. Substrate-dependent ALD of Cux on TiO2 and its performance in photocatalytic CO2 reduction. *Chem Eng J*. 2021;405:126654. doi:10.1016/j.cej.2020.126654

263. Ramachandran RK, Detavernier C, Dendooven J. Atomic Layer Deposition for Catalysis. In: *Nanotechnology in Catalysis*. John Wiley & Sons, Ltd; 2017:335-358. doi:10.1002/9783527699827.ch14

264. Assaud L, Monyoncho E, Pitzschel K, et al. 3D-nanoarchitectured Pd/Ni catalysts prepared by atomic layer deposition for the electrooxidation of formic acid. *Beilstein J Nanotechnol*. 2014;5(1):162-172.

265. Weber MJ, Mackus AJM, Verheijen MA, van der Marel C, Kessels WMM. Supported Core/Shell Bimetallic Nanoparticles Synthesis by Atomic Layer Deposition. *Chem Mater*. 2012;24(15):2973-2977. doi:10.1021/cm301206e

266. Mackus A, Dielissen S, Mulders J, Kessels W. Nanopatterning by direct-write atomic layer deposition. *Nanoscale*. 2012;4(15):4477-4480.

267. Hashemi FSM, Bent SF. Sequential Regeneration of Self-Assembled Monolayers for Highly Selective Atomic Layer Deposition. *Adv Mater Interfaces*. 2016;3(21):1600464.

268. Jiang X, Wang H, Qi J, Willis BG. In-situ spectroscopic ellipsometry study of copper selective-area atomic layer deposition on palladium. *J Vac Sci Technol Vac Surf Films*. 2014;32(4):041513.

269. Lv P, Zhao C, Lee WJ, et al. Less is more: Enhancement of photocatalytic activity of g-C3N4 nanosheets by site-selective atomic layer deposition of TiO2. *Appl Surf Sci*. 2019;494:508-518. doi:10.1016/j.apsusc.2019.07.131

270. Yang Y, Zheng W, Zhao L. BaZrO3/Au and BaZrO3/Au-Pd hetero-structures: The characteristics and mechanism for their photocatalytic performance. *Ceram Int*. 2019;45(17, Part B):23808-23814. doi:10.1016/j.ceramint.2019.07.319

Chapter 2: Tunable TiO_2-BN-Pd nanofibers by combining electrospinning and Atomic Layer Deposition to enhance photodegradation of acetaminophen

Table of contents

1. ABSTRACT

The demand for fresh and clean water sources increases globally, and there is a need to develop novel routes to eliminate micropollutants and other harmful species from water. Photocatalysis is a promising alternative green technology that has shown great performance in the degradation of persistent pollutants. Titanium dioxide is the most used catalyst owing to his attractive physico-chemical properties, but this semiconductor presents limitations in the photocatalysis process due to the high band gap and the fast recombination of the photogenerated carriers. Herein, a novel photocatalyst has been developed, based on titanium dioxide nanofibers (TiO_2 NFs) synthesized by electrospinning. The TiO_2 NFs were coated by atomic layer deposition (ALD) to grow boron nitride (BN) and palladium (Pd) on their surface. The UV-Vis spectroscopy measurements confirmed the increase of the band gap and the extension of the spectral response to the visible range. The obtained TiO_2/BN/Pd nanofibers were then tested for photocatalysis, and showed a drastic increase of acetaminophen (ACT) degradation (>90%), compared to only 20% degradation obtained with pure TiO_2 after 4h of visible light irradiation. The high photocatalytic activity was attributed to the good dispersion of Pd NPs on TiO_2-BN nanofibers, leading to a higher transfer of photoexcited charges carriers and a decrease of photogenerated electron-holes recombination. To confirm their reusability, recycling tests on the hybrid photocatalyst TiO_2/BN/Pd have been performed, showing a good stability over 5 cycles under UV and Visible light. Moreover, toxicity tests as well as quenching tests were carried out to check the toxicity in the formation of byproducts and to determine active species responsible for the degradation. The results presented in this work demonstrate the potential of TiO_2/BN/Pd nanomaterials, and open new prospects for the preparation of tunable photocatalysts.

Keywords: TiO_2-BN-Pd nanocomposites; nanofibers, electrospinning; atomic layer deposition; photocatalysis; acetaminophen

2. Graphical abstract

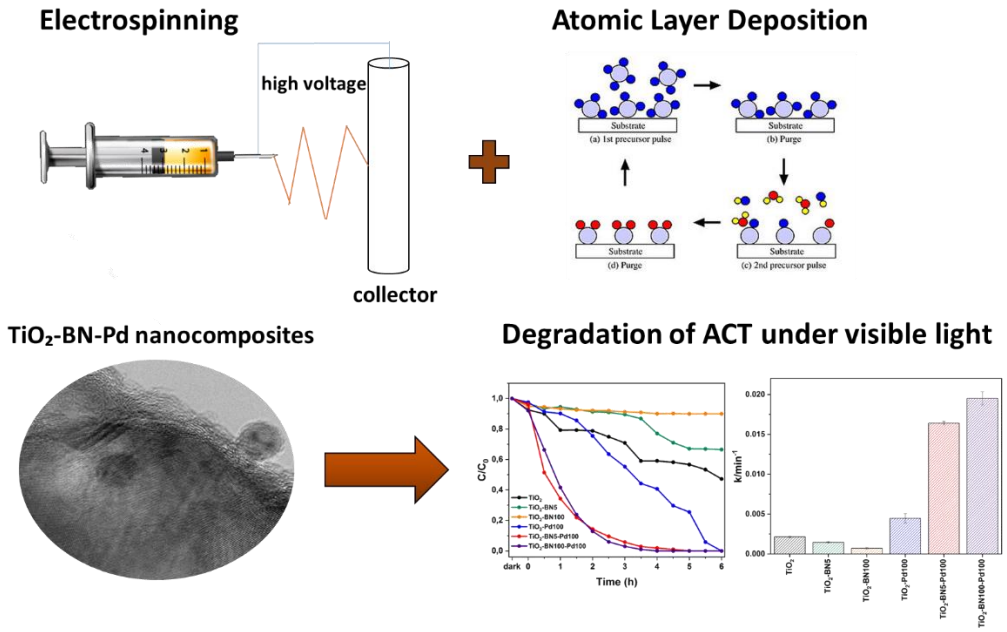

3. Highlights

- TiO_2-BN-Pd materials were successfully prepared by combining electrospinning and atomic layer deposition.
- The synthesized materials were used to study the degradation of acetaminophen (ACT) under UV and visible light.
- The degradation of ACT by TiO_2-BN100-Pd100 was 80% faster than pristine TiO_2 NFs.
- The photocatalysts showed high stability and recyclability after 5 successive cycles under UV and visible irradiation.
- The main active species that play a significant role in the degradation of ACT are $\cdot O_2^-$ and h^+.

4. Introduction

Water scarcity is a worldwide issue since the demand for clean water highly exceeds the freshwater sources.[1] To respond to this high demand, many sources of water have been considered such as wastewater, rainwater and seawater. However, these sources may contain harmful contaminants such as dyes, pesticides, pharmaceuticals and personal products, considered "emerging pollutants" [2]. Additionally, conventional wastewater treatment methods are inefficient in removing persistent organic substances such as drugs from the water and the presence of such contaminants, even at low concentrations, may be harmful on human health and aquatic organisms [3–7]. Many new techniques have been developed to overcome these limitations, such as ozonation, electrooxidation, photo-Fenton and photocatalysis[8,9]. Photocatalysis has attracted much attention in the last decades as a promising approach for water treatment [10–12]. It is an advanced oxidation process, based on the excitation of a semiconductor that will engender electron-hole pairs responsible of the degradation of pollutant[13–15]. Therefore, it is considered as an effective technique to remove trace contaminants and their intermediates products that could be more harmful [16–18].

In recent years, semiconductor photocatalysts have been considered for environmental and energy applications[19]. Among most of the semiconductors used in photocatalysis, titanium dioxide (TiO_2) has retrieved much attention for the removal of organic pollutants from wastewater. TiO_2 has several advantages regarding its high photocatalytic efficiency, high stability, low toxicity and low cost [20–22]. However, the wide band gap (~ 3.0-3.2 eV) limits the application of this photocatalyst under visible light. Another disadvantage is the fast recombination of photogenerated carriers, limiting its usages in large scale[23–25]**.**

During the last years, much research has focused on designing focus on the hybrid nanocatalysts to conquer their limitations[26–30] . Many studies have been presented, such as doping with metal ions (Pd, Ag, Pt…)[13,31–35] , nonmetal ions (B, N, Cu, Ni…)[36,37], and creation of heterojunctions with other semiconductors (BN, ZnO, CuO)[5,38–40]. Coupling TiO_2 with other semiconductors or metals will allow the formation of heterojunction that can increase the lifetime carrier charge, reduce the recombination of electron holes, and improve the photocatalysis efficiency of TiO_2 under visible light[41,42].

Many studies have reported the efficiency of doping TiO_2 with BN for dyes and pollutant degradation since BN has a high ability of energy storage to allow higher e^--h^+ transfers and a high chemical stability[43,44]. Nasr *et al.* reported that TiO_2-BN nanocomposites synthesized by electrospinning enhanced the degradation of methyl orange under UV light. They confirmed that BN could improve the photocatalytic activity of TiO_2 due to the migration of holes to the catalyst surface[13]. The photocatalytic oxidation of ibuprofen by TiO_2-BN nanocomposites were also studied by Lin *et al.*[45]. The photodegradation of ibuprofen was enhanced due to the incorporation of BN, and a complete degradation was obtained after 2h of UV irradiation. Sheng *et al.* prepared hexagonal boron nitride (h-BN)/titania (TiO_2) nanocomposites by sol-gel. They reported the degradation of rhodamine B (RhB) and methylene blue (MB) under UV light irradiation of 98% and 92% within 50 min irradiation,respectively[46].

In addition, loading noble metals such as palladium (Pd), platinum (Pt) and silver (Ag) on the surface of the substrate, appears to be effective for the elaboration of potential catalysts[47,48]. These metal nanoparticles (NPs) will allow the improvement of visible light excitation and reduce the recombination of e−/h+ pairs due to the surface plasmonic resonance effect and the metals' performance as charge acceptors, respectively[49]. Among these metals, loading Pd on the surface of TiO_2 has proven to be an effective method to improve visible light photocatalytic degradation. Mohapatra *et al.* prepared TiO_2-NTs with well-dispersed Pd NPs by incipient wetness method. The catalyst has shown effective degradation of dyes under solar light simulator[50]. Moreover, photocatalytic oxidation of nitrogen oxide (NO) was successful using Pd-modified TiO_2 prepared by thermal impregnation method[51].

Most of these studies have used several techniques such as electrospinning[25], sol-gel method[52], microwave-assisted synthesis[53], etc. Since visible photocatalysts are required for efficient catalytic applications, a highly structured material with a large specific area and more exposed active sites should be designed[54]. To our knowledge, no degradation of acetaminophen (ACT) was reported with TiO_2-BN-Pd nanocomposites. The major challenge is to design a semiconductor catalyst with a well-known structure, precise morphology and high

selectivity. Atomic layer deposition (ALD) combined with electrospinning shows potential advantages in fabricating highly effective and selective photocatalysts.

ALD is a vapor deposition technique that allows the preparation of thin films in the sub-nanometer scale with precise thickness and high conformality[55,56]. ALD enables the synthesis of nanoparticles and thin films with controllable dimensions at the subnanoscale, a unique capability[57–64]. The use of ALD in catalysis field is getting more attention since it enables the design of nanocatalyst with control over size, composition, thickness and distribution of the material[65]. For example, Weber *et al.* reported the synthesis of carbon paper-boron nitride-palladium electrodes using ALD, which electrochemical active surface was maintained stable even after applying an accelerated ageing program for 1000 cycles[66].

In their recent review, *Vempati et al.* reported the importance of the combination of ALD with electrospinning in the elaboration of catalytic materials[67]. Electrospinning is an easy technique to fabricate NFs with a controlled diameter in a range between 10-1000 nm, by applying a high electric field between the polymeric solution and the collector[68,69]. Preparation of TiO_2 nanofibers by electrospinning has been widely used, since electrospinning allows the fabrication of many nanostructures with low aggregation, high porosity, and large specific surface area, which can promote the charge and mass transfer for enhanced photocatalytic activities[70–72].

Recently nanocomposite materials for photocatalysis degradation of pharmaceuticals pollutants have involved many research studies[73–76]. Herein, we report for the first time the degradation of ACT with TiO_2-BN-Pd catalyst obtained by combining two major techniques, electrospinning and ALD. First, TiO_2 was synthesized by electrospinning, followed by a uniform deposition of BN by ALD. Pd nanoparticles was then added to obtain hybrid catalysts. Moreover, a variation of BN deposition cycles was also performed, and the degradation of ACT used as a model pollutant was compared under UV and visible light. TiO_2-BN100-Pd100 hybrid photocatalyst has shown the best photocatalytic activity among all prepared catalysts. Moreover, the catalyst has shown high stability even after 5 cycles. The toxicity was also evaluated during the degradation process to ensure that harmful byproductsgenerated during the process were degraded as well. Finally, scavengers study was conducted to get an idea

about the mechanism of degradation of ACT. The main species responsible of the degradation of acetaminophen were holes and superoxide radicals.

5. Experimental

5.1. Materials and chemicals

Titanium(IV) isopropoxide (TTIP, 97%, CAS: 546-68-9), polyvinyl pyrollidone (PVP, Mw=1300000, CAS: 9003-39-8), acetaminophen (ACT , ≥99% CAS: 103-90-2), formaline solution (HCHO, CAS: 50-00-0), boron tribromide(BBr_3, 99,9%, CAS :10294-33-4), nafion perfluorinated resin solution (CAS: 31175-20-9), sodium sulfate (Na_2SO_4, ≥99% ,CAS: 7757-82-6), sodium chloride (NaCl, , ≥99% ,CAS: 7647-14-5), 2-propanol (99.9%, CAS: 67-63-0), p-benzoquinone ($C_6H_4O_2$, ≥99.5%, CAS:106-51-4) and ethylenediaminetetraacetic acid (EDTA, 99.995%, CAS: 60-00-4) were purchased from Sigma-Aldrich. In addition, Pd palladium(II) hexafluoroacetylacetonate (≥95%, CAS: 64916-48-9) was purchased from Strem Chemicals. Acetic acid (CAS: 64-19-7) and ethanol (≥99.8% CAS: 64-17-5) were purchased from VWR chemicals and used as solvents. All chemicals were used without further purification. Indium tin oxide (ITO) deposited on quartz was purchased from Präzisions Glas & Optik. Deionized (DI) water (>18.2 MΩ) prepared by Millipore (Milli-Q® Academic) water purification system was used for all dilutions and reagent preparation. Argon gas and ammonia were bought from Linde and used as received.

5.2. Synthesis of TiO_2 nanofibers by electrospinning

The preparation of TTIP/PVP solution was similar to previous studies as shown in **Figure 2. 1**[22]. Acetic acid and ethanol are used as solvents. The suspension was stirred for 2h prior to spinning in order to increase the dielectric constant and obtain an electrospinnable solution. The resulting solution was then loaded in a 22 mL syringe and electrospun by a homemade electrospinning system. During the process, a high voltage of 25 kV and a flow rate of 1mL/h were applied. The distance between the 19 gauge needle and the collector was fixed at 10 cm. When the electric field is created, the polymer jet between the droplet and the grounded collector leads to fibres forming, overcoming the surface forces[71,77,78]. This

process was followed by calcination of obtained fibers at 400°C for 4h to remove the polymer and obtain crystalline TiO_2.

5.3. Modification of TiO_2 by Atomic Layer Deposition

5.3.1. Atomic Layer Deposition of Boron Nitride

The coating of BN was carried out on electrospun nanofibers at 750°C in a low-pressure homemade ALD reactor. The reactor was directly connected to the precursor and co-reactant lines through gate valves and heated at 110°C to avoid condensation. The deposition of BN was achieved using sequential exposures of BBr_3 and NH_3 (considered as co-reactant) separated by purge steps of argon with a flow rate of 100 sccm. One ALD cycle consisted of a 0.1 s BBr_3 pulse, 5 s exposure, and 15 s Ar purge, followed by a 5 s NH_3 pulse, 5 s exposure, and 20 s Ar purge. More details on the ALD reactor and on the process are listed elswhere[5]. In order to adjust the BN loading, the number of ALD cycles was varied. Thicknesses of deposited BN were chacaterized by ellipsometry on Si substrates added in the same of NFs using an optical model based on Cauchy fitting model (Semilab spectroscopic ellipsometer GES5E, Xe lamp 1.23eV-5eV).

5.3.2. Atomic Layer Deposition of Palladium

TiO_2-Pd were synthesized by atomic layer deposition in a low-pressure hot-wall (home-built) reactor, described earlier[79,80]. ALD of Pd was carried out with $Pd(hfac)_2$ and formalin. The highly dispersed Pd NPs were synthesized by applying 100 ALD cycles. The bubbler containing the $Pd(hfac)_2$ precursor was heated at 70 °C and the formalin container was kept at room temperature. The deposition chamber was set at a temperature of 220 °C, and the lines in the ALD system were heated at 80 °C to avoid any condensation [81]. The ALD cycle consisted of sequential pulse, exposure, and purge of Pd precursor and formalin, alternatively. The pulse, exposure, and purge durations were 5:15:10 s and 1:15:60 s for Pd(hfac)2 and formalin, respectively.

5.4. Characterization of the synthesized nanocomposites

A Hitachi S4800 emission scanning electron microscope (SEM, JAPAN) was used for morphology measurements of synthesized nanofibers. All samples were sputter coated with platinum/palladium before SEM measurement using a Polaron SC7620 Mini Sputter Coater. The crystal phases of the samples were examined by XRD diffractometer using Cu-Kα radiation (λ=1.5406 Å) in 2θ ranging from 10 to 80°. Fourier-transform infrared spectroscopy (FTIR) of TiO_2, TiO_2-BN, TiO_2-Pd and TiO_2-BN-Pd nanocomposites was recorded with the NEXUS instrument, equipped with an attenuated total reflection accessory in the frequency range of 400–4000 cm^{-1}. Raman spectra were measured by the dispersive Raman spectroscopy (Horiba XploRA), using a 659.55 nm laser and an objective lens of 100. Transmission electron microscopy (TEM) was performed using JEOL 2200FS (200 kV) and JEOL ARM-200F (200kV). X-ray photoelectron spectroscopy (XPS) measurements were conducted via ESCALAB 250 spectrometer from Thermo Electron using Al Kα monochromatic source (1486.6 eV) as an excitation source. In order to determine the band gaps of synthesized materials, the UV-vis spectra were measured by a UV–vis spectrophotometer (Jasco model V570) equipped with a diffuse reflectance (DR) attachment (Shimadzu IRS-2200) for optical absorbance measurements. Photoluminescence (PL) spectra were recorded with an optical fiber spectrometer (Ocean Optics usb2000) with an excitation wavelength of 266 nm by a nitrogen Nd:YAG laser, 9mW.

5.5. Electrochemical impedance spectroscopy measurement

An electrochemical system was used to carry out the EIS tests by a Solartron SI 1287 potentiostat/ galvanostat. Three-electrode cell were used to study the photoelectrochemical property: photocatalysts used as working electrode, Ag/AgCl as reference electrode and platinum wire as counter electrode immersed in Na_2SO_4 solution (0.1 mol/L) considered as electrolyte. The mixtures of 4 mg photocatalyst, 1 mL isopropanol and 40 µL nafion aqueous solution were homogeneously mixed by the ultrasonic cleaner for 30 min, then the slurry was dropped on the ITO glass (1x1cm), and the working electrode was achieved after the evaporation of isopropanol. Moreover, the measurements were done using a 150 W halogen lamp as the light source under visible light exposition.

5.6. Quantum efficiency measurements

The measurements were performed in the following way:

3.5 mL plastic cuvette was filled with 2.5 mL of mQ water and installed into a cuvette holder. Tungsten light source (Avantes) was used for absorbance measurements. The 1 $mg.mL^{-1}$ water solutions of TiO_2-X samples were prepared. 50 mL of solution was added to the cuvette and absolute irradiance spectra of the sample were recorded (**Figure S2. 1**).

According to Kubelka-Munk following equations are applicable for the calculation of quantum efficiency:[82]

$$R_\infty = \frac{(1+R_0^2-T^2)-\left((1+R_0^2-T^2)^2-4R_0^2\right)^{0.5}}{2R_0} \quad (1)$$

Where K, S, T, R_0, d are diffuse absorption coefficient, diffuse scattering coefficient, transmittance (%), reflectance (%) and sample thickness (cm).

Within this theory, absorption and scattering coefficients can be calculated, the detailed calculation is represented in supporting information[82].

The quantum efficiency for 1 cm^3 volume of 0.5 $mg.mL^{-1}$ photocatalyst solution was calculated as following equation 2:

$$QE = \frac{N_0-N}{\sum_{400\,nm}^{700\,nm}\eta(\lambda)\cdot N_{ph}(\lambda)} \quad (2)$$

Where N0, N, η(λ) and $N_{ph}(\lambda)$ are the initial concentration of organic molecules (cm^{-3}), concentration of organic molecules after 3 hours of exposure to visible light (cm^{-3}), part of absorbed light and number of incident photons (cm^{-2}) for wavelength λ.

5.7. Photocatalytic experiments of acetaminophen

Photocatalytic activity of the synthesized nanocomposite was evaluated on the degradation of acetaminophen under two light sources. A medium pressure metal halide UV lamp (400 W, Lampes France) and a visible light source provided by a linear halogen lamp

(400W, Avide) were used for the comparative study. The irradiation distance between the lamp and the sample was fixed to 10 cm for all experiments.

The photocatalysts (0.5 $g.L^{-1}$ - TiO_2, TiO_2-BN, TiO_2-Pd and TiO_2-BN-Pd) were added into 250 mL of ACT solution (1 $mg.L^{-1}$) in a 300 mL glass reactor. A water bath was used to minimize the temperature increase in the solution under the light irradiation and keep it stable at 37 °C. The solution was stirred for 30 minutes to ensure equilibrium adsorption in the dark and then exposed to irradiation. At certain time intervals, 3 ml aliquots were sampled and filtered with 0.22 µm filters. The ACT concentration was analyzed by high-performance liquid chromatography equipped with a C-18 column (RP18, Nucleoshell) and a Quattro-Micro mass spectrometer with an Electrospray probe (Waters Micromass, Wythenshawe, Manchester, UK) as a detector. An isocratic method (A/B=97/3) set at 0.25 $mL.min^{-1}$ flow rate was used. The phase A of eluents consisted of a mixture of acetonitrile/water (95/05), while the phase B was 100 % acetonitrile with 0.1 % formic acid for both phases.

The recyclability of the catalyst that showed the best degradation efficiency was further investigated. The nanocomposite was reused under UV and visible light for 5 cycles with the same initial conditions.

The degradation efficiency (D(%)), was calculated according to Eq. (3):

$$\boldsymbol{D}(\%) = [(\boldsymbol{C_0} - \boldsymbol{C})/\boldsymbol{C_0}\,] \times \mathbf{100} \quad \textbf{(3)}$$

where: C_0 and C are the initial and final concentrations at $mg.L^{-1}$.

5.8. Photocatalytic kinetic model

Typically, TiO_2 kinetics is usually characterized by Langmuir–Hinshelwood (L–H) model[45,83]. When the concentration of the pollutant is low , pseudo-first-order kinetics is applied[84], Eq.(4):

$$\boldsymbol{ln}\,(\boldsymbol{C_0}/\boldsymbol{C}) = \boldsymbol{kt} \quad \textbf{(4)}$$

where C_0 ($mg.L^{-1}$) is the initial concentration of the pollutant, C is the pollutant concentration at time t (min) and k (min^{-1}) is the pseudo-first-order rate constant.

5.9. Microtoxicity tests for determination of byproducts toxicity

During the degradation of acetaminophen, many byproducts could be formed [85]. In order to confirm or not the toxicity of these compounds, a bioluminescence toxicity study was carried out. This study is based on the measurements of the luminescence effect of marine bacteria. The bacteria used in this method was the strain Vibrio fischeri LCK 487 .All measurements were conducted using Microtox® Model 500 Analyzer (Modern Water Inc.; United Kingdom) coupled with MicrotoxOmni® software. First, the bacteria reconstitution was performed by adding 5mL of the reagent diluents at 5°C. Then 200 µL of the solution was transferred to the cuvettes, and the reagent was stabilized at 15°C for 15 min. In order to enhance the activity of Vibrio Fisheri bacteria, the samples were diluted at 81.8% of initial concentration by adding 22% NaCl solution. Based on luminescence intensity, the screening test 81.8% allow identifying samples toxicity. Bacteria's activity could be reduced by the presence of toxic elements that decrease luminescence. Before measuring the bacteria luminescence, all the samples were filtered with 0.2 mm filters to remove any precipitate or solid matter in the solution. The toxicity values are directly relative to the inhibition rate of bacteria's activity, calculated as following in equation (5)[85,86]:

$$\boldsymbol{Ic_{(t)}}(\%) = \left(\mathbf{1} - \frac{\boldsymbol{LU_{(t)}}}{\boldsymbol{LU_{(0)}} \times \boldsymbol{R_{(t)}}}\right) \times \mathbf{100} \qquad \textbf{(5)}$$

where $LU_{(t)}$ is the intensity of luminescence emitted by bacteria after t=15 min of contact with the sample; $LU_{(0)}$: is the initial intensity of luminescence emitted by bacteria before the addition of the sample; R(t): is the corrected term.

Since luminescence of bacteria decreases over time and under the action of environmental conditions in the absence of toxicity, it is necessary to compensate for the errors due to these factors by taking into account the variability of the luminescence R(t) of the bacteria in a control solution (MilliQ water and NaCl) which gives the LU_0 values. The corrected term is given by equation (6):

$$\boldsymbol{R_{(t)}} = \frac{\boldsymbol{LU_{0(t)}}}{\boldsymbol{LU_0}} \qquad \textbf{(6)}$$

where $LU_{0(t)}$ is the intensity of luminescence emitted by bacteria after a t=5 min or t=15 min of contact with the control solution (MilliQ water and NaCl); and LU_0: is the initial intensity of luminescence emitted by bacteria before the addition of the control solution (MilliQ water and NaCl).

5.10. Quenching tests

Scavengers test were performed in order to determine the main active species responsible of the degradation of ACT. Benzoquinone, isopropanol and EDTA were added to the solution at 10, 5 and 17 µM, respectively, before switching the light on. The experiments performed was the same as the degradation process, an aliquot was withdrawn at different times and LC-MS-MS detected the concentration of ACT.

6. Results and discussion

6.1. Characterization of synthesized nanocomposites

TiO_2-BN-Pd photocatalysts were prepared in three steps, as illustrated in **Figure 2. 1** In the first step, TiO_2 nanofibers (NFs) were prepared by electrospinning than calcined at 400°C under air. **Figure 2. 2** shows the scanning electron microscopy image of TiO_2 NFs after calcination. It can be clearly seen that we have continuous and randomly oriented nanofibers that preserved their morphologies after calcination. In the second step, atomic layer deposition was used to modify the surface of the prepared NFs. First, we have coated TiO_2 with a second semiconductor, Boron Nitride, at 750°C. To compare the effect of BN, 5 cycles (<0.5 nm) and 100 cycles (~8nm) depositions were realized. The as-prepared samples will be designated by TiO_2-BN5 and TiO_2-BN100, respectively. In the last step, a deposition of 100 cycles of Pd has been processed on pure TiO_2 NFs and TiO_2-BN composites (donated as TiO_2-Pd100, TiO_2-BN5-Pd100 and TiO_2-BN100-Pd100). The BN coating has been used to enhance the separation of charge carriers as for Pd, it was added to allow the shift of band gap in the visible. Nanofibers with diameter range between 50 and 400 nm with length of several microns were obtained.

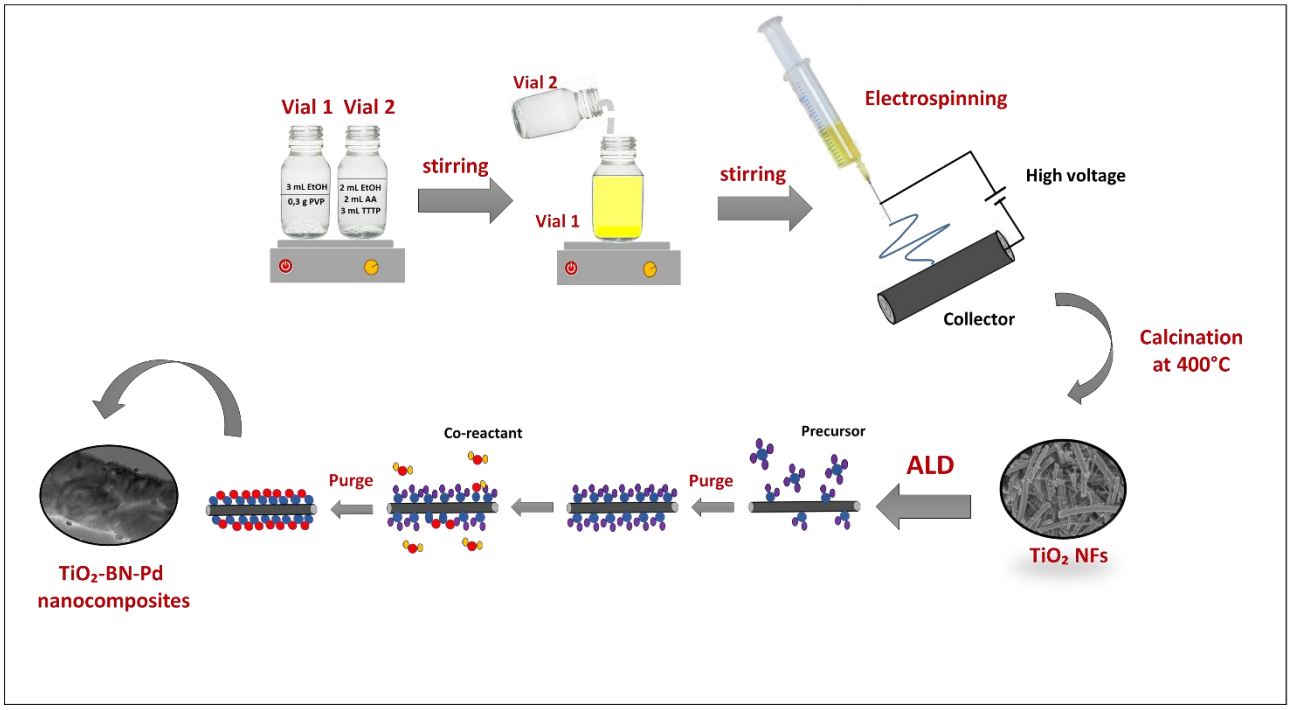

Figure 2. 1. Illustration of the steps for the preparation of nanocomposites, in the first step we prepared the polymeric solution, than electrospinning was performed. The collected nanofibers were then calcined before ALD process.

SEM images of nanocomposites TiO_2-BN5, TiO_2-BN100, TiO_2-Pd100, TiO_2-BN5-Pd100 and TiO_2-BN100-Pd100 (**Figure 2. 2**) show that after ALD deposition, the continuous morphology of TiO_2 was maintained. Nevertheless, when BN deposition increased from 5 to 100 cycles, the surface of TiO_2 NFs became rougher.

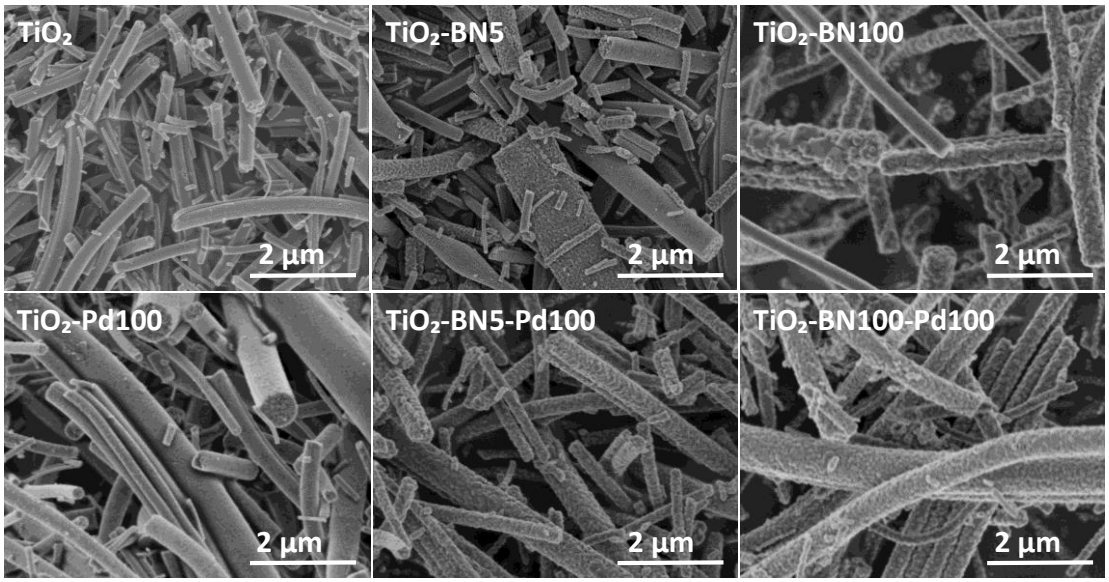

Figure 2. 2. SEM images of TiO_2, TiO_2-BN, TiO_2-Pd and TiO_2-BN-Pd nanocomposites.

In order to get a closer idea about the crystallinity of the prepared catalysts, XRD analysis were conducted. According to the XRD patterns (**Figure 2. 3 a**), pure TiO_2 obtained by electrospinning and calcined at 400°C shows a major peak at 25.3°, corresponding to anatase (101) plane. Furthermore, a small peak at 27.4° is assigned to rutile (110). XRD peaks at 25.3°, 37.9°, 48.2°, 55.1° and 62.9° 2θ diffraction angles were assigned to anatase (101), (004), (200), (211) and (204) crystal planes, whereas XRD peaks at 27.5°, 36.2°, 41.3°, 44.1°, 54,4°, and 69.1° were assigned to rutile TiO_2 (110), (101), (103), (100), (211) and (220) crystalline planes[20].

The concentration of rutile phase was determined using the spurr equation:

$$F_R = 1/(1 + 0.8[I_A(101)/I_R(110)\ ]\ ) \quad (7)$$

Where I_A and I_R are the integrated intensities of the diffraction peaks for anatase (101) and rutile (110) phases, respectively[87].

The anatase and rutile fractions were calculated for all the prepared samples. TiO_2 NFs was composed from 70.5% anatase phase while the anatase fraction varied for doped samples, the fraction was in a range between 43.6% (TiO_2-BN100) and 67.1% (TiO_2-Pd). The values of anatase/ rutile phase are represented in **Table 2. 1.** This decrease in anatase rate in TiO_2-BN100 is due to BN deposition at high temperatures (750°C) where the anatase is no

more stable. Anatase was proved to be the most active phase for photocatalytic degradation due to the lower rates of recombination and higher surface adsorptive capacity of anatase than that of rutile[88]. However, many studies confirmed that a mixture of crystalline phases 30% rutile and 70% anatase make the best photocatalyst for the oxidation of organics when applied to treat wastewater[89]. Hence, crystallinity is not the only parameter to be considered, many other factors could affect the activity and selectivity of photocatalysts, such as surface structure, surface defects, and surface charge[90].

In addition, diffraction peaks of Pd species were not depicted. This may be due to the low deposition loading or the small size of Pd NPs. For BN, the diffraction peak at 2θ = 26° of hexagonal BN related to the (002) direction has not been observed too, it is probably overlapped with the diffraction peak of TiO_2 at the same position[13]. Moreover, the grain sizes of the TiO_2 dominating phase crystals were calculated to be 11.5, 11.6, 23.5, 32.4 nm, 28.2nm and 35.3 for TiO_2, TiO_2-Pd, TiO_2-BN5, TiO_2-BN100, TiO_2-BN5-Pd100 and TiO_2-BN100-Pd100, respectively, based on the Scherrer equation described below:

$$\boldsymbol{D = \frac{K\lambda}{\beta cos\theta}} \qquad \textbf{(8)}$$

Where D is the crystallite size (nm); K is the Scherrer constant, 0.9; λ, is the X-ray wavelength, 0.15406 nm; β is the full-width at the half maximum intensity of the peak, in radians; and θ is the diffraction angle[91]. It can be concluded that the crystallite size increased remarkably when adding BN.

The increase in crystallite size when doping with BN could be due to the incorporation of B/N in the lattice of TiO_2 or to the higher deposition temperature of BN at 750°C and/or the generation of oxygen vacancies inside the TiO_2 lattice[92,93]. To confirm these results TEM and XPS has been performed and discussed below.

Figure 2. 3 b shows the Raman spectrum of TiO_2, TiO_2-BN5, TiO_2-BN100, TiO_2-Pd, TiO_2-BN5-Pd100 and TiO_2-BN100-Pd100. The Raman active mode revealed the characteristic peaks of both crystalline phases of TiO_2, anatase and rutile, confirming the XRD results. For all samples, we observe peaks corresponding to the active mode of anatase phase at 151 and 203 (Eg), 513 (B1g, A1g) and 638 (Eg) cm^{-1}. In addition, nanocomposites samples shows

three peaks corresponding to the active modes of rutile phase at 258 cm^{-1} (B1g), 447 cm^{-1} (Eg) and 633 cm^{-1} (A1g) [12,78]. Furthermore, **Figure 2. 3 c** shows the raman spectra of TiO_2-BN100, with a small band at 1328 cm^{-1} that could be attributed to h-BN active mode[7].

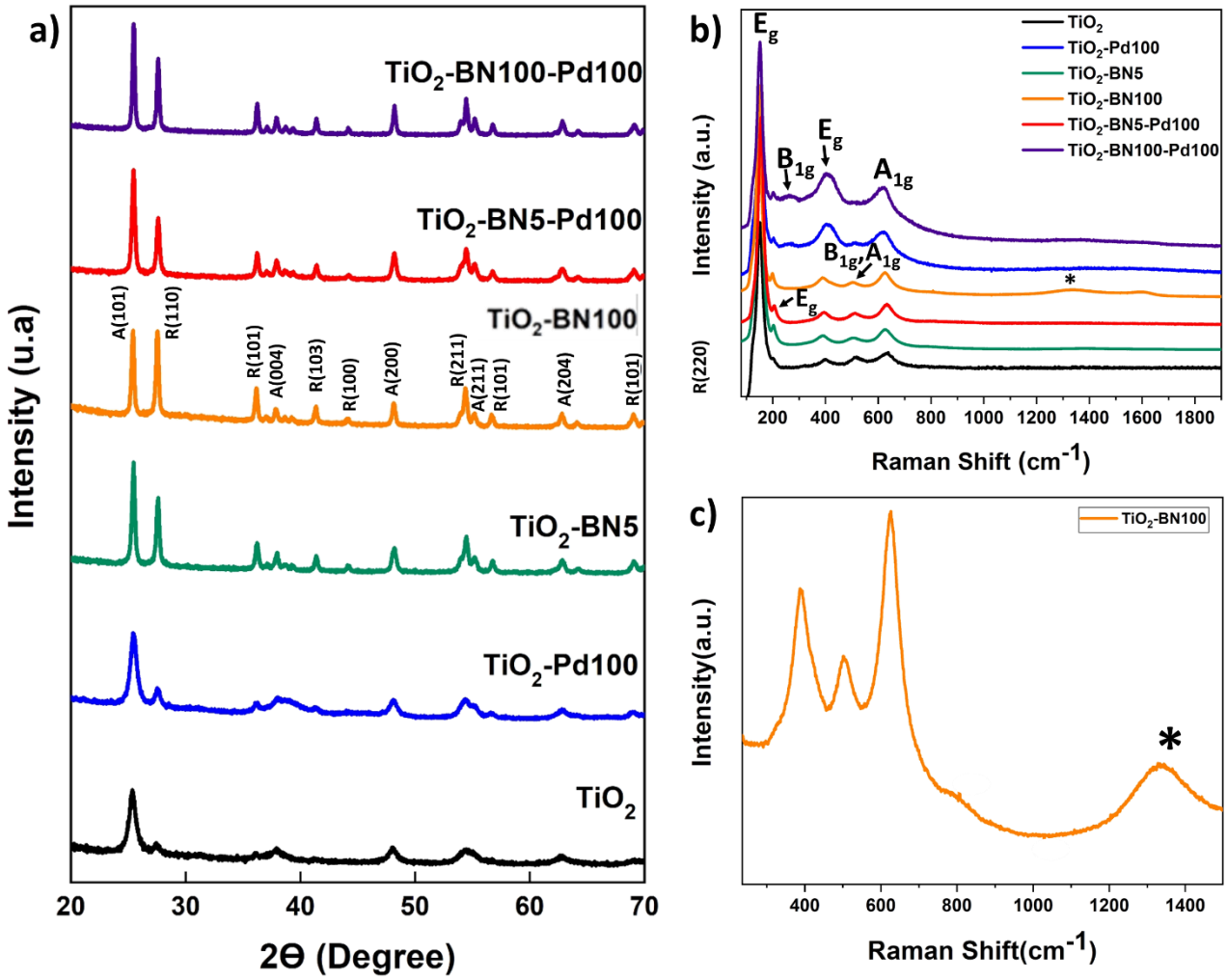

Figure 2. 3. a) XRD data b) Raman spectra of bare TiO_2 and synthesized nanocomposites and c) zoom on Raman spectra of TiO_2-BN100.

In addition to Raman and XRD spectra, Infrared spectroscopy was performed to confirm the functional groups of the prepared NFs**. Figure S2. 3** shows the characteristic absorption band of as-prepared samples. The large band at 800–1200 cm^{-1} is attributed to Ti–O bond. For TiO_2-BN100 and TiO_2-BN100-Pd100 in-plane B-N optical mode (1373 cm^{-1}) was observed. No

peaks could be detected in TiO_2-BN5 and TiO_2-BN5-Pd100, due to the low amount deposited by ALD (less than 0.5nm) and/or the incorporation of BN into the lattice of TiO_2.

Since none of the characterization techniques listed above has confirmed the deposition of Pd, high-resolution transmission electron microscopy (HRTEM) was employed. The state of dispersion of metal Pd particles and BN was examined by TEM for TiO_2-Pd100, TiO_2-BN5-Pd100 and TiO_2-BN100-Pd100. TEM images of TiO_2-Pd100, TiO_2-BN5-Pd100 and TiO_2-BN100-Pd100 photocatalysts (**Figure 2. 4**), shows that Pd NPs are dispersed uniformly on the surface of TiO_2 NFs. The dispersion of Pd decreases with the increase of BN thickness, this could be explained by the nucleation of the precursor on BN surface and/or to the decrease of the nucleation sites. The HRTEM image of **Figure 2. 4 c** shows that the Pd NPs are deposited on the surface lattice of TiO_2. Mackus *et al.* demonstrated that keeping the sites of TiO_2 catalysts available and depositing particles on preferential sites would enhance the selectivity of the synthesized catalysts [57]. The diameter of Pd NPs was in the range of 1 to 5nm. In **Figure 2. 5 f**, the boron nitride layer of TiO_2-BN5-Pd100 sample could not be detected by EDX due to the low deposition rate and since Boron is a light element that could not be easily detected by this technique. The presence of BN in TiO_2-BN5-Pd100 will be confirmed later by XPS. For TiO_2-BN100-Pd100, **Figure 2. 4 i**, the HRTEM image indicate that TiO_2 is covered by a layer of ~7nm of BN. Additionally, **Figure 2. 4 f** displays the SAED with a lattice spacing of 0.344 nm, which corresponds to the anatase (101), while a d-spacing of 0.208nm is attributed to the Pd (111).

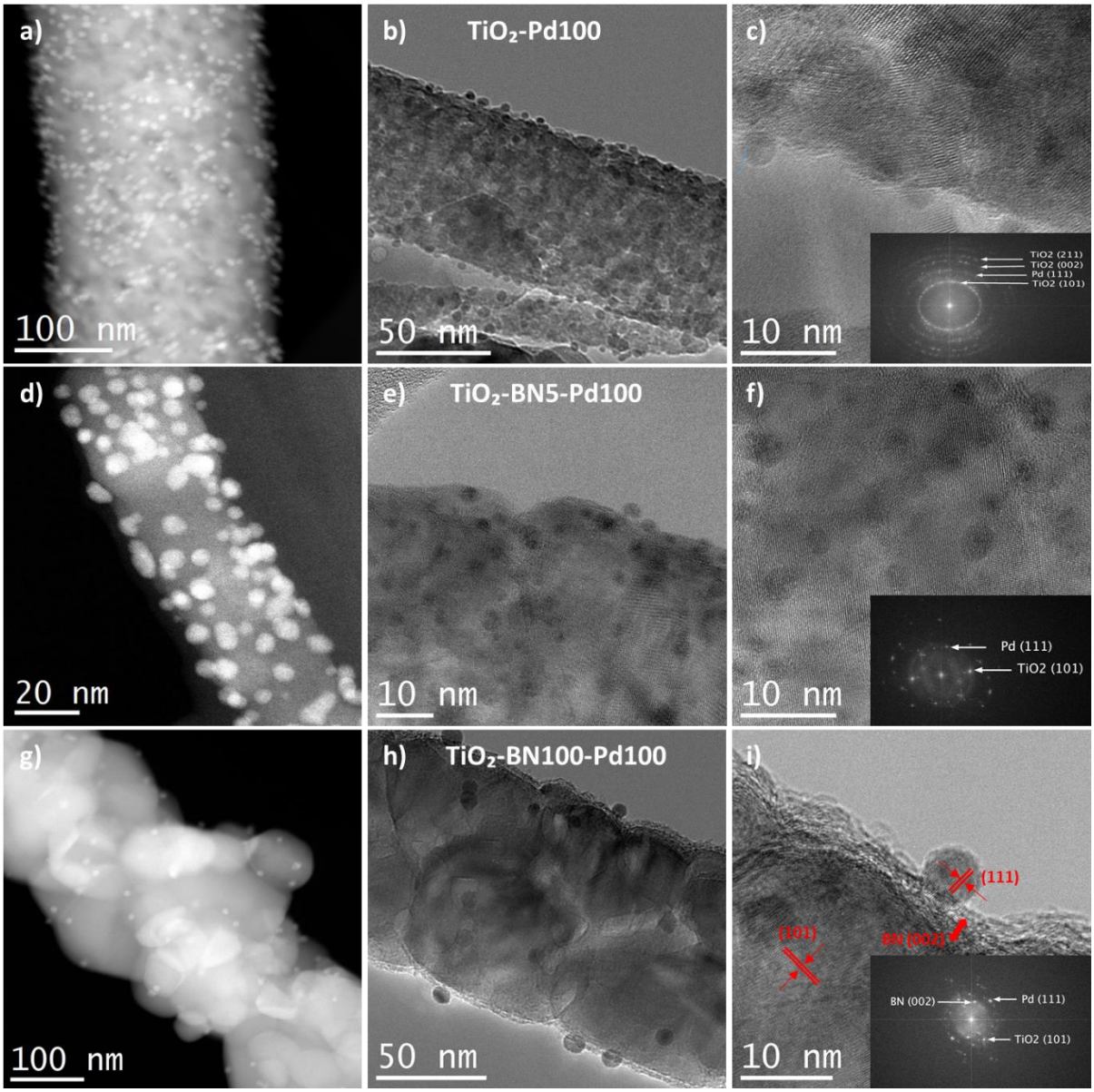

Figure 2. 4. TEM and HRTEM images of (a-c) TiO_2-Pd100; (d-f) $Ti0_2$-BN5-Pd100 and (g-i) TiO_2-BN100-Pd100.

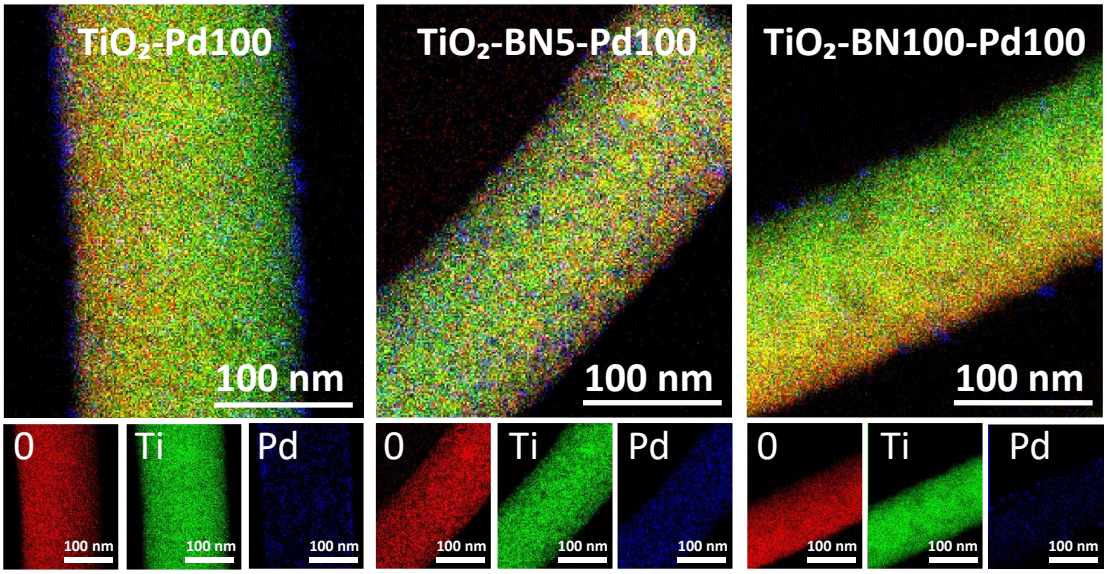

Figure 2. 5. EDS Elemental mapping of TiO_2-Pd100, TiO_2-BN5-Pd100 and TiO_2-BN100-Pd100 nanofibers.

As the obtained TiO_2-BN-Pd nanocomposites were designed and prepared for photocatalytic purposes, it is important to know the chemical state of each element via composition analysis using XPS technique. **Figure S2. 4 a** shows the survey spectra of TiO_2-BN100-Pd100, all elements were clearly seen. **Figure 2. 6 a** shows the Ti 2p XPS spectra of pure TiO_2, TiO_2-BN100, TiO_2-Pd100, TiO_2-BN5-Pd100 and TiO_2-BN100-Pd100 composites. For Ti 2p in TiO_2 sample, two peaks are positioned at 458.7 and 464.4 eV, corresponding to Ti $2p_{3/2}$ and Ti $2p_{1/2}$ states indicating that Ti is 4+ valence. For the TiO_2-BN and TiO_2-Pd samples, Ti 2p peaks are slightly shifted toward higher binding energy (+0.2 eV and + 0.3 eV) due to the inclusion of BN and Pd, respectively, into the TiO_2 lattice and the formation of oxygen vacancies exhibiting a high electron-attracting effect[95]. Similar behavior were observed for O 1s spectrum (**Figure 2. 6 b**). Considering TiO_2 spectrum as reference, O 1s spectra of TiO_2 show a peak at 529.9 eV attributed to Ti-O bond, while TiO_2-BN100-Pd100 shows two characteristic peaks at a higher binding energy 530.1 eV attributed to Ti–O bonds and at 532.6 corresponding to B-O-Ti groups. **Figure S2. 4 b** shows the deconvolution peaks of O 1s element for all samples. Doping TiO_2 with BN and Pd reducued the atomic percentage of Ti-O-Ti and generated new boron nitide bonds in the case of TiO_2-BN100 and more OH groups in the case of TiO_2-Pd100. For the samples with BN coating (**Figure 2. 6 c-d**), the B 1s and N1s elements

are identified. The peaks position of B 1s and N1s are shifted to higher binding energy when incorporating Pd NPs.

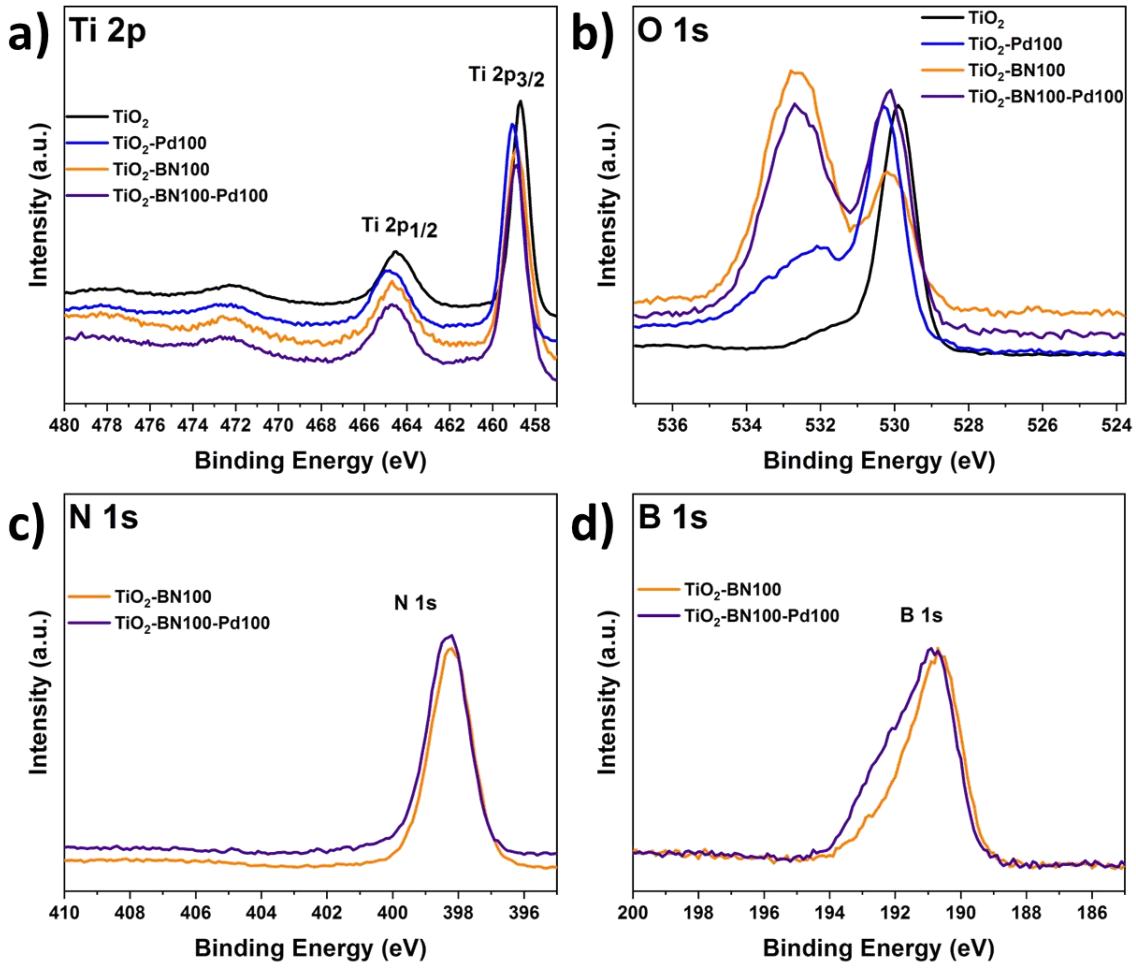

Figure 2. 6. XPS data of a) Ti 2p b) O 1s c) N 1s and B 1s of all prepared samples.

As shown in **Figure 2. 7 a**, the B 1s spectra consist of peaks at the binding energies of 190.5, 191.5 and 192.6 eV assigned to the edge or interfacial boron bonds connected with –N, –OH and -OTi, respectively. The presence of B–O–Ti bonds can also be proved by the O 1s spectra (**Figure S2. 5**) which is consigned to the formation of a chemical B-O-Ti bond between TiO_2 and boron at the edge of TiO_2[5]. For the TiO_2-BN100-Pd100 sample, the B-OH peak was not noticeable due to the incorporation of Pd NPs on BN surface. In **Figure 2. 7 b** the N 1s deconvolution peaks of TiO_2-BN100 composite revealed the presence of two peaks with binding energy at 398.2 and 398.6 eV ascribed to B–N linkages with Ti-O and the presence of

oxidized nitrogen such as N–O–Ti[95]. The atomic percentage and binding energy of all the elements obtained by XPS are resumed in **Table S2. 1**.

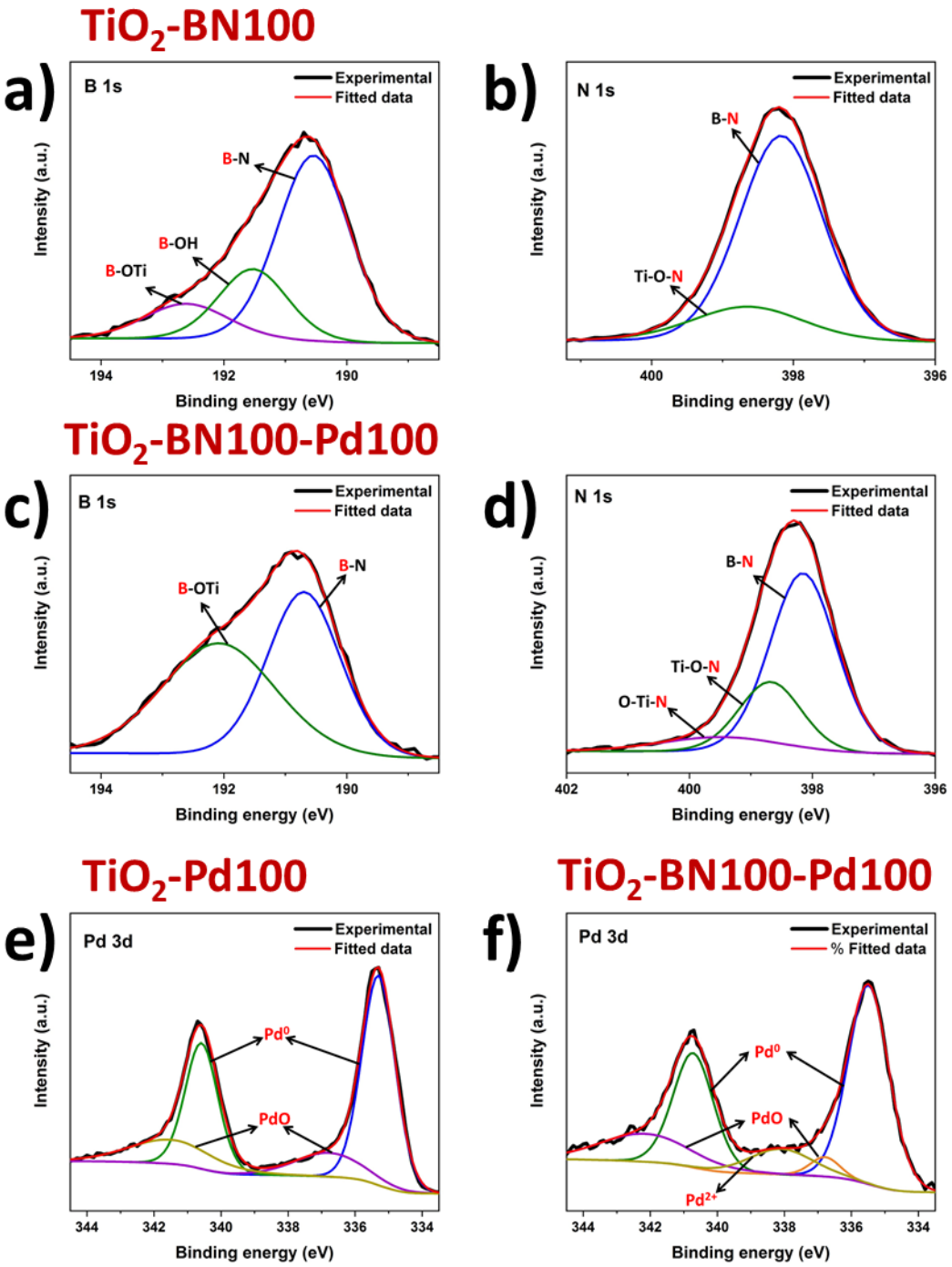

Figure 2. 7. Deconvoluted XPS spectra of B 1s (a-c), N 1s (c-e) and Pd 3d (f-h) for modified TiO_2 by ALD.

Deconvolution of the XPS spectrum was performed to further understand the incorporation of Pd NPs in the prepared samples. From **Figure S2. 4 c**, two peaks at 335.5 and 340.6 eV assigned to Pd $3d_{5/2}$ and Pd $3d_{3/2}$. **Figure 2. 7 e-f** shows a deconvoluted spectrum of Pd in sample TiO_2-Pd100 and TiO_2-BN100-Pd100 , with the main species being Pd^0 for all samples. Composite samples with BN and Pd shows an increase of oxidized Pd species, including PdO. This increase could be assigned to a higher Pd oxidation state on the sample's surface, even at low concentrations. Furthermore, the slight increase of oxidized Pd species in the TiO_2-BN-Pd material in comparison with TiO_2-Pd might be explained by the fact that boron nitride attracts electrons from Pd[96].

The optical properties of pure TiO_2 NFs and TiO_2 composite nanofibers were obtained by UV−Vis absorption spectroscopy measurement**. Figure 2. 8 a** indicates that TiO_2 NFs absorbs light at 378 nm corresponding to a band gap of 3.2±0.01 eV. For TiO_2 nanocomposites fibers, the absorption edges are red-shifted with the energy of 3.17±0.02, 3.11±0.03, 3.11±0.02, 3.10±0.03 and 3.09 ±0.02, corresponding to TiO_2, TiO_2-Pd100, TiO_2-BN5, TiO_2-BN100, TiO_2-BN5-Pd and TiO_2-BN100-Pd, respectively. Moreover, all nanocomposite samples have another absorption edge in the visible range. The observed broad absorption peak was observed in the range of 400-580 nm, centered at 540-550nm. Decrease of the band gap value in TiO_2/BN samples has been reported previously[13]. The explanation of redshift of the band gap and increase of visible absorption in BN samples could be explained by forming new defect states at BN/TiO_2 interface. Formation of Pd-TiO_2 composite resulted in redshift of the band gap and increase of the visible absorption. It was shown that Pd^{2+} states transfer d-electrons towards TiO_2. Depending on electronic configurations (work functions, Fermi level position, …) the d-electrons can reach for conductance band of TiO_2 or defect states[97].

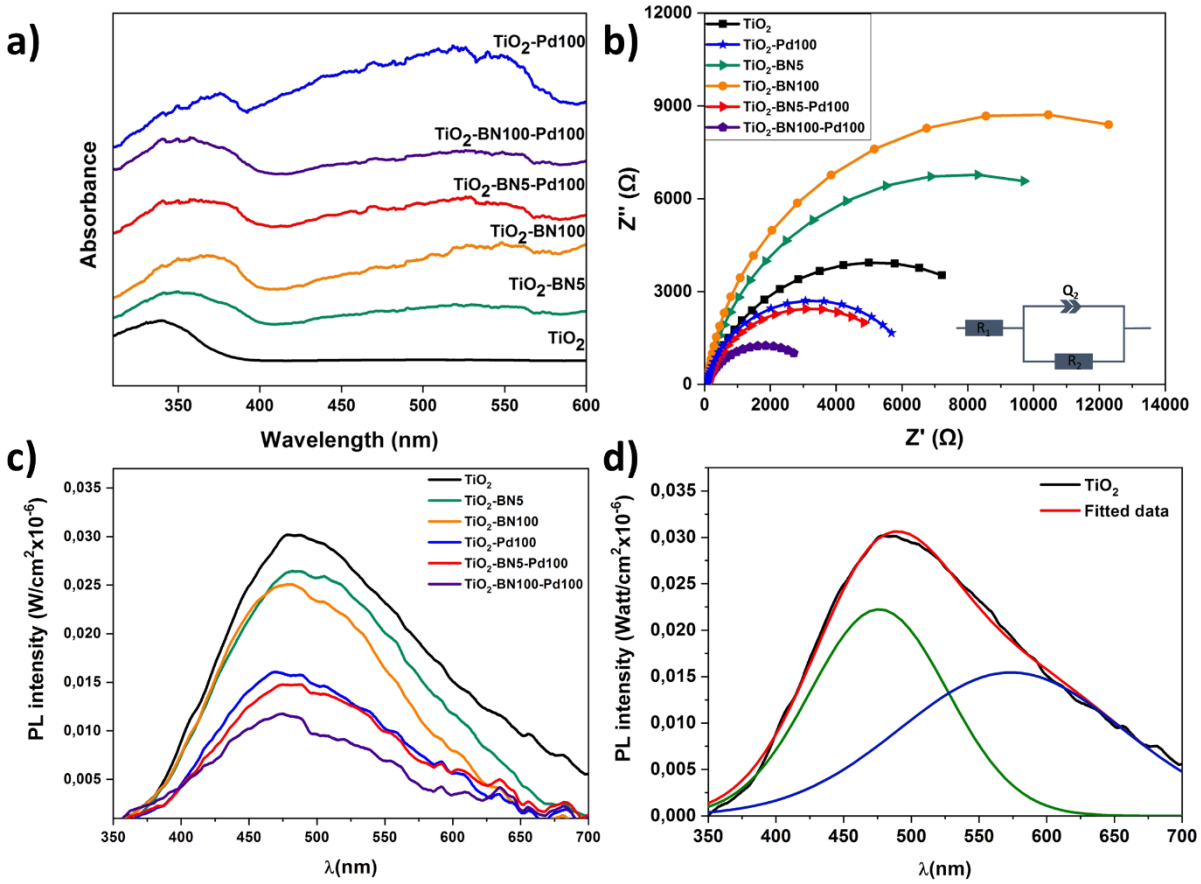

Figure 2. 8. a) UV-Vis diffused reflectance of TiO_2 NFs and nanocomposites; b) EIS Nyquist plots of prepared nanofibers; c) Photoluminescence of all synthesized NFs; d) deconvolution of TiO_2 PL spectra. The PL spectra of the samples is shown in **Figure 2. 8 c.** Typically to TiO_2-based nanostructures, the intensity of the PL was low (quantum efficiency of TiO_2 ~0.005-0.01). All samples showed wide peak, centered at 480 nm. The wide peak of prepared TiO_2 nanostructures could be split into two peaks, located at 476 and 573 nm (**Figure 2. 8 d**). These peaks correspond to self-trapped excitons and oxygen vacancies, respectively[20,98]. Modification of TiO_2 with Pd and BN nanostructures resulted in decreasing the PL. The lowest PL was observed for TiO_2-BN100-Pd100 pointing to higher charge separation rate. Photoluminescence of BN/TiO_2 was studied and explained by N*asr et al.*[13] Small concentrations of BN did not change PL, whereas high BN concentrations (5-10%) reduced PL intensity by 2 times. In addition, photoluminescence intensity decreased in samples with Pd due to formation of Schottky barrier between Pd and TiO_2[99]. Thus, Pd and BN act as additional quenching factors of PL. Values of quantum efficiency test were presented in **Table 2. 1**. It

should be noted that the yields reported by others cannot be directly compared as there are differences in reactor systems, source of irradiation, volume and concentration of the catalyst[100]. The apparent quantum yield is a parameter, which is usually defined as the ratio of converted reactant molecules over the number of photons entering the reactor. A metal oxide material such as TiO_2 (anatase and/or rutile) could never absorb all the incident photon flow from a given source, which can affect the calculation of QE[101]. The values of absorption and scattering coefficients are represented in **Figure S2. 2.** As shown in **Table 2. 1**, higher quantum yield efficiency was attributed to TiO_2-BN-Pd nanocomposite, which the higher ACT degradation can explain.

Table 2. 1: Anatase/ rutile faction, crystallite size, band gap and QE values of all catalysts.

Sample	Anatase (%)	Rutile (%)	Crystallite size (A) (nm)	Band gap (eV)	Quantum Efficiency (%)
TiO_2	70.5	29.5	11.5	3.2±0.01	2.5
TiO_2-Pd100	67.1	32.9	11.6	3.17±0.02	3.6
TiO_2-BN5	53.7	46.2	23.5	3.11±0.03	0.9
TiO_2-BN100	43.6	56.4	32.4	3.11±0.02	1.3
TiO_2-BN5-Pd100	57.2	42.8	28.2	3.10±0.03	12.5
TiO_2-BN100-Pd100	53.4	46.6	35.3	3.09±0.02	21.7

The charge transfer resistance of the photogenerated carriers is investigated through EIS experiments**. Figure 2. 8 b** shows the Nyquist diagrams of pristine TiO_2 and modified TiO_2 samples. It was found that the diameters of the semicircle decreased with the doped samples with Pd or BN- Pd and the lower value was obtained with TiO_2-BN100-Pd100 nanocomposites. The smaller EIS radius demonstrates the weaker electronic impedance and higher separation of photogenerated electron-hole pairs. This phenomenon benefits from the electronic band structure formed when TiO_2 is doped with BN and Pd, and through this structure, the ultimate catalytic activities can be promoted. Moreover, **Table 2. 2** shows that the smallest polarization resistances are obtained on TiO_2-BN100-Pd100, where R1 represents the bulk resistance of electrodes and electrolyte, R2 denotes the resistance formed at the nanofibers' and

electrolyte and Q2 designates the double layer capacitance at the nanofibers and the electrolyte interface. The lowest R_2 was attributed to TiO_2-BN100-Pd100 nanocomposites with a value of 3.74 KΩ, which refers to a lower resistance between fibers and electrolyte interface. TiO_2-BN100-Pd100 possesses a higher charge transfer rate and a better separation of photogenerated electron-hole than the other prepared catalysts, which is with good correlation with the degradation results.

Table 2. 2: Resistance values from EIS of all synthesized nanofibers.

Sample	R_1 (Ω)	R_2 (KΩ)
TiO_2	64.34	10.22
TiO_2-Pd100	65.56	6.44
TiO_2-BN5	76.88	15.86
TiO_2-BN100	83.17	19.82
TiO_2-BN5-Pd100	70.29	6.26
TiO_2-BN100-Pd100	63.66	3.74

6.2. PHOTOCATALYTIC DEGRADATION

In order to evaluate the modification of TiO_2 surface by ALD, photocatalytic performance of TiO_2 nanofibers with different amounts of Pd and BN were evaluated by degrading ACT in ultrapure water under UV and visible light**. Figure 2. 9 a-b** shows the degradation of ACT under UV light. Herein, the degradation rate was determined by LC-MS-MS every 5 minutes. It can be seen that the degradation with TiO_2-BN-Pd was faster than TiO_2. A total degradation of ACT was reached in less than 15 minutes with TiO_2-Pd100, TiO_2-BN5-Pd00 and TiO_2-BN100-Pd100 with a degradation rate of ACT corresponding to 0.06 $mg.L^{-1}.min^{-1}$ under UV irradiation. For TiO_2 catalyst, the process took 60 min until the degradation was complete. The fabrication of heterojunction with both BN and Pd at the same time has shown an efficient degradation under UV and visible light due to the enhancement of separation of electron-hole pairs as shown by PL and EIS results.

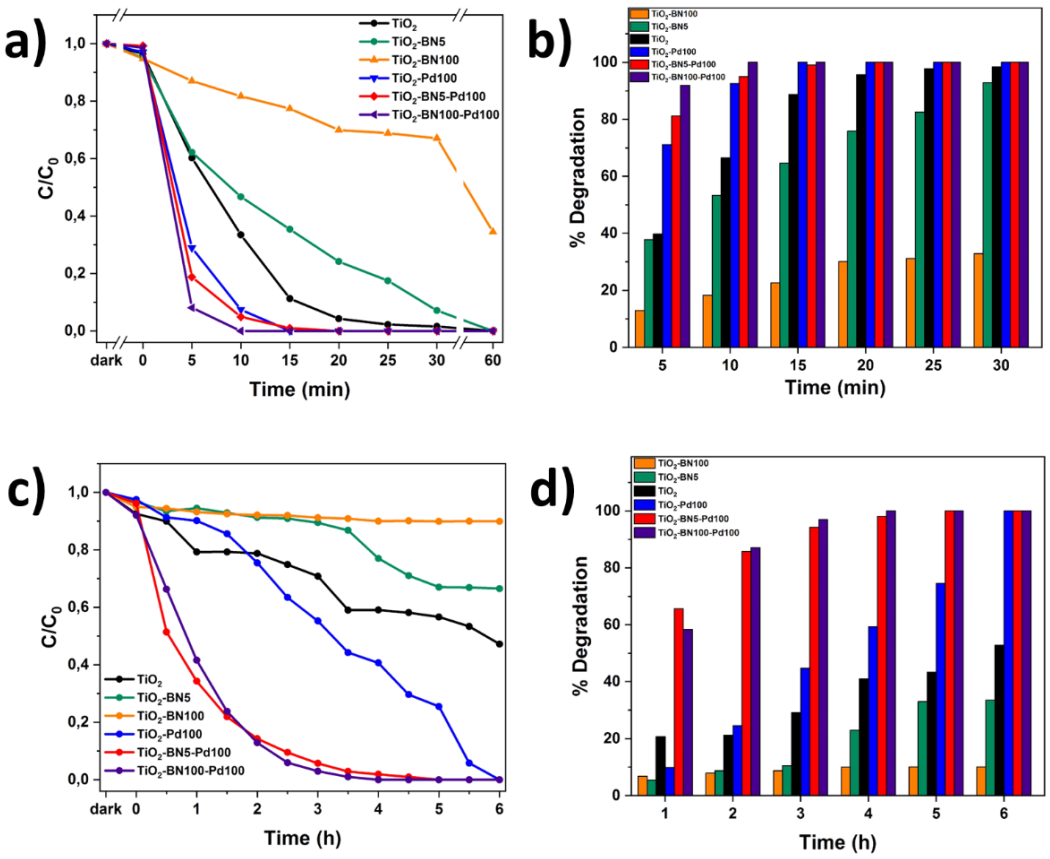

Figure 2. 9. All prepared catalysts were decomposition of ACT and degradation percentage under a-b) UV and c-d) visible light irradiation. Each experiment was conducted for at least three times with relative errors of less than 5%.

After 30 min in the dark, the equilibrium was reached. **Figure 2. 9 a-c** shows that the degradation of ACT by TiO_2-BN-Pd was faster than pristine TiO_2. The degradation of the pollutant reached 87% with TiO_2-BN100-Pd100 after 2h of visible irradiation comparing to just 20% with TiO_2 not modified (**Figure 2. 9 b**). Furthermore, it can be clearly seen that when we add the Pd, the degradation efficiency increases, and after 4 hours of irradiation, 100% of the pollutant was degraded. The degradation speed of ACT using TiO_2-BN100-Pd100 under visible irradiation after 4 hours was 0.004 $mg.L^{-1}.min^{-1.}$ This confirms that the Pd has shifted the band gap of TiO_2 to the visible range (confirmed by UV reflectance results), thus improving the catalytic activity under visible light[52]. Moreover, **Figure 2. 9 d** showed that when using TiO_2-Pd100 as a photocatalyst, the degradation has slightly improved compared to TiO_2 after 2 hours. A degradation percentage of 24% versus 21% was obtained. After 6 hours, the

nanocomposite has led to a total degradation of ACT in comparison with pure TiO_2 that had degraded only 50% of the pollutant. Doping with noble metals like Pd is an effective method to improve the photocatalytic efficiency of TiO_2 as this increases its visible-light capacity. When comparing TiO_2-BN-Pd nanocomposites and TiO_2-Pd, degradation of ACT was enhanced with TiO_2-BN-Pd. Shing *et al.* have already confirmed that heterojunction engineering promoted charge transfer and enhanced photocatalytic activities of photocatalysts[102]. This could be explained by the formation of Schottky junctions at the interface of noble metal nanoparticles and the semiconductor. The addition of Pd nanoparticles onto TiO_2-BN surface improves UV–visible light degradation of TiO_2 and creates Schottky junctions, which reduces the recombination of photogenerated carriers in TiO_2[103]. Moreover, TiO_2-BN100-Pd100 showed a better degradation efficiency than TiO_2-BN5-Pd100 and this is due to the lower amount of Pd deposited on TiO_2-BN100 as confirmed by TEM images. It was found that excessive Pd loading could decrease the performance of the catalyst. Moreover, Leong *et al.* demonstrated that the synergistic effects of the –O–Pd–O– surface species are mainly responsible for the enhanced photocatalytic activity, which confirms our findings since TiO_2-BN100-Pd100 possesses a higher % of Pd-O than TiO_2-BN5-Pd100 confirmed by deconvoluted XPS data[104].

The kinetic behavior of the as-prepared catalysts was also investigated under both lights. The photodegradation reactions follow a pseudo-first-order reaction[38]. **Figure 2. 10 a-c** shows the linear dependence between ln (C0/C) and time. The degradation rate increased as follow: TiO_2-BN100 < TiO_2-BN5 < TiO_2 < TiO_2-Pd100 < TiO_2-BN5-Pd100 < TiO_2-BN100-Pd100 under visible light as shown **in Figure 2. 10 b.** The degradation rate of TiO_2-BN100-Pd100 nanocomposite is 9 time higher than TiO_2 nanofibers under visible light and almost 2 times higher under UV light. These results confirm the role of heterojunction between TiO_2, BN and Pd in enhancing the degradation of ACT under visible light. Palladium decreases the band gap of TiO_2, as confirmed by UV reflectance and photoluminescence results, leading to a higher degradation in the visible range, while BN improves the separation efficiency of electron – holes (confirmed by PL results). The increase of photocatalytic degradation of ACT in the presence of BN and Pd could be attributed to the fast transfer of photogenerated electrons from the semiconductor (BN) to the metal NPs (Pd), which enhances the separation of the electrons and holes. Moreover, the shift in optical absorption of the catalyst in the visible

region is attributed to the Pd loading and the formation of B-O-Ti bond. This leads to an energy rearrangement that will affect the charge balance. Hence, the band gap of TiO_2-BN-Pd is narrowed and excited wavelength is extended from UV to visible light region[55,104,105].

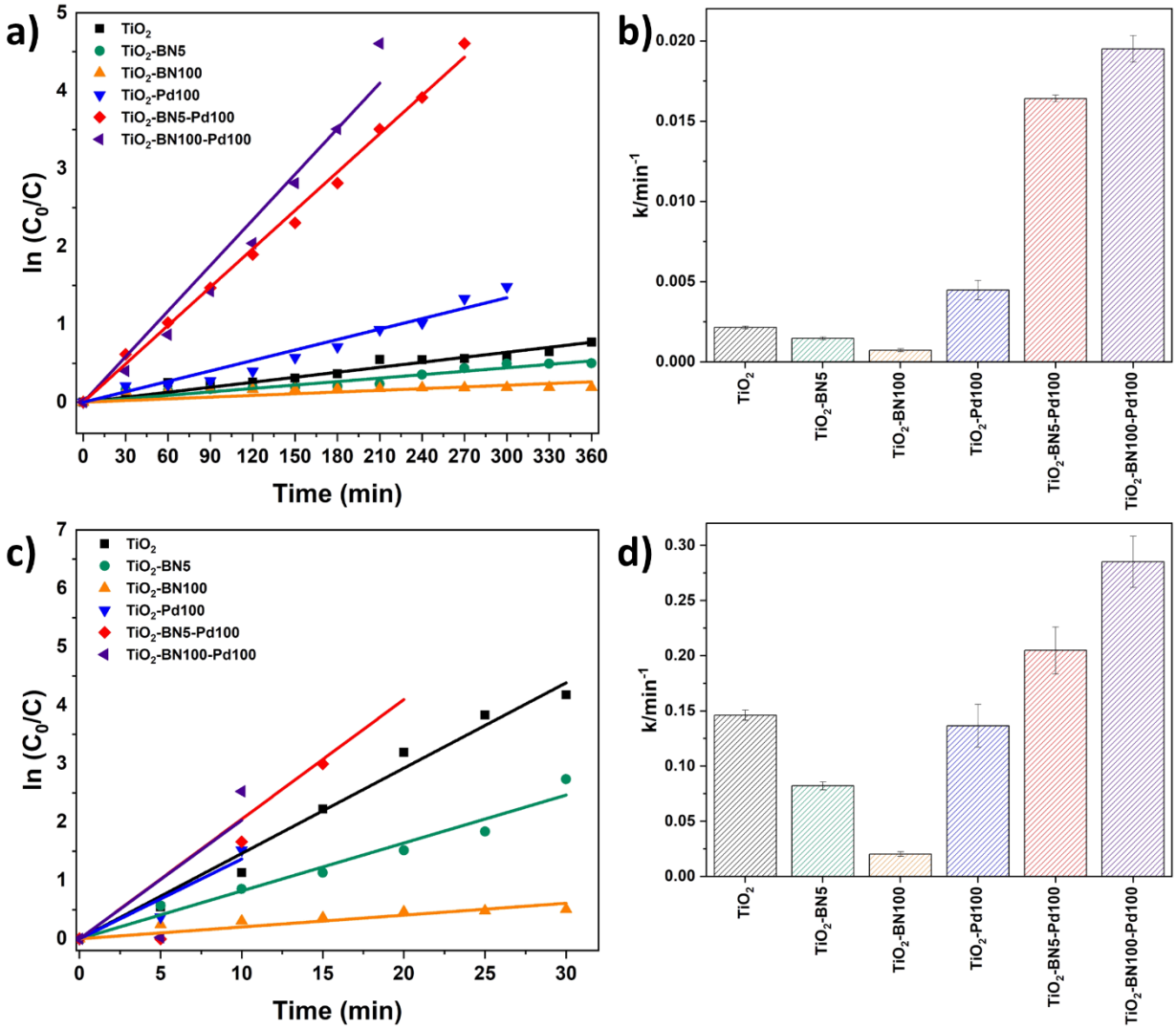

Figure 2. 10. Kinetics models and rate constant values of ACT degradation under a-b) UV and c-d) visible irradiation, respectively. All experiments were conducted for at least three times and relative errors were less than 5%.

Since TiO_2-BN100-Pd100 nanocomposites has shown the best degradation efficiency, a stability test was performed to confirm the reusability of the catalyst. After each cycle, the catalyst was filtered, washed with deionized water, dried at 100°C then reused with no further steps. In **Figure 2. 11 a**, the degradation of ACT remained unchanged under visible light after 5 cycles. For UV irradiation, the degradation efficiency dropped by less than 5% after the

second cycle, but kept almost stable until the fifth cycle (**Figure 2. 11 b)**. This reveals that using ALD allows enhancing the metal-support interaction, increasing the active sites, and improving the catalyst's stability. The prepared catalyst remains stable and can be reused to degrade water pollutants, thus aiming at the advantage of atomic layer deposition in the photocatalytic field.

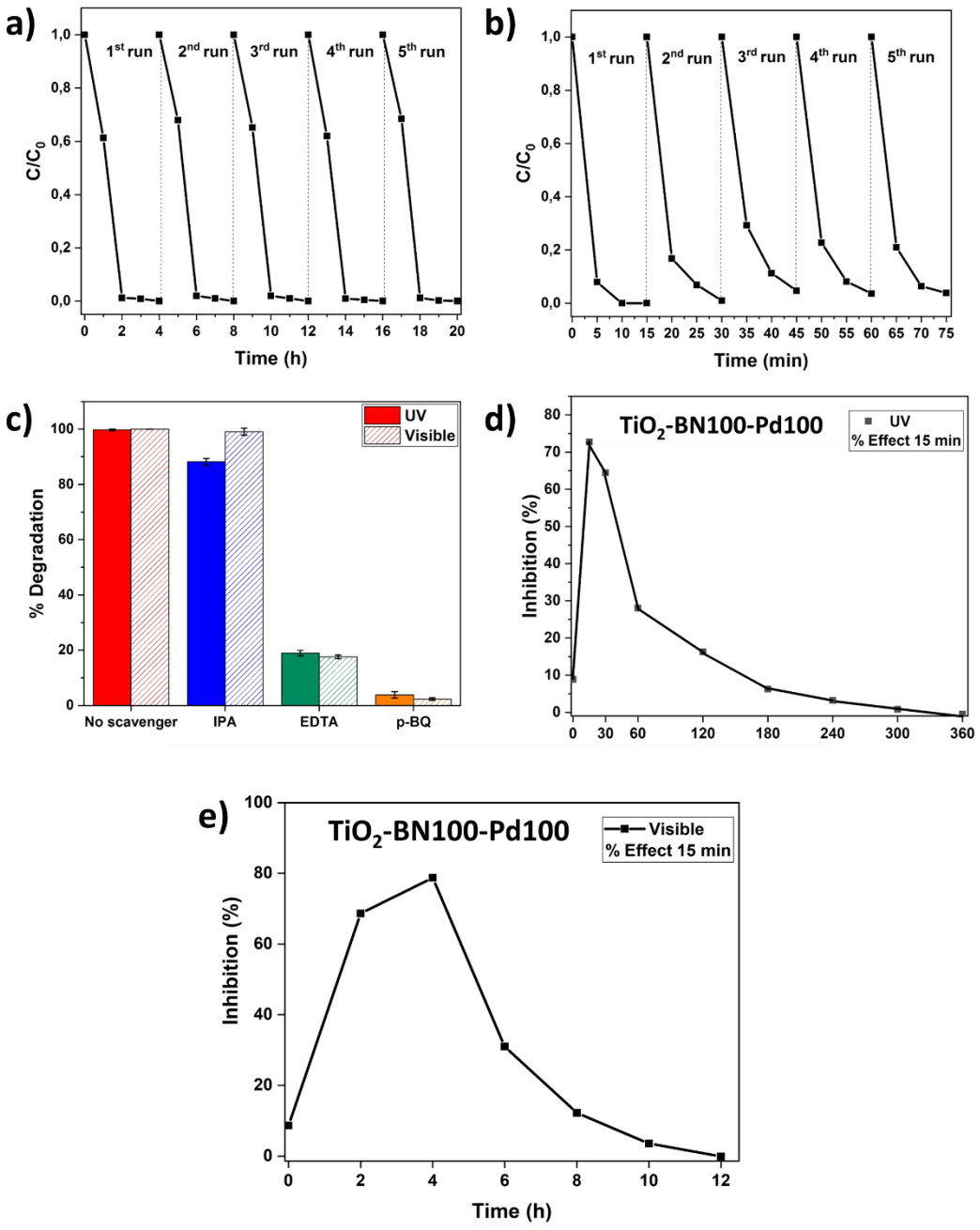

Figure 2. 11. Recycling test of TiO_2-BN100-Pd100 under a) visible and b) UV irradiation; c) Scavenger plot for determining reactive species in the degradation of ACT by TiO_2-BN100-Pd100; Inhibition of luminescence of V. fischeri marine bacteria during ACT photocatalysis after 15min exposure between the bacterial strain and the degradation solution d) under UV irradiation and e) under visible irradiation.

All further tests were done on TiO_2-BN100-Pd100 nanocomposites. It is known that three main active species could participate in the catalytic process. In order to understand the mechanism of the degradation of ACT by the catalyst, trapping experiments were carried out. Ethylenediaminetetracetate (EDTA), p-benzoquinone (p-BQ) and isopropanol (IPA) were used as trapping reagents for holes (h^+), superoxide radicals ($^{\cdot}O_2^-$) and hydroxyl radicals ($^{\cdot}OH$), respectively. **Figure 2. 11 c** shows that the degradation efficiency has clearly decreased from 100% to less than 20% when adding p-BQ and EDTA, while it remains almost unchanged when adding IPA under both lights UV and Visible, showing that $^{\cdot}OH$ do not contribute in the degradation. However, $^{\cdot}O_2^-$ and h^+, both has a major role in the photocatalytic degradation of ACT.

6.3. Toxicity tests

Identification of ACT intermediates and their metabolic pathways is essential to evaluate their potential impacts on human health, the environment and other aquatic life forms. In this work, we found that $^{\cdot}O_2^-$ and h^+ are the active species in the photocatalytic degradation of ACT, this agrees with previously published results [106]. Zhang *et al.* suggested a direct hole (h^+) oxidation route as the initial step for ACT degradation. Then the formed phenolic radical loses a cation and leads to phenoxyl radicals that will react with superoxide radical. During this route, harmful metabolites could be formed. Some of these intermediates could be more harmful than the initial pollutant, such as 1,4-benzoquinone, benzoic acid and benzaldehyde. In order to understand the pathways degradation, the global toxicity of the solution was studied. ACT itself shows a low inhibition percentage (8%) as it is not a hazardous pollutant for this strain of bacteria (**Figure 2. 11 c-d**). After 15 min time contact between the solution and V. fischeri bacteria, the acute toxicity of the treated solution strain increased rapidly at

the early stage of the treatment and reached 68% at 15 min UV irradiation (**Figure 2. 11 c**) and 72% after 2h visible irradiation (**Figure 2. 11 d**). This result is relevant and consistent with regard to the previously proved formation of toxic aromatic by-products such as 1,4-benzoquinone, benzoic acid and benzaldehyde[74–76]. After 3h UV irradiation and 12h degradation under visible light, the toxicity markedly declined to a value near 0% inhibition and lower than the initial % of inhibition of ACT. At that point, short-chain carboxylic acids and aromatic compounds could be formed continuously and then transformed to none toxic compounds. Further studies should be done to identify all the byproductsof this degradation mechanism. As mentioned before, the photocatalyst used in this work was not reported before, but a comparison with other works was summarized in **Table 2. 3**. The comparison is not easy since many factors could vary such as pollutant concentration, catalyst concentration, pH of the solution and most importantly the irradiation type. However, it can be clearly seen that the prepared catalyst (TiO_2-BN-Pd) showed interesting results with a high degradation efficiency, recyclability, and most importantly, fast degradation rate.

Table 2. 3: Comparison of degradation efficiency of differently prepared photocatalysts

Pollutant	$C_{Pollutant}$ ($mg.L^{-1}$)	Photocatalyst	$C_{Catalyst}$ ($g.L^{-1}$)	Type of irradiation	Energy ($W.m^{-2}$)	Degradation time (min)	pH	Removal efficiency (%)	References
ACT	**1**	**TiO_2-BN100-Pd100**	**0.5**	**Medium pressure metal halide UV**	**NA**	**10**	**6.8**	**100**	**In this work**
ACT	**1**	**TiO_2-BN100-Pd100**	**0.5**	**halogen linear lamp**	**NA**	**180**	**6.8**	**98**	**In this work**
ACT	20	Pt-TiO_2	0.4	Solar irradiation	500	180	6.3	100	[110]
ACT	20	Degussa P25	2	UV irradiation 365nm	NA	60	NA	98	[111]
ACT	0.08	TiO_2-Ag5%	1	UV irradiation 365nm	NA	180	NA	98	[112]
ACT	15	$K_2S_2O_8$-TiO_2	2	Visible irradiation LED lamps	168.5	390	6.9	93	[113]

MO	10	10%BN/TiO_2 NFs	0.4	UV irradiation	NA	75	NA	99	[13]
MB	10	BN/TiO_2 composite	0.33	Visible light	NA	200	NA	79	[5]
MB RhB Phenol	150	F-BN/TiO_2 composite	0.05	visible light irradiation	NA	105	NA	92 90.5 78	[114]
RhB	10	12 wt% BN/TiO_2	0.5	visible-light Xe lamp	1000	150	NA	99	[115]
ACT	10	MWCNT10%-TiO_2-SiO_2	NA	Visible irradiation high pressure mercury lamp	73.1–75.3	60	7	81.6	[116]
ACT	30	Fe_2O_3-TiO_2	0.25	solar simulator halogen lamp	140	180	8	94.8	[117]
ACT	5	$BaTiO_3$/TiO_2 (3 :1)	1	UV/Vis xenon lamp	NA	240	7	95	[118]
ACT	50	TiO_2@rGO TG_3	2	UVA/LED	950	50	5.4	100	[119]
RhB	10	12% h-BN/TiO_2	0.75	visible light	NA	120	NA	95	[14]
ACT	5	3% (w/w) WO_3/TiO_2/SiO_2	1.5	xenon lamp	NA	360	9	95	[120]
ACT	18	TiO_2-NFs-SSF	NA	UV light Blue lamps	27	200	6-7	40	[121]
MB	2	5%Pd/TiO_2	NA	visible white light	4	1500	NA	10	[105]
AMX	20	Pd/TiO_2	4	Visible light tungsten	NA	300	NA	97.5	[104]

7. Conclusion

To sum up, by combining two different techniques, electrospinning and ALD, six photocatalysts based on TiO_2 nanofibers coated by BN and Pd by ALD were synthesized: pristine TiO_2, TiO_2-Pd100, TiO_2-BN5, TiO_2-BN100, TiO_2-BN5-Pd100 and TiO_2-BN100-Pd100. The influence of nanocomposites catalyst on degradation of water pollutants was studied, using ACT as a model pollutant. XRD and RAMAN spectroscopy results indicate that the modification mechanism by ALD, allowed the combination of crystalline phases of TiO_2 with different percentages of anatase-rutile phase. Moreover, TEM images showed the good dispersion of Pd NPs on the surface of nanofibers, the amount of Pd decreased with the increase of BN cycles. TiO_2-BN-Pd samples showed the best photocatalytic activity regarding ACT visible light irradiation (9 times higher than bare TiO_2), though their efficiency depends on the Schottky barrier-type separation from the deposition of another heterojunction material and noble metals on TiO_2. PL and EIS results confirmed that TiO_2-BN-Pd hybrids own a superior charge separation ability from TiO_2, TiO_2-BN and TiO_2-Pd, which was devoted in the higher degradation efficiency. Finally, the use of the ALD technique to modify the interface of TiO_2 shows a very promising pathway to enhance degradation of micropollutant and their intermediates in wastewater, by allowing a conformal coating with thickness control and formation of composites materials. Although additional studies should be conducted with other pollutants and on wastewater to estimate the real efficiency of the prepared nanomaterials, the results presents open prospects for the tuning of photocatalysts by ALD.

References

1. Mekonnen MM, Hoekstra AY. Four billion people facing severe water scarcity. *Sci Adv*. 2016;2(2):e1500323.

2. Gopinath KP, Madhav NV, Krishnan A, Malolan R, Rangarajan G. Present applications of titanium dioxide for the photocatalytic removal of pollutants from water: A review. *J Environ Manage*. 2020;270:110906. doi:10.1016/j.jenvman.2020.110906

3. Hou C, Jiao T, Xing R, Chen Y, Zhou J, Zhang L. Preparation of TiO2 nanoparticles modified electrospun nanocomposite membranes toward efficient dye degradation for wastewater treatment. *J Taiwan Inst Chem Eng*. 2017;78:118-126. doi:10.1016/j.jtice.2017.04.033

4. Kyung H, Lee J, Choi W. Simultaneous and Synergistic Conversion of Dyes and Heavy Metal Ions in Aqueous TiO2 Suspensions under Visible-Light Illumination. *Environ Sci Technol*. 2005;39(7):2376-2382. doi:10.1021/es0492788

5. Singh B, kaur G, Singh P, et al. Nanostructured BN–TiO2 composite with ultra-high photocatalytic activity. *New J Chem*. 2017;41(20):11640-11646. doi:10.1039/C7NJ02509B

6. Carbonaro S, Sugihara MN, Strathmann TJ. Continuous-flow photocatalytic treatment of pharmaceutical micropollutants: Activity, inhibition, and deactivation of TiO2 photocatalysts in wastewater effluent. *Appl Catal B Environ*. 2013;129:1-12. doi:10.1016/j.apcatb.2012.09.014

7. Van Doorslaer X, Dewulf J, De Maerschalk J, Van Langenhove H, Demeestere K. Heterogeneous photocatalysis of moxifloxacin in hospital effluent: Effect of selected matrix constituents. *Photocatal Disinfect Remov Contam Emerg Concern*. 2015;261:9-16. doi:10.1016/j.cej.2014.06.079

8. Nada AA, Orimolade BO, El-Maghrabi HH, et al. Photoelectrocatalysis of paracetamol on Pd–ZnO/N-doped carbon nanofibers electrode. *Appl Mater Today*. 2021;24:101129.

9. Titchou FE, Zazou H, Afanga H, et al. Electrochemical oxidation treatment of Direct Red 23 aqueous solutions: Influence of the operating conditions. *Sep Sci Technol*. Published online September 26, 2021:1-20. doi:10.1080/01496395.2021.1982978

10. Wang H, Zhang L, Chen Z, et al. Semiconductor heterojunction photocatalysts: design, construction, and photocatalytic performances. *Chem Soc Rev*. 2014;43(15):5234-5244. doi:10.1039/C4CS00126E

11. Zhang J, Hou X, Pang Z, et al. Author ' s Accepted Manuscript Fabrication of hierarchical TiO 2 nanofibers by microemulsion electrospinning for photocatalysis applications. *Ceram Int*. Published online 2017. doi:10.1016/j.ceramint.2017.08.166

12. Stucchi M, Bianchi CL, Argirusis C, et al. Ultrasound assisted synthesis of Ag-decorated TiO2 active in visible light. *Ultrason Sonochem*. 2018;40:282-288. doi:10.1016/j.ultsonch.2017.07.016

13. Nasr M, Viter R, Eid C, Habchi R, Miele P, Bechelany M. Enhanced photocatalytic performance of novel electrospun BN/TiO2 composite nanofibers. *New J Chem*. 2017;41(1):81-89. doi:10.1039/C6NJ03088B

14. Li Q, Hou X, Fang Z, et al. Construction of layered h-BN/TiO2 hetero-structure and probing of the synergetic photocatalytic effect. *Sci China Mater*. 2020;63(2):276-287. doi:10.1007/s40843-019-1180-8

15. Nada AA, Nasr M, Viter R, Miele P, Roualdes S, Bechelany M. Mesoporous ZnFe2O4@TiO2 Nanofibers Prepared by Electrospinning Coupled to PECVD as Highly Performing Photocatalytic Materials. *J Phys Chem C*. 2017;121(44):24669-24677. doi:10.1021/acs.jpcc.7b08567

16. García-Zaleta DS, Torres-Huerta AM, Domínguez-Crespo MA, García-Murillo A, Silva-Rodrigo R, González RL. Influence of Phases Content on Pt/TiO2, Pd/TiO2 Catalysts for Degradation of 4-Chlorophenol at Room Temperature. Low J, ed. *J Nanomater*. 2016;2016:1805169. doi:10.1155/2016/1805169

17. Wang M, Liu Z, Fang M, et al. Enhancement in the photocatalytic activity of TiO 2 nano fi bers hybridized with g-C 3 N 4 via electrospinning. 2016;55:2-8. doi:10.1016/j.solidstatesciences.2016.02.002

18. Abellán MN, Giménez J, Esplugas S. Photocatalytic degradation of antibiotics: The case of sulfamethoxazole and trimethoprim. *Sel Pap Present 5th Eur Conf Sol Chem Photocatal Environ Appl SPEA 5 4-8th Oct 2008*. 2009;144(1):131-136. doi:10.1016/j.cattod.2009.01.051

19. Zhou C, Lai C, Zhang C, et al. Semiconductor/boron nitride composites: Synthesis, properties, and photocatalysis applications. *Appl Catal B Environ*. 2018;238:6-18. doi:10.1016/j.apcatb.2018.07.011

20. Nasr M, Abou Chaaya A, Abboud N, et al. Photoluminescence: A very sensitive tool to detect the presence of anatase in rutile phase electrospun TiO2 nanofibers. *Superlattices Microstruct*. 2015;77:18-24. doi:10.1016/j.spmi.2014.10.034

21. Sayed FarheenN, Jayakumar OD, Sasikala R, et al. Photochemical Hydrogen Generation Using Nitrogen-Doped TiO2–Pd Nanoparticles: Facile Synthesis and Effect of Ti3+ Incorporation. *J Phys Chem C*. 2012;116(23):12462-12467. doi:10.1021/jp3029962

22. Nasr M, Balme S, Eid C, Habchi R, Miele P, Bechelany M. Enhanced Visible-Light Photocatalytic Performance of Electrospun rGO/TiO2 Composite Nanofibers. *J Phys Chem C*. 2017;121(1):261-269. doi:10.1021/acs.jpcc.6b08840

23. Khan H, Jiang Z, Berk D. Molybdenum doped graphene/TiO2 hybrid photocatalyst for UV/visible photocatalytic applications. *Sol Energy*. 2018;162:420-430. doi:10.1016/j.solener.2018.01.055

24. Pascariu P, Airinei A, Iacomi F, Bucur S, Suchea MP. Chapter 12 - Electrospun TiO2-based nanofiber composites and their bio-related and environmental applications. In: Dinca V, Suchea MP, eds. *Functional Nanostructured Interfaces for Environmental and Biomedical Applications*. Elsevier; 2019:307-321. doi:10.1016/B978-0-12-814401-5.00012-8

25. Chen Z, Zhao J, Yang X, et al. Fabrication of TiO2/WO3 Composite Nanofibers by Electrospinning and Photocatalystic Performance of the Resultant Fabrics. *Ind Eng Chem Res*. 2016;55(1):80-85. doi:10.1021/acs.iecr.5b03578

26. Shanmugam V, Sanjeevamuthu S, Jeyaperumal KS, Vairamuthu R. Fabrication of heterostructured vanadium modified g-C3N4/TiO2 hybrid photocatalyst for improved photocatalytic performance under visible light exposure and antibacterial activities. *J Ind Eng Chem*. 2019;76:318-332. doi:10.1016/j.jiec.2019.03.056

27. Lin L, Wang H, Xu P. Immobilized TiO2-reduced graphene oxide nanocomposites on optical fibers as high performance photocatalysts for degradation of pharmaceuticals. *Chem Eng J*. Published online 2017. doi:10.1016/j.cej.2016.04.024

28. Tao W, Wang M, Ali R, et al. Multi-layered porous hierarchical TiO2/g-C3N4 hybrid coating for enhanced visible light photocatalysis. *Appl Surf Sci*. 2019;495:143435. doi:10.1016/j.apsusc.2019.07.177

29. Xu F, Zhang J, Zhu B, Yu J, Xu J. CuInS2 sensitized TiO2 hybrid nanofibers for improved photocatalytic CO2 reduction. *Appl Catal B Environ*. 2018;230:194-202. doi:10.1016/j.apcatb.2018.02.042

30. Barhoum A, El-Maghrabi HH, Iatsunskyi I, et al. Atomic layer deposition of Pd nanoparticles on self-supported carbon-Ni/NiO-Pd nanofiber electrodes for electrochemical hydrogen and oxygen evolution reactions. *J Colloid Interface Sci*. 2020;569:286-297. doi:10.1016/j.jcis.2020.02.063

31. Khojasteh H, Salavati-niasari M, Sadat F. Photocatalytic evaluation of RGO / TiO 2 NWs / Pd-Ag nanocomposite as an improved catalyst for ef fi cient dye degradation. 2018;746:611–618. doi:10.1016/j.jallcom.2018.02.345

32. Zhu Y, Gao C, Bai S, et al. Hydriding Pd cocatalysts: An approach to giant enhancement on photocatalytic CO2 reduction into CH4. *Nano Res*. 2017;10:1-11. doi:10.1007/s12274-017-1552-0

33. Sasikala R, Shirole AR, Sudarsan V, et al. Enhanced photocatalytic activity of indium and nitrogen co-doped TiO2–Pd nanocomposites for hydrogen generation. *Appl Catal Gen*. 2010;377(1):47-54. doi:https://doi.org/10.1016/j.apcata.2010.01.039

34. Duan H, Wang Z, Cui L, Lin B, Zhou Y. Stability Investigation of a Supported TiO2–Pd Bifunctional Catalyst over the One-Pot Liquid-Phase Synthesis of Methyl Isobutyl Ketone from Acetone and H2. *Ind Eng Chem Res*. 2018;57(37):12358-12366. doi:10.1021/acs.iecr.8b02854

35. Espino-Estévez MR, Fernández-Rodríguez C, González-Díaz OM, et al. Effect of TiO2–Pd and TiO2–Ag on the photocatalytic oxidation of diclofenac, isoproturon and phenol. *Chem Eng J*. 2016;298:82-95. doi:10.1016/j.cej.2016.04.016

36. Meng A, Zhang L, Cheng B, Yu J. Dual Cocatalysts in TiO 2 Photocatalysis. 2019;1807660:1-31. doi:10.1002/adma.201807660

37. Jiang G, Geng K, Wu Y, Han Y, Shen X. High photocatalytic performance of ruthenium complexes sensitizing g-C3N4/TiO2 hybrid in visible light irradiation. *Appl Catal B Environ*. 2018;227:366-375. doi:10.1016/j.apcatb.2018.01.034

38. Nasr M, Soussan L, Viter R, et al. High photodegradation and antibacterial activity of BN–Ag/TiO2 composite nanofibers under visible light. *New J Chem*. 2018;42(2):1250-1259. doi:10.1039/C7NJ03183A

39. Lee C, Na K, Kim W, Park D, Yang W, Choi W. applied sciences TiO 2 / ZnO Nanofibers Prepared by Electrospinning and Their Photocatalytic Degradation of Methylene Blue Compared with TiO 2 Nanofibers. Published online 2019.

40. Park S-M, Razzaq A, Park YH, et al. Hybrid CuxO–TiO2 Heterostructured Composites for Photocatalytic CO2 Reduction into Methane Using Solar Irradiation: Sunlight into Fuel. *ACS Omega*. 2016;1(5):868-875. doi:10.1021/acsomega.6b00164

41. Peng C, Yang X, Li Y, Yu H, Wang H, Peng F. Hybrids of Two-Dimensional Ti3C2 and TiO2 Exposing {001} Facets toward Enhanced Photocatalytic Activity. *ACS Appl Mater Interfaces*. 2016;8(9):6051-6060. doi:10.1021/acsami.5b11973

42. Coy E, Siuzdak K, Grądzka-Kurzaj I, et al. Exploring the effect of BN and BN bridges on the photocatalytic performance of semiconductor heterojunctions: Enhancing carrier transfer mechanism. *Appl Mater Today*. 2021;24:101095.

43. Bechelany M, Brioude A, Stadelmann P, Bernard S, Cornu D, Miele P. Preparation of BN Microtubes/Nanotubes with a Unique Chemical Process. *J Phys Chem C*. 2008;112(47):18325-18330. doi:10.1021/jp804286x

44. Gao X, Yao Y, Meng X. Recent development on BN-based photocatalysis: A review. *Mater Sci Semicond Process*. 2020;120:105256. doi:10.1016/j.mssp.2020.105256

45. Lin L, Lin L, Jiang W, Bechelany M, Nasr M, Jarvis J. Adsorption and photocatalytic oxidation of ibuprofen using nanocomposites of TiO2 nanofibers combined with BN nanosheets : Degradation products and mechanisms Chemosphere Adsorption and

photocatalytic oxidation of ibuprofen using nanocomposites of TiO 2 n. *Chemosphere*. 2019;220(December 2018):921-929. doi:10.1016/j.chemosphere.2018.12.184

46. Sheng Y, Yang J, Wang F, et al. Sol-gel synthesized hexagonal boron nitride/titania nanocomposites with enhanced photocatalytic activity. *Appl Surf Sci*. 2019;465:154-163. doi:10.1016/j.apsusc.2018.09.137

47. Li Z, Meng X. Recent development on palladium enhanced photocatalytic activity: A review. *J Alloys Compd*. 2020;830:154669. doi:10.1016/j.jallcom.2020.154669

48. Coy E, Siuzdak K, Pavlenko M, et al. Enhancing photocatalytic performance and solar absorption by schottky nanodiodes heterojunctions in mechanically resilient palladium coated TiO2/Si nanopillars by atomic layer deposition. *Chem Eng J*. 2020;392:123702. doi:https://doi.org/10.1016/j.cej.2019.123702

49. Linic S, Aslam U, Boerigter C, Morabito M. Photochemical transformations on plasmonic metal nanoparticles. *Nat Mater*. 2015;14(6):567-576. doi:10.1038/nmat4281

50. Mohapatra SK, Kondamudi N, Banerjee S, Misra M. Functionalization of Self-Organized TiO2 Nanotubes with Pd Nanoparticles for Photocatalytic Decomposition of Dyes under Solar Light Illumination. *Langmuir*. 2008;24(19):11276-11281. doi:10.1021/la801253f

51. Wu Z, Sheng Z, Liu Y, Wang H, Tang N, Wang J. Characterization and activity of Pd-modified TiO2 catalysts for photocatalytic oxidation of NO in gas phase. *J Hazard Mater*. 2009;164(2):542-548. doi:10.1016/j.jhazmat.2008.08.028

52. Rusinque B, Lasa H. Photoreduction of a Pd-Doped Mesoporous TiO2 Photocatalyst for Hydrogen Production under Visible Light. *Catalysts*. 2020;10:74. doi:10.3390/catal10010074

53. Drunka R, Grabis J, Krūmiņa A. Preparation of Au, Pt, Pd and Ag Doped TiO2 Nanofibers and their Photocatalytic Properties under LED Illumination. *Key Eng Mater*. 2018;762:283-287. doi:10.4028/www.scientific.net/KEM.762.283

54. Tang Q, Meng X, Wang Z, Zhou J, Tang H. One-step Electrospinning Synthesis of TiO 2 / g-C 3 N 4 Nanofibers with Enhanced Photocatalytic Properties. *Appl Surf Sci*. Published online 2017. doi:10.1016/j.apsusc.2017.07.288

55. Weber M, Julbe A, Ayral A, Miele P, Bechelany M. Atomic Layer Deposition for Membranes: Basics, Challenges, and Opportunities. *Chem Mater*. 2018;30(21):7368-7390. doi:10.1021/acs.chemmater.8b02687

56. Graniel O, Weber M, Balme S, Miele P, Bechelany M. Atomic layer deposition for biosensing applications. *Biosens Bioelectron*. 2018;122:147-159. doi:https://doi.org/10.1016/j.bios.2018.09.038

57. Mackus AJM, Weber MJ, Thissen NFW, et al. Atomic layer deposition of Pd and Pt nanoparticles for catalysis: on the mechanisms of nanoparticle formation. *Nanotechnology*. 2015;27(3):034001. doi:10.1088/0957-4484/27/3/034001

58. Najem M, Nada AA, Weber M, et al. Palladium/Carbon Nanofibers by Combining Atomic Layer Deposition and Electrospinning for Organic Pollutant Degradation. *Materials*. 2020;13(8). doi:10.3390/ma13081947

59. Weber M, Bechelany M. Combining nanoparticles grown by ALD and MOFs for gas separation and catalysis applications. *Pure Appl Chem*. 2019;92. doi:10.1515/pac-2019-0109

60. Sun S, Zhang G, Gauquelin N, et al. Single-atom Catalysis Using Pt/Graphene Achieved through Atomic Layer Deposition. *Sci Rep*. 2013;3(1):1775. doi:10.1038/srep01775

61. Ramachandran RK, Detavernier C, Dendooven J. Atomic Layer Deposition for Catalysis. In: *Nanotechnology in Catalysis*. John Wiley & Sons, Ltd; 2017:335-358. doi:10.1002/9783527699827.ch14

62. Backman L, Rautiainen A, Lindblad M, Jylhä O, Krause A. Characterisation of Co/SiO2 catalysts prepared from Co(acac)3 by gas phase deposition. *Appl Catal Gen*. 2001;208:223-234. doi:10.1016/S0926-860X(00)00707-9

63. George SM. Atomic Layer Deposition: An Overview. *Chem Rev*. 2010;110(1):111-131. doi:10.1021/cr900056b

64. Weber M, Verheijen M, Bol A, Kessels W. Sub-nanometer dimensions control of core/shell nanoparticles prepared by atomic layer deposition. *Nanotechnology*. 2015;26(9):094002.

65. Eswar NKR, Singh SA, Heo J. Atomic layer deposited photocatalysts: comprehensive review on viable fabrication routes and reactor design approaches for photo-mediated redox reactions. *J Mater Chem A*. 2019;7(30):17703-17734. doi:10.1039/C9TA04780H

66. Weber M, Tuleushova N, Zgheib J, et al. Enhanced electrocatalytic performance triggered by atomically bridged boron nitride between palladium nanoparticles and carbon fibers in gas-diffusion electrodes. *Appl Catal B Environ*. 2019;257:117917. doi:10.1016/j.apcatb.2019.117917

67. Vempati S, Ranjith KS, Topuz F, Biyikli N, Uyar T. Electrospinning Combined with Atomic Layer Deposition to Generate Applied Nanomaterials: A Review. *ACS Appl Nano Mater*. 2020;3(7):6186-6209. doi:10.1021/acsanm.0c01120

68. Barhoum A, Pal K, Rahier H, Uludag H, Kim IS, Bechelany M. Nanofibers as new-generation materials: From spinning and nano-spinning fabrication techniques to emerging applications. *Appl Mater Today*. 2019;17:1-35. doi:10.1016/j.apmt.2019.06.015

69. Pasini SM, Valério A, Yin G, et al. An overview on nanostructured TiO2–containing fibers for photocatalytic degradation of organic pollutants in wastewater treatment. *J Water Process Eng*. 2021;40:101827. doi:10.1016/j.jwpe.2020.101827

70. Mozzaquatro S, Valério A, Guelli SMA, et al. Journal of Environmental Chemical Engineering Plasma-modi fi ed TiO 2 / polyetherimide nanocomposite fi bers for photocatalytic degradation of organic compounds. 2019;7(June):2-11. doi:10.1016/j.jece.2019.103213

71. Reneker DH, Yarin AL. Electrospinning jets and polymer nanofibers. *Polym Aligned Carbon Nanotub Act Compos Mater*. 2008;49(10):2387-2425. doi:10.1016/j.polymer.2008.02.002

72. Tang Q, Meng X, Wang Z, Zhou J, Tang H. One-step electrospinning synthesis of TiO2/g-C3N4 nanofibers with enhanced photocatalytic properties. *2nd Int Workshop Graphene C3N4-Based Photocatal*. 2018;430:253-262. doi:10.1016/j.apsusc.2017.07.288

73. Basavarajappa PS, Patil SB, Ganganagappa N, Reddy KR, Raghu AV, Reddy ChV. Recent progress in metal-doped TiO2, non-metal doped/codoped TiO2 and TiO2 nanostructured hybrids for enhanced photocatalysis. *2nd Int Conf Sustain Environ Energy ICSEE-2019*. 2020;45(13):7764-7778. doi:10.1016/j.ijhydene.2019.07.241

74. Shende TP, Bhanvase BA, Rathod AP, Pinjari DV, Sonawane SH. Sonochemical synthesis of Graphene-Ce-TiO2 and Graphene-Fe-TiO2 ternary hybrid photocatalyst nanocomposite and its application in degradation of crystal violet dye. *Ultrason Sonochem*. 2018;41:582-589. doi:10.1016/j.ultsonch.2017.10.024

75. Meng A, Zhang L, Cheng B, Yu J. TiO2–MnOx–Pt Hybrid Multiheterojunction Film Photocatalyst with Enhanced Photocatalytic CO2-Reduction Activity. *ACS Appl Mater Interfaces*. 2019;11(6):5581-5589. doi:10.1021/acsami.8b02552

76. Cheng G, Xu F, Xiong J, et al. Enhanced adsorption and photocatalysis capability of generally synthesized TiO2-carbon materials hybrids. *Adv Powder Technol*. 2016;27(5):1949-1962. doi:10.1016/j.apt.2016.06.026

77. Nasr M, Eid C, Habchi R, Miele P. Recent Progress on Titanium Dioxide Nanomaterials for Photocatalytic Applications. Published online 2018:3023-3047. doi:10.1002/cssc.201800874

78. Chronakis IS. Novel nanocomposites and nanoceramics based on polymer nanofibers using electrospinning process — A review. 2005;167:283-293. doi:10.1016/j.jmatprotec.2005.06.053

79. Merenda A, Weber M, Bechelany M, et al. Fabrication of Pd-TiO2 nanotube photoactive junctions via Atomic Layer Deposition for persistent pesticide pollutants degradation. *Appl Surf Sci*. 2019;483:219-230. doi:10.1016/j.apsusc.2019.03.285

80. Weber M, Drobek M, Rebière B, et al. Hydrogen selective palladium-alumina composite membranes prepared by Atomic Layer Deposition. *J Membr Sci*. 2020;596:117701. doi:https://doi.org/10.1016/j.memsci.2019.117701

81. Weber M, Kim J-H, Lee J-H, et al. High-Performance Nanowire Hydrogen Sensors by Exploiting the Synergistic Effect of Pd Nanoparticles and Metal–Organic Framework Membranes. *ACS Appl Mater Interfaces*. 2018;10(40):34765-34773. doi:10.1021/acsami.8b12569

82. Molenaar R, Jaap J, Zijp JR. Determination of Kubelka–Munk scattering and absorption coefficients by diffuse illumination. *Appl Opt*. 1999;38(10):2068-2077.

83. Konstantinou IK, Albanis TA. TiO2-assisted photocatalytic degradation of azo dyes in aqueous solution: kinetic and mechanistic investigations: A review. *Appl Catal B Environ*. 2004;49(1):1-14. doi:10.1016/j.apcatb.2003.11.010

84. Konstantinou IK, Albanis TA. Photocatalytic transformation of pesticides in aqueous titanium dioxide suspensions using artificial and solar light: intermediates and degradation pathways. *Appl Catal B Environ*. 2003;42(4):319-335. doi:10.1016/S0926-3373(02)00266-7

85. Xuan T, Le H, Nguyen T Van, et al. Chemosphere Correlation between degradation pathway and toxicity of acetaminophen and its by-products by using the electro-Fenton process in aqueous media. 2017;172:1-9. doi:10.1016/j.chemosphere.2016.12.060

86. El Kateb M, Trellu C, Darwich A, et al. Electrochemical advanced oxidation processes using novel electrode materials for mineralization and biodegradability enhancement of nanofiltration concentrate of landfill leachates. *Water Res*. 2019;162:446-455.

87. Spurr RA, Myers H. Quantitative analysis of anatase-rutile mixtures with an X-ray diffractometer. *Anal Chem*. 1957;29(5):760-762.

88. Xu Q. *Nanoporous Materials: Synthesis and Applications*. CRC press; 2013.

89. Li H, Zhang W, Pan W. Enhanced Photocatalytic Activity of Electrospun TiO2 Nanofibers with Optimal Anatase/Rutile Ratio. *J Am Ceram Soc*. 2011;94(10):3184-3187. doi:10.1111/j.1551-2916.2011.04748.x

90. Fan X, Yu T, Zhang L, Chen X, Zou Z. Photocatalytic degradation of acetaldehyde on mesoporous TiO2: Effects of surface area and crystallinity on the photocatalytic activity. *Chin J Chem Phys*. 2007;20(6):733.

91. Ouyang W, Liu S, yao K, et al. Ultrafine hollow TiO2 nanofibers from core-shell composite fibers and their photocatalytic properties. *Compos Commun*. 2018;9:76-80. doi:10.1016/j.coco.2018.06.006

92. Kawrani S, Nada AA, Bekheet MF, et al. Enhancement of calcium copper titanium oxide photoelectrochemical performance using boron nitride nanosheets. *Chem Eng J*. 2020;389:124326. doi:10.1016/j.cej.2020.124326

93. Nada AA, El Rouby WMA, Bekheet MF, et al. Highly textured boron/nitrogen co-doped TiO2 with honeycomb structure showing enhanced visible-light photoelectrocatalytic activity. *Appl Surf Sci*. 2020;505:144419. doi:10.1016/j.apsusc.2019.144419

94. Bolokang AS, Motaung DE, Arendse CJ, Muller TFG. Morphology and structural development of reduced anatase-TiO2 by pure Ti powder upon annealing and nitridation: Synthesis of TiOx and TiOxNy powders. *Mater Charact*. 2015;100:41-49. doi:10.1016/j.matchar.2014.11.026

95. Zhang M, Lu D, Yan G, Wu J, Yang J. Fabrication of Mo+N-Codoped TiO2 Nanotube Arrays by Anodization and Sputtering for Visible Light-Induced Photoelectrochemical and Photocatalytic Properties. Zhu S, ed. *J Nanomater*. 2013;2013:648346. doi:10.1155/2013/648346

96. Byrne C, Fagan R, Hinder S, McCormack DE, Pillai SC. New approach of modifying the anatase to rutile transition temperature in TiO2 photocatalysts. *RSC Adv*. 2016;6(97):95232-95238. doi:10.1039/C6RA19759K

97. Yilmaz P, Lacerda AM, Larrosa I, Dunn S. Photoelectrocatalysis of Rhodamine B and Solar Hydrogen Production by TiO2 and Pd/TiO2 Catalyst Systems. *Electrochimica Acta*. 2017;231:641-649. doi:10.1016/j.electacta.2017.02.035

98. Iatsunskyi I, Pavlenko M, Viter R, et al. Tailoring the Structural, Optical, and Photoluminescence Properties of Porous Silicon/TiO2 Nanostructures. *J Phys Chem C*. 2015;119(13):7164-7171. doi:10.1021/acs.jpcc.5b01670

99. Safajou H, Khojasteh H, Salavati-Niasari M, Mortazavi-Derazkola S. Enhanced photocatalytic degradation of dyes over graphene/Pd/TiO2 nanocomposites: TiO2 nanowires versus TiO2 nanoparticles. *J Colloid Interface Sci*. 2017;498:423-432. doi:10.1016/j.jcis.2017.03.078

100. Levchuk I, Guillard C, Dappozze F, Parola S, Leonard D, Sillanpää M. Photocatalytic activity of TiO2 films immobilized on aluminum foam by atomic layer deposition technique. *J Photochem Photobiol Chem*. 2016;328:16-23. doi:10.1016/j.jphotochem.2016.03.034

101. Serpone N. Relative photonic efficiencies and quantum yields in heterogeneous photocatalysis. *J Photochem Photobiol Chem*. 1997;104(1):1-12. doi:10.1016/S1010-6030(96)04538-8

102. Singh J, Tripathi N, Mohapatra S. Synthesis of Ag–TiO2 hybrid nanoparticles with enhanced photocatalytic activity by a facile wet chemical method. *Nano-Struct Nano-Objects*. 2019;18:100266. doi:10.1016/j.nanoso.2019.100266

103. Khan H, Rigamonti MG, Boffito DC. Enhanced photocatalytic activity of Pt-TiO2/WO3 hybrid material with energy storage ability. *Appl Catal B Environ*. 2019;252:77-85. doi:10.1016/j.apcatb.2019.04.019

104. Leong KH, Chu HY, Ibrahim S, Saravanan P. Palladium nanoparticles anchored to anatase TiO2 for enhanced surface plasmon resonance-stimulated, visible-light-driven photocatalytic activity. *Beilstein J Nanotechnol*. 2015;6(1):428-437.

105. Chan C-C, Chang C-C, Hsu W-C, Wang S-K, Lin J. Photocatalytic activities of Pd-loaded mesoporous TiO2 thin films. *Chem Eng J*. 2009;152(2):492-497. doi:10.1016/j.cej.2009.05.012

106. Zhang X, Wu F, Wu X, Chen P, Deng N. Photodegradation of acetaminophen in TiO2 suspended solution. *J Hazard Mater*. 2008;157(2):300-307. doi:10.1016/j.jhazmat.2007.12.098

107. Luna MDG de, Veciana ML, Su C-C, Lu M-C. Acetaminophen degradation by electro-Fenton and photoelectro-Fenton using a double cathode electrochemical cell. *J Hazard Mater*. 2012;217-218:200-207. doi:https://doi.org/10.1016/j.jhazmat.2012.03.018

108. Vo HNP, Le GK, Nguyen TMH, et al. Acetaminophen micropollutant: Historical and current occurrences, toxicity, removal strategies and transformation pathways in different environments. *Chemosphere*. 2019;236:124391. doi:https://doi.org/10.1016/j.chemosphere.2019.124391

109. Le TXH, Nguyen TV, Yacouba ZA, et al. Correlation between degradation pathway and toxicity of acetaminophen and its by-products by using the electro-Fenton process in aqueous media. *Chemosphere*. 2017;172:1-9. doi:https://doi.org/10.1016/j.chemosphere.2016.12.060

110. Nasr O, Mohamed O, Al-Shirbini A-S, Abdel-Wahab A-M. Photocatalytic degradation of acetaminophen over Ag, Au and Pt loaded TiO2 using solar light. *J Photochem Photobiol Chem*. 2019;374:185-193. doi:10.1016/j.jphotochem.2019.01.032

111. Aguilar CA, Montalvo C, Ceron JG, Moctezuma E. Photocatalytic Degradation of Acetaminophen. *Int J Environ Res*. 2011;5(4):1071-1078. doi:10.22059/ijer.2011.465

112. Aguilar CA, Montalvo C, Zermeño BB, et al. Photocatalytic degradation of acetaminophen, tergitol and nonylphenol with catalysts TiO2/Ag under UV and Vis light. *Int J Environ Sci Technol*. 2019;16(2):843-852. doi:10.1007/s13762-018-1707-x

113. Lin JC-T, de Luna MDG, Aranzamendez GL, Lu M-C. Degradations of acetaminophen via a K2S2O8-doped TiO2 photocatalyst under visible light irradiation. *Chemosphere*. 2016;155:388-394. doi:10.1016/j.chemosphere.2016.04.059

114. Ahmad A ul, Abbas A, Ali S, et al. Visible-light driven photo-catalytic performance of novel composite of TiO2 and fluorinated hexagonal boron nitride nanosheets. *Ceram Int*. 2021;47(7, Part A):10089-10095. doi:10.1016/j.ceramint.2020.12.156

115. Ni G, Li Y, Wang S, Li Q. Construction of 1D/2D BN/TiO2 nanostructures for efficient photocatalytic degradation of dyes. *Mater Lett*. 2021;288:129385. doi:10.1016/j.matlet.2021.129385

116. Czech B, Tyszczuk-Rotko K. Visible-light-driven photocatalytic removal of acetaminophen from water using a novel MWCNT-TiO2-SiO2 photocatalysts. *Sep Purif Technol*. 2018;206:343-355. doi:10.1016/j.seppur.2018.06.025

117. Khasawneh OFS, Palaniandy P, Ahmadipour M, Mohammadi H, Bin Hamdan MR. Removal of acetaminophen using Fe2O3-TiO2 nanocomposites by photocatalysis under simulated solar irradiation: Optimization study. *J Environ Chem Eng*. 2021;9(1):104921. doi:10.1016/j.jece.2020.104921

118. Kurniawan TA, Yanyan L, Ouyang T, Albadarin AB, Walker G. BaTiO3/TiO2 composite-assisted photocatalytic degradation for removal of acetaminophen from synthetic wastewater under UV–vis irradiation. *Semicond Mater Green Energy Environ Appl*. 2018;73:42-50. doi:10.1016/j.mssp.2017.06.048

119. Cheshme Khavar AH, Moussavi G, Mahjoub AR. The preparation of TiO2@rGO nanocomposite efficiently activated with UVA/LED and H2O2 for high rate oxidation of acetaminophen: Catalyst characterization and acetaminophen degradation and mineralization. *Appl Surf Sci*. 2018;440:963-973. doi:10.1016/j.apsusc.2018.01.238

120. Yanyan L, Kurniawan TA, Ying Z, Albadarin AB, Walker G. Enhanced photocatalytic degradation of acetaminophen from wastewater using WO3/TiO2/SiO2 composite under UV–VIS irradiation. *J Mol Liq*. 2017;243:761-770. doi:10.1016/j.molliq.2017.08.092

121. Ramasundaram S, Yoo HN, Song KG, Lee J, Choi KJ, Hong SW. Titanium dioxide nanofibers integrated stainless steel filter for photocatalytic degradation of pharmaceutical compounds. *J Hazard Mater*. 2013;258-259:124-132. doi:10.1016/j.jhazmat.2013.04.047

8. Supporting Information

S1. Optical characterization: calculation details

Detailed calculation of the absorption and scattering coefficients for quantum efficiency values:

$$K = \frac{1}{2d}\frac{1-R_\infty}{1+R_\infty} ln\left(\frac{R_\infty(1-R_\infty R_0)}{R_\infty - R_0}\right) \quad \textbf{(1)}$$

$$S = \frac{1}{2d}\frac{R_\infty}{1-R_\infty^2} ln\left(\frac{R_\infty(1-R_\infty R_0)}{R_\infty - R_0}\right) \quad \textbf{(2)}$$

Linear absorption and scattering coefficients a and s can be calculated as:

$$K = 2a \quad \textbf{(3)}$$

$$S = \frac{3s(1-g)-a}{4} \quad \textbf{(4)}$$

where g is scattering anisotropy factor.

The concentration dependence of a and s have linear form:

$$a = a_s C \quad \textbf{(5)}$$

$$s = s_s C \quad \textbf{(6)}$$

where a_s and s_s are absorption and scattering coefficients per concentration unit

(cm.mg/ml)$^{-1}$ and C is a concentration of photocatalyst (mg/ml).

Total extinction coefficient γ can be calculated as a slope from:

$$I_T = I_0 \cdot e^{-\gamma \cdot C} \quad \textbf{(7)}$$

The total extinction coefficient γ can be described as:

$$\gamma = a_s + s_s \quad \textbf{(8)}$$

The T, R_0 and γ were measured and calculated for photocatalyst concentrations in the range 0.03-0.18 mg/ml. The measurements were performed per 1 cm^3 volume of solutions. Optimization of g, a_c and s_c have been performed by using two conditions

$$3s(1-g) > a\ (*) \quad \textbf{(9)}$$

$$\delta_{min} = |\gamma - a_s - s_s| \quad \textbf{(10)}$$

The obtained values of a_s and s_s are shown in **Figure S2. 2.**

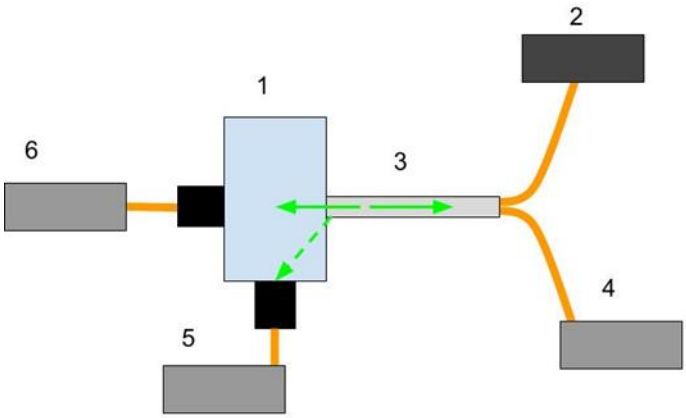

Figure S2. 1. Measurements setup. Quartz cuvette 1, tungsten-halogen light source – 2, 3 bifurcated diffuse reflectance, 4-6 probe fiber optic spectrometers.

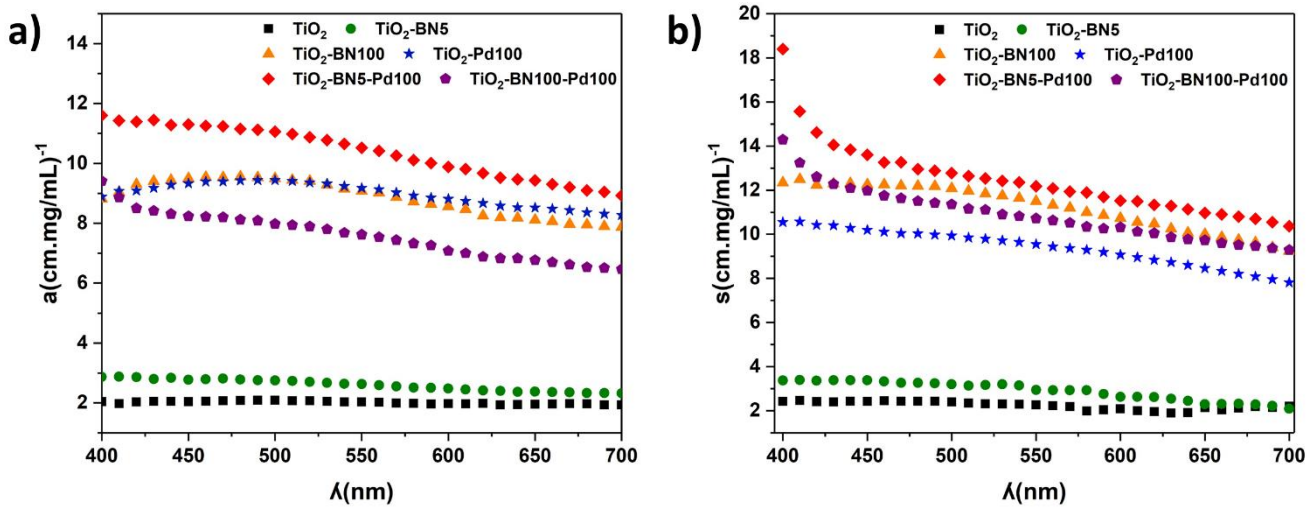

Figure S2. 2. absorption and scattering coefficients a and s of all prepared samples.

S2. Structural characterization: XRD and XPS

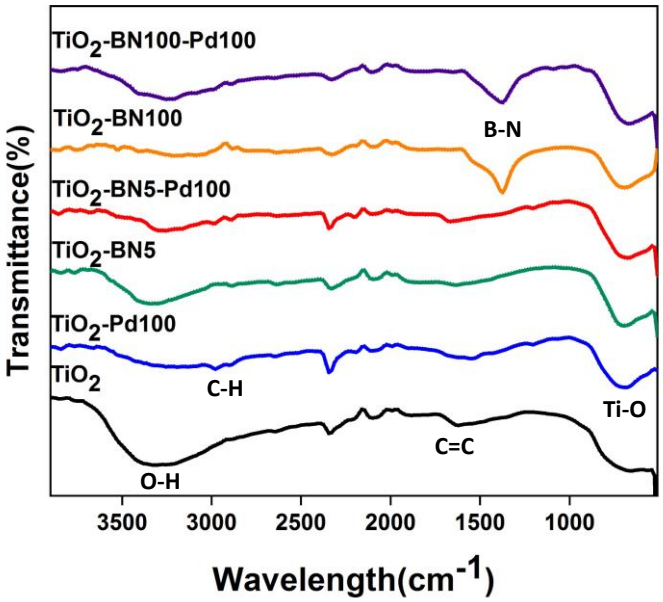

Figure S2. 3. FTIR spectra of undoped TiO_2 and nanocomposites TiO_2

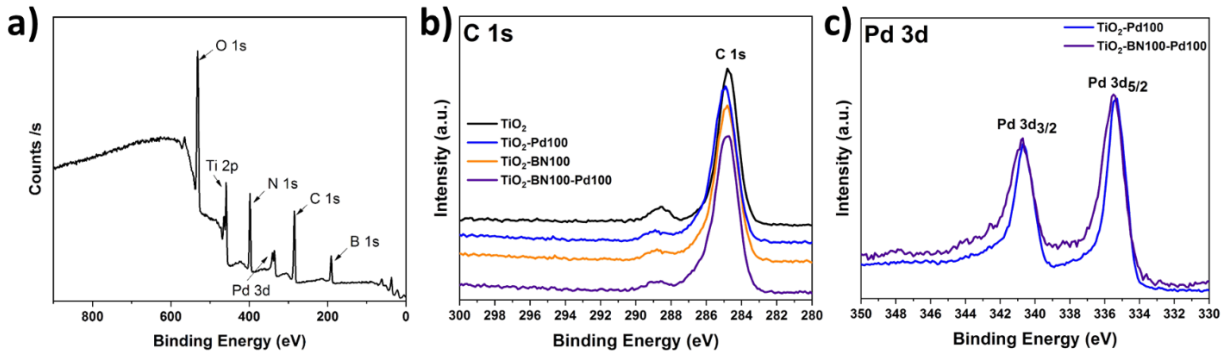

Figure S2. 4. a) Survey spectra of TiO_2-BN100-Pd100, XPS spectra of all prepared samples for b) C 1s and c) Pd3d

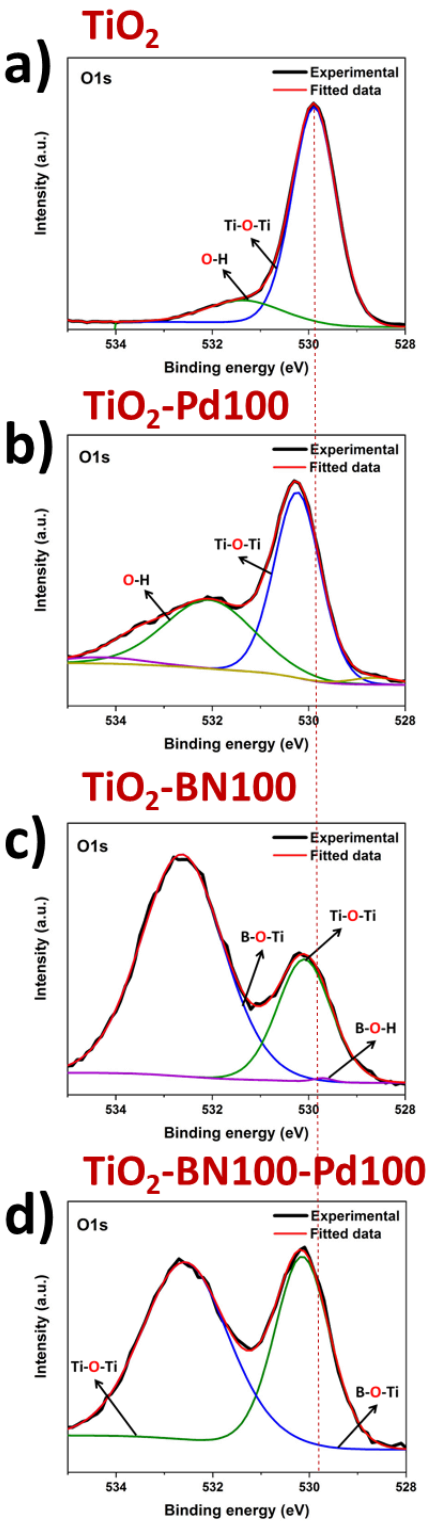

Figure S2. 5. Deconvoluted spectrum of O 1s element for a) TiO_2, b) TiO_2-Pd100, c) TiO_2-BN100 and d) TiO_2-BN100-Pd100.

Table S2. 1: Binding energy and atomic percentage of as-synthesized TiO_2 and doped TiO_2 samples by XPS.

Sample / Element	TiO_2 BE / Atomic %	TiO_2-Pd100 BE / Atomic %	TiO_2-BN100 BE / Atomic %	TiO_2-BN100-Pd100 BE / Atomic %
Ti2p	464.4 / 24.7	464.7/ 30.2	464.6 / 35.6	464.6 / 31.3
	458.7 / 75.2	459.1 / 69.8	458.9 / 64.3	458.9 / 68.7
O1s	531.4/ 14.7	532.1 / 36.4	532.6 / 50.8	532.6 / 49.5
	529.9 / 85.3	530.2 / 63.6	530.1 / 34.1	530.1 / 50.6
			529.7 / 15.1	
B1s			192.6 / 19.2	192.1 / 44.1
			191.5 / 27.3	190.7 / 55.9
			190.5 / 53.5	
N1s			398.6 / 19.8	399.5 / 14.9
			398.2 / 80.2	398.7 / 28.9
				398.2 / 56.2
Pd3d		341.6 / 13.9		342.2 / 16.1
		340.6 / 31.2		340.7 / 24.3
		336.8 / 11.5		338.2 / 14.7
		335.3 / 43.4		336.8 / 13.8
				335.5 / 31.1

Chapter 3: N-doped TiO_2 Nanotubes synthesized by Atomic Layer Deposition for the degradation of acetaminophen

Table of contents

1. ABSTRACT

Titanium dioxide is widely used in photocatalysis applications for wastewater treatment due to its benefits. However, its wide band gap and fast electron-holes recombination limits its use under visible light. Many techniques have been used for elaboration and modification of this catalyst. Investigations demonstrated that Titanium dioxide (TiO_2) structure plays a major role on enhancing the degradation efficiency of different micropollutants present in wastewater. Titanium dioxide (TiO_2) nanotubes have attracted much interest in photocatalytic degradation due to their large specific surface area and highly ordered structure. Atomic Layer Deposition (ALD) proves to be very suitable for elaboration of well-structured photocatalysts. In this work, N-doped TiO_2 nanotubes (NTs) were successfully prepared by ALD followed by a thermal treatment for nitrogen doping. The photocatalytic efficiency of these nanotubes was compared to TiO_2 nanofibers (NFs) for the degradation of acetaminophen (ACT). Therefore, the acetaminophen degradation performance on the nitrogen-doped photocatalyst is much enhanced and superior to that of TiO_2 nanofibers prepared by electrospinning. The morphology and structure of these materials were investigated by several characterization techniques such as scanning electron microscopy (SEM), X-ray diffraction (XRD), transmission electron microscopy (TEM) and X-ray photoelectron spectroscopy (XPS). Photolumiscence measurement were also achieved, and TiO_2 NTs shows a lower PL intensity than TiO_2 NFs. The lowest PL intensity correspond to a lower recombination of electron-holes, consequently higher degradation efficiency. The nanotubes were doped with Boron and/or nitrogen in order to enhance its photocatalytic activity for acetaminophen degradation. Among the different doping, nitrogen doped TiO_2 demonstrated the best catalytic properties. The degradation efficiency of N-TiO_2-NTs was 5 times higher than TiO_2-NFs with a degradation rate of 0.05 and 0.01 $mg.L^{-1}.min^{-1}$, respectively. In addition, the photocatalyst has shown a high stability after 4 repetitive cycles, then the stability slightly decreased after the fifth cycle. Acute toxicity assays confirm the release of high toxic sub-products during the first hours of ACT degradation but the toxicity decreased markedly to lower values than initial ACT toxicity after 5 hours irradiation.

Keywords: TiO_2 nantotubes; N doped TiO_2; atomic layer deposition; photocatalysis; acetaminophen

2. Graphical abstract

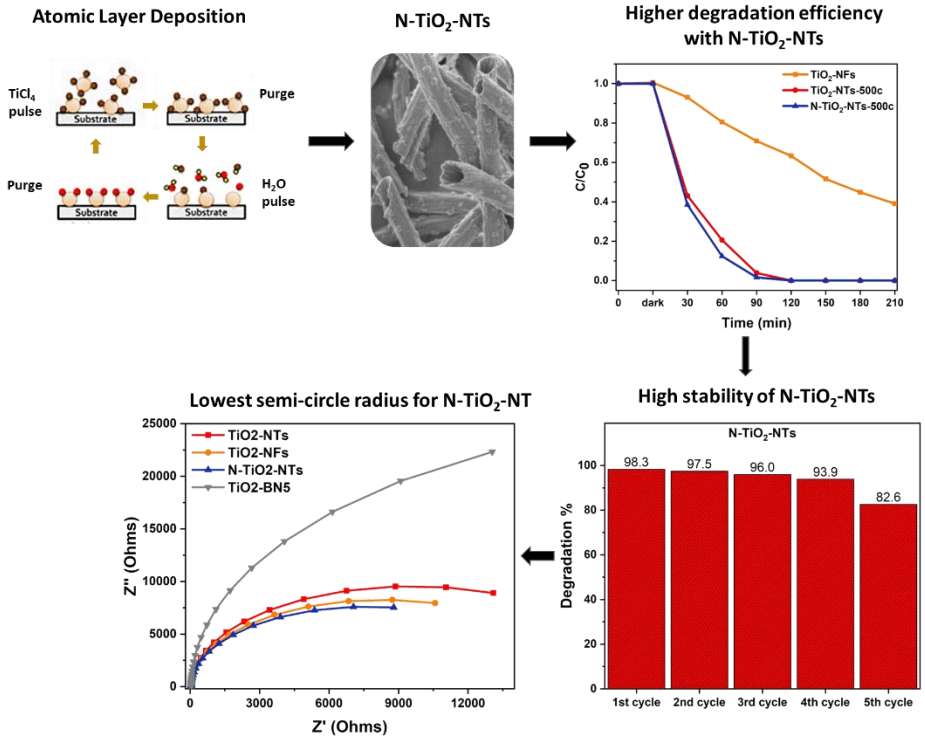

3. Highlights

- TiO_2 nanotubes were successfully elaborated by Atomic layer deposition on polyacrylonitrile nanofibers used as substrate.
- The as-prepared sample was highly active under visible light irradiation for acetaminophen degradation.
- The photocatalytic efficiency of TiO_2 nanotubes treated at 750°C was 3 times higher than TiO_2 nanofibers after 90 min visible irradiation.
- N doping further improved the degradation efficiency of TiO_2-NTs by increasing the separation time of photogenerated charge carriers.
- N-TiO_2-NTs holds the lowest resistance of charge transfer and highest electroactive surface area.

4. Introduction

The increase in fresh water demand during the last decades, has led the researchers to focus on developing new technologies for water treatments. Actually, the conventional methods in wastewater treatment plants have shown their inefficiency in degradation of micropollutants and elimination of bacterias[1,2]. Many chemical products such as pharmaceutical products, pesticides, personal care products and dyes can resist to the conventional methods and make it into the drinking water[3,4]. Even though these contaminants are detected at very low levels, they could be harmful on human health and the living organisms[5,6].

The need for new techniques to remove them with low cost and low energy consumption is the main challenge focus. Advanced oxidation processes (AOP) are good candidates in replacing or in combination with the conventional techniques[7–9]. Among the various AOP approaches, photocatalysis is a green technology technique focusing on the degradation of pollutants under visible irradiation with the final reaction products being CO_2 and H_2O[10,11]. The mechanism of photocatalysis involve the activation of a semiconductor by irradiating its surface by a photon energy (*hv*) equal or greater than its bandgap energy. The excitation of the semiconductor creates electron-hole pairs between the conduction and valence band. These photogenerated carriers will generate radicals that will participate in the mineralization of micropollutants[12,13].

One of the most used semiconductors is TiO_2 regarding its advantages, low cost, high chemical and thermal stability and most importantly low toxicity[14,15]. Hence, this material has two main drawbacks that limits its use under visible light, the wide band gap and the fast recombination of electron holes[16–18]. The effort on elaboration advanced materials and technologies with higher degradation efficiency for water treatment has been widely reported[19–21].The structure and morphology of the catalyst could play a major role in assuming its catalytic activity under visible light. The photocatalytic activity of TiO_2 is mainly dependent on its morphology, crystallinity, surface and textural properties. Tailoring TiO_2 with well-defined morphology that improves its photocatalytic properties is taking lot of attention[22–24]. Many structures have already been reported, 0D, 1D, 2D and 3D materials synthesized by

different techniques[25–27]. Synthesis of one-dimensional (1D) materials has remained a topic of intense interest due to the increased light absorption, and slower recombination rates which could allow a more efficient photocatalytic activity[28–30].

1D TiO_2 materials such as nanofibers (NFs), nanorods, nanotubes (NTs), nanowhiskers, and nanowires, possess potential properties and advantages for photocatalytic reactions[31–33]. Among these structures, tubular nanostructured TiO_2 is a versatile material and has generated great interest for its potential use in photocatalysis and photoelectrolysis[34–36]. So far, many preparation techniques were assessed to fabricate the 1D nanostructures, such as hydrothermal method, template method, anodization, electrospinning method and most recently Atomic Layer deposition (ALD) technique[37–40]. Among these techniques, Atomic Layer deposition is a great technique for elaboration of 1D catalyst with high thickness and structure control[41]. ALD is a thin film deposition technique based on gas phase precursors for the deposition of thin film layers controllable at the angstrom level[42,43]. Combining ALD with electrospinning for deposition of desired materials on polymeric fibers used as substrate was widely reported in the litterature[44–47]. When the polymeric core is removed by thermal treatment after ALD cycles, the formation of a tubular structure is witnessed[48]. McClure *et al.* reported the deposition of TiO_2 on polymeric nanofibers by ALD. The authors compared the precursor effect on the film coating and found that precursor choice could affect the final structure of TiO_2 NTs[49]. Su *et al.* reported the elaboration of TiO_2 NTs by ALD using titanium chloride ($TiCl_4$) and H_2O as precursors. The authors reported the effect of doping NTs on their photocatalytic and photoelectrochemical (PEC) activities[50]. Moreover, modifying the ALD number of cycles and the deposition temperature could affect the crystalline structure of the material[39].

Improvement in the morphology of TiO_2 could highly increase its photocatalytic behavior compared to the unmodified TiO_2 (commercial P25, Degussa)[51]. Hence, in many cases TiO_2 catalyst could not be stable and active under visible light irradiation. To extend the photoresponse of semiconductors to the visible light region several method were reported such as doping TiO_2 with metals, non-metals and coupling with other semi conductors[52–54]. Non-metal doping has been widely applied to decrease the recombination of photogenerated

electron-hole pairs in TiO_2. Several non-metal dopants were mentioned in the literature such as Carbon (C), sulfur (S), phosphorus (P) and nitrogen (N)[55–59]. N-doped TiO_2 is the most studied system of non-metal doped photocatalyst[60]. Nitrogen dopants allow the shift of TiO_2 band into the visible region[61]. Asahi *et al.* reported that nitrogen doping of TiO_2 extended the optical absorbance of TiO_2 into the visible light region[62]. Moreover, the presence of non-metal generally enhances the specific surface area, restrains the growth of crystallite size and increases the anatase phase percentage in TiO_2 photocatalyst[63]. Huang *et al.* reported the preparation of N-doped TiO_2 (N-TiO_2) by hydrothermal method with calcination under NH_3 atmosphere. The authors found that nitrogen doping increased the generation of hydroxyl and superoxide radicals that enhanced the photocatalytic activity of the catalyst[64]. In another study, researchers found that doping of nitrogen empowers the formation of oxygen vacancies that also contributes in the visible light absorbtion[53].

In this study, we successfully prepared 1D TiO_2 nanotubes by Atomic Layer Deposition for photocatalytic purposes. Variation of the number of ALD cycles confirmed that increasing NTs wall thickness could directly affect the photocatalytic efficiency. Moreover, doping TiO_2 with non-metal dopants such as nitrogen could further enhance the photocatlyst properties by modifying the characteristics properties specifically its charge transportation, surface area, reflection and absorption properties. The catalytic activity of these elaborated nanotubes was compared to TiO_2 nanofibers prepared by electrospinning. We found that ALD allow the formation of a well-structured nanotubular catalyst with higher degradation efficiency than nanofibers. The Nanotubes were doped with Boron and/or nitrogen in order to enhance its photocatalytic activity for acetaminophen degradation. We found that more than 98% of acetaminophen was degraded in presence of nitrogen doped TiO_2-NTs under visible light irradiation after 180 min of irradiation. Further studies on the recyclability of N-TiO_2-NTs and toxicity test, shows the potential of this catalyst for real applications. Quenching test were also performed to determine the active species responsible of the degradation of the pollutant.

5. Experimental

5.1. Materials and chemicals

Titanium(IV) isopropoxide (TTIP, 97%, CAS: 546-68-9), titanium (IV) chloride ($TiCl_4$, 99.9%, CAS: 7550-45-0) , polyacrylonitrile (PAN, Mw=150000, CAS: 25014-41-9), polyvinyl pyrollidone (PVP, Mw=1300000, CAS: 9003-39-8), acetaminophen (ACT , ≥99%, CAS: 103-90-2), formaline solution (HCHO, CAS: 50-00-0), boron tribromide (BBr_3, 99.9%, CAS :10294-33-4), nafion perfluorinated resin solution (CAS: 31175-20-9), potassium chloride (KCl, ≥99%, CAS: 7447-40-7), sodium sulfate (Na_2SO_4, ≥99%, CAS: 7757-82-6), sodium chloride (NaCl, ≥99%, CAS: 7647-14-5, potassium ferricyanide ($K_3[Fe(CN)_6]$, ≥99%, CAS 13746-66-2), 2-propanol (99.9%, CAS: 67-63-0), p-benzoquinone ($C_6H_4O_2$, ≥99.5%, CAS:106-51-4), and ethylenediaminetetraacetic acid (EDTA, 99.995%, CAS: 60-00-4) were purchased from Sigma-Aldrich. In addition, tetrahydrofuran (99.9%, CAS: 109-99-9) was bought from Honeywell. Acetic acid (CAS: 64-19-7) and ethanol (≥99.8% CAS: 64-17-5) were purchased from VWR chemicals and used as solvents. All chemicals were used without further purification. Indium tin oxide (ITO) deposited on quartz was purchased from Präzisions Glas & Optik. Deionized (DI) water (>18.2 MΩ) prepared by Millipore (Milli-Q® Academic) water purification system was used for all dilutions and reagent preparation. Argon gas, ammonia and nitrogen were bought from Linde and used as received.

5.2. Supports and catalysts preparation

5.2.1. Synthesis of TiO_2 nanofibers and PAN nanofibers by electrospinning

Electrospinnable solutions were prepared for the elaboration of TiO_2 and PAN nanofibers, For TiO_2 NFs, a mix of TTIP, PVP, acetic acid and ethanol were stirred for 2h before the electrospinning process. Than the solution was transverse to a 22 mL syringe and the needle was connected to high voltage. The distance between the needle and the collector was fixed to 10cm and a tension of 25kV was applied. The solution is conducted from the spinneret to the rotating collector with a fixed flow of $1mL.h^{-1}$. For the preparation of PAN nanofibers, 18mL of tetrahydrofuran were mixed with 2 mg of PAN for 24 h at 60 °C. A home-built electrospinning process was used for this purpose. For more details, the reader is referred to

our published papers[44,45]. The collected TiO_2 NFs were than calcined at 750 °C for 4h before testing their degradation efficiency. The PAN were stabilized at 250 °C for 2h with a heating rate of 1 °C.min^{-1} before ALD process.

5.2.2. Deposition of TiO_2 nanotubes and BN by Atomic Layer Deposition

Stabilized PAN nanofibers were used as substrates for TiO_2 deposition in a home-built ALD. The deposition process was achieved at 100°C using $TiCl_4$ and H_2O as precursors. Typical ALD cycle consisted of 0.2 s pulse of $TiCl_4$, followed by 10 s exposure and 60 s purge. Than H_2O valve was opened for 2 s, followed by an exposure of 10 s and purge with Ar gas for 60 s. The line connected to the reactor were heated at 100°C to avoid condensation. The thickness of TiO_2 shell could be controlled by the number of ALD cycles. After TiO_2 deposition, PAN-TiO_2 were heated at 750°C for 4 hours with a heating rate of 1 °C/min under air before further uses.

For TiO_2-BN based catalysts, the deposition of BN was performed according to the procedure described elsewhere[65]. The number of ALD cycles used for deposition of TiO_2 and BN is represented in **Table 3. 1**.

Table 3. 1: Variation of ALD number of cycles during TiO_2 and BN deposition

Sample	TiO_2 number of cycles	BN number of cycles
TiO_2-NTs-500c	500	×
TiO_2-NTs-800c	800	×
TiO_2-NTs-1000c	1000	×
TiO_2-NTs-500-BN2c	500	2
TiO_2-NTs-500-BN5c	500	5
TiO_2-NTs-500-BN10c	500	10

5.3. Nitrogen and Boron doped TiO_2 NTs

Titanium dioxide deposit after 500 cycles of ALD were treated under different atmospheres at 750°C for 15 min (**Table 3. 2**). For nitrogen doped, two sources were used,

ammonia and nitrogen gas, the samples were denoted N-TiO_2-NTs, NH_3-TiO_2-NTs. Boron doped TiO_2 (B-TiO_2-NTs) was obtained by thermal treatment under BBr_3 gas pulses.

Table 3. 2: Doping TiO_2-NTs-500c with nitrogen, ammonia and boron.

Sample	TiO_2 number of cycles	Doping at 750°C for 15 min
N-TiO_2-NTs	500	Nitrogen
NH_3-TiO_2-NTs	500	Ammonia
B-TiO_2-NTs	500	Boron tribromide

5.4. Characterization of the synthesized nanocomposites

The morphology of the elaborated nanotubes and nanofibers was analyzed by scanning electron microscope (SEM Hitachi S4800, JAPAN). The samples were supported on aluminum stubs and were sputter coated with platinum/palladium using a Polaron SC7620 Mini Sputter Coater. X-ray diffraction (XRD) studies of synthesized catalysts were carried out using Philips X'pert system with Cu K α radiation (k = 0.15406 nm). The diffraction patterns were measured between 10 and 80° with a step size of 0.0167°. The tubular morphology of nanotube was further confirmed by transmission electron microscope (TEM) analysis using JEOL 2200FS (200 kV) and JEOL ARM-200F (200kV). For TEM analysis, catalysts were dispersed in ethanol and a drop of the resultant suspension was dried on a carbon support film covering a standard copper grid. X-ray photoelectron spectroscopy (XPS) measurements were conducted via (XPS, Escalab 250 appartus, in order to define the chemical composition of the prepared samples. The band gap of the synthesized catalysts was determined by UV–Visible spectrophotometer (Jasco model V570) equipped with a diffuse reflectance (DR) attachment (Shimadzu IRS-2200). For optical absorbance measurements, photoluminescence (PL) spectra was recorded with an optical fiber spectrometer (Ocean Optics usb2000) with an excitation wavelength of 266 nm by a nitrogen Nd:YAG laser, 9mW.

5.5. Electrochemical measurements

Electrochemical impedance measurements and electroactive surface characterization cyclic voltammetry (CV) were performed in three-electrode cell system connected to a solartron SI 1287 galvanostatic-potentiostat. Halogen lamp (150 w) was used as light source and placed at a distance of 10 cm away from the electrode surface. Platinum wire and Ag/AgCl were used as counter and reference electrode, respectively. The working electrode (2x2.5cm) was prepared from a suspension of 5 mg photocatalyst, 1 mL isopropanol and 40 µL Nafion aqueous solution. After 30 min of mixture in ultrasonic cleaner, the slurry was dropped on the ITO glass, and the working electrode was achieved after the evaporation of isopropanol. For EIS measurements, the three electrodes were immersed in Na_2SO_4 solution (0.1 $mol.L^{-1}$) considered as electrolyte. For EAS analysis, 10 mM $K_3[Fe(CN)_6]$ and 1.0 M KCl were used as electrolytes. The electroactive surface of cathode materials was estimated from cyclic voltammetry performed in a voltage range of -0.4 to 0.8 V and at a scan rate of 20 $mV.s^{-1}$. The electroactive surface area was calculated using the Randles–Sevcik equation:

$$\mathbf{Ip = 2.69 \times 10^5 \times AD^{1/2} \times n^{3/2} \times Cv^{1/2}} \quad \textbf{(1)}$$

where Ip is the maximum current (A), n is the number of electrons transferred (n = 1), A is the area of the electrode (cm^2), D is the diffusion coefficient of $[Fe(CN)_6]^{3-}$ ($7.60 \times 10\text{-}6\ cm^2.s^{-1}$), C is the concentration of $[Fe(CN)_6]^{3-}$ ($1 \times 10^{-5}\ mol.cm^{-3}$) and v is the scan rate ($0.01\ V.s^{-1}$).

5.6. Photocatalytic experiments of acetaminophen

Degradation of acetaminophen (ACT) in aqueous solution was used to inspect the photocatalytic activity of as prepared TiO_2 samples under visible light source provided by a halogen linear lamp (400W, Avide). The solution containing the pollutants was maintained at 10 cm from the lamp for all experiments. At first, comparison between TiO_2-NTs with different wall thicknesses (different ALD cycles) was made. Than the catalytic efficiency of TiO_2-NTs with 500 cycles of ALD was compared to TiO_2- NFs and doped TiO_2-NTs.

The photocatalytic degradation experiments were performed as following: photocatalyst with initial concentration of 0.5 $g.L^{-1}$ was added into 250 mL of ACT solution (5 $mg.L^{-1}$) in a 600 mL glass reactor. A water bath was used to minimize the temperature increase in the solution

under the light irradiation. The solution was stirred for 30 minutes to ensure equilibrium adsorption in the dark and then exposed to irradiation. At certain time intervals, 2 mL aliquots were sampled and filtered with 0.22 µm filters. The concentration of ACT was analyzed by high performance liquid chromatography equipped with a C-18 column (RP18 Column, Nucleoshell) and a Quattro-Micro mass spectrometer with an Electrospray probe (Waters Micromass, Wythenshawe, Manchester, UK) as a detector. An isocratic method (A/B=97/3) set at a flow rate of 0.25 mL.min^{-1} was used. The phase A of eluents consisted on a mixture of Acetonitrile/water (95/5) while the phase B was 100% acetonitrile with 0.1% formic acid for both phases.

The recyclability of the catalyst that showed the best degradation efficiency was further investigated. The nanocomposite was reused under UV and visible light for 5 cycles with the same initial conditions.

The degradation efficiency (D(%)), was calculated according to Eq. (2):

$$\mathbf{D}(\%) = [(\mathbf{C_0} - \mathbf{C})/\mathbf{C_0}\,] \times \mathbf{100} \qquad \textbf{(2)}$$

where: C_0 and C are the initial and final concentrations of contaminant after tests, respectively.

5.7. Photocatalytic kinetic model

Typically, TiO_2 kinetics is usually characterized by Langmuir–Hinshelwood (L–H) model[66,67]. When the concentration of the pollutant is low, a pseudo-first-order kinetics is applied[68], Eq.(3):

$$\mathbf{ln}\,(\mathbf{C_0}/\mathbf{C}) = \mathbf{kt} \qquad \textbf{(3)}$$

where C_0 (mg/L) is the initial concentration of the pollutant, C is the pollutant concentration at time t (min) and k (min^{-1}) is the pseudo-first- order rate constant.

5.8. Mictoxicity tests for determination of sub-products toxicity

During the degradation of acetaminophen many sub-products could be formed [69]. In order to confirm or not the toxicity of these compounds bioluminescence toxicity study was carried

out. This study is based on the measurements of the luminescence effect of marine bacteria. The bacteria used in this method was the strain Vibrio fischeri LCK 487. All measurements were conducted using Microtox® Model 500 Analyzer (Modern Water Inc.; United Kingdom) coupled with MicrotoxOmni® software. First, the bacteria reconstitution was performed by adding 5mL of the reagent diluents at 5°C. Then 100 µL of the solution was transferred to the cuvettes and the reagent was stabilized at 15°C for 15 min. In order to enhance the activity of Vibrio Fisheri bacteria, the samples were diluted at 81.8% of initial concentration by adding 22% NaCl solution. Based on luminescence intensity, the screening test 81.8% allow to identify the toxicity of samples, as the activity of the bacteria could be reduced by the presence of toxic elements related to a decrease of bacteria luminescence. Before measuring the bacteria luminescence, all the samples were filtered with 0.2 mm filters to remove any precipitate or solid matter in the solution. The toxicity values are directly relative to the inhibition rate of bacteria's activity, calculated as follow in the equation (4):

$$\mathbf{Ic_{(t)}}(\%) = (\mathbf{1} - \frac{\mathbf{LU_{(t)}}}{\mathbf{LU_{(0)}} \times \mathbf{R_{(t)}}}) \times \mathbf{100} \quad \textbf{(4)}$$

where $LU_{(t)}$ is the intensity of luminescence emitted by bacteria after t=15 min of contact with the sample; $LU_{(0)}$: is the initial intensity of luminescence emitted by bacteria before the addition of the sample; R(t): is the corrected term.

Since luminescence of bacteria decreases over time and under the action of environmental conditions in the absence of toxicity, it is necessary to compensate the errors due to these factors by taking into account the variability of the luminescence R(t) of the bacteria in a control solution (MilliQ water and NaCl) which gives the LU_0 values. The corrected term is given by equation (5):

$$\mathbf{R_{(t)}} = \frac{\mathbf{LU_{0(t)}}}{\mathbf{LU_0}} \quad \textbf{(5)}$$

where $LU_{0(t)}$ is the intensity of luminescence emitted by bacteria after a t=5 min or t=15 min of contact with the control solution (MilliQ water and NaCl); and LU_0: is the initial intensity of luminescence emitted by bacteria before the addition of the control solution (MilliQ water and NaCl).

5.9. Quenching tests

Scavengers test were performed in order to determine the main active species responsible of the degradation of ACT. Benzoquinone, isopropanol and EDTA were added to the solution before switching the light on. The experiments performed was the same as degradation process, an aliquot was withdrawn at different times and the concentration of ACT was detected by LC-MS-MS.

6. Results and discussion

6.1. Morphological characterization

The morphology of all prepared materials was verified by scanning electron microscopy (SEM). Before the analysis, TiO_2 deposit on PAN nanofibers substrate by ALD and TiO_2 nanofibers elaborated by electrospinning were subject to thermal treatment at 750°C under air for 4h. A well nanotubular structure was depicted after ALD deposition when the time of pulse of TiO_2 was set at 0.2 s. Below this value the nanotubes were not well formed (**Figure S3. 1**). In addition, it was reported elsewhere that more than 200 cycles are necessary to obtain well-structured nanotubes[70]. Moreover, **Figure 3. 1 a** demonstrate the nanotubular morphology of TiO_2 after the removal of PAN substrate with several microns length. The PAN nanofibers served as an efficient “template” in the synthesis of titanium dioxide nanotubes. In **Figure 3. 1 b,** nanotubes with an inner diameter of approximatively 400 nm and high surface roughness were obtained after 500 cycles of ALD. Nanofibrous structure of TiO_2 obtained by electrospinning was presented in **Figure 3. 1 c.** The surface roughness is attributed to the crystalline structure of the nanofibers at 750°C. In **Figure 3. 1 d-e,** no distinct difference was depicted after doping the nanotubes, confirming the literature finding that introduction of nitrogen or BN cannot change the shape of TiO_2[64]. Thus, it was reported than doping with non-metals could occur into the bulk of nanotubes[71].

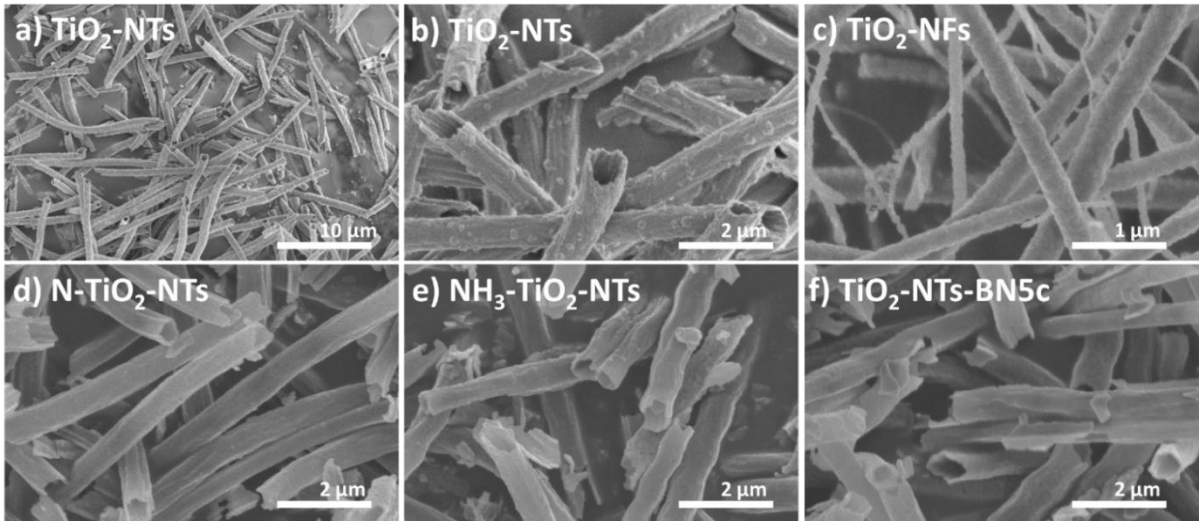

Figure 3. 1. SEM images of synthesized materials a-b)TiO_2-NTs, c)TiO_2-NFs, d)N-TiO_2-NTs, e)NH_3-TiO_2-NTs and f) TiO_2-NTs-BN5c.

TEM images (**Figure 3. 2**) confirm the nanotubular structure of TiO_2 with a nanotube wall thickness of ~60nm for both doped and undoped titanium. After doping with nitrogen, the nanotubular morphology of titanium was maintained, and the crystal lattice values remain unchanged (SAED images). Moreover, elemental mapping in **Figure 3. 2 b** confirms the presence of nitrogen dopants with T and O elements.

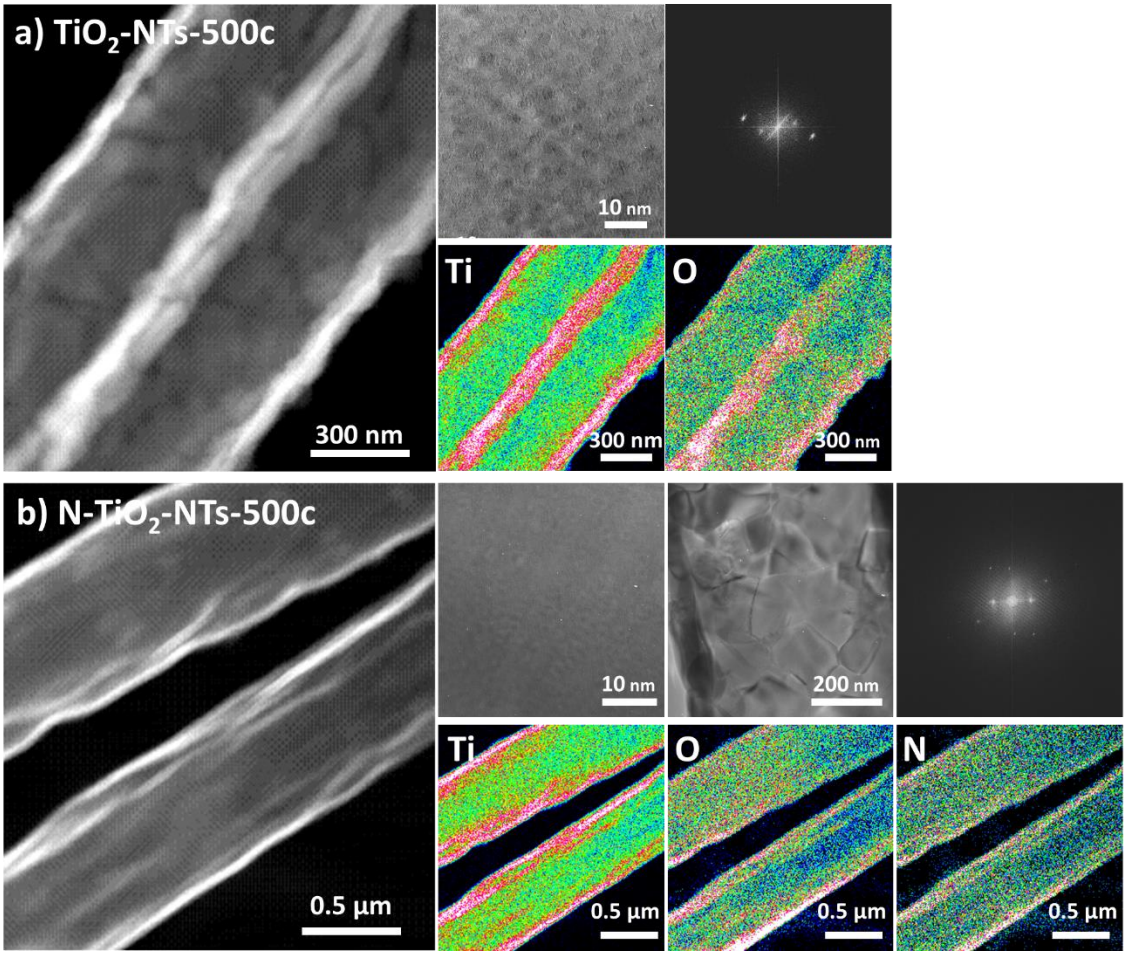

Figure 3. 2. HRTEM, elemental mapping and SAED of a) TiO_2-NTs-500c and b) N-TiO_2-NTs.

Characterization of crystalline structure of the prepared catalysts was determined by XRD. Nanotubes with different thicknesses were all composed of anatase phase at 750 °C, which is in good correlation with the literature[72] (**Figure 3. 3 and S3. 2**). TiO_2-NTs and N-TiO_2-NTs evidenced characteristics peaks of anatase crystalline structure at 2θ = 25.3, 36.9, 37.7, 38.5, 48.0, 53.8, 55.0, 62.6, 68.7, 70.2, 74.9 and 75.9° [73]. These peaks correspond to plans of anatase phase (101), (004), (200), (105), (211), (204), (116) and (107) (JCPDS-00-071-1167), respectively[74]. Anatase phase was known to be more active than rutile due to the presence of an indirect band gap in the anatase crystal which extends the electron–hole pair separation[75]. It should be noted that anatase peak at N-TiO_2-NTs was slightly shifted in comparison to TiO_2-NTs. This could be explained by the incorporation of dopants into the bulk or the crystal lattice of TiO_2 these results will be confirmed by XPS results[76] . Contrarily to boron and BN doping, nitrogen inhibit the formation of rutile phase. By doping TiO_2 NTs with B and BN, additional

peaks for rutile phase were observed in the XRD of B-TiO_2-NTs and TiO_2-NTs-BN5c[77]. The peak at 2θ = 28.0° indexed to rutile phase of (110) plane[78]. It was reported elsewhere that the percentage of incorporation of boron into TiO_2 can allow or not the formation of rutile phase. In our case, when the percentage of BN was increased **(Figure S3. 2**), the anatase phase was more stable and the rutile transformation was inhibited[79]. Finally, TiO_2 nanofibers shows formation of both crystalline phases, anatase and rutile with characteristic diffraction peaks of rutile phase (1 1 0), (1 0 1), (1 1 1), (2 1 0), (2 1 1), (2 2 0), (3 1 0) and (1 1 2) diffraction peak (rutile TiO2, JCPDS 21-1276)[80].

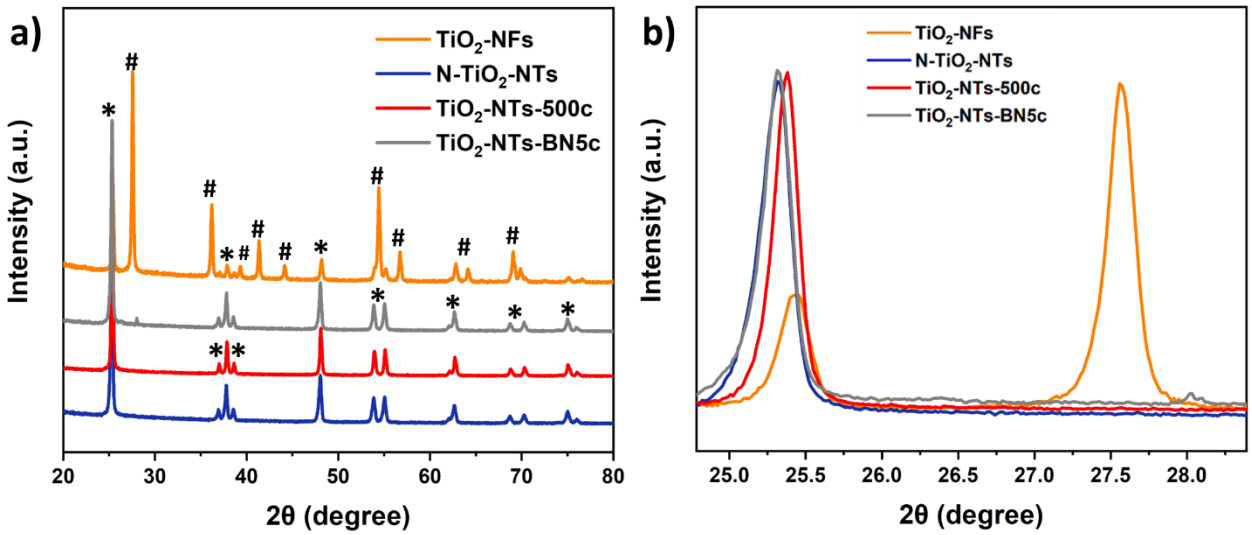

Figure 3. 3. X-Ray diffraction of TiO_2 NTs doped and undoped and TiO_2 nanofibers a) from 15 to 80° and b) zoom on peaks from 24 to 29°.

To understand the effect of different morphologies and modification on TiO_2 structure, percentage of anatase/rutile phase and crystallite sizes were calculated using the spurr equation (6) and Scherrer equation (7)[81,82]:

$$\%R = \frac{1}{1+0.8\left[\frac{I_A(101)}{I_R(110)}\right]} \quad (6)$$

$$D = \frac{k\lambda}{\beta\cos\theta} \quad (7)$$

Where I_A and I_R are the integrated intensities of the diffraction peaks for anatase (101) and rutile (110), D is the average size of crystallites, K is the shape factor of 0.89, λ is the X-ray wavelength, β is the full width at half maximum of a diffraction peak, and θ is the Bragg angle.

Table 3. 3 represents the % of anatase/ rutile phases and their particle sizes for all prepared samples calculated by Scherer and spurr formula, respectively. Modification of TiO_2-NTs with different dopants decreased the crystallite size of composite materials, owing to the inhibitory effect of dopants on the grain growth of TiO_2 particle. The anatase particle size of undoped TiO_2-NTs and N-TiO_2-NTs were 37.2 nm and 29.9 nm, respectively. This is probably due to the deformation of crystal lattice and oxygen vacancies left by the substitution of O atoms by N atoms. When the particle size decreases, it allows the photo-generated electrons to move faster to the surface of TiO_2, thus improves the degradation efficiency[61,83]. For TiO_2 NFs, crystallite sizes for both phases was calculated, with values of 30.9 and 34.3 nm for anatase and rutile, respectively. Hence, it was reported in the literature that rutile phase photocatalytic characteristics are lower than anatase phase[84].

To further understand the morphology of pristine TiO_2-NTs and nitrogen doped TiO_2 NTs with comparison with TiO_2-NFs, TEM and XPS measurements have been performed. The data will be reported later.

Table 3. 3: Percentage of anatase and rutile phases in all prepared samples and their crystallite sizes.

Sample	Anatase phase (%)	Rutile phase (%)	Crystallite Size (A) (nm)	Crystallite Size (R) (nm)
TiO_2-NTs-500c	100	-	37.2	-
TiO_2-NTs-1000c	100	-	42.1	-
TiO_2-NFs	24.5	75.5	30.9	34.3
TiO_2-NTs-BN2c	100	-	31.5	-
TiO_2-NTs-BN5c	91.0	9.0	32.1	46.5
TiO_2-NTs-BN10c	100	-	28.9	-
N-TiO_2-NTs	100	-	29.9	-
NH_3-TiO_2-NTs	100	-	27.2	-
B-TiO_2 NTs	65.8	34.2	31.8	52.1

The chemical composition of pristine TiO_2-NTs and doped TiO_2-NTs was assigned by XPS measurements. **Figure 3. 4 a** represents the XPS survey of nitrogen doped TiO_2 NTs and confirms the presence of the elements Ti, O, C and N. The presence of carbon could be assigned to the residues remained after calcination and removal of PAN nanofibers. High resolution spectra of Ti 2p shows two peaks at 458.4 and 464.1 eV attribuated to Ti 2p3/2 and Ti 2p1/2, respectively. The high-resolution XPS spectra for O 1s were deconvoluted into three peaks positioned at 529.5, 530.6 and 532.3 eV. The binding energies of Ti 2p and O 1s for TiO_2 NTs were represented in **Table S3. 1** and shows lower BE than doped TiO_2. These results are not in agreement with reported results in literature where nitrogen doping decrease the BE values[85,86]. Hence, these reports have proven the presence of oxygen vacancies due to the substitution of O state by N. In our case, the nitrogen peak (**Figure 3. 4 d**) at 399.9 eV could not be assigned to substitutional doping of TiO_2 lattice with nitrogen. But, to the presence of interstitial N atom in the environment of O–Ti–N. Interaction between N and O within the lattice of TiO_2 NTs increased the BE of the N 1s level which is correlated with our results[87].Moreover, the theory of the existence of Ti-N bond is excluded since N1s would be located at lower binding energies (BE lower than 397 eV)[88]. This result might be motivating for photocatalytic applications, since N-doping in TiO_2 without Ti–N bonding is responsible for visible-light sensitization. The total nitrogen amount of the N-TiO_2 nanotube was approximately 0.7%, whereas for TiO_2-NTs-BN5c, the B and N amounts were estimated to be 6.6 and 1.3%, respectively. The higher nitrogen values could be assigned to the different doping route where nitrogen was used. As seen in **Figure 3. 4 e,** only one peak at 192.3 eV was attributed to B 1s, which suggests the presence of B-O-Ti groups[89]. The B-N linkage was not formed which means that the sample is not doped by BN but is co-doped with B and N. N 1s peak at 398.2 eV (N 1s A) is typically assigned to the substitutional nitrogen atom replacing one O atom of the TiO_2 lattice. While the peak at 401.5 (N 1s B) eV corresponded to NH_4^+ions on the TiO_2 surface[90]. The site of the N atoms in the TiO_2 lattice depends on the synthetic route of N-doped TiO_2.

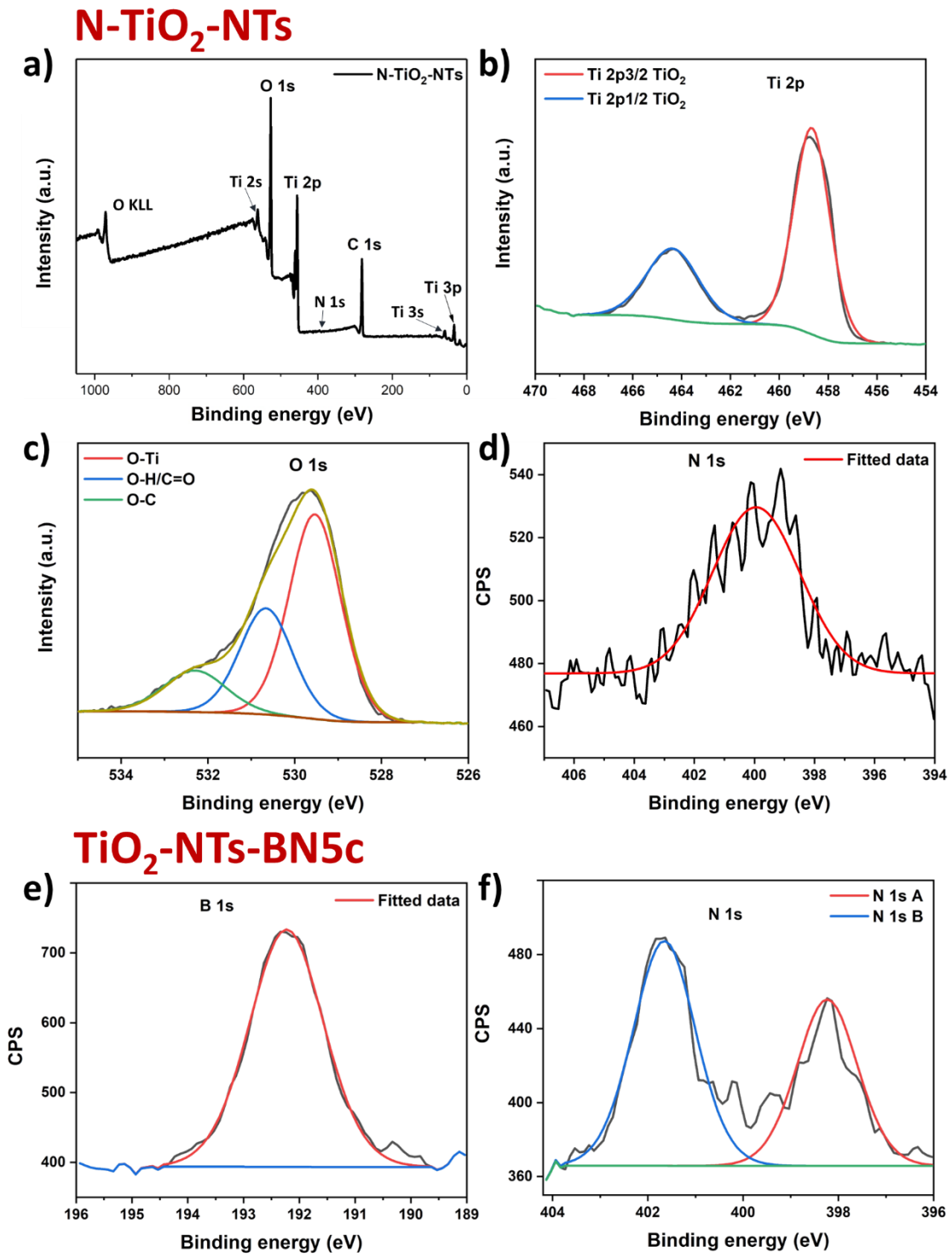

Figure 3. 4. XPS spectra of the N-TiO_2-NTs sample (a) Survey spectra, (b) Ti 2p, (c) O 1s, (d) N 1s; and TiO_2-NTs-BN5c sample e) B1s and f) N1s.

6.2. Electrochemical measurements

Elaboration of catalyst with a reduced e^-/h^+ recombination rate and enhanced electron-charge transport are of utmost importance for enhancing degradation efficiency under visible light. In addition to PL measurements (**Figure S3. 3**), EIS and EAS were carried out to investigate the interfacial charge transport process. **Figure 3. 5 a** shows the nyquist plot of TiO_2-NTs, TiO_2-NFs, N-TiO_2-NTs and TiO_2-BN5 prepared samples. TiO_2 nyquist plot is described by its semicircle frequency region in the Nyquist plot related to the electron transfer from the conduction band of TiO_2 to the electrolyte[91]. The radius arc resistance is directly correlated with charge transport ability of the prepared photocatalyst. N-TiO_2-NTs holds the lowest radius arc than other prepared samples, associated to the higher ability of charge transports and the lowest recombination rate. Charge transfer resistances values were represented in **Table 3. 4**, nitrogen-doped TiO_2-NTs possesses the lowest R_2 of 15.22 kΩ compared to 19.11 kΩ for undoped TiO_2 NTs. The increase in charge transfer resistance suggests that nitrogen dopant increases the surface resistance of TiO_2 electrode and retards charge recombination at the TiO_2/electrolyte interface. Comparing TiO_2 morphology, TiO_2 nanofibers have shown a better resistance of the separation of e^--h^+, this could be assess with its higher crystalline that favored the separation and transport of charge carriers[22]. Hence, doping TiO_2 NTs with BN affected negatively the charge kinetics indicating the occurrence of trap states and recombination centers caused by this type of doping[92]. To investigate the effect of morphology structure and doping titanium dioxide materials on electroactive surface, cyclic voltammograms were performed in **Figure 3. 5 b.** Nitrogen doped TiO_2 resulted in the highest current response toward $[Fe(CN)_6]^{3/4}$ which proposed that the electrode reaction rate is higher. Doping TiO_2 NTs with nitrogen improved the electron-transfer efficiency, leading to the enlargement of electroactive surface area. **Table 3. 4** summarized the electrochemical properties of prepared catalysts using the $[Fe(CN)_6]^{3-}/[Fe(CN)_6]^{4-}$ couple.

Table 3. 4: Electrochemical results for TiO_2-NTs, TiO_2-NFs, TiO_2-NTs-BN5c and N-TiO_2 NTs

Sample	R_2 (KΩ)	Ip (A)	ΔE (mV)	EAS (cm^2)
TiO_2-NTs	19.11	1.86	0.38	1.78
TiO_2-NFs	16.52	1.94	0.43	1.85
TiO_2-NTs -BN5c	51.31	2.0	0.40	1.9
N-TiO_2 NTs	15.22	2.5	0.37	2.4

The values of $\Delta E=E_{anode} - E_{cathode}$ were also calculated. N-TiO_2-NTs electrode exhibits a shorter average peak-to-peak separation of 0.3711 mV at V= 20 mV/s. When ΔE is smaller, faster electron transfer occurred in the redox reaction and demonstrates a more conductive electrode surface. The EAS values increased following this order TiO_2-NTs-500c < TiO_2-NFs < TiO_2-NTs-BN5c < N-TiO_2 NTs with 1.78, 1.85, 1.9 and 2.4 cm^2, respectively[93]. This confirms that doping TiO_2 play a major role on enhancing the photocatalytic reaction by improving the separation of the electron-holes which was confirmed by PL results. According to the literature, a smaller grain size can increase not only the number of active surface sites but also the transfer rate of surface charge carrier in 1D structured photocatalyst, thus higher photocatalytic activity could be reported [94]. N-TiO_2-NTs possesses the lowest crystallite grain size than TiO_2 NFs, undoped TiO_2-NTs and BN doped TiO_2.

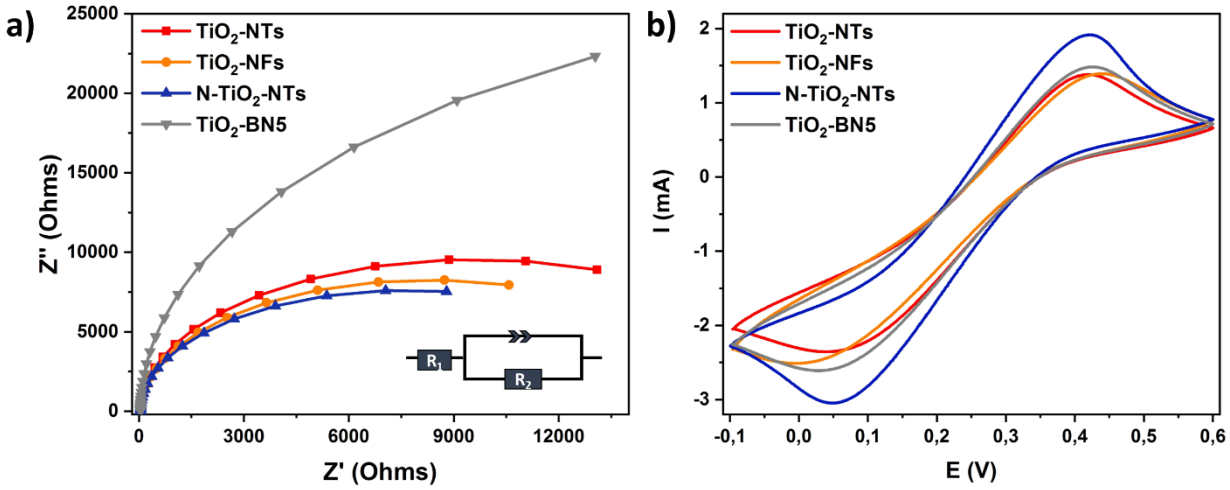

Figure 3. 5. a) Nyquist plots of TiO_2-NTs, TiO_2-NFs, N-TiO_2-NTs and TiO_2-BN5; b) Cyclic voltammograms (CVs) in potassium hexacyanoferrate solution at scan rate 20 mV/s of prepared TiO_2 catalysts.

6.3. Photocatalytic experiments

6.3.1. Photocatalytic degradation

Visible light photodegradation of ACT (**Figure 3. 6**) was compared by studying the effect of TiO_2 modification. First, the ALD parameters were varied and it was found that increasing the ALD cycles, lead to an increase of wall thickness (not presented in this paper). These parameters could highly affect the degradation efficiency as presented in **Figure 3. 6 a** and reported in litterature[72]. TiO_2 nanotubes after 500 cycles of ALD shows the highest degradation of 95.7 % after 120 minutes irradiation compared to 76.6 % and 56.0 % for 800 and 1000 cycles, respectively. Regarding the best performance for TiO_2-NTs-500c, the photocatalyst was selected for further investigation. Since the morphology plays a major role on the degradation efficiency of pharmaceutical pollutants taking into consideration the surface area, crystallinity, recombination of electron-holes, bang gap, it is important to understand the effect of these parameters on the photocatalytic properties[85]. We synthesized TiO_2 NFs by electrospinning followed by a thermal treatment at 750°C for 4h. The visible light catalytic properties of these nanofibers were compared to TiO_2 nanotubes in **Figure 3. 6** As proven from EIS and EAS measurements, N-TiO_2 nanotubes possess the lowest recombination rate and a higher surface area than nanofibers which enhance its photocatalytic activity.

Degradation efficiency with anatase TiO_2 was reported to have higher degradation efficiency than a catalyst with both crystalline phase[72,83]. Wang *et al.* reported that TiO_2 structure plays a major role on the degradation efficiency. They found that TiO_2 nanosheets presents a better photocatalytic degradation of methylene blue than TiO_2 nanoparticles. Moreover, they reported that the higher surface area further improve the degradation under visible light[95].

Based on the performance of TiO_2-NTs, different modified samples were prepared by varying the dopants nature. These modifications are essential in order to explore how to restrain the recombination of photogenerated electron-hole pairs for feasible charge separation and transfer, and expand the absorption edge to the visible-light region. The order of photocatalytic activity of the catalysts is as follow N-TiO_2-NTs > TiO_2-500c-750°C-NH3 > TiO_2-NTs-BN5c > B-TiO_2-500c-750°C with degradation percentage of 98.3, 38.9, 31.9 and 13.4 %, respectively (**Table S3. 2**). As a result, nitrogen dopants have shown high efficiency for fastest pollutants degradation. Hence, better degradation were obtained when using nitrogen as a gas source and not ammonia. It seems that the modification step could be affected by many factors, one of them runs in the types and level of nitrogen doping and the concentration of oxygen vacancies, that will greatly influences the photocatalytic activity[96,97].

The effect of nitrogen doping on improving catalyst properties have been widely reported in the literature. It was found that effect of doping by nitrogen creates oxygen vacancies that participate in trapping the photoinduced electron and acting as a reactive center for the photocatalytic process. Thousands of paper were published on the modification of TiO_2 by nitrogen doping, hence a clear comparison between these papers remain difficult since many parameters could vary in the same time (structure of the catalyst, concentrations, matrix, lamp source….)[63,83,98–100].

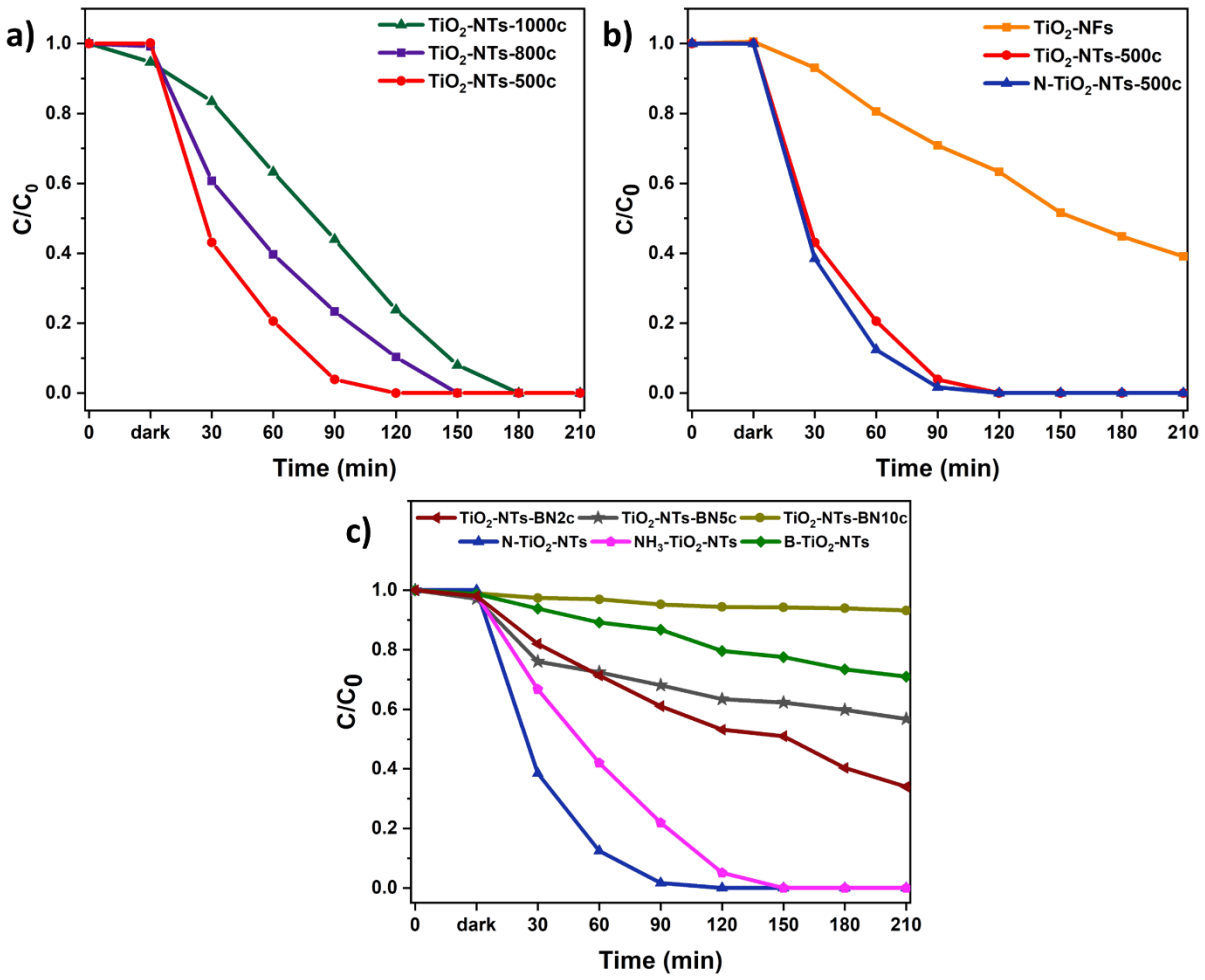

Figure 3. 6. Degradation efficiency of acetaminophen under visible light by studying the effect of a) TiO_2 wall thickness, b) TiO_2 structure morphology and c) TiO_2 modification by different dopants.

6.3.2. Photocatalytic kinetic model

The photocatalytic degradation of ACT under visible light irradiation follows the pseudo-first order kinetics. As shown in **Figure 3. 7 a**, the closely linear relationship between $\ln(C_0/C)$ and irradiation time (t) fits well with the first order reaction rate of ACT degradation. The degradation rate of ACT over N-TiO_2-NTs was 0.045 min^{-1}, which is 4 times higher than TiO_2-NFs. This increase in degradation efficiency of TiO_2 nanotubes over TiO_2 nanofibers was proved by the lower recombination rate of e^--h^+ in PL and EIS measurements. Moreover, the presence of high fraction of rutile phase in TiO_2 NFs have reduced the degradation efficiency of the catalyst. It can be clearly concluded that atomic layer deposition is a promising

technique for elaboration of highly active catalyst with well organized structure and higher degradation performance under visible light.

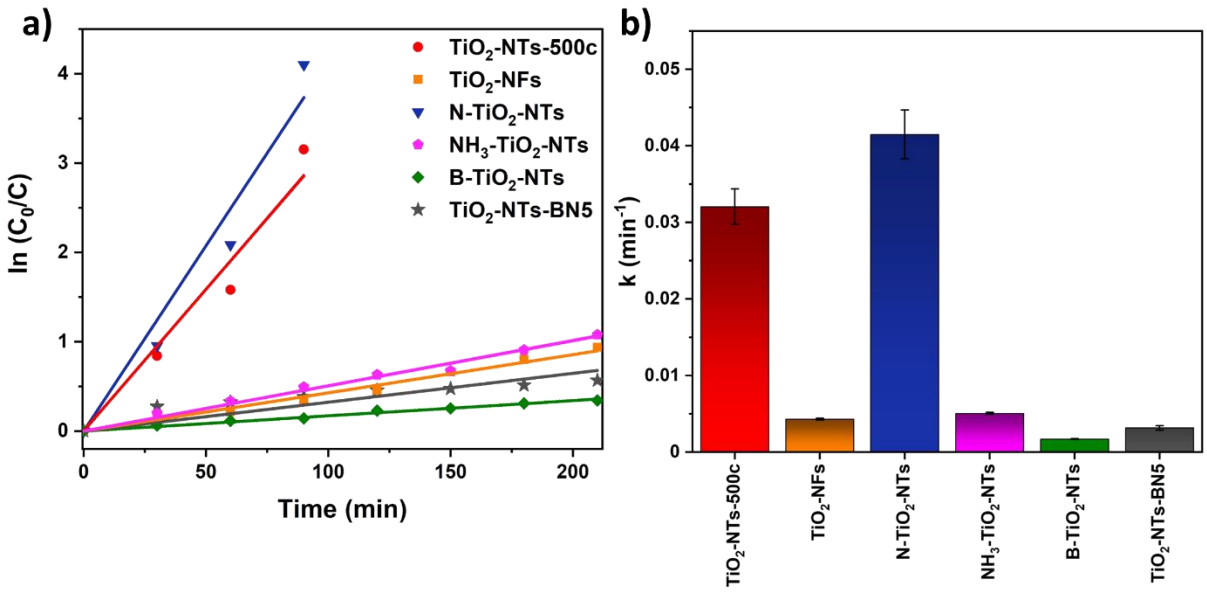

Figure 3. 7. Photocatalytic ACT degradation by as-prepared TiO_2 a) plot of ln(C0/Ct) versus time (fitted to first order rate law) and b) values the first order rate constant.

6.3.3. Stability, quenching and toxicity tests

The recycling and stability of N-TiO_2-NTs photocatalyst was tested for five consecutive cycles and the results are presented in **Figure 3. 8 a**. After each cycle, the catalyst was rinsed several times with distilled water and dried at 70 °C before being used for the next cycle. In the first run, paracetamol degradation reached 98.3 % after 90 min of visible irradiation. While 97.5, 96.0 and 93.9 % were achieved for the second, third and fourth runs, respectively. Only 82.6% paracetamol removal were obtained at 5th runs within 90 min. It is clear that a little loss happened in the ACT degradation efficiency during reusing cycles of the catalyst, but the decontamination percentage was still over 82% after five runs. The reasons in the decrease of catalytic activity could be related to the loss of nitrogen in the catalyst after consecutive cycles, or the accumulation of sub-products formed during the degradation of the surface of the catalyst, thus decreasing the active sites available[101]. Although the prepared nitrogen doped catalyst show a loss of activity (less than 20 %) after five cycles, it is considered as a promising stable catalyst for industrial applications. It was reported in literature, that treatment of

organic pollutants might generate the formation of sub-products during advanced oxidation processes[102,103]. These byproducts exhibit cyclic and aromatic structure that are highly toxic even more than the initial pollutant itself. Consequently, it is of utmost importance to evaluate the toxicity of such intermediates during the phototodegradation of ACT. The acute toxicity of the treated solution after 15-min time contact with V. fischeri bacterial strain is represented in **Figure 3. 8 b**. The initial toxicity of ACT is very low at this concentration, as proved in previous works[104]. Hence, the toxicity increased drastically at the early stage of degradation and reached ~90 % after 1h visible irradiation. This result is relevant and consistent with previously published reports that proved formation of toxic aromatic by-products such as 1,4-benzoquinone, hydroquinone, benzoic acid and benzaldehyde during ACT degradation[105,106]. After 1h irradiation, the toxicity begins to decrease and reached less than 20% at 3h irradiation. During this stage, the formation of lower-toxic aromatic compounds is proposed. The solution toxicity remains stable after 6h irradiation at a very low value less than 5 % where short-chain carboxylic acids were continuously transformed to CO_2 and H_2O.

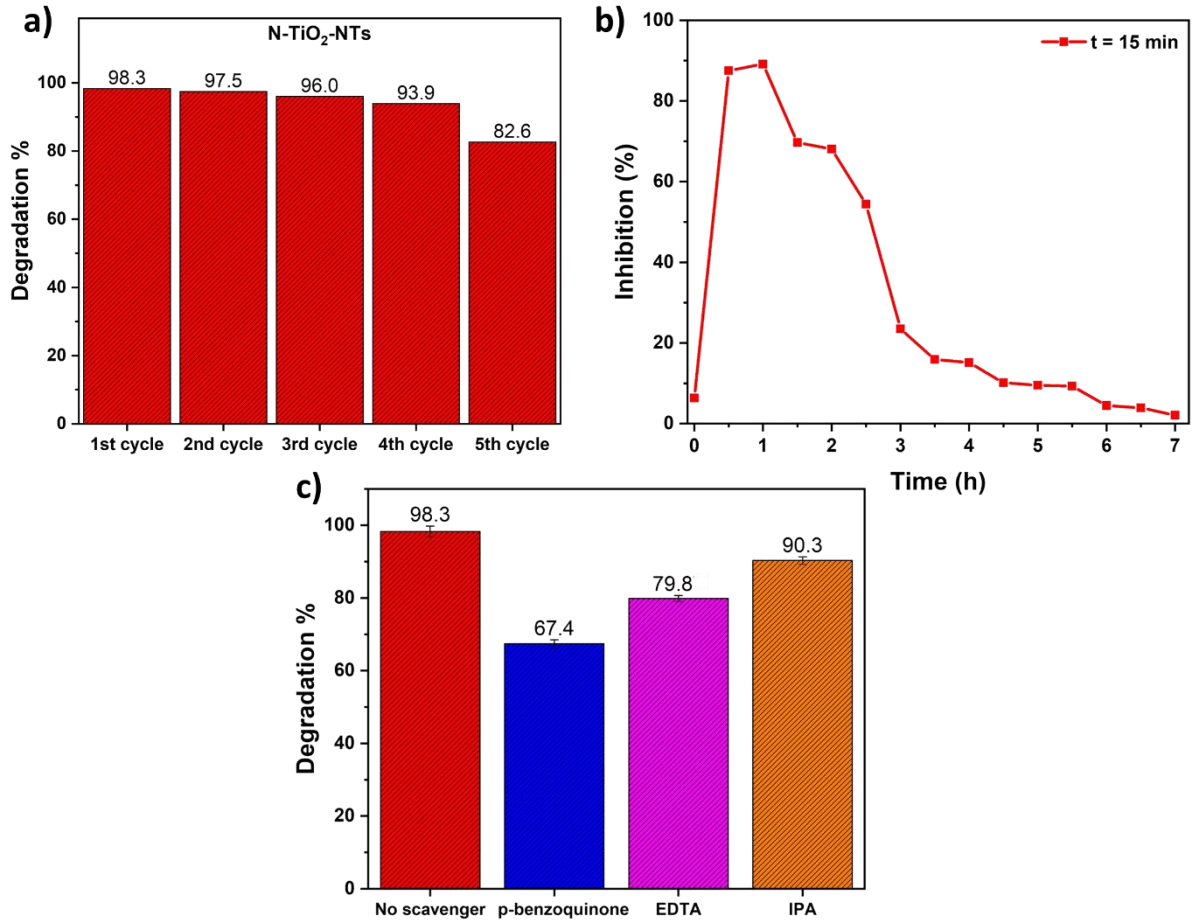

Figure 3. 8. a) Reusability of N–TiO_2-NT for photocatalytic activity, b) Inhibition of luminescence of V. fischeri marine bacteria during photodegration of ACT and c) effect of radical scavengers on acetaminophen degradation.

During the photodegradation, OH radicals, h^+ and O_2^- radicals are generally considered as active species. In order to determine reactive radicals responsible of the degradation of ACT, scavengers tests were performed. The trapping experiments were performed with different scavengers EDTA for h^+, isopropanol (IPA) for OH radicals and p-benzoquinone (BQ) for O_2^- radicals using N-TiO_2-NTs catalyst. The results presented in **Figure 3. 8 c** suggest that all three active radical species are responsible for the degradation of ACT, since a decrease of photodegradation was depicted with the three scavengers. Among them, benzoquinone reduced the degradation rate of ACT from 98.3 % to 67.4 % this clearly indicated that O_2^- radical played a major role during the degradation process under visible light irradiation.

7. Conclusion

In comparison between TiO_2 nanofibers elaborated by electrospinning and TiO_2 NTs prepared by ALD, the nanotubes structure exhibited higher photocatalytic activity. Coupling TiO_2 NTs with non-metal dopants such as nitrogen enhanced further the degradation efficiency of the catalyst and shows higher degradation efficiency under visible light. N-TiO_2-NTs catalyst shows a lower recombination rate of the electron-holes and a higher electroactive surface area that explains its better degradation efficiency. The elaborated catalysts maintain a high stability after four consecutive cycles with a loss of less than 5% of the catalytic activity. Moreover, scavengers tests attested that the main reactive specie responsible of the degradation of ACT was the superoxide radicals. ALD is a promising technique for tuning photocatalysts on immobilized supports with good degradation efficiency and high stability. Further studies using these elaborated catalysts should be developed on the mechanism of degradation of organic pollutant in real wastewater.

References

1. Takeuchi N, Yasuoka K. Review of plasma-based water treatment technologies for the decomposition of persistent organic compounds. *Jpn J Appl Phys*. 2020;60(SA):SA0801. doi:10.35848/1347-4065/abb75d

2. Gehrke I, Geiser A, Somborn-Schulz A. Innovations in nanotechnology for water treatment. *Nanotechnol Sci Appl*. 2015;8:1-17. doi:10.2147/NSA.S43773

3. World Health Organization. Pharmaceuticals in drinking-water. Published online 2012.

4. Houtman CJ. Emerging contaminants in surface waters and their relevance for the production of drinking water in Europe. *J Integr Environ Sci*. 2010;7(4):271-295.

5. Tran NH, Reinhard M, Gin KYH. Occurrence and fate of emerging contaminants in municipal wastewater treatment plants from different geographical regions-a review. *Water Res*. 2018;133:182-207.

6. Nam SW, Jo BI, Yoon Y, Zoh KD. Occurrence and removal of selected micropollutants in a water treatment plant. *Chemosphere*. 2014;95:156-165. doi:10.1016/j.chemosphere.2013.08.055

7. Stasinakis A. Use of selected advanced oxidation processes (AOPs) for wastewater treatment–a mini review. *Glob NEST J*. 2008;10(3):376-385.

8. Rodriguez-Narvaez OM, Peralta-Hernandez JM, Goonetilleke A, Bandala ER. Treatment technologies for emerging contaminants in water: A review. *Chem Eng J*. 2017;323:361-380.

9. Teodosiu C, Gilca AF, Barjoveanu G, Fiore S. Emerging pollutants removal through advanced drinking water treatment: A review on processes and environmental performances assessment. *J Clean Prod*. 2018;197:1210-1221. doi:10.1016/j.jclepro.2018.06.247

10. Friedmann D, Mendive C, Bahnemann D. TiO2 for water treatment: parameters affecting the kinetics and mechanisms of photocatalysis. *Appl Catal B Environ*. 2010;99(3-4):398-406.

11. Chong MN, Jin B, Chow CWK, Saint C. Recent developments in photocatalytic water treatment technology: A review. *Water Res*. 2010;44(10):2997-3027. doi:10.1016/j.watres.2010.02.039

12. Ameta R, Solanki MS, Benjamin S, Ameta SC. Chapter 6 - Photocatalysis. In: Ameta SC, Ameta R, eds. *Advanced Oxidation Processes for Waste Water Treatment*. Academic Press; 2018:135-175. doi:10.1016/B978-0-12-810499-6.00006-1

13. Serpone N. Photocatalysis. In: *Kirk-Othmer Encyclopedia of Chemical Technology*. American Cancer Society; 2000. doi:https://doi.org/10.1002/0471238961.1608152019051816.a01

14. Gaya UI, Abdullah AH. Heterogeneous photocatalytic degradation of organic contaminants over titanium dioxide: a review of fundamentals, progress and problems. *J Photochem Photobiol C Photochem Rev*. 2008;9(1):1-12.

15. Hong SP, Park J, SM Bhat S, et al. Comprehensive study on the morphology control of TiO2 nanorods on foreign substrates by the hydrothermal method. *Cryst Growth Des*. 2018;18(11):6504-6512.

16. Nakata K, Fujishima A. TiO2 photocatalysis: Design and applications. *J Photochem Photobiol C Photochem Rev*. 2012;13(3):169-189. doi:10.1016/j.jphotochemrev.2012.06.001

17. Nasr M, Eid C, Habchi R, Miele P, Bechelany M. Recent Progress on Titanium Dioxide Nanomaterials for Photocatalytic Applications. *ChemSusChem*. 2018;11(18):3023-3047. doi:10.1002/cssc.201800874

18. Nasr O, Mohamed O, Al-Shirbini AS, Abdel-Wahab AM. Photocatalytic degradation of acetaminophen over Ag, Au and Pt loaded TiO2 using solar light. *J Photochem Photobiol Chem*. 2019;374:185-193. doi:10.1016/j.jphotochem.2019.01.032

19. Bui XT, Chiemchaisri C, Fujioka T, Varjani S. Introduction to Recent Advances in Water and Wastewater Treatment Technologies. In: Bui XT, Chiemchaisri C, Fujioka T, Varjani S, eds. *Water and Wastewater Treatment Technologies*. Springer Singapore; 2019:3-12. doi:10.1007/978-981-13-3259-3_1

20. Xiang Q, Ma X, Zhang D, et al. Interfacial modification of titanium dioxide to enhance photocatalytic efficiency towards H2 production. *J Colloid Interface Sci*. 2019;556:376-385. doi:10.1016/j.jcis.2019.08.033

21. Bethi B, Sonawane SH, Bhanvase BA, Gumfekar SP. Nanomaterials-based advanced oxidation processes for wastewater treatment: A review. *Chem Eng Process - Process Intensif*. 2016;109:178-189. doi:10.1016/j.cep.2016.08.016

22. Akple M, Low J, Qin Z, et al. Nitrogen-doped TiO2 microsheets with enhanced visible light photocatalytic activity for CO2 reduction. *Chin J Catal*. 2015;36:2127-2134.

23. Klavarioti M, Mantzavinos D, Kassinos D. Removal of residual pharmaceuticals from aqueous systems by advanced oxidation processes. *Environ Int*. 2009;35(2):402-417.

24. Katal R, Masudy-Panah S, Tanhaei M, Farahani MHDA, Jiangyong H. A review on the synthesis of the various types of anatase TiO2 facets and their applications for photocatalysis. *Chem Eng J*. 2020;384:123384. doi:10.1016/j.cej.2019.123384

25. Yang HG, Liu G, Qiao SZ, et al. Solvothermal Synthesis and Photoreactivity of Anatase TiO2 Nanosheets with Dominant {001} Facets. *J Am Chem Soc*. 2009;131(11):4078-4083. doi:10.1021/ja808790p

26. Ramakrishnan VM, Natarajan M, Santhanam A, Asokan V, Velauthapillai D. Size controlled synthesis of TiO2 nanoparticles by modified solvothermal method towards effective photo catalytic and photovoltaic applications. *Mater Res Bull*. 2018;97:351-360. doi:10.1016/j.materresbull.2017.09.017

27. Mamaghani AH, Haghighat F, Lee CS. Role of titanium dioxide (TiO2) structural design/morphology in photocatalytic air purification. *Appl Catal B Environ*. 2020;269:118735. doi:10.1016/j.apcatb.2020.118735

28. Ge M, Li Q, Cao C, et al. One-dimensional TiO2 Nanotube Photocatalysts for Solar Water Splitting. *Adv Sci*. 2017;4(1):1600152. doi:10.1002/advs.201600152

29. Feng T, Feng GS, Yan L, Pan JH. One-dimensional nanostructured TiO2 for photocatalytic degradation of organic pollutants in wastewater. *Int J Photoenergy*. 2014;2014.

30. Shahrezaei M, Babaluo AA, Habibzadeh S, Haghighi M. Photocatalytic properties of 1D TiO2 nanostructures prepared from polyacrylamide gel–TiO2 nanopowders by hydrothermal synthesis. *Eur J Inorg Chem*. 2017;2017(3):694-703.

31. Rosales M, Zoltan T, Yadarola C, Mosquera E, Gracia F, García A. The influence of the morphology of 1D TiO2 nanostructures on photogeneration of reactive oxygen species and enhanced photocatalytic activity. *J Mol Liq*. 2019;281:59-69. doi:10.1016/j.molliq.2019.02.070

32. Guo MY, Fung MK, Fang F, et al. ZnO and TiO2 1D nanostructures for photocatalytic applications. *J Alloys Compd*. 2011;509(4):1328-1332. doi:10.1016/j.jallcom.2010.10.028

33. Erdogan N, Park J, Choi W, Kim SY, Ozturk A. Alkaline hydrothermal synthesis, characterization, and photocatalytic activity of TiO2 nanostructures: the effect of initial TiO2 phase. *J Nanosci Nanotechnol*. 2019;19(3):1511-1519.

34. Chatzitakis A, Grandcolas M, Xu K, et al. Assessing the photoelectrochemical properties of C, N, F codoped TiO2 nanotubes of different lengths. *Sel Contrib 9th Eur Meet Sol Chem Photocatal Environ Appl SPEA-9*. 2017;287:161-168. doi:10.1016/j.cattod.2016.11.040

35. Roy P, Berger S, Schmuki P. TiO2 nanotubes: synthesis and applications. *Angew Chem Int Ed*. 2011;50(13):2904-2939.

36. Paramasivam I, Jha H, Liu N, Schmuki P. A review of photocatalysis using self-organized TiO2 nanotubes and other ordered oxide nanostructures. *small*. 2012;8(20):3073-3103.

37. Zhu S, Nie L. Progress in fabrication of one-dimensional catalytic materials by electrospinning technology. *J Ind Eng Chem*. 2021;93:28-56. doi:10.1016/j.jiec.2020.09.016

38. Kowalski D, Kim D, Schmuki P. TiO2 nanotubes, nanochannels and mesosponge: Self-organized formation and applications. *Nano Today*. 2013;8(3):235-264. doi:10.1016/j.nantod.2013.04.010

39. Meng X, Banis MN, Geng D, et al. Controllable atomic layer deposition of one-dimensional nanotubular TiO2. *Appl Surf Sci*. 2013;266:132-140. doi:10.1016/j.apsusc.2012.11.116

40. Liang HC, Li XZ, Nowotny J. Photocatalytical properties of TiO2 nanotubes. In: Vol 162. Trans Tech Publ; 2010:295-328.

41. Gao Z, Qin Y. Design and Properties of Confined Nanocatalysts by Atomic Layer Deposition. *Acc Chem Res*. 2017;50(9):2309-2316. doi:10.1021/acs.accounts.7b00266

42. Weber M, Julbe A, Kim SS, Bechelany M. Atomic layer deposition (ALD) on inorganic or polymeric membranes. *J Appl Phys*. 2019;126(4):041101. doi:10.1063/1.5103212

43. George SM. Atomic Layer Deposition: An Overview. *Chem Rev*. 2010;110(1):111-131. doi:10.1021/cr900056b

44. Abi Younes P, Sayegh S, Nada AA, et al. Elaboration of porous alumina nanofibers by electrospinning and molecular layer deposition for organic pollutant removal. *Colloids Surf Physicochem Eng Asp*. 2021;628:127274. doi:10.1016/j.colsurfa.2021.127274

45. Najem M, Nada AA, Weber M, et al. Palladium/Carbon Nanofibers by Combining Atomic Layer Deposition and Electrospinning for Organic Pollutant Degradation. *Materials*. 2020;13(8). doi:10.3390/ma13081947

46. Kim WS, Lee BS, Kim DH, Kim HC, Yu WR, Hong SH. SnO2 nanotubes fabricated using electrospinning and atomic layer deposition and their gas sensing performance. *Nanotechnology*. 2010;21(24):245605.

47. Kim GM, Lee SM, Michler G, Roggendorf H, Gosele U, Knez M. Nanostructured pure anatase titania tubes replicated from electrospun polymer fiber templates by atomic layer deposition. *Chem Mater*. 2008;20(9):3085-3091.

48. Szilágyi IM, Nagy D. Review on one-dimensional nanostructures prepared by electrospinning and atomic layer deposition. *J Phys Conf Ser*. 2014;559:012010. doi:10.1088/1742-6596/559/1/012010

49. McClure CD, Oldham CJ, Walls HJ, Parsons GN. Large effect of titanium precursor on surface reactivity and mechanical strength of electrospun nanofibers coated with TiO2 by atomic layer deposition. *J Vac Sci Technol Vac Surf Films*. 2013;31(6):061506.

50. Su CY, Wang LC, Liu WS, Wang CC, Perng TP. Photocatalysis and Hydrogen Evolution of Al- and Zn-Doped TiO2 Nanotubes Fabricated by Atomic Layer Deposition. *ACS Appl Mater Interfaces*. 2018;10(39):33287-33295. doi:10.1021/acsami.8b12299

51. Lee SY, Park SJ. TiO2 photocatalyst for water treatment applications. *J Ind Eng Chem*. 2013;19(6):1761-1769.

52. Fang W, Xing M, Zhang J. Modifications on reduced titanium dioxide photocatalysts: A review. *J Photochem Photobiol C Photochem Rev*. 2017;32:21-39.

53. Fujishima A, Zhang X, Tryk DA. TiO2 photocatalysis and related surface phenomena. *Surf Sci Rep*. 2008;63(12):515-582. doi:10.1016/j.surfrep.2008.10.001

54. Khaki MRD, Shafeeyan MS, Raman AAA, Daud WMAW. Application of doped photocatalysts for organic pollutant degradation - A review. *J Environ Manage*. 2017;198:78-94. doi:10.1016/j.jenvman.2017.04.099

55. Mrowetz M, Balcerski W, Colussi A, Hoffmann MR. Oxidative power of nitrogen-doped TiO2 photocatalysts under visible illumination. *J Phys Chem B*. 2004;108(45):17269-17273.

56. Park JH, Kim S, Bard AJ. Novel carbon-doped TiO2 nanotube arrays with high aspect ratios for efficient solar water splitting. *Nano Lett*. 2006;6(1):24-28.

57. Tachikawa T, Tojo S, Kawai K, et al. Photocatalytic Oxidation Reactivity of Holes in the Sulfur- and Carbon-Doped TiO2 Powders Studied by Time-Resolved Diffuse Reflectance Spectroscopy. *J Phys Chem B*. 2004;108(50):19299-19306. doi:10.1021/jp0470593

58. Takeshita K, Yamakata A, Ishibashi T aki, Onishi H, Nishijima K, Ohno T. Transient IR absorption study of charge carriers photogenerated in sulfur-doped TiO2. *J Photochem Photobiol Chem*. 2006;177(2-3):269-275.

59. Ohno T, Akiyoshi M, Umebayashi T, Asai K, Mitsui T, Matsumura M. Preparation of S-doped TiO2 photocatalysts and their photocatalytic activities under visible light. *Appl Catal Gen*. 2004;265(1):115-121.

60. Liu R, Yang F, Xie Y, Yu Y. Visible-light responsive boron and nitrogen codoped anatase TiO2 with exposed {0 0 1} facet: Calculation and experiment. *Appl Surf Sci*. 2019;466:568-577.

61. Wang SQ, Liu WB, Fu P, Cheng WL. Enhanced photoactivity of N-doped TiO2 for Cr(VI) removal: Influencing factors and mechanism. *Korean J Chem Eng*. 2017;34(5):1584-1590. doi:10.1007/s11814-017-0003-7

62. Dong F, Wang H, Wu Z, Qiu J. Marked enhancement of photocatalytic activity and photochemical stability of N–doped TiO2 nanocrystals by Fe3+/Fe2+ surface modification. *J Colloid Interface Sci*. 2010;343(1):200-208. doi:10.1016/j.jcis.2009.11.012

63. Zhang Z, Wang X, Long J, Gu Q, Ding Z, Fu X. Nitrogen-doped titanium dioxide visible light photocatalyst: Spectroscopic identification of photoactive centers. *J Catal*. 2010;276(2):201-214. doi:10.1016/j.jcat.2010.07.033

64. Huang J, Dou L, Li J, Zhong J, Li M, Wang T. Excellent visible light responsive photocatalytic behavior of N-doped TiO2 toward decontamination of organic pollutants. *J Hazard Mater*. 2021;403:123857. doi:10.1016/j.jhazmat.2020.123857

65. Weber M, Lamboux C, Navarra B, et al. Boron nitride as a novel support for highly stable palladium nanocatalysts by atomic layer deposition. *Nanomaterials*. 2018;8(10):849.

66. Lin L, Lin L, Jiang W, Bechelany M, Nasr M, Jarvis J. Adsorption and photocatalytic oxidation of ibuprofen using nanocomposites of TiO2 nanofibers combined with BN nanosheets : Degradation products and mechanisms Chemosphere Adsorption and photocatalytic oxidation of ibuprofen using nanocomposites of TiO 2 n. *Chemosphere*. 2019;220(December 2018):921-929. doi:10.1016/j.chemosphere.2018.12.184

67. Konstantinou IK, Albanis TA. TiO2-assisted photocatalytic degradation of azo dyes in aqueous solution: kinetic and mechanistic investigations: A review. *Appl Catal B Environ*. 2004;49(1):1-14. doi:10.1016/j.apcatb.2003.11.010

68. Konstantinou IK, Albanis TA. Photocatalytic transformation of pesticides in aqueous titanium dioxide suspensions using artificial and solar light: intermediates and degradation pathways. *Appl Catal B Environ*. 2003;42(4):319-335. doi:10.1016/S0926-3373(02)00266-7

69. Xuan T, Le H, Nguyen T Van, et al. Chemosphere Correlation between degradation pathway and toxicity of acetaminophen and its by-products by using the electro-Fenton process in aqueous media. 2017;172:1-9. doi:10.1016/j.chemosphere.2016.12.060

70. Borbón-Nuñez HA, Dominguez D, Muñoz-Muñoz F, et al. Fabrication of hollow TiO2 nanotubes through atomic layer deposition and MWCNT templates. *Powder Technol*. 2017;308:249-257. doi:10.1016/j.powtec.2016.12.001

71. Lazar MA, Varghese S, Nair SS. Photocatalytic Water Treatment by Titanium Dioxide: Recent Updates. *Catalysts*. 2012;2(4). doi:10.3390/catal2040572

72. Wang CC, Kei CC, Perng TP. Fabrication of TiO2 nanotubes by atomic layer deposition and their photocatalytic and photoelectrochemical applications. *Nanotechnology*. 2011;22(36):365702.

73. López de Dicastillo C, Patiño C, Galotto MJ, Palma JL, Alburquenque D, Escrig J. Novel Antimicrobial Titanium Dioxide Nanotubes Obtained through a Combination of Atomic Layer Deposition and Electrospinning Technologies. *Nanomaterials*. 2018;8(2). doi:10.3390/nano8020128

74. Thamaphat K, Limsuwan P, Ngotawornchai B. Phase characterization of TiO2 powder by XRD and TEM. *Agric Nat Resour*. 2008;42(5):357-361.

75. Soo JZ, Lee KM, Ang BC, Ong BH. Optimal electrospun TiO2 nanofiber photocatalytic performance via synergistic morphology and particle crystallinity with anatase/rutile phase tuning. *Phys Status Solidi A*. 2019;216(16):1900066.

76. Sinha I, De AK. Chapter 1 - An overview of synthesis techniques for preparing doped photocatalysts. In: Singh P, Borthakur A, Mishra PK, Tiwary D, eds. *Nano-Materials as Photocatalysts for Degradation of Environmental Pollutants*. Elsevier; 2020:1-13. doi:10.1016/B978-0-12-818598-8.00001-8

77. Lu N, Quan X, Li J, Chen S, Yu H, Chen G. Fabrication of Boron-Doped TiO2 Nanotube Array Electrode and Investigation of Its Photoelectrochemical Capability. *J Phys Chem C*. 2007;111(32):11836-11842. doi:10.1021/jp071359d

78. Natarajan TS, Natarajan K, Bajaj HC, Tayade RJ. Enhanced photocatalytic activity of bismuth-doped TiO 2 nanotubes under direct sunlight irradiation for degradation of Rhodamine B dye. *J Nanoparticle Res*. 2013;15(5):1-18.

79. Gombac V, De Rogatis L, Gasparotto A, et al. TiO2 nanopowders doped with boron and nitrogen for photocatalytic applications. *Doping Funct Photoactive Semicond Met Oxides*. 2007;339(1):111-123. doi:10.1016/j.chemphys.2007.05.024

80. Doh SJ, Kim C, Lee SG, Lee SJ, Kim H. Development of photocatalytic TiO2 nanofibers by electrospinning and its application to degradation of dye pollutants. *J Hazard Mater*. 2008;154(1):118-127. doi:10.1016/j.jhazmat.2007.09.118

81. Yang Z, Shi Y, Wang B. Photocatalytic activity of magnetically anatase TiO2 with high crystallinity and stability for dyes degradation: Insights into the dual roles of SiO2 interlayer between TiO2 and CoFe2O4. *Appl Surf Sci*. 2017;399:192-199. doi:10.1016/j.apsusc.2016.12.078

82. Jin X, Yuan K, Xu C, et al. Water steam modified crystallization and microstructure of mesoporous TiO2 nanofibers. *Ceram Int*. 2018;44(2):2158-2164. doi:10.1016/j.ceramint.2017.10.168

83. Vaiano V, Sannino D, Sacco O. Heterogeneous photocatalysis: how doping with nitrogen can improve the performance of semiconductor nanoparticles under visible light irradiation. In: *Nanomaterials for the Detection and Removal of Wastewater Pollutants*. Elsevier; 2020:285-301.

84. Lai Y, Sun L, Chen Y, Zhuang H, Lin C, Chin JW. Effects of the Structure of TiO[sub 2] Nanotube Array on Ti Substrate on Its Photocatalytic Activity. *J Electrochem Soc*. 2006;153(7):D123. doi:10.1149/1.2203112

85. Sauthier G, György E, Figueras A, Sánchez RS, Hernando J. Laser Synthesis and Characterization of Nitrogen-Doped TiO2 Vertically Aligned Columnar Array Photocatalysts. *J Phys Chem C*. 2012;116(27):14534-14540. doi:10.1021/jp304324e

86. Calisir MD, Gungor M, Demir A, Kilic A, Khan MM. Nitrogen-doped TiO2 fibers for visible-light-induced photocatalytic activities. *Ceram Int*. 2020;46(10):16743-16753.

87. Sathishkumar P, Pugazhenthiran N, Mangalaraja RV, Guesh K, Contreras D, Anandan S. Contemporary Achievements of Visible Light-Driven Nanocatalysts for the Environmental Applications. In: *Photocatalytic Functional Materials for Environmental Remediation*. John Wiley & Sons, Ltd; 2019:69-129. doi:https://doi.org/10.1002/9781119529941.ch3

88. Di Valentin C, Finazzi E, Pacchioni G, et al. N-doped TiO2: Theory and experiment. *Doping Funct Photoactive Semicond Met Oxides*. 2007;339(1):44-56. doi:10.1016/j.chemphys.2007.07.020

89. Liu D, Zhang M, Xie W, Sun L, Chen Y, Lei W. Porous BN/TiO2 hybrid nanosheets as highly efficient visible-light-driven photocatalysts. *Appl Catal B Environ*. 2017;207:72-78. doi:10.1016/j.apcatb.2017.02.011

90. Tran VA, Truong TT, Phan TAP, et al. Application of nitrogen-doped TiO2 nano-tubes in dye-sensitized solar cells. *Appl Surf Sci*. 2017;399:515-522. doi:10.1016/j.apsusc.2016.12.125

91. Shu T, Xiang P, Zhou ZM, et al. Mesoscopic nitrogen-doped TiO2 spheres for quantum dot-sensitized solar cells. *Electrochimica Acta*. 2012;68:166-171. doi:10.1016/j.electacta.2012.02.068

92. Garlisi C, Lai CY, George L, Chiesa M, Palmisano G. Relating Photoelectrochemistry and Wettability of Sputtered Cu- and N-Doped TiO2 Thin Films via an Integrated Approach. *J Phys Chem C*. 2018;122(23):12369-12376. doi:10.1021/acs.jpcc.8b03650

93. Le TXH, Charmette C, Bechelany M, Cretin M. Facile preparation of porous carbon cathode to eliminate paracetamol in aqueous medium using electro-Fenton system. *Electrochimica Acta*. 2016;188:378-384.

94. Li H, Zhang W, Pan W. Enhanced Photocatalytic Activity of Electrospun TiO2 Nanofibers with Optimal Anatase/Rutile Ratio. *J Am Ceram Soc*. 2011;94(10):3184-3187. doi:10.1111/j.1551-2916.2011.04748.x

95. Wang B, Leung MKH, Lu XY, Chen SY. Synthesis and photocatalytic activity of boron and fluorine codoped TiO2 nanosheets with reactive facets. *Appl Energy*. 2013;112:1190-1197. doi:10.1016/j.apenergy.2013.03.084

96. Film N, HaiyingWang, Hu Y. The Photocatalytic Property of Nitrogen-Doped TiO 2. In: ; 2015.

97. Wang H, Hu Y. The Photocatalytic Property of Nitrogen-Doped TiO2 Nanoball Film. *Int J Photoenergy*. 2013;2013:1-6.

98. Li X, Liu P, Mao Y, Xing M, Zhang J. Preparation of homogeneous nitrogen-doped mesoporous TiO2 spheres with enhanced visible-light photocatalysis. *Appl Catal B Environ*. 2015;164:352-359. doi:10.1016/j.apcatb.2014.09.053

99. Bakar SA, Ribeiro C. Nitrogen-doped titanium dioxide: An overview of material design and dimensionality effect over modern applications. *J Photochem Photobiol C Photochem Rev*. 2016;27:1-29. doi:10.1016/j.jphotochemrev.2016.05.001

100. Choi WH, Lee CH, Kim H eun, Lee SU, Bang JH. Designing a high-performance nitrogen-doped titanium dioxide anode material for lithium-ion batteries by unravelling the nitrogen doping effect. *Nano Energy*. 2020;74:104829. doi:10.1016/j.nanoen.2020.104829

101. Noorisepehr M, Kakavandi B, Isari AA, et al. Sulfate radical-based oxidative degradation of acetaminophen over an efficient hybrid system: Peroxydisulfate decomposed by ferroferric oxide nanocatalyst anchored on activated carbon and UV light. *Sep Purif Technol*. 2020;250:116950. doi:10.1016/j.seppur.2020.116950

102. Dirany A, Sirés I, Oturan N, Özcan A, Oturan MA. Electrochemical treatment of the antibiotic sulfachloropyridazine: kinetics, reaction pathways, and toxicity evolution. *Environ Sci Technol*. 2012;46(7):4074-4082.

103. Le TXH, Nguyen TV, Yacouba ZA, et al. Correlation between degradation pathway and toxicity of acetaminophen and its by-products by using the electro-Fenton process in aqueous media. *Chemosphere*. 2017;172:1-9. doi:https://doi.org/10.1016/j.chemosphere.2016.12.060

104. Zhang J, Sun B, Xiong X, et al. Removal of emerging pollutants by Ru/TiO2-catalyzed permanganate oxidation. *Water Res*. 2014;63:262-270. doi:10.1016/j.watres.2014.06.028

105. Zhao B, Yu H, Liu Y, et al. Enhanced photoelectrocatalytic degradation of acetaminophen using a bifacial electrode of praseodymium-polyethylene glycol-PbO2//Ti//TiO2-nanotubes. *Chem Eng J*. 2021;410:128337. doi:10.1016/j.cej.2020.128337

106. Yang L, Yu LE, Ray MB. Photocatalytic Oxidation of Paracetamol: Dominant Reactants, Intermediates, and Reaction Mechanisms. *Environ Sci Technol*. 2009;43(2):460-465. doi:10.1021/es8020099

107. Sridhar S, Arunnellaiappan T, Rameshbabu N, Mika S, Viswanathan A. Solar photocatalytic activity of nitrogen doped TiO2 coating by micro-arc oxidation. *Surf Eng*. 2017;33(10):779-786. doi:10.1080/02670844.2016.1259090

108. Liu X, Liu Z, Zheng J, et al. Characteristics of N-doped TiO2 nanotube arrays by N2-plasma for visible light-driven photocatalysis. *J Alloys Compd*. 2011;509(41):9970-9976. doi:10.1016/j.jallcom.2011.08.003

8. Supporting information

Figure S3. 1 shows spots in red were incomplete tubular TiO_2 were formed proving that pulse time below 0.2 s was not sufficient to obtain good tubular structure.

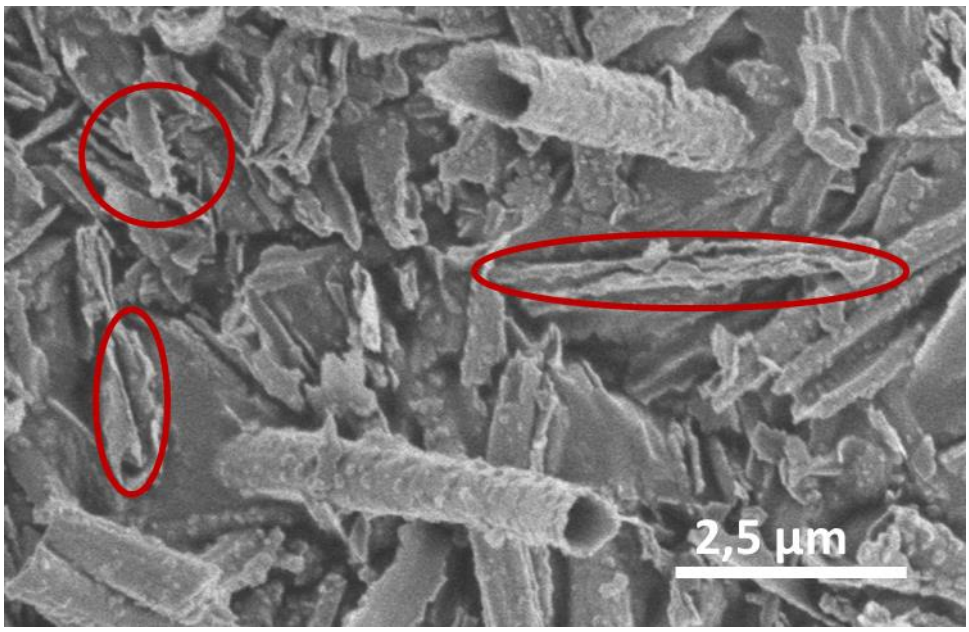

Figure S3. 1. SEM image of TiO_2-NTs-500 cycles using a pulse time of $TiCl_4$ of 0.1 s.

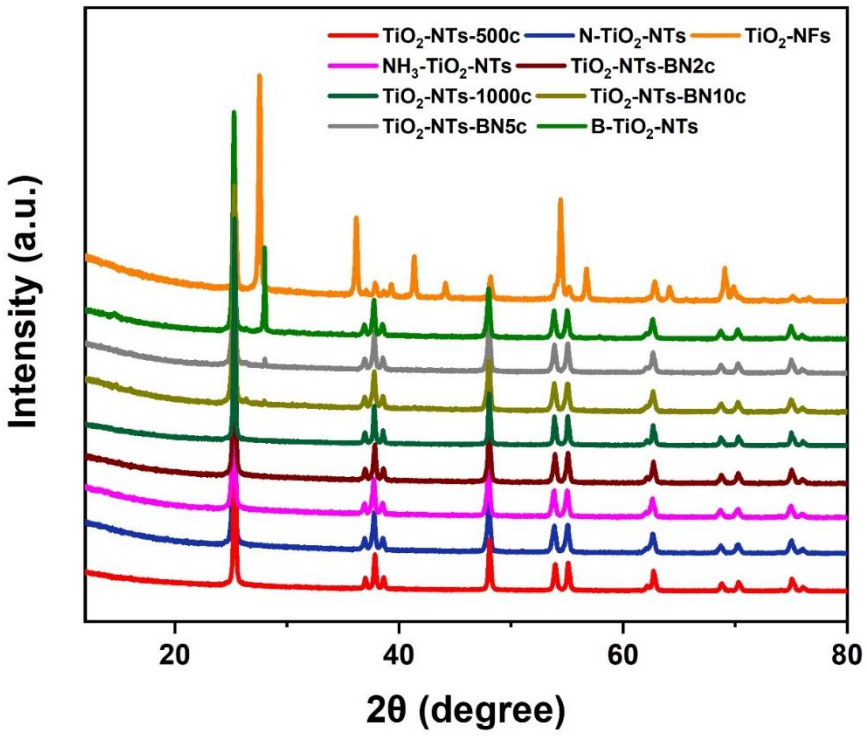

Figure S3. 2. X-ray diffraction spectrum of all prepared samples.

Table S3. 1: Binding energies of Ti, O, B and N element for undoped and nitrogen doped TiO_2 nanotubes.

Sample / Element	TiO_2-NTs BE (eV)	N-TiO_2-NTs BE (eV)	TiO_2-NTs-BN5c BE (eV)
Ti2p	458.4	458.7	458.5
O1s	529.5	529.6	529.7
B1s	-	-	192.3
N1s	-	399.9	398.2/401.6

Figure S3. 3 a, represents the band gap values of TiO_2 samples with 3.16, 3.18 and 3.22 for N-TiO_2-NTs, TiO_2-NTs and TiO_2-NTs-BN5, respectively. These values are in good agreement with the photocatalytic degradation efficiency of the photocatalyst, whereas the lowest band gap is more active under visible irradiation. Despite having the same anatase crystalline phase, it is evident that the morphology of the dopants had a certain extent of influence on the band gap values. Photoluminescence measurements were performed to investigate the effect of TiO_2 morphology and doping on the charge carrier generation. **Figure S3. 3 b** shows the excitation sharp peaks located at ~500 nm. An important decrease of the photoluminescence intensity of TiO_2 NTs compared to nanofibers can be clearly seen. Charge carrier transport in TiO2 nanotubes can be significantly different from comparable 1D systems, as bulk states present in anodic nanotube structures are found to strongly affect the trapping/detrapping transport of majority carrier transport. The PL intensity quenching could be attributed to the different structure of TiO_2, with anatase being the major phase in TiO_2 NTs while TiO_2 NFs has rutile as a major phase (75.5%). Furthermore, the photoluminescence intensity of N-TiO_2-NTs was lower than undoped nanotubes TiO_2, which is in good agreement with the literature[107]. Therefore, nitrogen doping enhanced the separation of the photo-generated electron–hole pairs of TiO_2 with the lowest PL intensity[108].

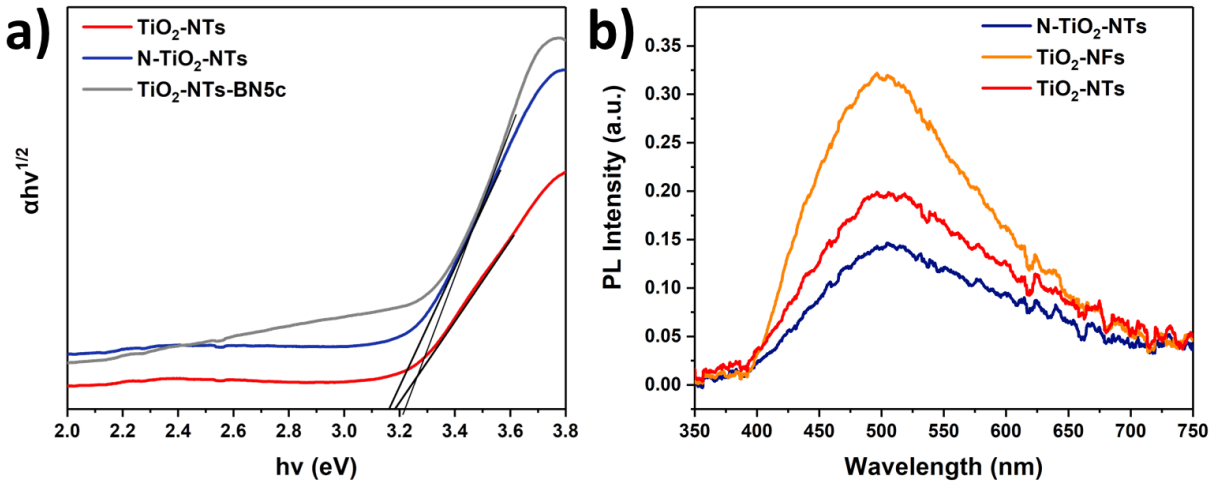

Figure S3. 3. a) band gap values of TiO_2-NTs and doped TiO_2-NTs and b) PL spectra of TiO_2-NFs, TiO_2-NTs and N-TiO_2-NTs.

Table S3. 2: Degradation percentage of ACT after 1h30min visible irradiation with all prepared catalysts

Sample	Degradation efficiency (%)
TiO_2-NTs-500c	95.7
TiO_2-NTs-800c	76.6
TiO_2-NTs-1000c	56.0
TiO_2-NFs	29.0
TiO_2-NTs-BN2c	33.8
TiO_2-NTs-BN5c	31.9
TiO_2-NTs-BN10c	0.4
N-TiO_2 NTs	98.3
NH_3-TiO_2-NTs	38.9
B-TiO_2 NTs	13.4

Chapter 4: Elaboration of photocatalytic membranes with TiO_2 coating by ALD and evaluation of photocatalytic membrane reactor performance for degradation of ACT

Table of content

1. Abstract

Among the advance oxidation processes photocalysis appear to be one of the most promising technology for organic micropollutant removal. However, catalyst used in suspension in water requires more energy and are time consuming to be removed and recycled. One other limitation is the partial penetration of light irradiation due to light absorption and scattering by the catalyst. To overcome these limitations, fixed photocatalysts reactors have been already developed, where the catalyst is fixed on nanofibers, nanotubes, nanosheets and membranes. Photocatalytic membrane reactors combine the membrane separation and advanced oxidation processes (AOPs). These type of reactors have been denoted as effective for water and wastewater treatments. Herein, Commercial α-Al_2O_3 membranes with a pore size of 200-nm were modified by Atomic layer Deposition (ALD) for photocatalytic purposes.TiO_2 is the material of choice for functionalization of ceramic membrane supports due to its high photocatalytic activity, low toxicity and high stability. Preliminary results shows that the permeability of the membrane decreased with the increase of TiO_2 ALD cycles. To understand the effect of this modification, further experiments are looked-for in the future. Design of new photocatalytic reactor is under process to report the photocatalytic efficiency of these modified membranes.

2. Highlights

- Commercial ceramic membrane α -Al_2O_3 was coated with TiO_2 using atomic layer deposition (ALD).
- Increase in the coating layer decreased the permeability of Al_2O_3 membranes.
- New design of photocatalytic membrane reactor is still in process for an efficient degradation step.

3. Introduction

Pharmaceuticals residues and many other pollutants have been detected in effluents of sewage treatment plants, surface, ground and drinking water in Europe and the US[1]. These findings confirm that conventional waste water treatment cannot face the increase of water pollution and remove all the poluttants[2–4]. In recent years, research has focused on produced water treatment by membranes. Many reviews on advancement in membrane technology were published during the last five years[5–8]. Membranes can be used in different fields and for several approaches according to their properties[9–11].

Membrane filtration is a chemical-less/free technology effective to remove particles, microorganisms and organic matter from drinking waters. Compared to conventional waste water treatment, this technique can provide higher water quality, minimize disinfectant demand, provide easier operational control and less maintenance, and finally generates less sludge[12]. We can distinct microfiltration (MO) membranes with pore diameters (dp) ranging from 0.05 to 5 mm, ultrafiltration (UF) with pore diameter comprise between 2nm <dp< 50nm, nanofiltration (NF) for pore diameter below 2 nm until 0.5 nm and finally reverse osmosis (RO) for membranes with dp less than 0.5 nm[13,14].

Current research on produced water treatment by membranes is mainly focused on improving existing processes and investigate the complex interactions at the produced water/membrane to achieve better efficient degradation.[15] Many limitations are confronted in membranes technology and the most important one is membrane fouling. Moreover, membrane processes are only separation step generating a product (purified water) and a concentrate. Regarding organic micropollutant issue, separation process alone is not appropriate as micropollutants will be discharged again in the environment[16,17].

One of the most innovative step is combining membrane process with advanced oxidation processes. Catalytic membranes as heterogeneous advanced oxidation microreactors are interesting for organic pollutants treatment[18,19]. Coupling of membrane separation technique with the photocatalytic process can result in a profit of the synergy of both technologies, which makes a powerful system. The membrane in this system will have a simultaneous task,

first supporting photocatalyst and second acting as a selective barrier for species to be degraded[20–23]. Yu *et al.* prepared a photocatalytic polysulfone based membrane with graphitic carbon nitride/titanium dioxide (mpg-C_3N_4/TiO_2) nanocomposite. The authors explored the photocatalytic activity of this membrane for degradation of sulfamethoxazole (pharmaceutical pollutant). The synthesized membrane showed a great potential of degradation of the pollutant into nontoxic products[24]. In another study, titanium dioxide (TiO_2) composite fiber membranes were tested in a photocatalytic membrane reactor (PMR) for the degradation of pollutants based on dead-end filtration process and photocatalytic degradation. The study was based on the flux values and the removal of the organic pollutant measurments[25].

Different membrane reactors and systems can be designed based on the membrane separation mode (dead end or cross flow or continuous flow**, Figure 4. 1**), membrane process (MF, UF, NF, etc.), membrane configuration (flat sheet, hollow fiber, spiral wound, and tubular) and light irradiation. Hence, the catalyst is still the most important parameter to be considered in these processes. Many modifications of catalysts during the last decades have been reported to enhance the band gap to the visible range. Therefore, the membrane material to support the catalyst influences the robustness of the technique[26,27]. Many requirements are settled on the support material in order to obtain a well-designed PM. The material should have a high chemical stability, high abrasion and be compatible with the catalyst. Photocatalytic membrane can be categorized into two classes based on the support materials: inorganic membrane and inorganic polymer hybrid membrane such as regenerated cellulose membrane, polyvinylidene fluoride (PVDF), polyethersulfone (PES), ceramic, fibers and many more[28–30].

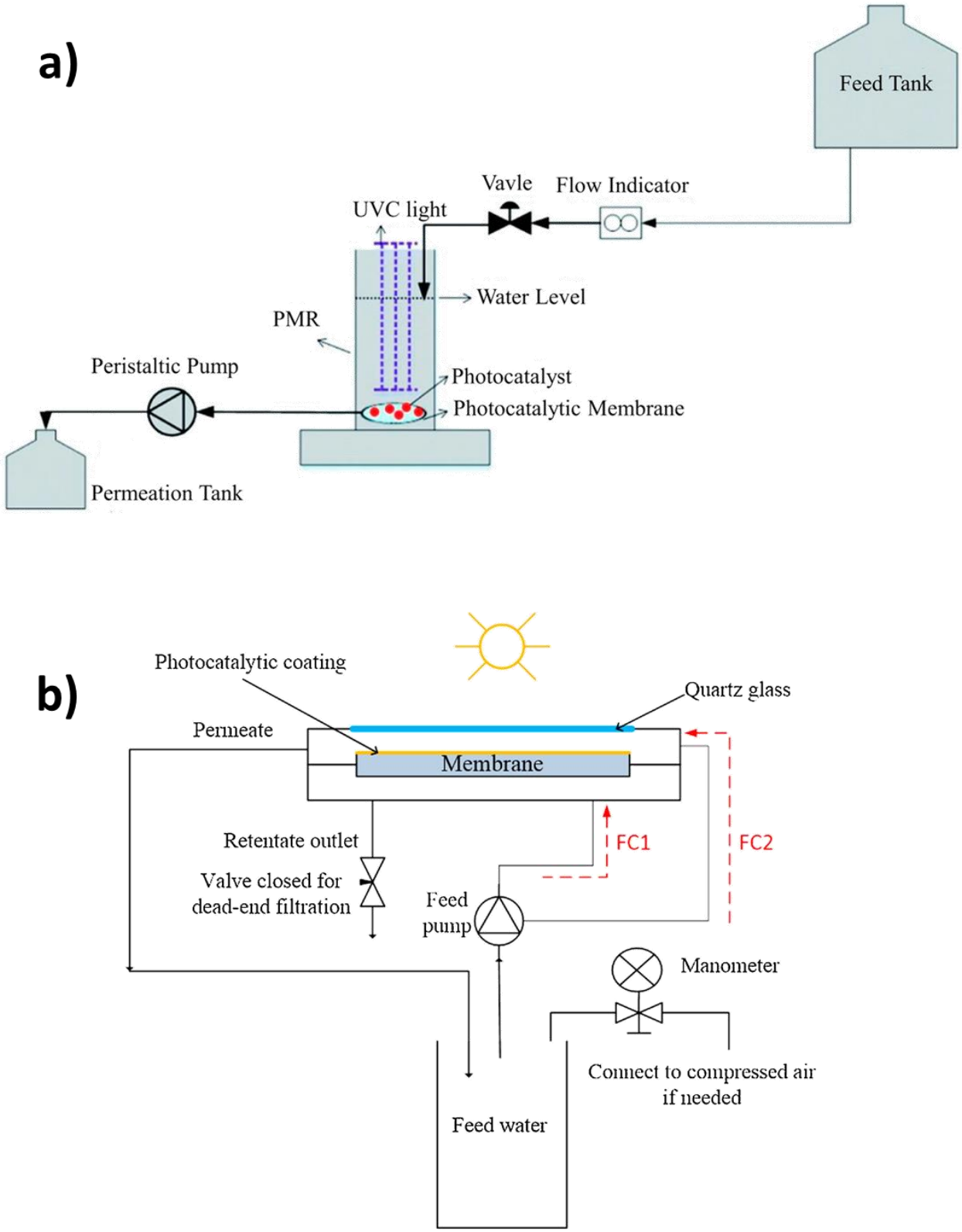

Figure 4. 1. Schematic diagram of a lab-scale PMR system with a) dead-end configuration and b) cross-flow configuration (figure reported from article as it is)[31].

The choice of membrane support is based on the pollutant size, the water matrix and the oxidant reaction. Polymeric membranes could have some limitations regarding thermal, chemical and photo resistance for AOPs mechanism in wastewater. Ceramic membranes are considered as competitive candidates due to their intrinsic hydrophilicity and excellent chemical, mechanical and thermal stability. Herein, we will discuss the advantageous of using ceramic membranes in water treatment for removal of polluttant[32,33]. Owing to their advantages, ceramic membranes are being increasingly applied in wastewater treatment, chemical, beverage and pharmaceutical industry[34,35]. Several parameter could affect the catalytic efficiency of the membrane as per structure design and surface functionalization. Tuning the pore diameter and hydrophobicity of the membrane by applying an active layer on the surface allow their immersion in high-efficiency filtration, retard fouling and increase its service-life[36–38]. Functionalization of the membrane could be done by many approaches already developed by coating in active layer by using one of these techniques sol-gel, anodization, electrospinning, etc.[39,40]. Ren *et al.* converted the surface of alumina membrane from hydrophilic to hydrophobic by grafting with a fluoroalkylsilane. The performance of the membrane on water desalination was reported to be very promising with a salt rejection over 99.5% [34]. Functionalization of ceramic membrane by TiO_2 was found effective to reduce the fouling due to the increase of hydrophilicity, surface area and the decrease of the mass transfer resistance[41].

However, the conventional coating methods such as impregnation, sol gel and anodizing have some drawbacks. Consequently, deactivation of photocatalyst may happen due to the limited mass transfer and hindrance of active surface area for adsorption and catalyst reactions. Another major drawback in ceramic membranes are the higher fabrication cost than polymeric membranes. Although ceramic membrane presents high mechanical strength and chemical resistance, decline in flux or permeation rate is believed to be the major limitation for industrial applications[42,43]. Modification of the membrane, improves its photocatalytic performance in water and wastewater with a longer life span and less maintenance requirement[36,44]. The synthesis of TiO_2 nanoparticles on the surface of hydrophilic membrane improved its anti-fouling properties and demonstrated a highly active capability for photocatalytic oxidation of pharmaceuticals[45]. In another study, TiO_2 catalyst was coated on

the surface of a porous ceramic tube for degradation of model pollutant Acid Red 4 dye. Effect of physical parameters on the degradation efficiency were stated. It was found that dead-end system presents higher degradation rates that cross-flow system. Moreover, increase in catalyst loading improved the degradation efficiency whereas increase in the flow rate limited the decomposition of the dye[46]. However, in most studies, deterioration of the membrane structure, low photocatalytic activity and loss of TiO_2 layer was reported. To prevent these problems, deposition technique with high control of the deposited layer are necessary[47]. Among all the existing techniques (sol–gel, coprecipitation, hydrolysis, anodization and electrospinning), atomic layer deposition is a promising way to functionalize ceramic membrane with high control.

From few years, the application of ALD was extended to membrane preparation and surface modification for water treatment due to its excellent controllable coating performance[48]. This technique is based on separated gas pulses, self-limiting and saturated reaction for growth of few nanometer layers with the highest precision and homogeneity on membrane surface. Since the membrane performance is highly dependent on the physical and chemical properties (pore structure, thickness, roughness, hydrophilicity, surface charge), high controllable coating is a must to tune the membrane properties. ALD offers the possibility of deposition of different materials even on 3D structure supports (tubular membranes)[49] and high-aspect-ratio structures, such as membrane pores[50]. Many researches have been investigated the coating of membranes with TiO_2 using ALD[51,52]. Hence, comparison between these systems is not easy, since many parameter are being changed. Chen *et al.* reported the efficiency of ALD for coating tubular membranes over sol-gel method. The authors coated the membrane with titanium alkoxide (titanicone) by ALD. Than calcination step was added to degrade the polymeric layer and allow the formation of microporous membrane. Changing ALD cycle numbers, decreased the pore diameter of the membrane and allow the formation of nanofiltration membrane and the variation of permeability[53].

In this work, Atomic Layer Deposition was opted for coating commercial ceramic membrane α-Al_2O_3. Variation of ALD number of cycle was investigated on two types of membranes with pore diameter of 200nm. The effect of TiO_2 ALD cycles on membrane

permeability was achieved. A custom-built photocatalytic membrane reactor was tested on the modified membranes. Two membrane modules were compared and more work is still needed, since both module shows low reproducibility and repeatability.

4. Materials and methods

4.1. Materials and chemicals

Titanium (IV) chloride (TiCl4, 99.9%, CAS: 7550-45-0)) and ethanol (≥99.8% CAS: 64-17-5) were purchased from Sigma-Aldrich. Deionized (DI) water (>18.2 MΩ) prepared by Millipore (Milli-Q® Academic) water purification system was used for all reagent preparation and in distillation process. Argon gas was bought from linde and used as received. Commercial microfiltration ceramic membrane were bought from Fraunhofer, Germany. Silicium of p type Si(100) wafers were used as substrates for film deposition and thickness study by SEM and ellipsometry. Prior to use a step of cleaning with pure ethanol and water was performed.

4.2. Fabrication of TiO_2/Al_2O_3 membrane by ALD

Deposition of TiO_2 was carried out in a home-built ALD, on commercial ceramic membrane α-Al_2O_3 (d = 27 mm, dp = 200 nm, thickness 1 mm) purchased from Fraunhofer. $TiCl_4$ and H_2O were used as precursors and co-reactants and the substrate temperature was maintained at 100 °C. Typical ALD cycle consisted of pulse of $TiCl_4$ and H_2O for 0.2 s and 2 s, respectively. The exposure time and purge time were set at 30 and 60s, respectively, for both precursors. The lines were heated at 80 °C to avoid any precursor condensation and the growth-per-cycle (GPC) of TiO_2 was approximately 2 Å per cycle. The number of ALD cycles was varied depending on the initial pore diameter of the membrane.

Deposition of aluminum oxide Al_2O_3 on the membrane substrate before TiO_2 coating layer was also realized. It was reported in the literature that this layer allow the formation of more active sites for a homogeneous deposition. A typical ALD cycle consisted of a pulse of trimethylaluminum (TMA) for 0.4 s followed by an exposure for 30 s and a purge with Argon gas for 40s. H_2O half cycle was presented by 0.2-30-40 s of pulse, exposure and purge correspondingly. The deposition temperature was maintained at 100°C and 5 cycles were repeated to get a 1 nm Al_2O_3 layer.

4.3. Morphology characterizations

4.3.1. Scanning Electron Microscopy and spectroscopic ellipsometry

The TiO_2 growth rate per ALD cycle was characterized by ellipsometry using an optical model based on Cauchy fitting (Semilab spectroscopic ellipsometer GES5E, Xe lamp 1.23eV-5eV). The results were confirmed via scanning electron microscopy (SEM Hitachi S4800, JAPAN) on Si-500 TiO_2 cycles that was ALD-coated in the same time as ceramic membranes. SEM images of coated ceramic membrane were not reported here. The coating layer of TiO_2 on membranes will be reported later by SEM analysis.

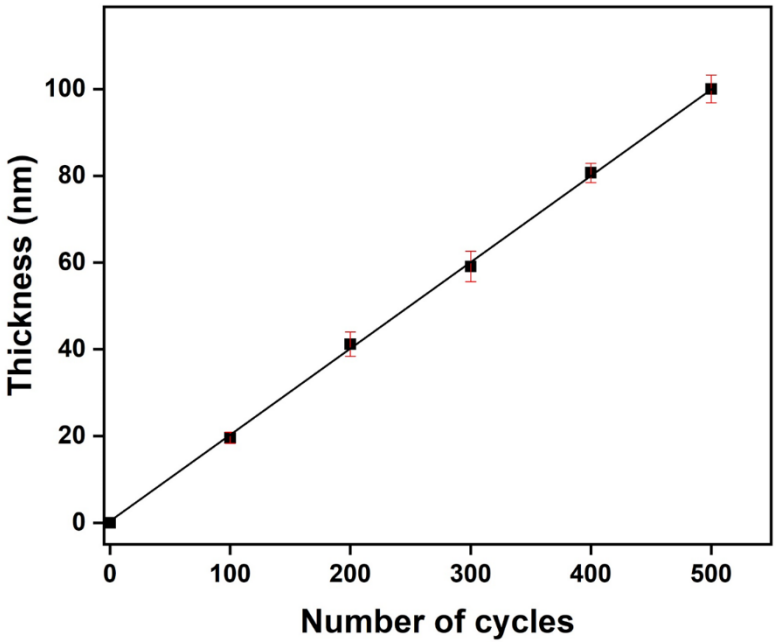

Figure 4. 2. Thickness of TiO_2 films as function of ALD cycles on Si substrate.

The deposition rate of TiO_2 by ALD was also calculated by SEM images after deposition of 500 cycles on Si substrate in **Figure 4. 3.** The coated layer after 500 cycles was almost 101.6 nm, which corresponds to ~ 0.2 nm/cycle and confirm the results obtained by ellipsometry.

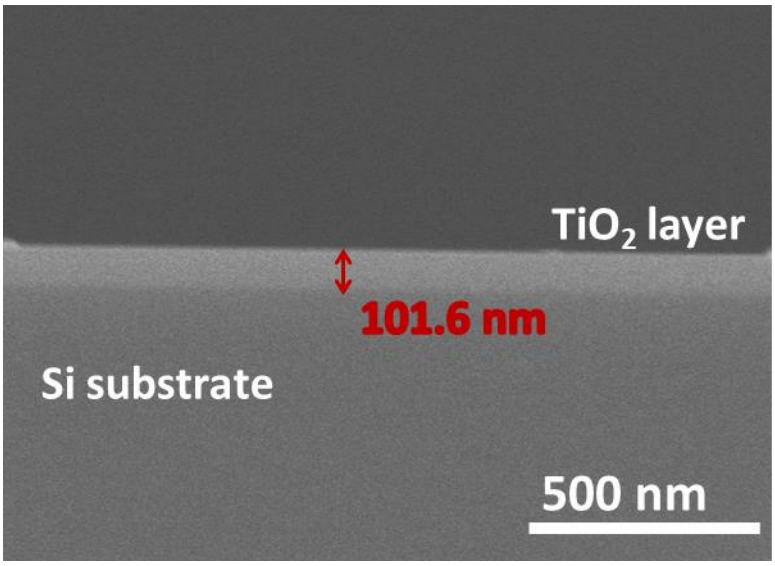

Figure 4. 3. Scanning electron microscopy of Si substrate coated with 500 cycles of TiO_2.

4.3.2. X-Ray Diffraction

X-ray diffraction analysis were performed on pristine membrane and 500c TiO_2 coated membrane. We chose the highest number of ALD cycle to be able to detect the coated layer otherwise the layer is too thin to be depicted. **Figure 4. 4** shows that no characteristic peak of TiO_2 crystalline phase were depicted. Two hypothesis could be proposed, even the deposited TiO_2 layer is amorphous as confirmed in literature[50] or the layer is too thin to be detected by XRD.

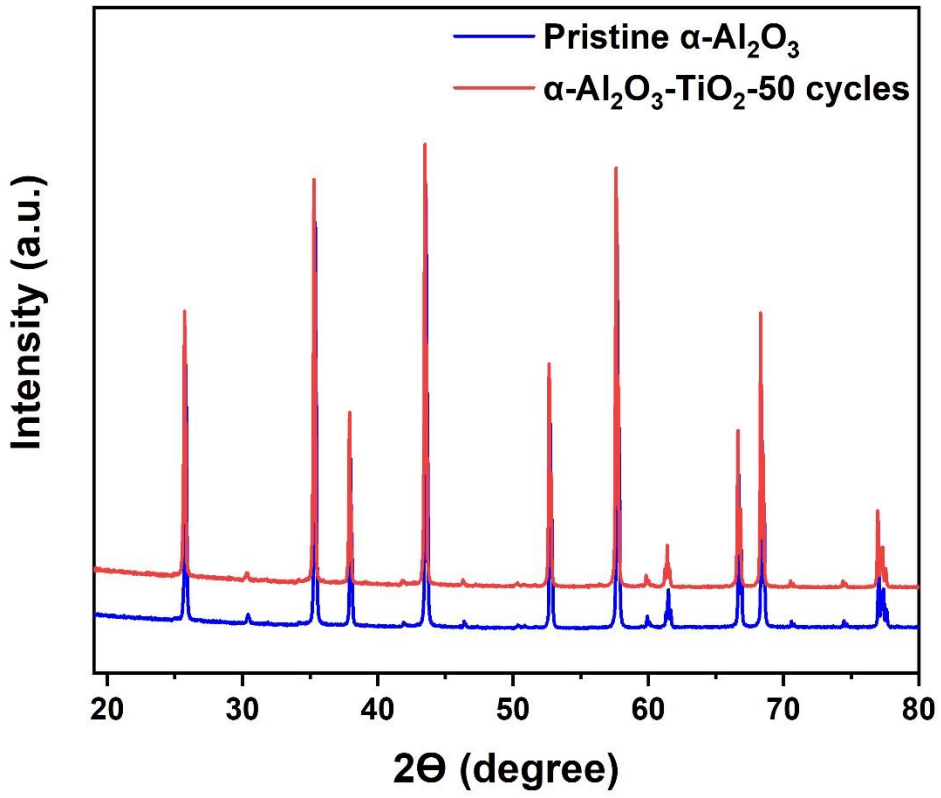

Figure 4. 4. X-ray diffraction of pristine and TiO_2 coated ceramic membrane.

4.3.3. Contact angle measurements

Since the membrane surface was hydrophilic, values were presented as time dependence of water contact angle (CA) changes on membrane surfaces. Contact angle of ceramic membrane with 50 cycles TiO_2 layer has shown inhomogeneity in the absorption time of the water droplet. This could be due to the non-uniform coated layer of TiO_2 by ALD. Owing to this problem, ceramic membrane was coated with a thin layer of Al_2O_3 (1 nm) before TiO_2 coating to increase the active sites for a uniform deposited layer. All used membranes in following steps were coated with 1 nm Al_2O_3 prior to TiO_2 coating. Coated membranes with TiO_2 shows an increase in hydrophilicity represented by the lower absorption time (in less than 3s) of the water droplet compared to pristine membrane. The decrease in adsorption time suggested that hydrophilicity and/or smoothness of the membrane was improved by the

coated TiO_2 layer. The contact angle of the composite membrane decreased due to the presence of –OH functional groups of TiO_2.

4.4. Permeability measurements

Water permeability of the ceramic membranes (pristine and coated) used in this study were estimated by measuring water flux (filtration of pure water Eq. 1) at different transmembrane pressures according to Darcy's law (Eq. 2). Permeability measurement of all membranes tested are compared in **Figure 4.** 5**.** Water permeability of bare α-Al_2O_3 membrane was given around 5000L.m^{-2}.$h^{-1}$$bar^{-1}$ which is in agreement with the membrane cut-off . However, after coating with TiO_2 layer onto ceramic substrate, water permeability decreased with the increase of ALD cycles. This is due to the resistance provided by the active layer formed on the membrane against water flow. The uniform TiO_2 coating on Al_2O_3 substrate reduce porosity of the pristine membrane and thus increase significantly the resistance of water flow [44]. When the coated layer of TiO_2 increase (500 cycles), the membranes pores were blocked and the permeability decreased brutally. In addition, the values of the contact angle measured also indicate that the surface of TiO_2/Al_2O_3 membrane is more hydrophilic than the uncoated membrane. Higher membrane hydrophilicity can improve water permeability but also decrease membrane fouling propensity. The TiO_2 layer thickness will determine the membrane permeability by refining its porosity and hydrophilicity.

The membrane flux (L.m^{-2}.h^{-1}) was calculated using equation 1:

$$J_w = \frac{V}{A \times t} \quad (1)$$

Where V is the permeate in L, A is the active surface area of the membrane in m^2 and t is the time of the measurement.

$$J_w = Lp_0 \times \Delta P \quad (2)$$

Where Lp_0 is the permeability of the membrane L.m^{-2}.h^{-1}.bar^{-1} toward solvents and ΔP is the transmembrane pressure in bar.

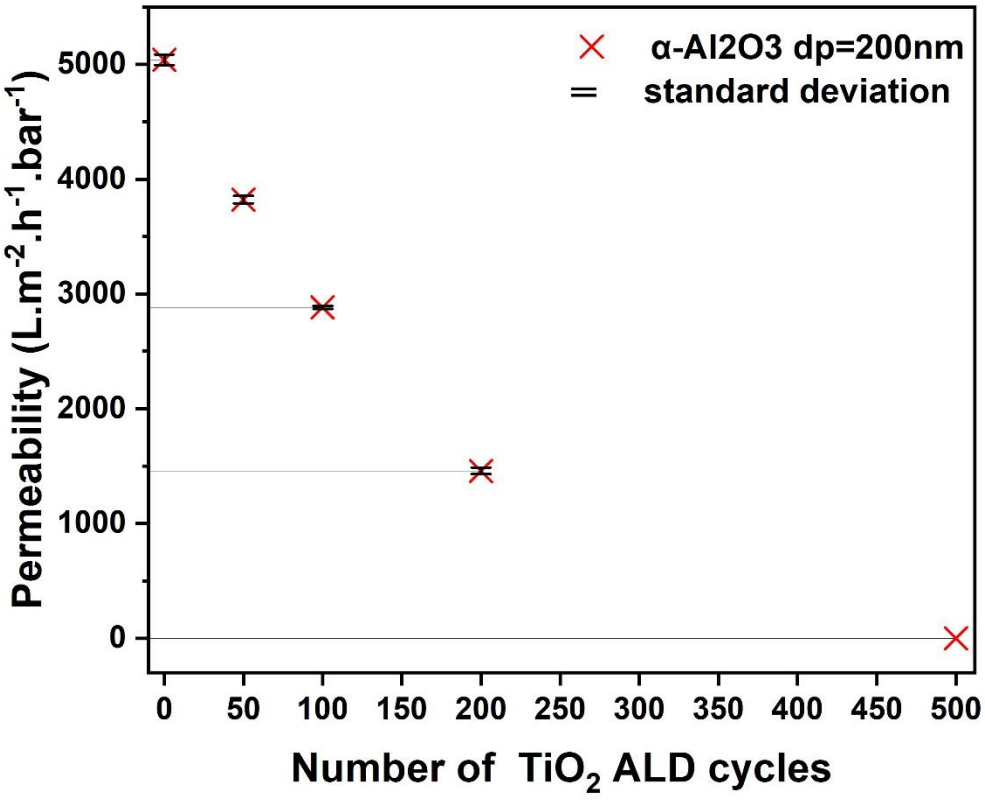

Figure 4. 5. Permeability results versus TiO_2 ALD number of cycles.

4.5. Photocatalytic membrane reactor performance (PMR)

Unfortunately, the preliminary test conducted with the PMR did not lead to logic results and permeability was lower than expected. Moreover, fouling behavior was observed by using the TiO_2 coated membrane in the photocatalytic membrane reactor (PMR) even with clean water. The permeability of the membrane decreased after three consecutive tests with α-Al_2O_3-TiO_2-50c (**Figure 4. 7**) and the membrane surface turned to a yellowish color (**Figure 4. 6**). This problem was not detected when using close module membrane in permeability tests. This could be attributed to a contamination from the connections or the rubber O rings used in the new cellule module. A step of cleaning the rings and test their stability will be implemented in the future before their use in the membrane module.

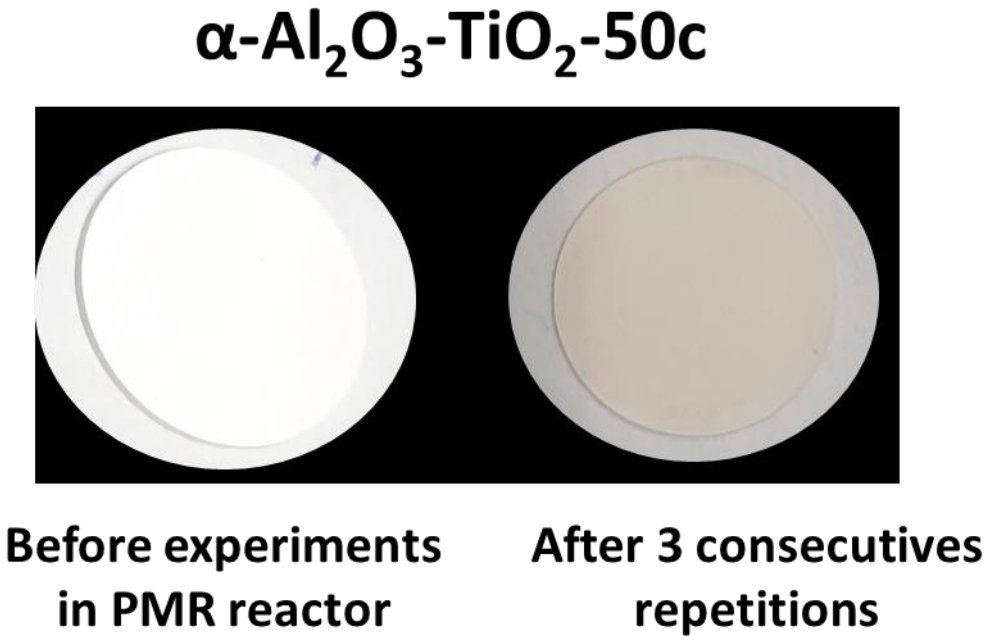

Figure 4. 6. Photograph of pristine and coated ceramic membrane before the experiments in PMR and after three consecutive tests.

The membrane flux ($L.m^{-2}.h^{-1}$) was calculated using equation 2 and the values of membrane permeability were represented in **Figure 4. 7**.

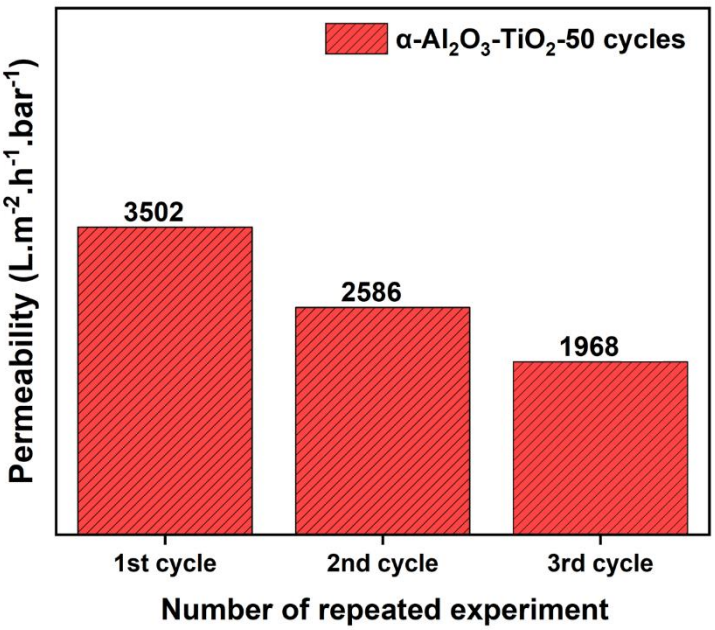

Figure 4. 7. Permeability of α-Al_2O_3-TiO_2-50cycles after three experiments using the PM reactor with the second membrane module.

5. Conclusion and Perspectives

Coating ceramic membrane by ALD was found to be an effective coating technique for the reduction of pore sizes and by that reduce the permeability of the membranes. Before coating with TiO_2, a thin layer of Al_2O_3 (1 nm) was deposit by ALD to increase the active sites yet to enhance the coating process. When coating α-Al_2O_3 with 1 nm Al_2O_3 and 10 nm TiO_2, the hydrophilicity of the membrane was decreased and more homogeneous deposition was found. The permeability was decreased with the increase of TiO_2 ALD cycles. ALD is an effective technique for modification of not only the membrane surface but also the pores. Hence, the photocatalytic reactor that was created at IEM still need more modification to meet the requirements.

The following points are still need to be executed to achieve this study:

- New membrane module should be elaborated taking into account the dynamic flow and the active surface area.
- Studied comparing TiO_2-Al_2O_3 membrane with and without thermal treatment should be conducted.
- Many parameters should be taken into account when opting for ceramic membrane support.
- These membranes could not be used with high pressure systems because of their brittle nature.
- Fouling aspect of the membrane should also be considered.

References

1. Doll TE, Frimmel FH. Cross-flow microfiltration with periodical back-washing for photocatalytic degradation of pharmaceutical and diagnostic residues–evaluation of the long-term stability of the photocatalytic activity of TiO_2. *Water Res*. 2005;39(5):847-854. doi:10.1016/j.watres.2004.11.029

2. Li N, Lu X, He M, et al. Catalytic membrane-based oxidation-filtration systems for organic wastewater purification: A review. *J Hazard Mater*. Published online 2021:125478.

3. Nam S-W, Jo B-I, Yoon Y, Zoh K-D. Occurrence and removal of selected micropollutants in a water treatment plant. *Chemosphere*. 2014;95:156-165. doi:10.1016/j.chemosphere.2013.08.055

4. Kim M-K, Zoh K-D. Occurrence and removals of micropollutants in water environment. *Environ Eng Res*. 2016;21(4):319-332.

5. Sundar KP, Kanmani S. Progression of Photocatalytic reactors and it's comparison: A Review. *Chem Eng Res Des*. 2020;154:135-150.

6. Molinari R, Argurio P, Szymański K, Darowna D, Mozia S. Photocatalytic membrane reactors for wastewater treatment. *Curr Trends Future Dev Bio- Membr*. Published online 2020:83-116.

7. Molinari R, Lavorato C, Argurio P. Recent progress of photocatalytic membrane reactors in water treatment and in synthesis of organic compounds. A review. *Catal Today*. 2017;281:144-164.

8. Nasrollahi N, Ghalamchi L, Vatanpour V, Khataee A. Photocatalytic-membrane technology: a critical review for membrane fouling mitigation. *J Ind Eng Chem*. Published online 2020.

9. Munirasu S, Haija MA, Banat F. Use of membrane technology for oil field and refinery produced water treatment—A review. *Process Saf Environ Prot*. 2016;100:183-202. doi:10.1016/j.psep.2016.01.010

10. Curcio E, Profio GD, Fontananova E, Drioli E. 13 - Membrane technologies for seawater desalination and brackish water treatment. In: Basile A, Cassano A, Rastogi NK, eds. *Advances in Membrane Technologies for Water Treatment*. Woodhead Publishing; 2015:411-441. doi:10.1016/B978-1-78242-121-4.00013-7

11. Bodzek M. 15 - Membrane technologies for the removal of micropollutants in water treatment. In: Basile A, Cassano A, Rastogi NK, eds. *Advances in Membrane Technologies for Water Treatment*. Woodhead Publishing; 2015:465-517. doi:10.1016/B978-1-78242-121-4.00015-0

12. Karnik BS, Davies SHR, Chen KC, Jaglowski DR, Baumann MJ, Masten SJ. Effects of ozonation on the permeate flux of nanocrystalline ceramic membranes. *Water Res*. 2005;39(4):728-734. doi:10.1016/j.watres.2004.11.017

13. Jaffrin M. Membrane Filtration process. Published online 2015.

14. Teodosiu C, Gilca A-F, Barjoveanu G, Fiore S. Emerging pollutants removal through advanced drinking water treatment: A review on processes and environmental performances assessment. *J Clean Prod*. 2018;197:1210-1221. doi:10.1016/j.jclepro.2018.06.247

15. Dickhout JM, Moreno J, Biesheuvel PM, Boels L, Lammertink RGH, de Vos WM. Produced water treatment by membranes: A review from a colloidal perspective. *J Colloid Interface Sci*. 2017;487:523-534. doi:10.1016/j.jcis.2016.10.013

16. Hashino M, Hirami K, Katagiri T, et al. Effects of three natural organic matter types on cellulose acetate butyrate microfiltration membrane fouling. *J Membr Sci*. 2011;379(1):233-238. doi:10.1016/j.memsci.2011.05.068

17. Ang WS, Tiraferri A, Chen KL, Elimelech M. Fouling and cleaning of RO membranes fouled by mixtures of organic foulants simulating wastewater effluent. *J Membr Sci*. 2011;376(1):196-206. doi:10.1016/j.memsci.2011.04.020

18. Lin H, Fang Q, Wang W, et al. Prussian blue/PVDF catalytic membrane with exceptional and stable Fenton oxidation performance for organic pollutants removal. *Appl Catal B Environ*. 2020;273:119047. doi:10.1016/j.apcatb.2020.119047

19. Lee WJ, Bao Y, Guan C, Hu X, Lim T-T. Ce/TiOx-functionalized catalytic ceramic membrane for hybrid catalytic ozonation-membrane filtration process: Fabrication, characterization and performance evaluation. *Chem Eng J*. 2021;410:128307. doi:10.1016/j.cej.2020.128307

20. Mahdavi HR, Arzani M, Mohammadi T. Synthesis, characterization and performance evaluation of an optimized ceramic membrane with physical separation and photocatalytic degradation capabilities. *Ceram Int*. 2018;44(9):10281-10292. doi:10.1016/j.ceramint.2018.03.035

21. Wu H, Xu X, Shi L, et al. Manganese oxide integrated catalytic ceramic membrane for degradation of organic pollutants using sulfate radicals. *Water Res*. 2019;167:115110. doi:10.1016/j.watres.2019.115110

22. Mandal MK, Sharma M, Pandey S, Dubey KK. Membrane technologies for the treatment of pharmaceutical industry wastewater. In: *Water and Wastewater Treatment Technologies*. Springer; 2019:103-116.

23. Azrague K, Aimar P, Benoit-Marquie F, Maurette M. A new combination of a membrane and a photocatalytic reactor for the depollution of turbid water. *Appl Catal B Environ*. 2007;72(3-4):197-204.

24. Yu S, Wang Y, Sun F, Wang R, Zhou Y. Novel mpg-C3N4/TiO_2 nanocomposite photocatalytic membrane reactor for sulfamethoxazole photodegradation. *Chem Eng J*. 2018;337:183-192. doi:10.1016/j.cej.2017.12.093

25. Hatat-Fraile M, Liang R, Arlos MJ, et al. Concurrent photocatalytic and filtration processes using doped TiO_2 coated quartz fiber membranes in a photocatalytic membrane reactor. *Chem Eng J*. 2017;330:531-540. doi:10.1016/j.cej.2017.07.141

26. Sacco O, Vaiano V, Sannino D. Main parameters influencing the design of photocatalytic reactors for wastewater treatment: a mini review. *J Chem Technol Biotechnol*. 2020;95(10):2608-2618.

27. Kumari P, Bahadur N, Dumée LF. Photo-catalytic membrane reactors for the remediation of persistent organic pollutants–A review. *Sep Purif Technol*. 2020;230:115878.

28. Rosman N, Salleh WNW, Mohamed MA, Jaafar J, Ismail AF, Harun Z. Hybrid membrane filtration-advanced oxidation processes for removal of pharmaceutical residue. *J Colloid Interface Sci*. 2018;532:236-260. doi:10.1016/j.jcis.2018.07.118

29. Bakr AR, Rahaman MdS. Crossflow electrochemical filtration for elimination of ibuprofen and bisphenol a from pure and competing electrolytic solution conditions. *J Hazard Mater*. 2019;365:615-621. doi:10.1016/j.jhazmat.2018.11.015

30. Tijing LD, Yao M, Ren J, Park C-H, Kim CS, Shon HK. Nanofibers for water and wastewater treatment: Recent advances and developments. *Water Wastewater Treat Technol*. Published online 2019:431-468.

31. Zheng X, Shen Z-P, Shi L, Cheng R, Yuan D-H. Photocatalytic Membrane Reactors (PMRs) in Water Treatment: Configurations and Influencing Factors. *Catalysts*. 2017;7(8). doi:10.3390/catal7080224

32. Koe WS, Lee JW, Chong WC, Pang YL, Sim LC. An overview of photocatalytic degradation: photocatalysts, mechanisms, and development of photocatalytic membrane. *Environ Sci Pollut Res*. 2020;27(3):2522-2565. doi:10.1007/s11356-019-07193-5

33. Asif MB, Zhang Z. Ceramic membrane technology for water and wastewater treatment: a critical review of performance, full-scale applications, membrane fouling and prospects. *Chem Eng J*. Published online 2021:129481.

34. Ren C, Fang H, Gu J, Winnubst L, Chen C. Preparation and characterization of hydrophobic alumina planar membranes for water desalination. *J Eur Ceram Soc*. 2015;35(2):723-730.

35. Cassano A, Rastogi NK, Basile A. 18 - Membrane technologies for water treatment and reuse in the food and beverage industries. In: Basile A, Cassano A, Rastogi NK, eds.

Advances in Membrane Technologies for Water Treatment. Woodhead Publishing; 2015:551-580. doi:10.1016/B978-1-78242-121-4.00018-6

36. Gu Q, Ng TCA, Bao Y, Ng HY, Tan SC, Wang J. Developing better ceramic membranes for water and wastewater Treatment: Where microstructure integrates with chemistry and functionalities. *Chem Eng J*. 2022;428:130456. doi:10.1016/j.cej.2021.130456

37. Moustakas NG, Katsaros FK, Kontos AG, Romanos GEm, Dionysiou DD, Falaras P. Visible light active TiO_2 photocatalytic filtration membranes with improved permeability and low energy consumption. *Photocatalytic Process Environ Remediat Honor Prof Jincai Zhao Chin Acad Sci*. 2014;224:56-69. doi:10.1016/j.cattod.2013.10.063

38. Horovitz I, Avisar D, Baker MA, et al. Carbamazepine degradation using a N-doped TiO_2 coated photocatalytic membrane reactor: Influence of physical parameters. *J Hazard Mater*. 2016;310:98-107. doi:10.1016/j.jhazmat.2016.02.008

39. Radeva J, Roth AG, Göbbert C, et al. Hybrid Ceramic Membranes for the Removal of Pharmaceuticals from Aqueous Solutions. *Membranes*. 2021;11(4):280.

40. Mendret J, Hatat-Fraile M, Rivallin M, Brosillon S. Hydrophilic composite membranes for simultaneous separation and photocatalytic degradation of organic pollutants. *Sep Purif Technol*. 2013;111:9-19. doi:10.1016/j.seppur.2013.03.030

41. Sarasidis VC, Plakas KV, Patsios SI, Karabelas AJ. Investigation of diclofenac degradation in a continuous photo-catalytic membrane reactor. Influence of operating parameters. *Chem Eng J*. 2014;239:299-311.

42. Sondhi R, Lin YS, Alvarez F. Crossflow filtration of chromium hydroxide suspension by ceramic membranes: fouling and its minimization by backpulsing. *J Membr Sci*. 2000;174(1):111-122. doi:10.1016/S0376-7388(00)00384-7

43. Yang T, Xiong H, Liu F, Yang Q, Xu B, Zhan C. Effect of UV/TiO_2 pretreatment on fouling alleviation and mechanisms of fouling development in a cross-flow filtration process using a ceramic UF membrane. *Chem Eng J*. 2019;358:1583-1593. doi:10.1016/j.cej.2018.10.149

44. Ahmad R, Lee CS, Kim JH, Kim J. Partially coated TiO_2 on Al_2O_3 membrane for high water flux and photodegradation by novel filtration strategy in photocatalytic membrane reactors. *Chem Eng Res Des*. 2020;163:138-148. doi:10.1016/j.cherd.2020.08.027

45. Rodriguez-Narvaez OM, Peralta-Hernandez JM, Goonetilleke A, Bandala ER. Treatment technologies for emerging contaminants in water: A review. *Chem Eng J*. 2017;323:361-380.

46. Wang W-Y, Irawan A, Ku Y. Photocatalytic degradation of Acid Red 4 using a titanium dioxide membrane supported on a porous ceramic tube. *Water Res*. 2008;42(19):4725-4732. doi:10.1016/j.watres.2008.08.021

47. Chong MN, Jin B, Chow CWK, Saint C. Recent developments in photocatalytic water treatment technology: A review. *Water Res*. 2010;44(10):2997-3027. doi:10.1016/j.watres.2010.02.039

48. Weber M, Julbe A, Ayral A, Miele P, Bechelany M. Atomic Layer Deposition for Membranes: Basics, Challenges, and Opportunities. *Chem Mater*. 2018;30(21):7368-7390. doi:10.1021/acs.chemmater.8b02687

49. Lee J, Kim IS, Hwang M-H, Chae K-J. Atomic layer deposition and electrospinning as membrane surface engineering methods for water treatment: a short review. *Env Sci Water Res Technol*. 2020;6(7):1765-1785. doi:10.1039/C9EW01134J

50. Berger TE, Regmi C, Schäfer AI, Richards BS. Photocatalytic degradation of organic dye via atomic layer deposited TiO_2 on ceramic membranes in single-pass flow-through operation. *J Membr Sci*. 2020;604:118015. doi:10.1016/j.memsci.2020.118015

51. Chen H-S, Chen P-H, Huang S-H, Perng T-P. Toward highly efficient photocatalysis: a flow-through Pt@TiO_2@AAO membrane nanoreactor prepared by atomic layer deposition. *Chem Commun*. 2014;50(33):4379-4382. doi:10.1039/C4CC01166J

52. Chen H, Lin Q, Xu Q, Yang Y, Shao Z, Wang Y. Plasma activation and atomic layer deposition of TiO_2 on polypropylene membranes for improved performances of lithium-ion batteries. *J Membr Sci*. 2014;458:217-224. doi:10.1016/j.memsci.2014.02.004

53. Chen H, Jia X, Wei M, Wang Y. Ceramic tubular nanofiltration membranes with tunable performances by atomic layer deposition and calcination. *J Membr Sci*. 2017;528:95-102. doi:10.1016/j.memsci.2017.01.020

General conclusion

Currently, the world faces unprecedented challenges concerning energy and environmental topics. The continuous increase of environmental pollution has directly affected the water quality. Pollutants such as dyes, heavy metals, pharmaceuticals, personal care products etc. were detected in drinking water. With the increase demand of fresh water, new technologies for water treatment have been considered. Photocatalysis have drawn much attention for degradation of pollutants to less harmful products. Hence, the design of highly active photocatalyst under visible light is still needed.

In this work, elaboration and functionalization of highly active TiO_2 under visible light were performed using two techniques electrospinning and atomic layer deposition. The photocatalytic activity of the prepared samples was tested on the degradation of pharmaceutical pollutants acetaminophen. The effect of the morphology and structure of TiO_2 after several modifications was reported.

First, TiO_2 nanofibers were successfully prepared by electrospinning technique. The obtained nanofibers were calcined at 400°C for 4h for removal of organic layer. Than modification of these nanofibers to enhance their photocatalytic activity was done by atomic layer deposition. The TiO_2 was coated with boron nitride layer of different thicknesses, followed by doping with Pd nanoparticles. The morphological and structural properties of TiO_2 after modification have shown the efficiency of ALD to prepare enhanced catalyst. TiO_2-BN100-Pd100 with 100 cycles of BN and Pd have shown a degradation efficiency 9 time higher than pristine TiO_2 under visible light irradiation. Modification of TiO_2 by ALD, decreased the recombination of photogenerated charges and shifted the band gap to the visible range. This was confirmed by optical and electrochemical measurements. The active species responsible of ACT degradation are superoxide radicals ($\cdot O_2^-$) and holes (h^+). Moreover, the modified catalyst have also shown great stability after five repeatable cycles. Toxicity test revealed that all harmful sub-products were completely mineralized after 8 hours visible irradiation.

Second, elaboration of TiO_2 nanotubes was performed using atomic layer deposition on PAN substrate prepared by electrospinning. Calcination of the samples was than undergo at 750°C for 4h under air. Variation of ALD parameters could highly influence the photocatalytic activity. The increase of ALD cycles decreased the degradation efficiency of the nanotubes.

The best degradation efficiency was obtained after 500 cycles of TiO_2. The pulse time of $TiCl_4$ was also optimized and SEM images showed an incomplete tubular structure when the pulse time was below 0.2 s. Moreover, the morphology and structure of TiO_2 play a major role in the degradation of ACT. TiO_2 nanotube has much higher degradation efficiency that nanofibers heated at the same temperature. The nanotubular structure enhanced the separation rate of the electron- holes. Another modification of TiO_2 was tested by doping he nanotubes with non- metals. Nitrogen doping was found to be effective in enhancing the optical and electrochemical properties of TiO_2.

Finally, photocatalysis combined with membrane processes have shown a high potential in translation and commercialization of this technology. Commercial ceramic membrane with initial pore diameter of 200 nm were purchased from Franhaufer. These membranes were coated with an active layer of TiO_2 using ALD. The TiO_2 coated layer was amorphous and the increase of coated layer thickness decreased the permeability of the membranes. ALD is an efficient technique for uniformly coating of the membrane surface and an increase of the long-term stability. Design of photocatalytic membrane reactor was developed at IEM. The PMR with membrane module containing quartz window for light penetration still need improvement for repeatability and reproducibility of the experiments. Photocatalytic degradation using this system was not performed yet. New membrane module is being designed to investigate the effect of membrane functionalization by ALD in the PMR system.

Perspectives

With the rapid increase and evolution of the pollution in the world, many information are still missing and many efforts should be done for the improvements of water treatment technologies. Several key technical issues limit the applicability of the heterogeneous photocatalytic technology for water treatment. This involve the photocatalysis system, the material synthesis, the substrate choice, the membrane reactor and the upscaling of the process.

Everyday new work on photocatalysis is emerging and over the years thousands of reports were published on improvements of photocatalytic activity using different catalysts for the degradation of organic and inorganic compounds. This photocatalytic process effectively

removed different water contaminants, ranging from hazardous contaminants of pesticides, herbicides, pharmaceuticals compounds and viruses. Researchers found that the pollutant structure and the catalyst surface are highly correlated. They also proved that for each pollutant, a unique set of conditions might be needed for optimal performance which makes the application of photocatalysis more complicated since every pollutant should be considered. More efforts for standardization of this technique are still needed to enable its commercialization. Furthermore, sub-products formed during the degradation process should take more attention since these metabolites could be toxic and harmful on human health and could react with each other's as well. Another important fact should be considered as real wastewater could contain not only organic and inorganic pollutants but many more contaminants could be detected. To date, no clear image was released on the effect of photocatalysis in treating real wastewater in the presence of different pollutants. Therefore, it is difficult to consider a viable treatment of wastewater without a comprehensive investigation of the real circumstance in the industrial plant.

As mentioned before, the catalyst design and structure are two factors that affect the photodergadation of pollutants. TiO_2-based catalyst have been widely reported due to its many advantages: low cost, non-toxicity, high chemical stability and good photocatalytic efficiency. Hence, improvement of the catalyst is necessary for applicability in visible light range and increase of the separation of electron-holes. 0D, 1D, 2D and 3D structure materials were reported in the literature. Modification of these structures by doping with metals or non-metals and coupling with other semiconductor have proven to be efficient for the increase of the catalytic activity. Hence, it is essential to find an optimum amount of dopant to increase the separation of charge carriers and prevent the formation of a recombination center. Therefore, further research and development in TiO_2-based materials are indispensable for exploring sufficient functionality required from the industry. More importantly, choosing an appropriate synthesizing or coating method to improve the catalyst features should also be considered.

Atomic layer deposition among many others techniques could be an important technique for elaboration of highly structured material with control over the thickness of coating layer. This technique was proven to be efficient and started to get more attention in the catalysis

field. It allows the deposition of different materials such as oxides, metals, non-metals over different substrate types. Furthermore, modifications of this technique could be addressed to allow the deposition on high aspect ratio materials such as membranes. This technique could elaborate robust materials for wastewater treatment. It is also an effective technique for large-scale photocatalyst preparation. Hence, the cost of the material synthesis has to be evaluated considering the long-term stability of the catalyst.

To exclude some of the drawbacks associated with the individual techniques, photocatalysis has been recently combined with membrane filtration processes. The photocatalytic membrane reactors have been addressed using organic and inorganic materials. Hence, membranes are associated with fouling, a major drawback that can limits their effectiveness. Functionalized ceramic membranes by coating with highly active catalyst are good candidate for real wastewater applications. Hence, the long-term stability and high cost effectiveness should be developed before upscaling. Mathematical modeling for optimization of the reaction parameters could be an effective solution.

Finally, successful applications of TiO_2 photocatalyst under visible light for water and wastewater treatment were carried out at the laboratory scale. Future research should focus on the use of novel TiO_2 photocatalyst for large-scale applications. Optimization of the process for up-scaling is mandatory and overall cost should be considered.

Scientific contributions

Publications

1. **Sayegh, S.**, Tanos, F., Nada, A.A., Lesage, G., Zaviska, F., Petit, E., Rouessac, V., Iatusnkyi, I., Coy, E., Viter, R., Damberga, Weber, M., Razzouk, A., Estephan J., D., & Bechelany, M.

Tunable TiO_2-BN-Pd nanofibers by combining electrospinning and Atomic Layer Deposition to enhance photodegradation of acetaminophen .

Dalton Transactions, 2022, **51**, 2674-2695

2. **Sayegh, S.**, Zaviska, F., Lesage, G., Razzouk, A. & Bechelany, M.

Atomic Layer Deposition (ALD) an innovative technique for photocatalysts preparation: Review.

In progress

3. **Sayegh, S.**, Abid, M., Tanos, F., Zaviska, F., Lesage, G., Petit, E., Estephan J., Iatusnkyi, I., Coy, E., Viter, Razzouk, A. & Bechelany, M.

N-doped TiO_2 Nanotubes synthesized by Atomic Layer Deposition for the degradation of acetaminophen.

Submission in march 2022

4. **Sayegh, S.**, Lee, J-H., Yang, D-H., Weber, M., Razzouk, A., Iatusnkyi, I., Coy, E., Kim, S. S. & Bechelany, M.

Humidity Resistant Gas Sensors Based on SnO_2 Nanowires Coated with a Porous Alucone Converted Nanomembrane by Molecular Layer Deposition.

Sensors and Actuators B: Chemical Volume 344, 1 October 2021, 130302

5. **Sayegh, S.**, Majhi, S. M., Kim, H. W., Kim, S. S. & Bechelany, M.

Atomic Layer Deposition: a unique tool for gas sensing application-an overview.

Submitted in Journal of Materials Chemistry A.

6. Zebiri, H., Van Den Berghe, H., **Sayegh, S.**, Chammas, P. E., Pompée, C., Chammas, M., & Garric, X. (2021).

Synthesis of PLA–poly (ether urethane)–PLA copolymers and design of biodegradable anti-adhesive membranes for orthopaedic applications.

Journal of Materials Chemistry B, *9*(3), 832-845.

7. Barhoum, A., El-Maghrabi, H. H., Iatsunskyi, I., Coy, E., Renard, A., Salameh, C., Weber, M., **Sayegh, S.**, Nada, A. A., Roualdes, S. & Bechelany, M. (2020).
Atomic layer deposition of Pd nanoparticles on self-supported carbon-Ni/NiO-Pd nanofiber electrodes for electrochemical hydrogen and oxygen evolution reactions.
Journal of colloid and interface science, *569*, 286-297.

8. Najem, M., Nada, A. A., Weber, M., **Sayegh, S.**, Razzouk, A., Salameh, C., Eid, C. & Bechelany, M. (2020).
Palladium/carbon nanofibers by combining atomic layer deposition and electrospinning for organic pollutant degradation.
Materials, *13*(8), 1947.

9. Abi younes, P., **Sayegh, S.**, Nada, A., Weber, M., Abboud, N. & Bechelany,M.
Elaboration of Porous Alumina Nanofibers by Electrospinning and Molecular Layer Deposition for Organic Pollutant Removal.
Colloids and Surfaces A: Physicochemical and Engineering Aspects, Volume 628, 5 November 2021, 127274

10. Siuzdak, K., Grądzka-Kurzaj, I., **Sayegh, S.**, Weber, M., Ziółek, M., Bechelany, M., Iatsunskyi, I. & Coy, E.
Exploring the Effect of BN and B-N Bridges on the Photocatalytic Performance of Semiconductor Heterojunctions: Enhancing Carrier Transfer Mechanism.
Applied Materials Today, Volume 24, September 2021, 101095

11. Barhoum, A., Favre, T., **Sayegh, S.**, Tanos, F., Emerson. C., Razzouk, A., Iatusnkyi I., Cretin. M. & Bechelany, M.
3D Self-supported Nitrogen-Doped Carbon Nanofiber Electrodes incorporated Co/CoOx Nanoparticles: Application to Dyes Degradation by Electro-Fenton-based Process.
Nanomaterials 2021, 11(10), 2686

12. Mirek, A., Grzeczkowicz, M., Lamboux, C., **Sayegh, S.**, Bechelany, M., LewińskaKunene, D.

Formation of disaggregated polymer microspheres by a novel method combining pulsed voltage electrospray and wet phase inversion techniques.

Submitted to Journal of Colloid And Interface Science

13. Kunene, K., **Sayegh, S.,** Weber, Sabela M., Voiry D., Emerson. C., Iatusnkyi I., Kanchi S. & Bechelany, M.

Electrochemical immunosensor for detection of Aflatoxin B1 in wine using Pd nanoparticles supported on boron nitride coated carbon felt electrode: A screening tool to wine industries

In progress

Conferences: Oral communication

1. **Sayegh S.**, 7th workshop RAFALD: ALD Nov. 2021, Marseille, France.

"N-doped TiO_2 Nanotubes synthesized by Atomic Layer Deposition for the degradation of acetaminophen"

2. **Sayegh S.**, Balard Chemistry Conferences 2021, June 2021, Montpellier, France.

"Design of Advanced Photocatalytic Materials by Atomic layer Deposition (ALD)"

3. **Sayegh S.**, 6th workshop RAFALD: ALD Nov. 2020, zoom webinar.

"Humidity Resistant Gas Sensors Based on SnO2 Nanowires Coated with a Porous Alucone Converted Nanomembrane by Molecular Layer Deposition (MLD)"

4. **Sayegh S.**, 5th International Conference on Bioinspired and Biobased Chemistry & Materials, Oct. 2020, Nice, France

"Design of Advanced Photocatalytic Materials by Atomic layer Deposition (ALD)"

5. **Sayegh S.**, 20th International Conference on Atomic Layer Deposition (ALD/ALE 2020), June 2020, Ghent, Belgium (zoom webinar)

"Design of Advanced Photocatalytic Materials by Atomic layer Deposition (ALD)"

6. **Sayegh S.**, 5th workshop RAFALD: ALD, Nov. 2019 , Toulouse, France

"Design of Advanced Photocatalytic Materials by Atomic layer Deposition (ALD)"

Conferences: Poster

1. **Sayegh S.**, 7th workshop RAFALD: ALD Nov. 2021, Marseille, France.

   "Tunable TiO_2-BN-Pd nanofibers by combining electrospinning and Atomic Layer Deposition to enhance photodegradation of acetaminophen"